NIELS BOHR INSTITUTE
FACULTY OF SCIENCE
UNIVERSITY OF COPENHAGEN

PhD thesis

Sune Olander Rasmussen

Improvement, dating, and analysis of Greenland ice core stratigraphies

The cold climate period Younger Dryas, dated in the new Greenland Ice Core Chronology 2005 to 10897 – 9704 years B.C., takes its name from the flower Dryas Octopetala, fossil remains of which were found in glacial clay deposits in Denmark by Hartz and Milthers.

Main supervisor: Katrine Krogh Andersen.

Submitted August 4, 2006.

Contents

Preface

This thesis is submitted in partial fulfillment of the requirements for the PhD degree at the Niels Bohr Institute, Faculty of Science, University of Copenhagen, Denmark. The thesis consists of the present text and five enclosed papers and manuscripts encompassing several separate topics. In order to make the thesis readable as a whole, the papers and manuscripts are summarized in the thesis text, but the main theory and literature discussions are contained in the papers and manuscripts. In accordance with this, the evaluation of the thesis should be based upon the thesis text and papers in conjunction.

Ice core science is teamwork, and the work presented here relies on the efforts of many people involved in the Greenland deep drilling projects and the related measurement campaigns. Their work is gratefully acknowledged.
I would like to express my thanks to my colleagues at the Ice and Climate Research Group in Copenhagen for continued support and cooperation. Special thanks goes to Katrine Krogh Andersen for exemplary supervision and cooperation. Timely and valuable input from co-supervisors Peter Thejll, Danish Meteorological Institute, and Ole Winther, Institute for Informatics and Mathematical Modelling, Technical University of Denmark, is greatly appreciated.

The study has been financed by the Carlsberg Foundation and the Copenhagen Global Change Initiative (COGCI). Rob Mulvaney, British Antarctic Survey, is gratefully acknowledged for hosting me and my family during our visit to Cambridge in summer 2004 and for additional financial support.

Copenhagen, Denmark, August 4, 2006.

Sune Olander Rasmussen

Introduction

The large ice caps covering Greenland and Antarctica comprise a fantastic archive of information about the palaeoclimate. This information has been made available through the drilling of ice cores, which represent samples of millennia of precipitation. However, the value of this information can only be fully appreciated if reliable chronologies can be established. Much work has therefore gone into constructing time scales for ice cores, using a variety of methods and data sources. During the most recent deep ice core drilling project in Greenland, the North Greenland Ice Core Project (NGRIP), it became apparent that the NGRIP ice core would be exceptionally suitable for establishing a chronology for the climate of the last glacial period. By means of a generous grant from the Carlsberg Foundation, the Copenhagen Dating Initiative was initiated in 2002 with the objective of constructing the optimal chronology for the NGRIP ice core by counting annual layers in the upper part of the ice core, linking this chronology to that of other palaeoclimate records, and developing measurement techniques that will allow dating of the deeper parts of the core. The primary result from the Copenhagen Dating Initiative is a new ice core chronology, the so-called Greenland Ice Core Chronology 2005 (GICC05), which has been constructed by counting annual layers in several ice cores. The work reported in this thesis is a contribution to the construction of the GICC05 time scale.

The GICC05 time scale represents a new approach to ice core dating, because it is a composite stratigraphic time scale based on data from several ice cores to ensure optimal quality and coverage. Differences in accumulation and flow conditions mean that ice cores retrieved from different parts of the ice cap are optimal for dating different age intervals, and this fact is utilized in the construction of the GICC05. The drill site of the DYE-3 ice core in South Greenland receives more than twice as much accumulation as Central Greenland, and the annual layers are thus very well resolved in the upper part of the DYE-3 ice core. In the most recent 7.9 ky, annual layers have therefore been identified using stable isotope ratio data from the DYE-3 ice core, supported by data from the GRIP and NGRIP ice cores in the youngest part. High accumulation rates result in relatively rapid ice flow, and due to flow-induced layer thinning and diffusion of the isotopes, DYE-3 data can not be used for annual layer counting much more than 8 ky back in time. In the more recent GRIP and NGRIP ice cores, continuous measurements of the concentration of a number of impurities in the ice have been performed. Impurity data are not significantly influenced by diffusion, and can be used for identification of annual layers that are much thinner than if using isotope data. The impurity records are, however, also less straight-forward to interpret, as the impurities originate from sources exhibiting both annual and non-annual variations. In order to identify the annual layers correctly, the resolution and quality of the data is therefore of paramount importance.

The first part of this thesis presents methods for improving the resolution of the Continuous Flow Analysis (CFA) impurity data. The aim of this work is to improve the quality of the data in order to make annual layer detection more certain, and to deal with problems of missing data. The missing data problem has been handled by developing a Maximum Entropy Method prediction algorithm, and resolution enhancement has been performed using a spectral deconvolution technique. The latter method is compared with a Monte Carlo resolution enhancement approach, and it is discussed how integration of the resolution enhancement methods into the CFA data processing line can be used to improve future CFA measurements.

Dating by annual layer counting is the subject of the second part of the thesis. A short overview of existing Greenland ice core chronologies is given, and the importance of independent dating is discussed. The NGRIP CFA data set contains multiple series with an annual signal, and different approaches to multi-parameter dating using this data set are developed and demonstrated. The key element of this section is the description of the construction of the GICC05 time scale across the last termination, the period 7.9 – 14.8 ka before A.D. 2000 (b2k).

The third part of the thesis deals with interpretation of the dated records. In the Holocene, the GICC05 time scale is common to the DYE-3, GRIP, and NGRIP ice cores, and in the most recent millennia the records of the three deep cores are synchronized with annual precision to the records of the Crête and Milcent intermediate length ice cores. The tight synchronization makes it possible to compare the records on the same time scale and to extract a common regional accumulation and isotope signal. The same approach has been applied to the 7.9 – 11.7 ka b2k section, which is characterized by a number of prominent climate anomalies: the 8.2 ka event, the 9.3 ka event, and the Preboreal Oscillation. It is discussed how these events are represented in the Greenland ice core records and how climatic events and transitions can be defined in an objective way. Currently, the GICC05 time scale has been extended back to 42 ka b2k in the NGRIP ice core, and the thesis describes how the GRIP and GISP2 ice core records have been synchronized with the NGRIP records, making it possible to apply the GICC05 time scale to all three cores. The synchronization allows for the first time a comparison of the climate records of the three cores on a sub-centennial scale throughout the late glacial period, and unveils hitherto unknown differences between these key records of the glacial climate.

Part 1

Enhancing NGRIP CFA data

During the NGRIP field season in year 2000, impurity measurements were performed on the NGRIP deep ice core using a Continuous Flow Analysis (CFA) setup. The type of measuring system used is described in Röthlisberger et al. (2000), and more specific investigations of the setup and data are reported in Bigler (2004). In the depth interval from 1404.7 to 2930.4 m, a 3 cm by 3 cm cross section was cut from the main core in 1.65 m pieces and was melted continuously on a special melt head at a speed of 3 – 4 cm min^{-1}. The melt water from the clean inner part of the core was debubbled and passed to the analysis systems measuring the concentrations of NH_4^+, Ca^{2+}, NO_3^-, Na^+, SO_4^{2-}, HCHO, and H_2O_2. The electrolytical conductivity of the melt water was also measured, together with the dust content (Ruth et al., 2003). The melting device is shown on Fig. 1.1 .

The resolution of the resulting impurity records is governed by the amount of mixing that takes places as the melt water passes through the sampling and analysis system. The sampling system and the [Ca^{2+}], [NH_4^+], and conductivity measuring sub-systems are illustrated

Figure 1.1: The melt head of the CFA system ready for ice samples (left) and during sampling (right). The center hole through which melt water from the inner part of the core is collected is visible. The ring is intended to separate the melt water from the clean inner part from the contaminated melt water from the outer parts. Picture provided by M. Bigler.

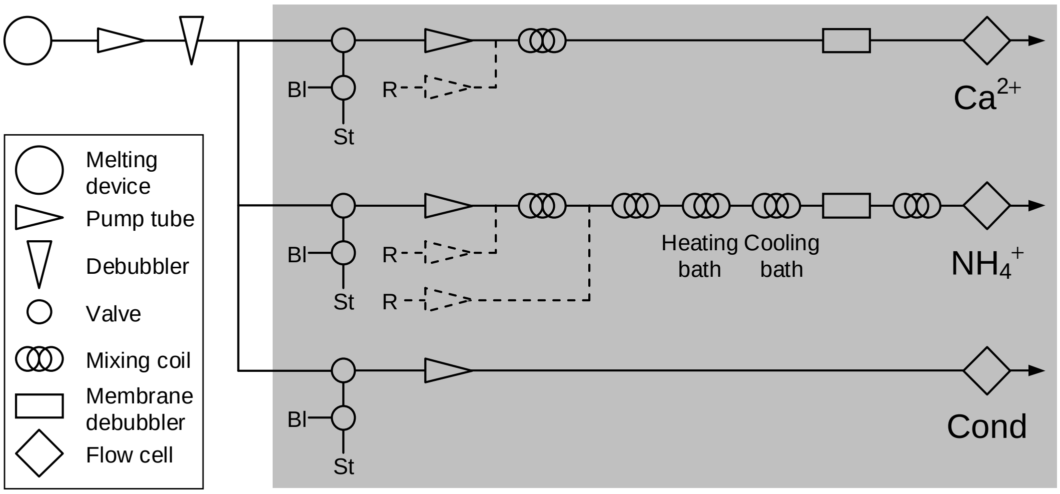

Figure 1.2: Simplified flowchart of the CFA setups for [Ca^{2+}], [NH_4^+], and electrolytical meltwater conductivity. The remaining analysis sub-systems are in principle similar to the [Ca^{2+}] and [NH_4^+] sub-systems shown, while the dust measurement sub-stream resembles the illustrated conductivity sub-stream. Sample water from continuously melted ice is pumped to the warm lab, debubbled and split into sub-streams to feed the different analysis subsystems, where specific reagents (R) are added. Valves allow switching between sample, blank (Bl) or standard solution (St), which are used to establish baselines and to calibrate the measurements. Figure from Rasmussen et al. (2005).

schematically in Fig. 1.2 and the main components are described below.

The melt head. The inner part of the melt head used for the NGRIP setup slopes gently inwards, which means that the center of the ice rod is melted at the same time as ice from an area a few millimeters above in the outer part of the ice rod. The result is that the melt water at any time originates from a section of ice that is approximately 3 mm thick.

Pump tubing. The melt water and air bubbles are pumped through thin tubes to the warm lab. The air content means that the flow is so-called *segmented flow*, where very small volumes of melt water are separated by small volumes of air. The mixing can thus only take place within these confined volumes, which limits the dispersion of the signal.

Debubbler. As most of the analysis systems are sensitive to air, the air is removed in a debubbler. The debubbler is basically a small reservoir into which the melt water drips, before it is pumped further into the system. The volume of the debubbler is critical to the resolution obtainable, and is kept as small as possible by adjusting the melting and pump speeds and by removing excess melt water not needed for the measurements. Despite the efforts to keep the mixing volume small, the mixing taking place in the debubbler is one of the more important contributions to the total mixing.

Reaction columns and mixing coils. After the debubbler, the sample flow is divided into sub-streams that are fed into the individual analysis systems. The conductivity and dust measurements are direct measurements, but for each of the chemical species, a reagent is added with the purpose of forming fluorescent or absorbent complexes that can be detected using spectrophotometric detectors. The individual measurement sub-systems contain different components needed for the formation of the complex, such as reaction columns and mixing coils. Mixing takes place in these components, meaning that the mixing strengths for the different sub-systems are different.

Flow cells. The concentration measurements are performed in flow cells. Mixing takes place in these volumes as well, and for the conductivity and dust measurements the flow cells are the main mixing volumes in question apart from the debubbler.

Even though data from the CFA setup are collected in sub-millimeter resolution, the mixing means that the real resolution only makes identification of cycles with wavelengths down to between one and two centimeters possible. However, some of the details lost in the mixing can be restored. Two different restoration approaches have been applied in this work. The first method is a spectral method that utilizes information about the mixing strength obtained from calibration measurements, while the second method is a Monte Carlo based method where the mixing strength estimation is performed automatically.

1.1 Spectral resolution enhancement

In order to convert the voltage output of the spectrophotometric detectors to impurity concentrations, calibration measurements are performed. The measurements are performed on ice core samples of 1.65 m length, the so-called *runs*. Ultra-pure water (blank) is passed through the system before and after each run, and standard solutions with known concentrations are measured between approximately every second ice core run. Raw data from a typical run, including standard measurements, are shown in Fig. 1.3.

Using the baseline established by the blank and the known concentrations of the standards, the measured voltage can be converted to a concentration scale, but the standard measurements can also be used to estimate the mixing strength in the analysis system. When switching between blank and standard solutions, the input to each analysis sub-system represents a step function from one concentration level to another, and the measured soft response curves (red curve sections of Fig. 1.3) thus contain information about the strength of the mixing in that specific analysis sub-system. This information can be used to restore some of the details lost by mixing, but it should be noted that only the mixing taking place in the analysis systems are considered in this way (corresponding to the grey shaded area in Fig. 1.2). In order to estimate the total mixing, the system's response to blank-standard and standard-blank shifts must be known, e.g. by measuring the response when melting a block of ice containing a step concentration change. However, it is not possible to obtain such a sample from natural

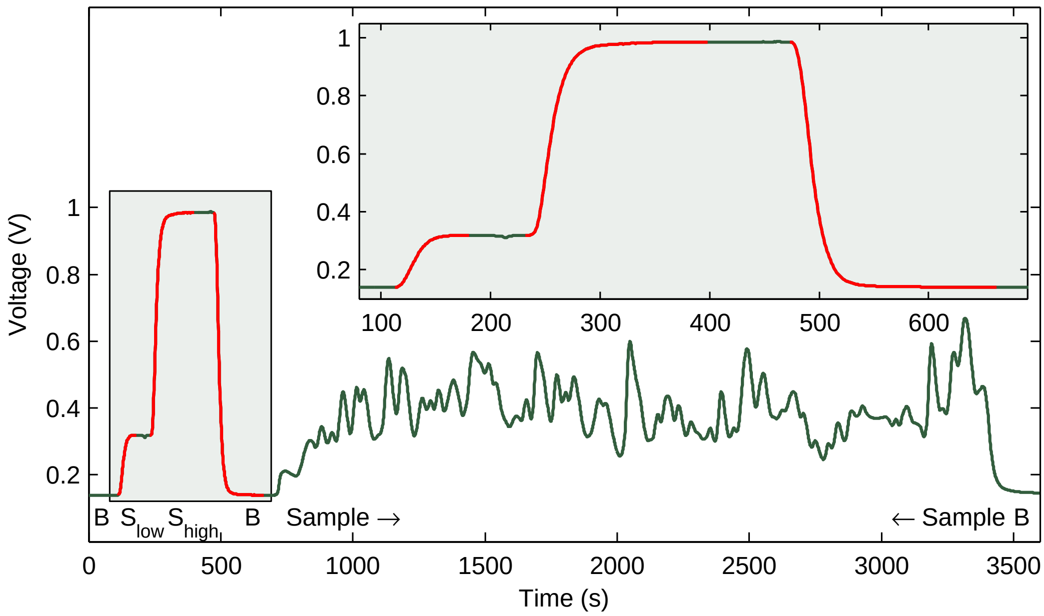

Figure 1.3: Raw data from a typical CFA ice core impurity measurement run. First ultra-clean water (B for "blank") is passed through the system. For calibration purposes, two standard solutions are measured (S_{low} and S_{high}). Before the actual sample, a block of frozen ultra-clean water is inserted to eliminate transients in the melting (the small bump between the blank and sample labels). After the sample has been measured, blank is passed through the system again. The B $\rightarrow S_{low}$, $S_{low} \rightarrow S_{high}$, and $S_{high} \rightarrow$ B step responses (red parts of the curve, also shown in the insert) are used to estimate the mixing strength.

sources, and making a realistic ice sample with a step change in concentration is very difficult. Freezing a standard solution will not produce ice with uniform concentration, and the ice should have a clean air content similar to that of glacier ice for the flow to resemble the segmented flow from the melting device to the debubbler unit. The resolution enhancement method presented here has therefore been developed to account only for the mixing in the analysis system. The concept is developed in Rasmussen et al. (2005), which is enclosed in this thesis and briefly summarized below.

1.1.1 Summary of Rasmussen et al. (2005)

The resolution enhancement method is developed using CFA data from the NGRIP and Berkner Island (Antarctica) ice cores. The impurity concentrations are generally much lower in Antarctic ice cores, and the signal-to-noise level is therefore lower in the Berkner Island data. The Berkner data are included to illustrate that the method is generally applicable and robust to the presence of noise.

Step-response curves are extracted from the raw data to estimate the strength of the part of the mixing that takes place in the $[Ca^{2+}]$ and $[NH_4^+]$ analysis sub-systems, and in the conductivity measurement sub-stream. A spectral filter $\widetilde{M}$ describing the effect of the mixing is constructed from the response curves (Fig. 1.4b, brown curve), but in the presence of noise

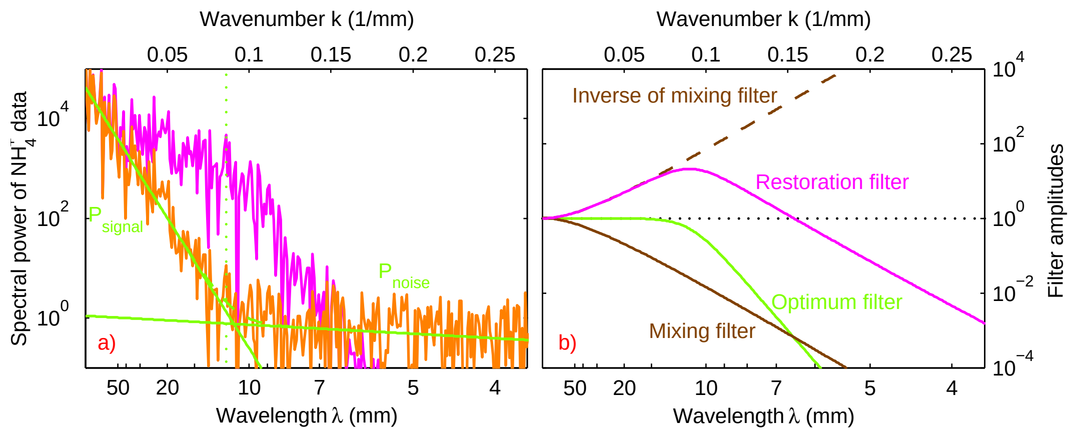

Figure 1.4: Data used to construct the deconvolution filters needed for signal restoration (a) and the resulting filters (b). The spectral power of a one meter NH_4^+ data section from about 1622 m depth (a, orange) has distinct signal and noise parts, P_{signal} and P_{noise}. This separation of the data spectral power into signal and noise parts defines the optimum filter (b, light green line) that allows restoration of the original signal without blowing up the noise. The strength of the mixing in the analysis system is estimated from the response curves (b, brown line). The inverted mixing filter (b, dashed brown line) is combined with the optimum filter (b, light green line), forming the restoration filter (b, magenta line). From Rasmussen et al. (2005).

the application of $\widetilde{M}^{-1}$ to the measured data will result in noise blow-up, as the short wavelengths are heavily amplified. The filter correcting for the mixing must therefore be combined with a so-called optimum filter $\widetilde{F}$ (Fig. 1.4b, green curve), which is constructed from the data by identifying the noise and signal parts of the data spectrum, P_{signal} and P_{noise} (Fig. 1.4a, green curves). The optimum filter $\widetilde{F}$ represents the optimal trade-off between noise robustness and the goal of restoring as much of the signal as possible. The mixing correction filter (Fig. 1.4b, brown dashed curve) and the optimum filter are combined to form the restoration filter $\widetilde{R} \equiv \widetilde{F}\widetilde{M}^{-1}$ (Fig. 1.4b, magenta curve) which leaves the long wavelengths untouched (as the mixing has not affected those, and no correction is needed), cuts away the short wavelengths (because the short-wavelength part of the data has been obliterated by the mixing and thus cannot be safely restored in the presence of noise), and amplifies wavelengths in the middle part of the spectrum. The amplification is illustrated most clearly by the comparison of the spectrum of the raw data (Fig. 1.4a, orange curve) with the spectrum of the resolution enhanced data (Fig. 1.4a, magenta curve). For the NGRIP data, the maximum amplification is attained for wavelengths in the $10-15$ mm interval, which is not far from the expected annual layer thickness in the glacial part of the NGRIP core. The P_{signal} and P_{noise} curves intersect at $\lambda \approx 11$ mm for the original data, while the signal part of the enhanced data spectrum intersects P_{noise} at $\lambda \approx 7$ mm, and the limit of how thin layers can be detected from the data is thus pushed accordingly.

The application of the method to the Berkner Island data shows that the method is robust to high levels of noise, but that the high noise levels limit the usefulness of the resolution enhancement because only few details can be safely restored. However, the integrated noise filtering is convenient, because it is performed without manually choosing at which frequency to cut away the noise, as the optimum filter automatically accommodates to the frequency-dependent signal-to-noise ratio of the data section in question.

Finally, it is argued that integration of the method into the CFA data processing line can improve the results further. By doing so, the response curves can be extracted without much additional work and the resolution enhancement can be performed with almost no extra effort. Also, the information needed to construct the filters can at the same time yield valuable information about the system stability. The combination of system stability check, noise filtering, and resolution enhancement means that the usefulness and reliability of data produced can be significantly improved.

1.1.2 Making an operational algorithm

The construction of the restoration filter and the method's application to data examples are described in Rasmussen et al. (2005), but making the method applicable to the large amounts of NGRIP CFA data requires elements other than the mathematical model itself. It is described in the following how the method was applied to 6 species of the NGRIP CFA data in the 1404-1640 m depth interval, corresponding to almost 900 data files.

The method has been applied successfully to the Ca^{2+}, NH_4^+, and conductivity data series. For the NO_3^-, Na^+, and SO_4^{2-} setups, the voltage output from the detector is not linearly related to concentration, and as the step response curves used for the calculations are the (time, voltage) rather than (time, concentration) curves, the step response curves used are slightly distorted. Formally correct resolution enhancement calculations require calibrated step response curves to be used, but the effort needed to perform this calibration is large compared to the small error made. The NO_3^-, Na^+, and SO_4^{2-} data series have therefore been resolution enhanced using the (time, voltage) step response curves, and the provisional results have been used for annual layer identification, but the results have not been published.

Dealing with missing values

All samples for the CFA measurements had to be cleaned on the end faces, and around irregular core breaks the sample pieces had to be trimmed to be perpendicular to the core axis. In addition, small gaps in the data are caused by bubbles originating from incomplete debubbling or bubbles formed by the chemical reactions in the analysis sub-systems. Short gaps of 1 – 20 mm in the CFA data thus occur frequently, typically several times per meter of data. In the Ca^{2+} record, for example, 94% of the data gaps in the 1404 – 1640 m data section are shorter than 20 mm. Although most of these gaps imply no problems for the interpretation of the records, they complicate the resolution enhancement method as they make standard Fourier transformation impossible. Methods for spectral power estimation of unevenly sampled data are becoming rather standard (e.g. the Lomb-Scargle approach), but for unevenly sampled data, spectral amplitude estimation, which is needed for the resolution enhancement approach described in Rasmussen et al. (2005), is less straightforward (see e.g. Qi et al., 2002, for a recent approach). Instead, the problem of missing data is solved by filling in values in the shorter data gaps, thereby ensuring that the distance between neighbouring data gaps is sufficiently large to allow ordinary Fourier transformation of each unbroken data segment.

When filling in values, it is essential to use a method that distorts the spectral properties of the data as little is possible. Most simple interpolation methods (linear, cubic, spline etc.) will fill in the gaps with data that have a spectral signature different from that of the surrounding data. When the resolution enhancement procedure is applied, these features may be amplified, thereby introducing spurious features in the resulting data series. It is therefore essential to fill in values that change the spectrum of the data as little as possible. For this purpose, the Maximum Entropy Method (MEM) has been applied. This method is described in Johnsen and Andersen (1978) and was originally developed for spectral power estimation, but the filter constructed can equally well be used as a prediction filter. All data gaps less than 100 mm wide have been filled with values predicted using the MEM method, which in practice consists of the following steps:

1. All data gaps shorter than 100 mm are filled with values obtained by linear interpolation to produce a first estimate of a data series without gaps, S_1.

2. MEM prediction filters are constructed using the numerical method of Johnsen and Andersen (1978) with a filter length of 150 points (chosen by trial and error). For each data gap, a filter is constructed using the 1000 data points from S_1 just prior to the beginning of each gap. The filter is used to estimate which values should be inserted (the forward prediction). Similar calculations are performed moving backwards through the data series, using the 1000 points below each gap to construct the filter (the backward prediction).

3. For each missing data point, the second estimate S_2 is calculated as a weighed mean of the forward and backward predicted values, where the weights are proportional to the distances to the gap end points. For a gap of length N, the i$^{\text{th}}$ value is thus calculated as $\frac{N+1-i}{N+1}$ of the forward prediction plus $\frac{i}{N+1}$ the backward prediction.

4. Steps 2 and 3 are repeated, so that the predicted values in S_n are used to construct the filters needed to calculate the predicted values S_{n+1}.

5. After about 5 prediction runs, the average difference between the predicted values of two subsequent estimates (e.g. S_5 and S_6) is less than 10^{-4} of the mean value, and the influence of the initial linear interpolated values have thus been "forgotten".

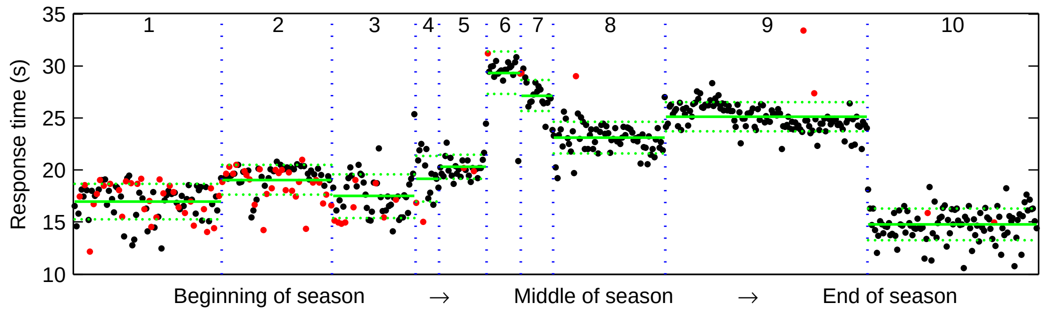

Figure 1.5: Response times for the CFA Ca^{2+} sub-system. Red marks are low → high concentration steps and black marks are high → low concentration steps. There is no systematic difference between the steepness of these two categories of step responses. The season has been divided into sections based on the response times, and within each section the average response time plus/minus one standard deviation is indicated by green lines.

This recursive approach is chosen to ensure that the prediction filters can be based on relatively long data sections (1000 points, or 1 meter of data) even in sections where the gaps are closely spaced. This means that prediction filters are calculated from data values of which some are predicted in a previous prediction round themselves, and thus the recursion procedure is necessary to eliminate the impact of the linear interpolation performed in the first step.

Step response curve extraction and treatment

Throughout the measuring campaign, standards were measured approximately every second run[1]. To investigate the temporal variance in the mixing strength, all step response curves from the Ca^{2+} sub-system have been extracted from the raw data files. Some of the response curves are unusable for estimating the mixing strength because the valves (see Fig. 1.2) sometimes introduce a bubble on the flank of the response curve, especially when switching from blank to standard, but a total of 567 intact response curves are available. Denoting the initial concentration C_0 and the end concentration C_1, the response time is defined as the time spent to go from $C_0 + 0.2 \cdot (C_1 - C_0)$ to $C_0 + 0.8 \cdot (C_1 - C_0)$. The response times of the Ca^{2+} sub-system are shown in Fig. 1.5 as red and black points, representing the blank → standard and standard → blank step responses, respectively.

It is apparent from Fig. 1.5 that the response times change abruptly several times during the season, and based on visual inspection the season has been divided into 10 sections with approximately constant response times as indicated in the figure. Some of these changes

[1]The electrolytical conductivity measurements are direct measurements that do not require calibration. Unfortunately, step response curves were only measured in the beginning of the season, and are not available below 1493.25 m depth. In the deconvolution calculations, the mixing characteristics of the 1404 – 1493 m section have been used for the entire 1404 – 1640 m depth interval considered. As the conductivity measurement setup is very simple and not modified during measurements of samples from the 1404 – 1640 m depth interval, this simple approach is reasonable.

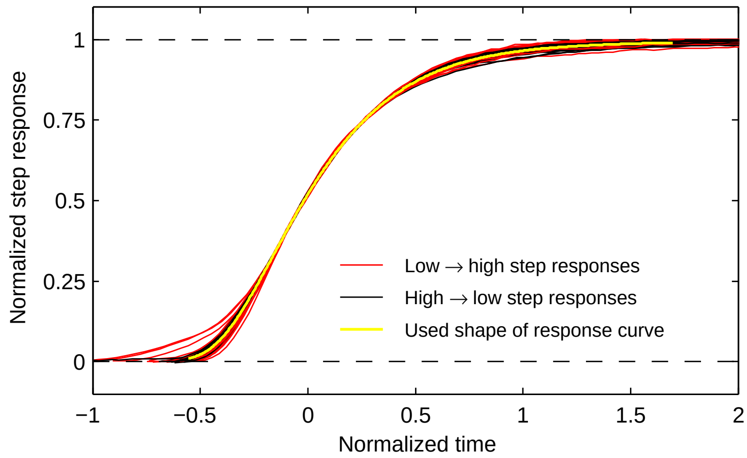

Figure 1.6: Shape of response curves from section 2 of Fig. 1.5 (red, black). The curves have been normalized to a $0 \rightarrow 1$ concentration step, and so that the mean slope of the steepest part is unity (see text). The yellow curve is the average shape curve used for the filter construction.

can be explained by known modifications of the setup (changed tubes, flow cells etc.) and changing melt speed as recorded in the laboratory journal, but other changes cannot readily be explained by known changes in the experimental design.

The shapes of the response curves vary slightly, and for some of the curves, the measurement noise level is significant compared to the signal magnitude. To obtain consistent results within each of the sections of Fig. 1.5, the step response curves are therefore combined to define the average curve shape, which is then used for that entire section.

- The curves are normalized to a $0 \rightarrow 1$ concentration step and aligned so that the concentration is 0.5 at time 0.
- For each curve, the slope of the steepest part is computed as the mean slope in the part with values in the [0.2, 0.8] interval. Each curve is then stretched in time so that the mean slope of the middle part is unity. The normalized and time-stretched response curves for the Ca^{2+} sub-system are shown in Fig. 1.6.
- For each time value, the average value of the response curves is determined. The average curve is shown as the yellow curve in Fig. 1.6.
- Using the average value of the slope steepness and the average melt speed, the normalized time scale of the average shape response curve is transformed into a depth scale, comparable to that of the ice samples.

Using the method of Rasmussen et al. (2005), the step response curve is differentiated with respect to time and then Fourier transformed to estimate the mixing filter $\widetilde{M}$. Noise on the measurements and numerical problems mean that the pulse response curve $\frac{ds}{dt}$ derived from the average shape curve described above often has small ripples imposed on the general curve

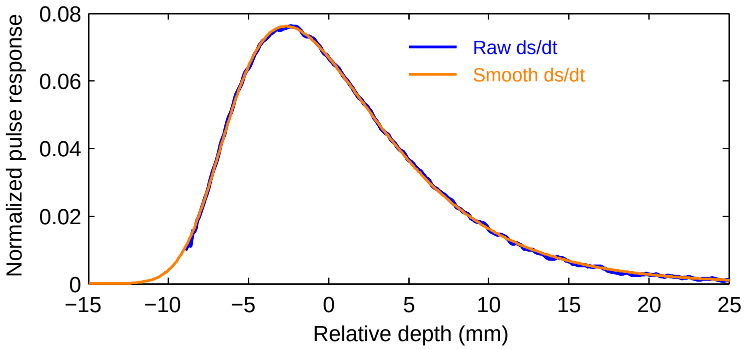

Figure 1.7: Normalized pulse response obtained by differentiating the scaled average step response curve of Fig. 1.6 (blue curve) and the corresponding smooth curve obtained by fitting equation 1.1 to the experimental data (orange curve).

shape (blue curve in Fig. 1.7).
When performing a Fourier transformation, these ripples sometimes cause numerical oddities. Other numerical problems are encountered because a small kink is introduced when zeros are padded to the ends of the curve in order to have 1024 point long series for a FFT calculation. To solve this, a function has been fitted to the experimental $\frac{ds}{dt}$ curve, and values have then been sampled from this analytical function to obtain a smooth $\frac{ds}{dt}$ curve. The curve type to be fitted must be able to represent the characteristics of the pulse response curves, namely the different steepness and curvature of the rising and falling slopes. A product of two logistic functions has proven to be rather successful in approximating the pulse response curves, but in order to fully represent the rising and falling slopes, an additional parameter has been added. The resulting function is

$$y = a \cdot [1 + \exp(-b_1 (x - c_1))]^{-d_1} \cdot [1 + \exp(b_2 (x - c_2))]^{-d_2} \tag{1.1}$$

where the parameters are determined using non-linear multi-parameter least squares regression within the intervals $a \in [0, 1], b_i \in [0, \infty[, c_i \in] - \infty, \infty[, d_i \in [0, \infty[$. Example of the original and smoothed $\frac{ds}{dt}$ curves are shown in Fig. 1.7.

Performing the deconvolution

As described above, the restoration filter $\widetilde{R}$ is the product of the inverse mixing filter $\widetilde{M}^{-1}$ and the optimum filter $\widetilde{F}$. The filter $\widetilde{M}^{-1}$ is taken to be constant as long as the response times do not change abruptly. This means, for example, that 10 different filters are used during the season for the Ca^{2+} sub-system in accordance with Fig. 1.5. The filter $\widetilde{F}$ depends on the signal-to-noise ratio, and will to some degree depend on the mean annual layer thickness and the impurity concentration levels. The optimum filter has been calculated for each species for each measurement run, and a visual inspection of the several thousand resulting filters has revealed no abrupt changes in $\widetilde{F}$. The inflection point of P_{signal} and P_{noise} is determined automatically as indicated in Fig. 1.4a, but the inflexion point is not always well-defined from the spectra of single runs. The optimum filters used for the deconvolution are therefore constructed from average spectra of 10 meters of data.

In this way, the restoration filters are constant within every 10 meters of data, except from where the step response times change abruptly as illustrated in Fig. 1.5. For the deconvolution of the NGRIP 1404 – 1640 m depth interval, such abrupt changes occur at the depth 1531.20 m for the Ca^{2+} sub-system (section 1→2 transition in Fig. 1.5), and at 1494.90 m for the NO_3^- subsystem. Within each interval where $\widetilde{R}$ is constant, the deconvolution is performed for 1024 points at a time with at least 100 points of overlap between neighbouring pieces. In the overlap, the results are combined using weighed averaging to ensure smoothness of the final results. The results are exemplified in Rasmussen et al. (2005) and have been used for annual layer counting as described in section 2.2.1.

1.2 Monte Carlo based resolution enhancement

The spectral resolution enhancement approach described above is based upon measured mixing characteristics and only corrects for the mixing in the analysis system as described in section 1.1. An alternative Monte Carlo-based method for resolution enhancement has been developed in cooperation with Susanne Lilja Buchardt to circumvent this problem and to validate the results of the spectral approach.

When applying the spectral resolution enhancement approach, an estimate of the original data $D(t)$ is calculated in the spectral domain from the measured data $d(t)$ using the restoration filter $\widetilde{R}$, which is estimated from the data and step response curves. In the alternative Monte Carlo approach, both the original unmixed data (in the following denoted the "true" data) and the mixing strength are estimated from the measured data series alone. Thus, the problem is to find true data $D(t)$ and a mixing response function $M(\tau)$ that satisfy

$$d(t) = \int_{-\infty}^{\infty} D(\tau) \cdot M(t-\tau) d\tau \tag{1.2}$$

where only the measured data $d(t)$ are known. Many combinations of $D(t)$ and $M(\tau)$ exist that satisfy Eq. 1.2, but as discussed below, constraints can be derived from a priori knowledge about the nature of the mixing and the nature of the true data.

1.2.1 Parameterizing the mixing strength

A simple yet reasonable model of the mixing is to represent the mixing in the melting and analysis systems as taking place in a series of well-mixed volumes $V_1, V_2, \ldots, V_N$ as illustrated in Fig. 1.8 (Sigg, 1990). These volumes represent the elements of the physical setup, such as the melt head, tubing, and debubbler, but can also be regarded as abstract parameters. Given a steady flow rate v through the CFA system and a sampling time interval r, a constant

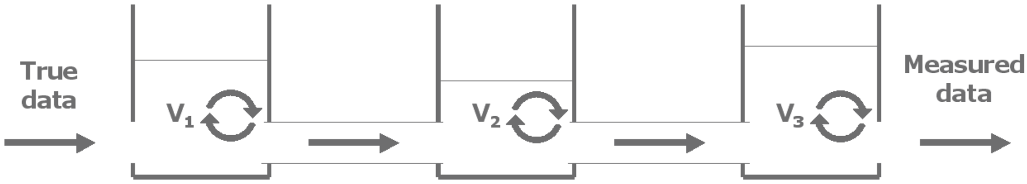

Figure 1.8: The mixing model used for the Monte Carlo based resolution enhancement method. The mixing takes place in a series of well-mixed volumes $V_1, \ldots, V_N$, in which the mixing is assumed to be instantaneous. Here $N = 3$.

fraction $dV_i = \frac{vr}{V_i}$ of the i$^{\text{th}}$ volume is replaced per time step r. Assuming that V_i is mixed instantaneously in every time step, the mixing response function is given by

$$M_i(\tau) = dV_i \cdot (1 - dV_i)^\tau \tag{1.3}$$

where τ is time measured in units of r. The mixing is thus described by the value of N and $dV_1, \ldots, dV_N$, and the effect of the mixing on the true data is described by consecutive convolution with the response functions $M_i(\tau)$. By taking $N \geq 3$ and adjusting the fractional volumes dV_i (or equivalently V_i), $i = 1, \ldots, N$, the modelled step response curves can be made to resemble those measured for the analysis sub-systems, while for $N = 2$ the different curvatures of the first and second halves of the curve are not successfully modelled. In Fig. 1.9, a measured Ca^{2+} sub-system step response function is shown together with modelled step response curves for $N = 3$ and $N = 5$, respectively. The values of dV have been determined using nonlinear constrained least-squares minimization. For $N = 3$ the fractional volumes are determined to $\{0.182, 0.091, 0.163\}$, while for $N = 5$ the values obtained are $\{0.428, 0.219, 0.395, 0.080, 0.353\}$. It is seen that for $N = 5$ the first and third of the dV values are significantly bigger than both the remaining values and the values obtained for $N = 3$,

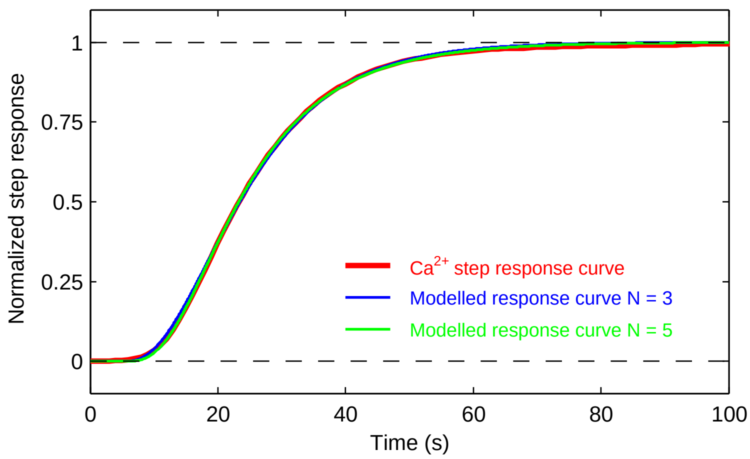

Figure 1.9: Measured (red) and modelled (blue, green) step response curves for the Ca^{2+} sub-system. As what may be expected because of the larger number of degrees of freedom, the green ($N = 5$) curve matches the measured curve slightly better than the blue ($N = 3$) curve, but the differences are small. See text for further explanation.

corresponding to very small mixing volumes. The results show that 3 mixing volumes are essentially sufficient to model the mixing process. From Fig. 1.9 it can be seen that the $N = 5$ curve does fit the measured step response curve best, but that the improvement relative to the $N = 3$ curve is small. To keep the number of model parameters as small as possible while still representing the mixing process well, the value $N = 3$ has been applied in the presented work. However, any number $N \geq 3$ can be used, or the number of volumes can be taken as a model parameter itself.

1.2.2 Data regularization

In the case of NGRIP CFA data, the sampling rate is approximately 1 Hz, corresponding to a depth sampling resolution of $0.6 - 0.7$ millimeter. The mixing practically eliminates oscillations with very short wavelengths, and especially "oscillations" consisting of single-point outliers. Using the data from the NH_4^+ sub-system in Rasmussen et al. (2005) as an example, the amplitude of oscillations with wavelength 2.6 mm, corresponding to 4 data points in the original data, will be reduced by the mixing to about 10^{-9} of the original amplitude. Hence, if a certain pair $D(t)$ and $M(\tau)$ satisfy Eq. 1.2, a data series $D^*(t)$ made from $D(t)$ by adding a number k to every second data value and subtracting the same number from the other half of the data values will satisfy Eq. 1.2 equally well as long as k is small compared to 10^9 times the typical amplitude of the signal.

In this way, the true data $D(t)$ estimated by the Monte Carlo approach will have a tendency to be highly oscillatory, indicating a need for regularization. Regularization has been implemented by preferring models with fewer single-point outliers in the Monte Carlo sampling algorithm. The numerical details are described below.

1.2.3 Monte Carlo modelling

With Eq. 1.3 parameterizing the effect of the mixing, a Monte Carlo method may be used to solve the inverse problem of estimating the true data $D(t)$ and the mixing volumes dV_1, dV_2, dV_3 from the measured data. In order to reduce the computation time, the analysis is performed using data at 2 mm resolution, corresponding to about one third of the original sampling resolution. As argued in section 1.2.2, a 2 mm sampling interval is sufficient to resolve everything in the original signal but the very shortest wavelengths, which have been so strongly dampened by the mixing that they cannot be safely restored in any way.

The Monte Carlo sampling is performed using the Metropolis algorithm, and has been implemented by Susanne Lilja Buchardt. The sampling is performed as described below

1. Initial values of the unknown model parameters are chosen. These consist of 3 fractional mixing volumes (dV_1, dV_2, dV_3) and 825 values $(D_1, \ldots, D_{825})$ because the analysis is performed with 2 mm resolution on sections of 1.65 m of ice core at a time, corresponding to a core section measured in one run. As initial values for D, the mean of the 825

measured d values is used. For the fractional mixing volumes, starting values of 0.5 are chosen, as $0 \leq dV_i \leq 1$.

2. Using the calculated mixing response function $M(\tau)$ and the true data D, a modelled output profile d_{est} is calculated using Eq. 1.2.

3. The misfit between d_{est} and the measured signal d is calculated as $\sum_{i=1}^{825}\left(\frac{d_{\text{est},i}-d_i}{\sigma_d}\right)^2$, where σ_d is the noise level of the measurements. In addition to the misfit, a regularization term is added as described in section 1.2.2, giving the total cost function S:

$$S = \sum_{i=1}^{825}\left(\frac{d_{\text{est},i}-d_i}{\sigma_d}\right)^2 + C\frac{1}{824}\sum_{i=1}^{824}(D_{i+1}-D_i)^2 \tag{1.4}$$

   where C is a parameter that represents the level of smoothness wanted. The value has been chosen by trial and error: $C = 1000$ for conductivity, $C = 800$ for NH_4^+, and $C = 0.1$ for Ca^{2+}. The C-values are different for the different components because of differences in noise level and signal amplitude, and scale approximately with the variance of the data series.

4. One of model parameter is selected and perturbed by a random number $0 < n < 1$ multiplied with a user-supplied maximum stepsize.

5. A new modelled profile d_{est} is calculated and the new cost function S_{new} is determined by Eq. 1.4.

6. The perturbed model is rejected or accepted according to the so-called Metropolis Criterion: if $S_{\text{new}} < S$ the model is accepted, otherwise it is accepted with the probability $\exp\left(\frac{1}{2}\left(S - S_{\text{new}}\right)\right)$ (Mosegaard and Tarantola, 1995).

7. Steps 4 through 6 are repeated until at least 10^6 models have been accepted. Typical acceptance rates are $70 - 80\%$ which is in the high end of the optimal range.

Results of the Monte Carlo modelling are shown in Fig. 1.10 together with the corresponding results from the spectral resolution enhancement method described in Rasmussen et al. (2005). The Monte Carlo results presented are the mean D values from all of the accepted models, and the shaded areas indicate the $\pm 1\sigma$ band. As expected, the Monte Carlo resolution enhanced data series are shifted slightly to the left of the measured data, because the mixing introduces a phase lag while the results of the spectral method are in phase with the measured data because the filters are constructed to be phase-neutral (Rasmussen et al., 2005). It is seen that the Monte Carlo results have larger amplitudes than the results from the spectral method, especially for the conductivity series, but also that these series have more small bumps than those produced by the spectral method. The latter is a consequence of the application of the optimum filter, which means that data filtering is integrated in the resolution enhancement procedure, but also the value of C influences the amplitudes as well as the amount of small

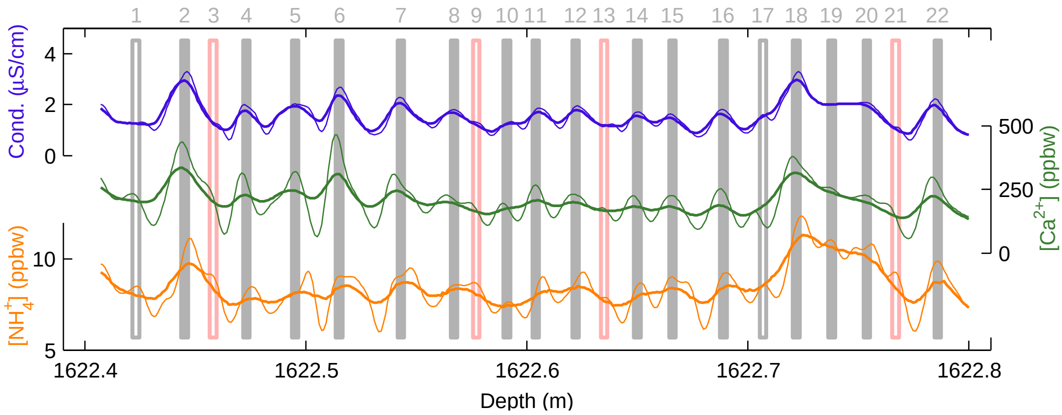

↑ (a) Results of spectral resolution enhancement of NGRIP data.

↓ (b) Results of Monte carlo based resolution enhancement of NGRIP data.

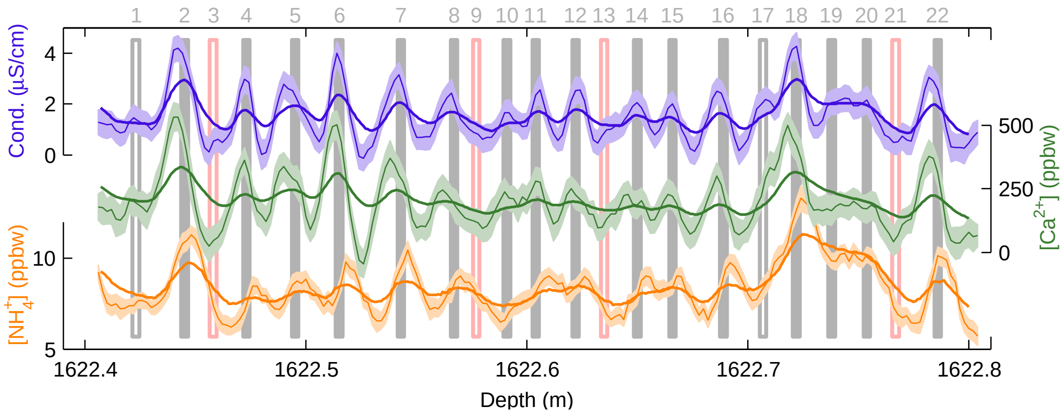

Figure 1.10: Results from the two resolution enhancement approaches (thin curves) and measured data (thick curves). In part (b), the shaded areas show the $\pm 1\sigma$ band of the 10^6 accepted solutions. The grey vertical bars represent annual layers as identified from the measured data, while the open grey bars are "uncertain annual layers" (further discussed in the second part of this thesis). That these features do represent annual layers is supported by the restored data. In addition, smaller features not visible in the measured data appear in the resolution enhanced data (open magenta bars). The grey and magenta bars are placed using the data in (a) and are reproduced in (b) for comparison only. In general the two sets of profiles agree on the position of annual layers although the detailed curve shapes are different.

bumps. For the purpose of annual layer counting, however, the results are very similar. The uncertain layer marks (open gray bars, no. 1 and 17 in Fig. 1.10) are supported by both sets of resolution enhanced data, and almost all the hints of annual peaks that appear when performing spectral resolution enhancement (magenta bars, no. 3, 9, 13, and 21) also appear in the Monte Carlo results, although the exact position varies. The agreement is fairly good, even across the feature comprising bars no. 17 through 21, which is hard to interpret because of the long, soft slope.

1.3 Conclusion

The results – as exemplified in Fig. 1.10 – show that the two methods perform well and produce consistent results. Due to the very different nature of the two methods and the different requirements with regard to data and processing time, the methods have different advantages and should be used in different situations.

The main advantage of the spectral method is that it can be seamlessly integrated into the data processing line, thereby improving data resolution with almost no extra work or time required. By performing the resolution enhancement in the data processing line, benefits other than the data improvement itself are obtainable:

- The transitions from blank to sample and vice versa are soft slopes as seen in Fig. 1.3 (at approx. 800 s and 3400 s). When assigning the depth scale to the measured signal, the position of the start and end of the sample must be set. When the resolution enhancement has been performed the onset and end slopes become steeper, and the depth assignment becomes more precise, which is of paramount importance when interpreting changes in seasonal-scale variability.
- If the mixing filter is constructed and noise-signal separation is performed after each measuring run, changes in the system response are detected immediately. The data collected for the resolution enhancement can thus be used for monitoring the measurement system stability and preventing data loss.

The main drawbacks are that the method requires significant amounts of work if the data used for mixing strength estimation have not been extracted during data processing, that data gaps cause problems, and that the noise level assessment and signal/noise separation can be difficult. For the NGRIP CFA data, the latter problem has been of minor importance, because the signal and noise parts of the spectrum are clearly distinct, as illustrated in Fig. 1.4a. For Berkner Island CFA data, the noise separation is more tricky, because the spectra often consist not of two distinct parts, but rather 3 linear parts. The interpretation of this observation is non-trivial, but it is possible that the middle part of the spectrum is related to resampling during the data processing, or to so-called glaciological noise, arising from the formation of sastrugi and other effects related to uneven small-scale distribution of snow (discussed further in section 3.1).

The Monte Carlo method has very different requirements. The mixing process must be well-understood and parameterizable, but the actual mixing strength does not need to be known as it is estimated by the model. Explicit signal/noise separation is not necessary either. The most important advantage is thus that very little needs to be known in advance, and that the results are very robust from a numerical point of view, even in the presence of small gaps in the measured data. The cost of this is that the method is rather demanding when it comes to computation time, and that the regularization described in section 1.2.2 involves some kind of model tuning when choosing the smoothness requirement. When using the regularization condition presented here, the constant C in Eq. 1.4 determines how smoothness is prioritized relative to model misfit. In this work, the value of C has been chosen manually by trial and error.

The Monte Carlo resolution enhancement approach presented here is very general, and can be used to correct for any type of smoothing (e.g. dampening, diffusion, mixing) of any type of signal, as long as the smoothing process can be parameterized. Experiments with diffusion correction of isotope data have been made in collaboration with Ole Winther, Susanne Lilja Buchardt, Bo M. Vinther, and Hans-Christian Steen-Larsen. Preliminary results show that the method also performs very well in this case.

In summary, both methods provide robust and efficient data resolution enhancement when applied in the correct setting, and can significantly improve the quality of the NGRIP CFA data, e.g. for annual layer counting purposes.

Part 2

Dating ice cores by counting of annual layers

Many different types of palaeoclimate records are used to reconstruct the past climate, but ice core records stand out due to a very attractive combination of resolution and time coverage. For the last 100,000 years, ice core records represent the only archive that covers the entire period with annual resolution, and independent and precise chronologies of ice core records are therefore of huge importance to the palaeoclimate community. This is also reflected by the attention received by the Central Greenland records from GRIP and GISP2, which for a decade have been the standard references when studying the climate back through the last glacial period, and the records from the more recent NGRIP (Dansgaard et al., 1993; Johnsen et al., 1997; Grootes and Stuiver, 1997; Meese et al., 1997; Alley et al., 1997b; NGRIP members, 2004). Ice core chronologies can essentially be dated by three different approaches:

- The depth-age relationship can be derived from modelling of past accumulation rates and flow patterns.
- Reference horizons that can be found in both the ice core and in other independently dated records can be used to transfer the dates of well-dated reference horizons to the ice core.
- Annual layers can be identified and counted continuously.

Often these three approaches are combined. For example, observed palaeo-accumulation rates are essential input data to flow models, and the free parameters of the model will often be determined by fitting the model results to observed annual layer thicknesses or independently obtained age estimates of reference horizons. On the other hand, annual layer counting is often only feasible in the upper part of an ice core, because flow-induced thinning of the annual layers makes detection of the annual signal difficult at greater depths. Modelling is therefore often the only available dating strategy for the lower part of an ice core. The difficulties of constructing precise time scales for deep ice cores is illustrated by the fact that most deep ice core time scales have been constructed using reference horizons from other dated archives or by "wiggle-matching" the records with those of other dated archives. For example, the GISP2 time scale was made to comply with the dated sea-sediment SPECMAP time scale around 45 ky before present (Meese et al., 1997), and also Antarctic cores are dated using correlation with marine records in the deeper parts (Parrenin et al., 2001).

The model time scales of the GRIP ice core are based on a combination of the three above-mentioned approaches. The accumulation at the DYE-3 drill site is several times greater than that at the GRIP drill site, and the DYE-3 ice core therefore has relatively thick annual layers in the upper parts, making the core ideal for dating the most recent millennia. Hence, the time scale of the most recent 8 ka is based on stable isotope and electrical conductivity data from DYE-3 and has been transferred to the GRIP core using a volcanic event inside the 8.2 ka cold event as a reference horizon (Hammer et al., 1986; Hammer, 1989; Johnsen et al., 1992). In the remaining part of the Holocene, the time scale is based on counting of annual layers using CFA impurity measurements, and in the late glacial part of GRIP, results from discontinuous annual layer counting have been used to establish a relationship between δ^{18}O and the annual accumulation rate. Together with an independently obtained age estimate of 113 ka at the termination of the last interglacial period, the Eemian, these elements constitute the basis for the so-called ss09 time scale (Dansgaard et al., 1993; Johnsen et al., 1995). The ss09sea flow model time scale is a revision hereof, taking into account the δ^{18}O offset caused by the large ice volumes of the glacial (Johnsen et al., 1995, 2001).

The GISP2 time scale is based on counting annual layers as defined primarily from the visual stratigraphy (Meese et al., 1997; Alley et al., 1997b). Isotope ratios, laser light scattering data (LLS), and electrical conductivity measurement data (ECM) are used to support that the layering observed in the visual stratigraphy (VS) indeed represents annual layers, and the time scale is thus formally based upon multi-parameter data. However, in long sections, only VS data are available, and as seen in Fig. 2.1, the examples of annual layer identification in (Meese et al., 1997) indicate that VS data are given very high priority in the annual layer identification process. In the most recent millennium (Fig. 2.1a), isotope ratios are available to support the interpretation, and the VS and isotope data seem to carry approximately equal weight. For example, the layer at 271.75 m is not seen in VS data, but is included as it is clearly visible in the δ^{18}O profile, and conversely are the two peaks in the VS profile at 273.8 m accepted as layers although they are not resolved by the δ^{18}O data. The relation of the ECM data to the annual signal (as defined by VS and isotope data) is not straightforward, and even though the total number of annual layers defined from the LLS data is rather close to the number derived from VS and δ^{18}O data, there seems to be no consistent year-to-year relationship between the records. The LLS peaks are believed to be connected to dust peaks that most often occur in the spring, while the VS signal in the Holocene is taken to be a summer signal (Alley et al., 1997b). In contrast to observation, a rather constant phase relation between the VS and LLS

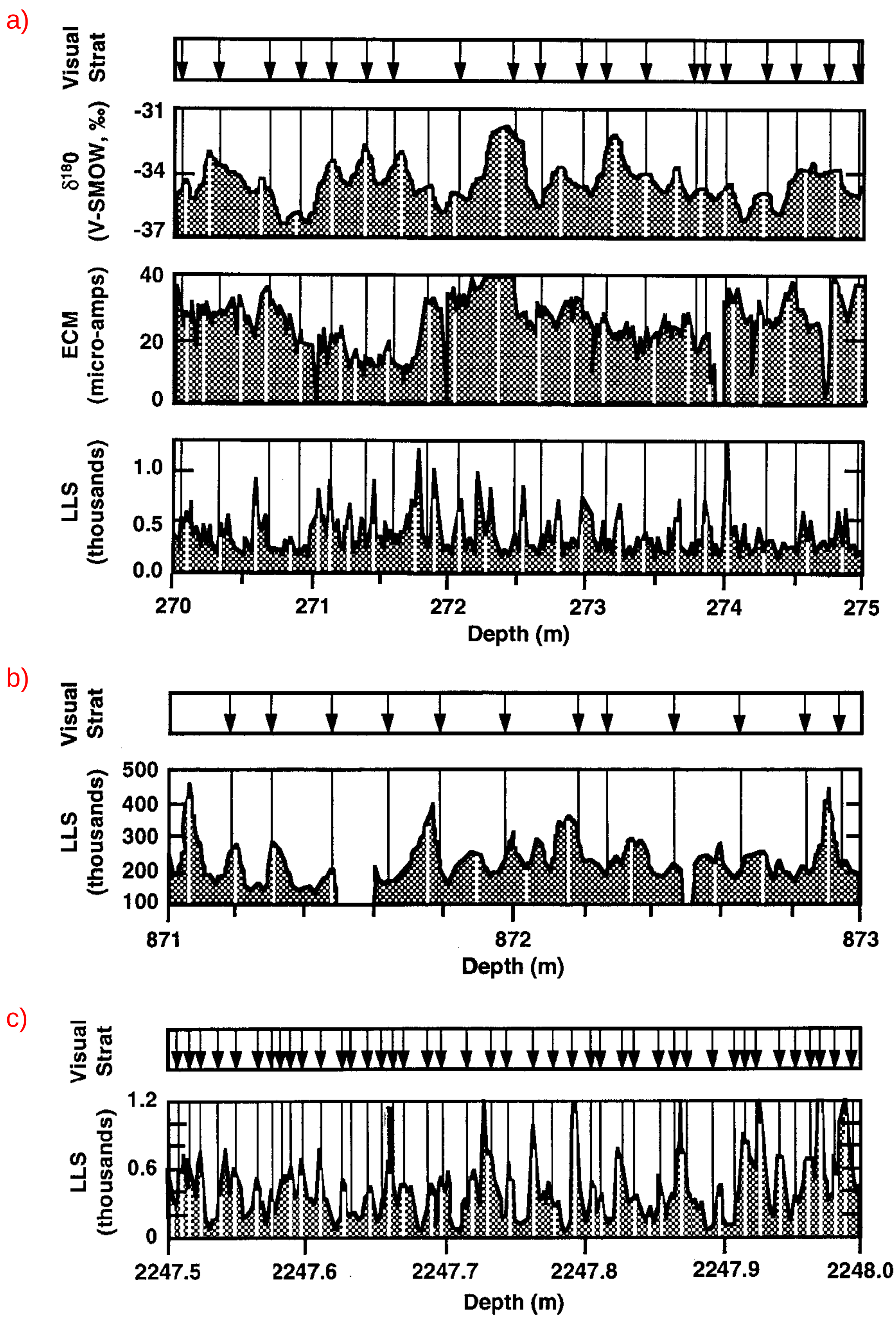

Figure 2.1: Examples from Meese et al. (1997) of how annual layers are identified using the different data series available for the construction of the GISP2 time scale. In all figures, the vertical black lines indicate the annual layers, the arrows in the top show the layering when based on VS alone, and the white vertical lines show the layers if defined from each of the other data series. The annual layer identification is discussed in section 2.

peaks should therefore be anticipated. Isotope data with sufficient resolution to allow annual layer identification are not available below 1.2 ka b2k[1], and in large parts of the 3 – 8 ka b2k zone, only VS data are available. Fig. 2.1b shows a section around 4ka b2k where VS and LLS data are available, and the quoted uncertainty of the annual layer identification procedure is 2%. There is only a one-to-one correspondence between the peaks of the VS and LLS series in the half meter farthest left, while the VS data clearly takes precedence over the LLS data in the remaining section illustrated. Again it is clear that even though approximately the same numbers of annual layers are identified from the two series (8 in LLS versus 9 in VS), there is no consistent phase relation. The same situation is seen in the glacial (Fig. 2.1c), although the resolution of the plot is marginal. A section with 42 annual layers is shown, of which all are identified in the VS data. Approximately 10% of those are not supported by corresponding peaks in the LLS data, and a few peaks that have not been identified in the VS data are visible in the LLS profile. Again the VS data seem to take precedence in all cases where the two profiles disagree, and it is thus reasonable to conclude that except for the section comprising the last millennium, the GISP2 time scale can essentially be regarded as a single-parameter time scale. Nevertheless, the GISP2 time has been the most widely used ice core time scale in the palaeoclimate community, and as will be discussed in section 2.2.1, it generally agrees well with the results of other dating approaches.

Two other examples of single parameter time scales are those of the Byrd ice core, which has been dated by counting of annual layers in the ECM data (Hammer et al., 1994), and the DYE-3 ice core, which has been dated back to 8 ka b2k using mainly δ^{18}O (Hammer et al., 1986; Vinther et al., 2006). Dating by counting of annual layers from the top of an ice core provides an opportunity to construct a fully independent time scale. The main problem to consider when performing independent dating by counting of annual layers is to verify that the peaks interpreted as annual layers represent a strictly annual signal. This assumption is rather well-established for the δ^{18}O signal, which is closely related to condensation temperature and thus carries a direct imprint of the annual temperature variation. Using independently dated reference horizons of e.g. volcanic origin, is has been verified that the δ^{18}O signal in Greenland indeed exhibits annual variations in the last millennia, and there is little reason to suspect that this does not hold under past climatic conditions as well, even though the intra-annual distribution of accumulation probably is different under glacial and interglacial conditions, respectively. In contrast, the apparent annual variations observed in e.g. impurity records are not directly related to a physical parameter with annual variation (as for δ^{18}O and temperature). Instead, the annual variations occur because the concentration of the different impurities have a tendency to peak at different seasons, and the annual signal thus results from

[1]The notation b2k means before A.D. 2000, and is introduced in Rasmussen et al. (2006) as an alternative to the conventional BP (before present). The BP notation has been used in some instances in ice core science with *present* being the starting year of the drilling of the particular ice core rather than the convention A.D. 1950. The b2k notation is introduced to clear up this confusion.

a complex combination of seasonal variations of sources, circulation patterns, and depositional conditions. A continuous profile of discretely sampled ion chromatography impurity data are available from the most shallow 350 m of the NGRIP ice cores, and a comparison of this data set with the δ^{18}O profile and independently dated reference horizons support that the concentration of several impurities vary on an annual basis and thus can be used for annual layer identification. However, the annual peak is occasionally missing in one or more of the records, and in a similar way one or more of the impurity records sometimes contain additional peaks that are not related to the annual signal, but originate from volcanic events, biomass burning events, or other episodical events. Hence, it is vital to base the identification of annual layers on all available data series rather than using a single species.

In a case where a data set is available in which several series contain an annual component, it should be thoroughly considered which annual layer identification strategy should be applied. Essentially, there are two conceptually different approaches to apply:

The "one-at-a-time" approach, in which the proposed annual peaks are identified from one data series at a time, after which these profiles of annual peaks are combined to produce the final time scale.

The simultaneous multi-parameter approach, where all data series are considered simultaneously, and the annual layers are defined in one operation based on all available data series.

Using the one-at-a-time approach, the identification of annual peaks in each series is a well-defined problem, that can be handled by manual inspection or by (semi-)automatic routines. In Rasmussen et al. (2002) a simple method using filtering and threshold-crossing detection is described and tested, and if a priori information on e.g. the statistics of the annual layer thicknesses is available, more advanced methods can be constructed to reproduce the results of a manual count. The next step is to combine the annual layer marks derived from each data series and decide which marks should be interpreted as annual layers. An attempt to date a section of the NGRIP ice core by letting many investigators mark annual peaks in single series and combine these marks to form an annual layer sequence is described in section 2.1 below.

The main problem of the simultaneous multi-parameter approach is to define the criteria to be used when determining which features are annual layers. The typical way of circumventing this problem is to let a number of investigators mark the annual layers by visual inspection, and then average the results of the different investigators or reach consensus by discussing and agreeing upon the interpretation at each point of disagreement. The averaging approach was adopted by the investigators dating the Antarctic Siple Dome ice core based on multi-parameter data (Taylor et al., 2004), and the latter approach has been applied in the construction of the GICC05 time scale across the last glacial termination (7.9-14.8 ka b2k) described in Rasmussen et al. (2006) and summarized in section 2.2.1. It is difficult to quantify the criteria used for visual annual layer identification, because each of the investigators use different criteria that are products of the experience of that individual. The Siple Dome investigators decline to discuss the criteria used in the manual annual layer identification process in detail, and state

> It is difficult to discuss the details of manual decisions because they are subjective and the number of decisions made is so large. Interpreters can spend days in seemingly non-productive discussions trying to justify to each other why they decided to lump two features into a single year instead of splitting them into two separate years. (Taylor et al., 2004, p. 456 – 457)

Large parts of the glacial periods, and the last glacial termination in particular, are characterized by highly variable climatic conditions, where both the impurity levels and the relative phasing of the annual signal in the different species change often and abruptly. When marking annual layers by visual inspection, these changes are detected and the criteria used for annual layer detection are adapted dynamically. The need for dynamic criteria makes it even more difficult to use automated methods based on simple criteria for annual layer identification, especially when several data series are used simultaneously. In the Holocene, climate conditions are rather stable over longer periods of time, and semi-automatic methods thus have better chances of performing well. In section 2.2.2 a method is presented that extracts the mean annual layer thickness from all the available data series without the need of actual annual layer identification. The criteria for annual signal extraction are quantifiable and the results are thus reproducible and more objective.

2.1 "One-at-a-time" multi-parameter approaches

When only one data series is used, the annual layer identification process is essentially a question of identifying which peaks in a data series are related to the annual signal. Most data series will contain many small peaks not related to the annual signal, and only peaks with a certain peak-to-peak distance and peak amplitude are therefore accepted. Depending on the criteria used for peak detection, many methods will have a tendency to either favour uniform layer thickness (that is, the criteria indicate how far away from the previous peak to look for the next peak) or favour the highest peaks (that is, the criteria define how high the peaks have to be).

In the Siple Dome dating effort, an automated approach was developed to perform annual layer detection using conductivity data (Taylor et al., 2004). In order to obtain a balance between the above-mentioned two tendencies, the Siple Dome method comprise a 15-step peak search sequence with different search windows and threshold values. In this way the method contain a number of adjustable parameters, on which the resulting number of annual layers depend critically. The parameter values are not chosen based on an analysis of the nature of the annual signal, but are determined so that the obtained depth-age relation is consistent with independently dated depth-age control points (or reference horizons) obtained from matching the records to the GISP2 records. The automated annual layer identification method therefore plays the role of an advanced interpolation algorithm rather than an independent dating method, although the method can be used for independent dating. The method is applied to two data series one by one, but systematical comparisons of the two peak sequences results are not reported. Comparison is also hampered by the fact that the parameters of the method are tuned for each data series to obtain agreement with the depth-age control points, and the results obtained from applying the method to the two data series are thus not independent.

Another single-species approach is presented by Pohjola et al. (2002), using the points where the curvature (the second derivative with respect to depth of the data series) changes sign as an indicator for change of season. The analytical uncertainty of the measurements and the sampling resolution define the lower bounds for which peaks are accepted as annual layers, but apart from this, no a priori information about e.g. mean annual layer thickness is used. The concept of using the change of sign of the curvature as criterium has the advantage that peaks of any size (larger than the analytical uncertainty) will be detected equally well, which reflects the general observation that peak amplitudes in ice core data vary significantly even on the year-to-year scale. The method has a tendency to pick out too many peaks as annual layers in the δ^{18}O signal, but this is counteracted by the fact that about 10% of the layers are missed when using impurity records. The method is applied to several data series independently, but the results are not compared between the data series on a year-to-year basis, so it is not clear which mechanisms are responsible for the discrepancies and missing years. The results can thus not be used to evaluate in detail which records are best for annual layer identification, or whether the differences between species are more or less pronounced than what is observed when peaks are picked by visual inspection.

The examples presented by Taylor et al. (2004) and Pohjola et al. (2002) illustrate that automated peak detection is indeed possible, but that there is no easy way of combining results obtained from identifying annual layers in multiple parallel data series. The situation is essentially similar to when annual layers are marked by visual inspection, as different investigators working on different data series inevitably produce different sets of annual peaks due to the subjectivity of the peak detection procedure. Typically, this fact is handled by averaging the results of different investigators working on different data series, thereby obtaining an average annual layer thickness estimate for each section. As an alternative, a method is presented below where annual peaks are picked using each of the NGRIP CFA data series, and subsequently combined to form an annual layer sequence based on quantifiable criteria. The peaks are identified by visual inspection in the presented work, but the methods to combine the peaks from different data series can be applied to results of the single-species peak detection approaches of Taylor et al. (2004) or Pohjola et al. (2002) equally well. The differences between different investigators and between different data series are evaluated peak-by-peak to decide whether a certain feature can be regarded as an annual layer. The criteria used obviously imply that the result can be biased, but by varying the criteria, the robustness of the results can be tested and the bias partially assessed. An important advantage of this approach compared to averaging the results in intervals is that the result is an annual layer sequence rather than a mean annual layer thickness estimate, and the distribution of annual layer thicknesses can thus be investigated. The procedure is described below in sections 2.1.1 through 2.1.4.

2.1.1 Marking the annual peaks

A dedicated data visualization and annual peak mark-up tool has been constructed as part of the thesis work to facilitate the annual layer mark-up procedure, and to collect the data in a format suitable for comparison. The tool, named *Datetool*, allows display and free scaling of any number of simultaneous data series and makes it possible to mark annual peaks (and remove the marks) with a single mouse click. In order to ease the comparison of marks from different investigators, the tool by default places the annual peak marks in local data maxima. Each investigator has marked annual peaks with only one data series on the screen, marking good candidates and doubtful features with different marks, in the following referred to as *peaks* and *uncertain peaks* for brevity. Across the late glacial transition (1404 – 1640 m NGRIP depth), up to 12 investigators have marked peaks in up to 8 different series, depending on data quality and amplitude of the annual signal. Most investigators have refrained from identifying annual peaks based on the ECM signal alone, and the liquid conductivity signal has only been used in the cold periods where the annual signal is most clear. At all depths at least 8 investigators have marked peaks in at least 5 series. Fig. 2.2 shows annual peaks as identified by the investigators in a 1.65 m section of data from the Bølling interstadial.

2.1.2 Combining the annual peaks for each series

The annual peaks marked by the different investigators are combined first for each data series, and then between different data series. Even though Datetool by default tries to place the annual peak marks in local data maxima, the investigators sometimes prefer to disable this function in order to place the peaks exactly at the mouse click location. Differences between peak mark locations are also observed where a peak consists of two maxima close together and the investigators disagree on which of the two peaks should be regarded at the annual peak (e.g. Fig. 2.2, [Na^+], depth 1590.75 m), and when a poorly resolved annual peak is represented as a shoulder on a neighbouring peak (e.g. Fig. 2.2, [Ca^{2+}], depth 1591.68 m). Hence, the annual peaks are sometimes marked at slightly different depths by different investigators, making a simple stacking of the marks little useful. Instead of attempting to combine the marks themselves, each annual peak mark is replaced by a probability distribution with a certain width. A peak picked by all investigators at a certain depth will thus be replaced

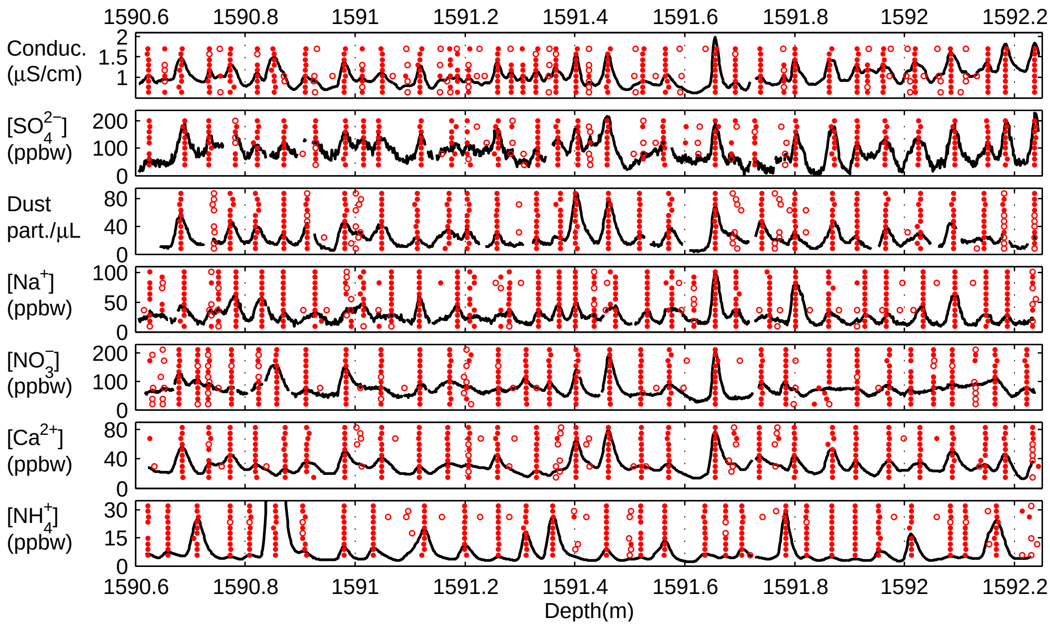

Figure 2.2: 1.65 m of NGRIP CFA data (black lines) and annual peaks set in each data series by up to 12 investigators. The red dots are certain peaks, while the open dots mark uncertain annual peaks, and each horizontal line corresponds to one investigator. It is clearly seen that the different investigators use rather different criteria for what is considered to be an annual peak.

by a narrow distribution with unity probability mass, while another not so well-defined peak only marked by six of ten investigators at slightly different depths will be represented by a broader distribution with probability mass 0.6. The uncertain peaks are included with a weight factor w, which is at least one half. The advantage of this procedure is that it combines the many individual peaks into one probability density profile for each data series, retaining the information on how well the investigators agree on both the number of peaks (as reflected by the probability mass of the peaks) and on the position of the peaks (as reflected by the width of the individual peaks in the distribution). It also accommodates dealing with a varying number of investigators, as the distributions are normalized to unity whenever there is agreement between all the investigators who marked peaks in the section in question.

2.1.3 Combining the layer markings across series

The probability density functions for each series are now combined. In some climatic periods, the different data series used for the dating have annual peaks at different times of the year. The annual peaks may be offset by as much as half a year due to the differences in seasonality (as discussed in Rasmussen et al. (2006)) and additional artificial offsets caused by imperfect depth assignment during the CFA data processing (see Rasmussen et al., 2005). The annual peaks in the different series are offset approximately by a fraction of a year due to different seasonality and by a constant depth value due to the artificial depth offset. When combining the probability density profiles from section 2.1.2, this offset must be taken into consideration.

In the present work, one series is chosen to be fixed, while the remaining series are shifted depth-wise in order to align the annual peaks of the different series as well as possible. The shifts applied to the series are calculated by maximizing the cross-correlation between the probability density profiles of the fixed series and each of the other series. Alternatively, the cross-correlation between the different data series can be used, but the density profiles are used because this approach is robust to the presence of occasional very high peaks in the data series. If, for example, a data section contain a single very tall peak that is not connected to the annual signal but occur simultaneously in all data series, this peak will contribute disproportionately much to the cross-correlation, and drown out the part of the cross-correlation that comes from alignment of the annual peaks. The [Ca^{2+}] profile is used as the fixed series in the examples shown here, because it has a strong annual signal and very few data gaps. In order to prevent the series from being shifted a full year or more, only shifts up to two thirds of the mean annual layer thickness are allowed, where the mean annual layer thicknesses from the ss09sea flow model time scale are used (Johnsen et al., 2001).

After shifting the series, the probability density profiles are summed and divided by the number of data series used for that interval, ensuring that the total probability mass is still unity for a peak marked by all investigators in all the series used. The probability density profiles obtained by replacing the marks of Fig. 2.2 with Gaussian probability distributions and aligning the series as described above are shown in Fig. 2.3. The lower panel show the combined probability density profile, where the blue shaded areas represent the part of the density that originates from uncertain peak marks.

2.1.4 Counting the annual peaks

The combined probability density profile is now divided into single peaks with the purpose of defining the position of each of the annual peaks. Individual peaks are defined by where the density drops below a certain threshold value. The probability mass of each peak is then calculated by integration from one local minimum to the next. Most peaks have probability mass (in the following just *mass*) close to unity, corresponding to well-defined annual layers, present in all data series and agreed upon by all investigators. Two annual layers not well separated, or two annual layers with unusual phasing of the different series, will appear as a broad peak with mass close to two. When counting the annual peaks, those with mass less than a lower limit are discarded, and the rest of the peaks are classified as representing one, two, or three annual layers by rounding off the mass to the nearest integer value. Although this is clearly a crude procedure, only a small fraction of the peaks have mass values close to 1.5 or 2.5, and the problem is therefore of limited significance. One example of the procedure is shown in Fig. 2.4, where the threshold value used to separate the peaks is 0.15 of the height of the Gaussian distributions representing the annual peaks and the minimum mass for a peak to be counted as an annual layer is 0.6.

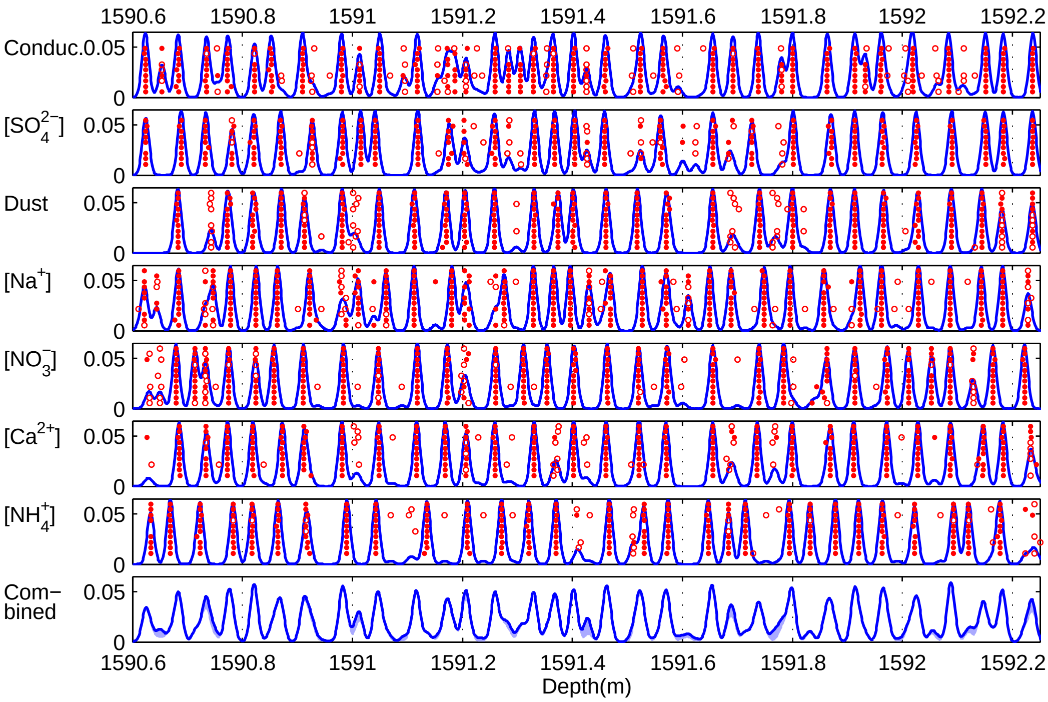

Figure 2.3: Probability profiles obtained by replacing each of the annual marks also shown in Fig. 2.2 with Gaussian probability distributions. The contributions from all investigators are summed for each data series, resulting in a single probability density profile for each data series. These profiles are then aligned by maximizing the cross-correlation between the [Ca^{2+}] probability density profile and each of the other probability density profiles. Finally, the profiles are combined to form the probability profile shown in the lower panel, based on which the annual layers are identified. The pale blue areas show the part of the density that originates from uncertain peaks.

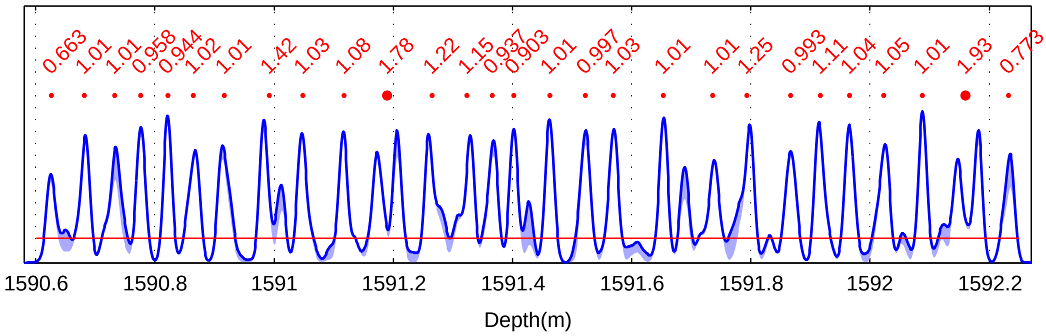

Figure 2.4: The combined probability density profile (the lowest panel of Fig. 2.3) separated into individual peaks using a threshold value of 15% of the height of the Gaussians representing the annual peak marks (red line). The probability mass of each of the peaks is given in red above each peak. The section contains 26 single-year peaks (red points) and 2 double-years peaks (large red points), totalling 30 annual layers. The peaks at 1591.43 m, 1591.69 m, and 1591.83 m are discarded as their probability masses (0.24, 0.58, and 0.17, respectively) do not exceed the minimum value for a peak to be accepted as an annual layer, here chosen as 0.6.

There are 30 annual layers in the 1.65 m data example presented in Fig. 2.4, but the result obviously depends on the values used for the numerical parameters of the method. By varying the parameter values used in the procedure within wide but reasonable limits, different annual layer sequences are produced, and the uncertainty of the method to the exact choice of parameter values can thus be estimated in an objective way. A sensitivity study has been performed by varying the following parameters:

Shape and width of the probability distributions representing the annual peaks.
Gaussian distributions give the best results and are generally used, but also boxcar distributions have been tested. The width (represented by the standard deviation parameter σ) of the Gaussian distributions is chosen as a constant (between three and five millimeters) plus a fraction of the mean annual layer thickness (from three to five percent) derived from the ss09sea model. The ranges of values have been determined partially by assessing the typical depth difference between marks set by different investigators, and partially by and trial and error, limited upwards by the condition that the distributions of neighbouring well-defined peaks should not overlap significantly. The concept of using a constant plus a fraction of the modelled mean annual layer thickness reflects the assumption that the spread in the position of an annual layer marking comes both from variations in the shape of the annual peaks and measurement noise (assumed to be virtually independent of depth), and from variations in the seasonality (assumed to scale with the annual layer thickness). The same width is used for each 1.65 m run.

Weight attributed to uncertain annual peak marks. The uncertain peak marks have been placed as representing 0.5 ± 0.5 year, but realizing that the resolution of the individual data series is marginal in some sections, the weight has been adjusted upwards. Values in the interval $[0.5, 1]$ are used.

Threshold value separating peaks in the combined probability density profile.
The value is given as a fraction of the height of the Gaussian used. Low values lead to many peaks with mass above 1.5 (double and triple peaks) because closely spaced peaks are not separated properly, while high values result in broad peaks with multiple maxima being split in two. These features often represent annual layers with unusual relative seasonality, and when split into two or more peaks they fall below the threshold probability mass and are thus not detected as annual layers. Values in the interval [0.05, 0.25] are observed to balance these two effects.

Threshold probability mass for a peak to be accepted as an annual layer.
The value is varied in the interval $[0.5, 0.7]$.

The parameters are changed stepwise one by one, thereby producing $\approx 10^3$ different annual layer profiles. The variation in the number of annual layers gives a robust estimate of the

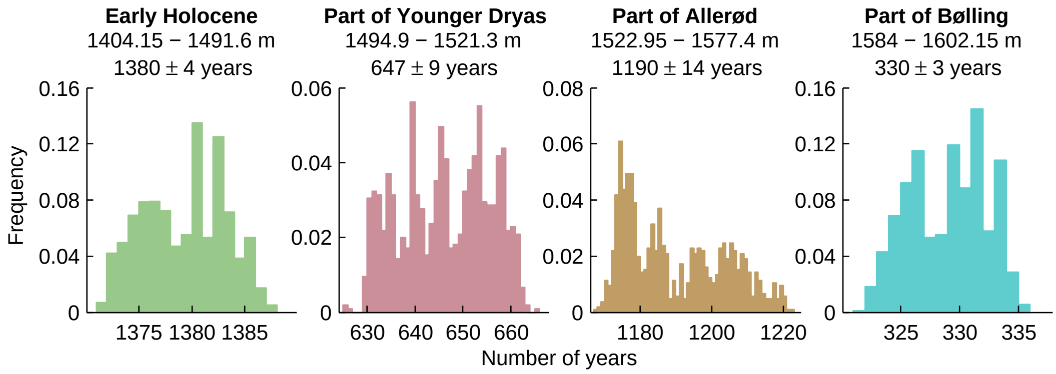

Figure 2.5: Distributions of the number of annual layers in 4 sections of NGRIP data obtained by varying the parameters as described in section 2.1.4. The sections are parts of the Younger Dryas, Allerød, and Bølling periods, respectively, and the number of years in each section should thus not be taken as the duration of these periods. The distribution of the number of annual layers in the early Holocene and Bølling sections indicate that the method produces a well-defined annual layer count. In the Younger Dryas and Allerød periods, the distributions are wide and multi-modal, indicating that the method does not produce a well-defined number of annual layers.

uncertainty related to the choice of parameters in the procedure. The distribution of the number of annual layers within 4 sections of the late glacial oscillation and the early Holocene is shown in Fig. 2.5. The periods are chosen so that abrupt climatic shifts are excluded to make sure that effects related to the rapidly changing annual signal properties do not influence the results.

For the early Holocene and Bølling sections, Fig. 2.5 show that the number of annual layers obtained by the annual peak combination procedure is rather well-defined. The distributions are reasonable narrow ($\sigma = 3\,‰$ and $\sigma = 1\%$ of the mean, respectively) and does not contain many clearly separated peaks. For the Younger Dryas and Allerød periods, however, the distributions are wider and show strong modality (the distributions consist of separate peaks) and the tails of the distributions are heavy. In these sections, the uncertain peaks are more common than in the early Holocene and Bølling section, in which the mean annual layer thickness is more than double the data resolution. Hence, the data resolution seems to be sufficient in the warm periods, while more features become hard to interpret in the colder Younger Dryas and Allerød periods. The number of annual layers produced by the described method depend critically on the weight attributed to the uncertain annual peaks. The value of this parameter is varied in steps of 0.1 between 0.5 and 1 in the sensitivity analysis, leading to six more or less separate maxima in the distribution of the number of annual layers in the colder periods.

In addition, a comparison of the annual layer thicknesses obtained from this procedure with modelled annual layer thicknesses from the ss09sea model of Johnsen et al. (2001) and with the results from the multi-parameter method presented in Rasmussen et al. (2006) show that too few annual layers are identified in the Younger Dryas and the colder parts of Allerød. A visual inspection of the Younger Dryas results together with the original data indicate that the main problem is that the annual peaks are not resolved in all series, and that they consequently are not identified as certain annual peaks when using only one series at a time. In some sections as much as every fourth layer is weak or missing in at least one series. Layers are missing in the different series in turn, making it very hard to make simple rules for which features should be regarded as annual layers. Some investigators spot and mark the less well-resolved features as annual peaks every time, while other investigators either miss them or consider them not to be certain annual layers. The different approaches taken by the different investigators thus turns out to be an important problem rather than being one of the strong points of the approach. By a similar argument, the advantage of having multiple series turns into a weakness when each layer is only resolved by a few of the data series,

The combination of the individual annual peak series to a final annual layer sequence can be performed in other ways than presented here, but the results indicate that a one-at-a-time approach is problematic when using data where the annual layers are not well-resolved in all data series. An annual layer that is only marginally resolved in each of the series, for example because it is relatively thin, will simply not be identified in sufficiently many of the individual series, and will thus rarely obtain a sufficiently high probability mass to be classified as an annual layer.

2.2 Simultaneous multi-parameter approaches

As described above, the resolution of each of the data series in the CFA data is marginal for annual layers detection in the Younger Dryas and cold parts of the Allerød period, even when the resolution enhancement described in section 1.1 has been applied. The dating of the last glacial transition (7.9 – 14.8 ka b2k) has therefore been performed using a classical simultaneous multi-parameter approach, where the annual layers are marked by visual inspection by a number of investigators. The work is a contribution to the Greenland Ice Core Chronology 2005 (GICC05), which is a composite time scale, based on different data series from several cores in different intervals. The section from present day to 7.9 ka b2k is dated using δ^{18}O data from DYE-3, GRIP, and NGRIP (Vinther et al., 2006). The 7.9 – 14.8 ka b2k section is dated using CFA data from GRIP and NGRIP (Rasmussen et al., 2006, summarized below), and in the Holocene part the time scale has been transferred to the DYE-3 core by matching the ECM records of the cores (Rasmussen et al., accepted). During the cold stadials of the glacial period, the annual layers are too thin to be resolved by the majority of the CFA data series, and more weight is put on the ECM, electrolytical conductivity, and visual stratigraphy records. The construction of the GICC05 in the interval 14.7 – 42 ka b2k is described in Andersen et al. (submitted) and compared to other records and chronologies in Svensson et al. (submitted).

In order to validate the results obtained by the visual layer identification approach of

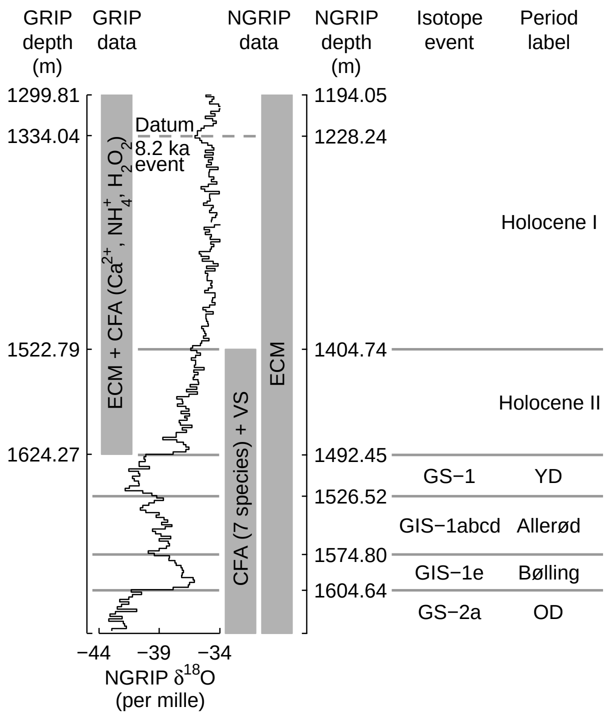

Figure 2.6: Overview of the data series used for the different parts of the GRIP and NGRIP ice cores. The period labels are the names used to identify the different time periods. YD and OD refer to the Younger Dryas and Oldest Dryas, respectively. The isotope event names refer to those of Björck et al. (1998). Figure from Rasmussen et al. (2006).

Rasmussen et al. (2006), and to explore the potential for extending the dating using automated methods, an automated simultaneous multi-parameter approach has been developed. The concept is to extract the common annual signal and determine the annual layer thickness without the need for manual annual layer identification. This approach is described in section 2.2.2.

2.2.1 Summary of Rasmussen et al. (2006)

A new chronology for the last glacial termination has been constructed using ECM data and CFA impurity records from the GRIP and NGRIP ice cores. The name of the chronology is Greenland Ice Core Chronology 2005 (GICC05). CFA data from GRIP are available in the section older than 7.9 ka b2k and resolve the annual layers throughout the Holocene, while the NGRIP CFA data are available from 10.3 ka b2k and back to the early glacial. The available data are illustrated in Fig. 2.6, which also shows how the terms Holocene, Younger Drays, Allerød, Bølling, and Older Dryas are used for different time intervals[2].

[2]The Greenland Stadial / Interstadial (GS/GI) terminology of INTIMATE (Björck et al., 1998) is in general preferable to the bio-stratigraphical terms Younger Dryas, Allerød, Bølling, and Older Dryas. However, the division into GI/GS made by the INTIMATE group relies on GRIP $\delta^{18}O$ data only, while ongoing work in the Copenhagen Dating Initiative aims at defining the climate transitions from all available ice core data sources.

The counting method is based on visual inspection by several investigators. For each section, three investigators have identified annual layers using a simultaneous multi-parameter approach. A typical Holocene annual layer is characteristic by having the sea salt dominated [Na^+] peaking in late winter. The VS record generally contains more than one peak per year and is not simple to interpret, but in general there are layers of high refraction (cloudy bands) at springtime, coinciding with high dust content, high [Ca^{2+}] and dips in the [H_2O_2] curve. Summer is characterized by high concentration of [NH_4^+], [NO_3^-], and sometimes of [SO_4^{2-}]. In general, dips in the ECM correlate with peaks in [NH_4^+] and [Ca^{2+}], while the conductivity is related to the total content of ions present in the meltwater and thus contains several peaks per year due to the different seasonality of the individual species. In the colder periods, the differences in seasonality almost vanish and most series peak simultaneously, making the conductivity record useful for identification of annual layers. The [NH_4^+] signal does not consistently show clear annual cycles in the cold periods. An example of the data series used and the annual layer marks is presented in Fig. 2.7.

Differences between the annual layer counts of the three or four investigators amount to a few percent in the relatively warm periods (Holocene II, Bølling, and most of Allerød), while the differences are up to 5% in the Younger Dryas and late Allerød and up to 10% in the Older Dryas, just prior to the onset of Bølling. The changes reflect the different criteria used for annual layer identification and in the cold periods also different interpretation of features possibly representing two annual layers that appear merged due to marginal data resolution. The annual peak markings of the three investigators have been reviewed with a fourth investigator acting as mediator. Ambiguous features and points where unanimity could not be reached were marked by uncertain layer marks, counting as $\frac{1}{2} \pm \frac{1}{2}$ year in the final time scale. The so-called maximum counting error (henceforth *mce*) is defined as the sum of all these "half years" and represents a conservative estimate of the uncertainty of the annual layer identification procedure, under the assumption that the underlying criteria used when identifying the layers are essentially correct.

The GRIP CFA data have previously been used to date the early Holocene part of the GRIP core, forming some of the empirical basis of the model time scales known as ss09 and ss09sea time scales (Johnsen et al., 1992, 1995, 2001). Using the GRIP CFA data together with the new NGRIP CFA data, that contain more species and are better resolved, a revised chronology of the early Holocene has been constructed (the section is denoted Holocene II in Fig. 2.6). A comparison with the previous GRIP time scale shows that the GRIP CFA data resolution is marginal in the very early part of the Holocene, and that the previous time scale contains too few annual layers. Using the experiences obtained from the Holocene II section

The onset depths of the Bølling, Allerød, and Holocene periods used in Rasmussen et al. (2006) are based on this recent work, and the terms Holocene, Younger Dryas, Allerød, Bølling, and Older Dryas have thus been adopted because they are well known to most readers, and because it allows the use of the newly obtained transition depths rather than those used by INTIMATE

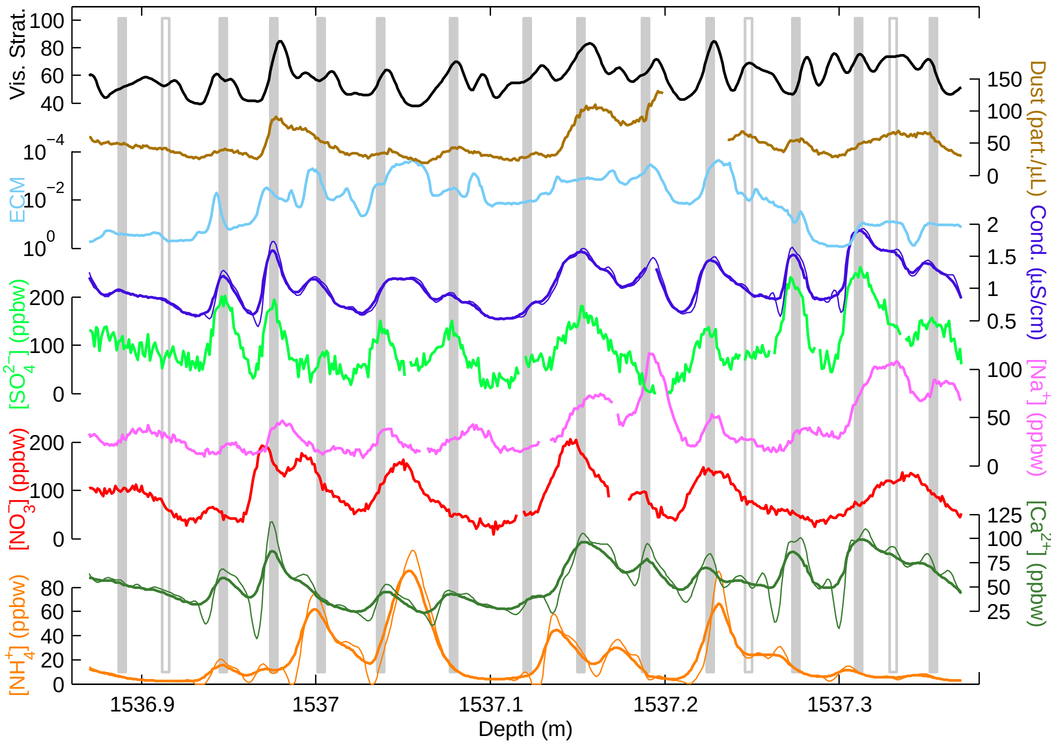

Figure 2.7: Example of data (heavy lines), resolution enhanced data (thin lines), and certain / uncertain annual layer markings (solid grey bars / open grey bars) from a cold period in Allerød. In this section the $[NH_4^+]$ and $[NO_3^-]$ series do not show clear annual cycles, while the other series peak almost simultaneously. The annual layer marks have been set in the annual peaks of $[Ca^{2+}]$. Figure from Rasmussen et al. (2006).

where both GRIP and NGRIP CFA data are available, the time scale of the Holocene I section was revised, linking in a consistent way the isotope-based dating of the DYE-3 core down to 7.9 ka b2k with the interval where NGRIP CFA data have been measured. In this section, the GRIP-based time scale is transferred to NGRIP depths by matching the ECM records. The combined time scale starts at 7903 b2k and dates the transition from the Younger Dryas to the Preboreal to 11,703 b2k (mce 99 years). Below this depth, the time scale is based on NGRIP data alone, reaching back to 14,776 b2k, or about hundred years into the Older Dryas. The onset of Bølling is dated to 14,692 (mce 186 years).

The total uncertainty of a stratigraphic time scale consists of contributions from imperfect stratigraphy, data gaps and measurement problems, limited resolution, and erroneous interpretation of the annual layer record. The first two of these contributions are negligible for the GICC05. Due to the rather high accumulation rates at the DYE-3, GRIP, and NGRIP drill sites it is unlikely that layers are missing from the annual layer sequence in the Holocene, and even in the glacial where the accumulation rate is lower and only NGRIP data are used, it is unlikely that a significant number of layers is lost by wind scouring or similar post-depositional effects. The quality of the ice core is excellent and there are very few data gaps of a size that cause problems then identifying annual layers. The resolution of the data is a potential problem in the coldest parts of the period considered, but the main source of uncertainty is uncertainty in the interpretation of the annual signal. This part of this uncertainty consist of two inherently different contributions, one of which comes from unusually shaped annual layers or other features that are hard to interpret (in the following called the *interpretation uncertainty*), while the other comes from possible imperfectness of the criteria used for identifying annual layers (a *possible bias*). The uncertain layer marks can be used to assess the interpretation uncertainty, but not the possible bias. As described, each of the uncertain layer marks are counted as $\frac{1}{2} \pm \frac{1}{2}$ years in the final time scale, but it is not a priori clear how these errors should be added to form the interpretation uncertainty, because the errors are neither uncorrelated nor fully correlated. A conservative approach is adopted, defining the maximum counting uncertainty as half the number of uncertain layer marks. This corresponds to regarding the errors as fully correlated, but in return the maximum counting error is interpreted as the total uncertainty, including the above-mentioned smaller contributions from imperfect stratigraphy, data gaps, and insufficient data resolution. The maximum counting error does, however, not include a possible bias in the counting procedure, as this bias cannot be evaluated without the use of independent dating methods.

The distribution of the strain-corrected annual layer thicknesses is observed to be approximately log-normal within climate periods with relatively stable conditions. This implies that the mean and standard deviation values of accumulation rates should be calculated from logarithmic transformed data rather than from the observed annual layer thicknesses, contrary to common usage, because the notion of standard deviation makes more sense when calculated for data that are approximately symmetrically distributed. The accumulation rate in the Younger Dryas and Bølling periods are 47% and 88% of the Holocene II values when calculated from logarithmically transformed data, respectively, indicating a smaller contrast between the stadial and interstadial accumulation rates than those observed in the GISP2.

In Fig. 2.8, 20 year mean values of NGRIP δ^{18}O data are shown on the GICC05 time scale and on the previously used time GRIP/NGRIP time scales. The 20 year resolution GISP2 isotope profile of Grootes and Stuiver (1997) and Stuiver and Grootes (2000) is presented on the time scale of Meese et al. (1997). The differences between the time scales are apparent in Fig. 2.9, where the differences in the dating of 46 selected ECM horizons are shown. Compared to the previous GRIP/NGRIP time scales, the GICC05 time scale has more annual layers in the early Holocene, pushing the Younger Dryas-Preboreal transition about 150 years back, while the number of annual layers in GICC05 is smaller in Allerød and Bølling, meaning that the time scales differ by only 50 year at the onset of the Bølling interstadial. The GICC05 and the GISP2 time scale agree almost to the year on the age of the Younger Dryas-Preboreal transition, while significant relative differences of 5% or more are observed in the Holocene I, Younger Dryas, and Bølling periods. These relative differences are well beyond the error bounds of the GICC05 and GISP2 time scales, and the time scales are thus significantly different although the absolute differences are rather small.

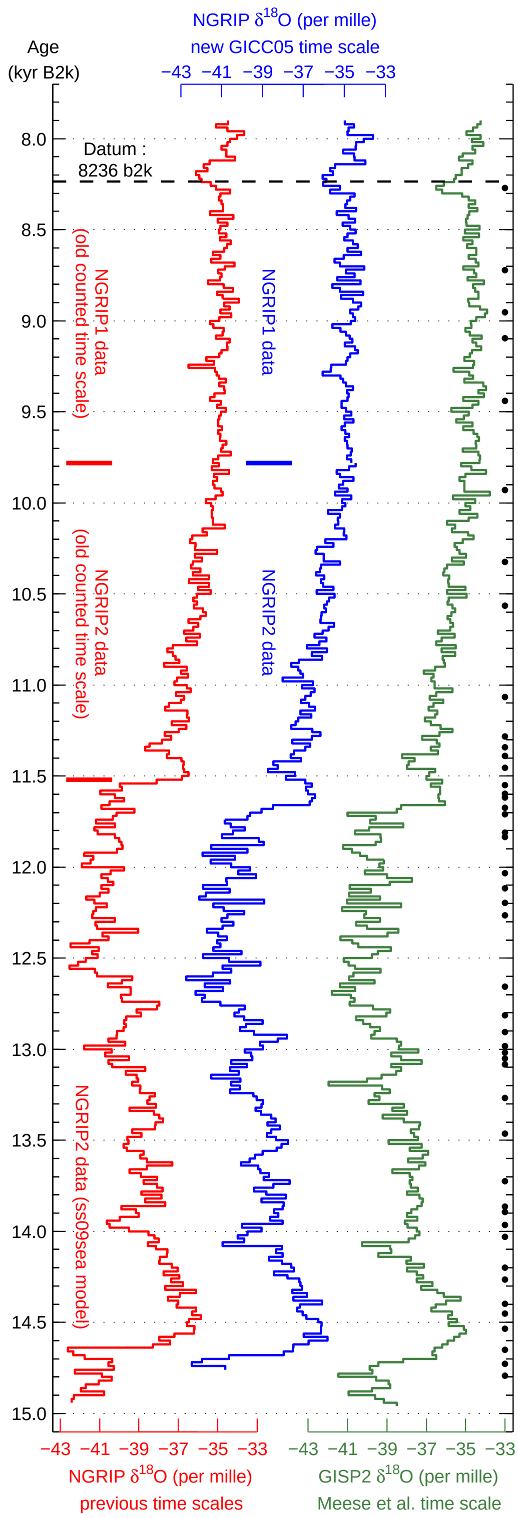

Figure 2.8: Stable isotope profiles from NGRIP and GISP2 across the last termination. The red curve shows 20 year mean values of NGRIP δ^{18}O data on the existing counted time scale (Holocene part) and ss09sea model time scale (glacial part). The blue curve shows the same data on the new GICC05 time scale. The green curve show GISP2 δ^{18}O data on the time scale of Meese et al. (1997). The black bullets to the right, plotted relative to the GISP2 curve, are the match points used for the comparison in Fig. 2.9. Figure from Rasmussen et al. (2006).

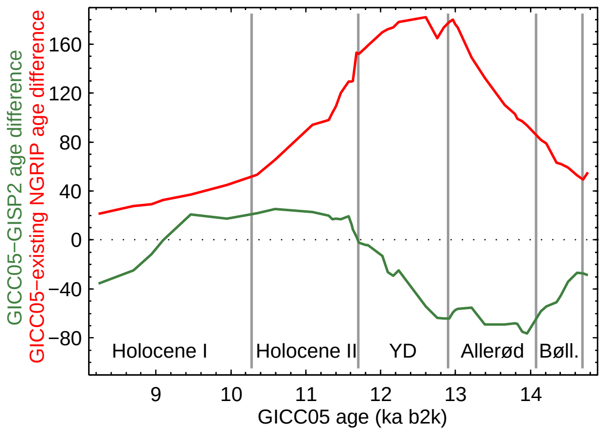

Figure 2.9: Detailed comparison of the GICC05 time scale with the existing GRIP/NGRIP time scales and the GISP2 time scale of Meese et al. (1997) using the dates of 46 common ECM events in the NGRIP, GRIP, and GISP2 cores (see Fig. 2.8). Positive values indicate that an event is older according to the GICC05 time scale. Figure from Rasmussen et al. (2006).

2.2.2 Extracting the annual signal by Dynamical Decorrelation

In the construction of the GICC05 time scale, the annual layer identification is based on synchronous inspection of all data series, and the identification of the annual layers thus relies on simultaneous interpretation of the annual signal as it is represented in several data series. It is difficult to automate this process where information from several data series is combined with different weights in different situations. When constructing automated annual layer detection methods, it is therefore more straightforward to use either a one-at-time approach as described in section 2.1, or to refine the signal before the annual layers are identified, because the criteria for annual layer identification in this way can be more directly specified. An approach is presented here in which the common annual signal present in the data series is extracted. The resulting annual signal can then be used for annual layer identification, or the mean annual layer thickness can be calculated directly. The method is based on the assumption that the measured data series contain imprints of a common annual signal, which can be extracted from the set of data series by time series analysis methods. The concept is somewhat similar to that of Principal Component Analysis (PCA) or Empirical Orthogonal Function (EOF) analysis, in that the measured data series $x_i, i \in [1, N]$ are regarded as linear combinations of some underlying source series $s_j, j \in [1 : M]$. In PCA, the number of source series and data series are equal ($N = M$), and the source series are defined as orthogonal. The principal component is the direction in data-space where there is most variance, the second component captures as much of the remaining variance as possible given the orthogonality constraint, and so forth. PCA is very useful for exploratory data analysis or dimension reduction purposes, but there is no generally valid reason to believe that the decomposition of the data set X into a set of sources series S will isolate the annual signal in one source series. Furthermore, the orthogonality requirement is a mathematical necessity rather than a realistic assumption about the possible source series. A number of so-called *Independent Component Analysis* (ICA) methods have been developed where the orthogonality requirement has been replaced with a requirement of statistically independent source series. The assumption of independence is not as strong as the orthogonality requirement, and thus other information or assumptions are needed in order to perform the decomposition into source series. Many different assumptions can be made, depending on the context and on the available a priori knowledge about possible source series (see Hyvärinen et al., 2001, for an overview). In many applications the approximate wavelength of the signal of interest is known. More specifically for ice core dating, the mean annual layer thickness can be estimated from surface observations and simple modelling, and this fact can be used in the ICA decomposition, because the temporal signature of the annual signal is different from that of most other source series.

Dynamical Decorrelation

The measured data series $x_i, i \in [1, N]$ are regarded as linear combinations of a number of source series $s_j, j \in [1, M]$. In addition to the annual signal, which is assumed to be contained in one of the source series, the measured data series may contain contributions from lower-frequency regional signals (related to e.g. the North Atlantic Oscillation, the sunspot cycle, or other quasi-periodic variations) and high-frequency contributions (e.g. sub-seasonal variations, episodic events, and noise). These different possible source series have very different auto-correlation functions and the so-called *Dynamical Decorrelation* (DD) method uses this information to perform the ICA decomposition of the data set X into the source set S. The DD method was originally suggested by Molgedey and Schuster (1994) and further developed by Hansen et al. (2000), and has been adapted and applied for ice core dating purposes as described in Rasmussen et al. (2002) and Rasmussen (2002). In the following, the concept of DD will be briefly reviewed, and the application of the method to the NGRIP data set will be presented. However, as the calculations are performed exactly as described in Rasmussen (2002), the mathematical details of the DD method will not be discussed further in this thesis[3].

The assumption that one of the source series (say, s_k) is dominated by the annual signal can be utilized in the ICA decomposition, because this source series will have large positive auto-correlation values c_{s_k} for time-lags equal to any integer number of years, and large negative auto-correlation values for time-lags of $\frac{1}{2}, \frac{3}{2}, \frac{5}{2}, ...$ years. Given the fact that ice core records are not time series, but rather depth series, the source series containing the annual signal must be expected to have local maxima at depth-lags[4] $\tau = \lambda_{\text{mean}}, 2\lambda_{\text{mean}}, 3\lambda_{\text{mean}}, ...$ and local minima at $\tau = \frac{\lambda_{\text{mean}}}{2}, \frac{3\lambda_{\text{mean}}}{2}, \frac{5\lambda_{\text{mean}}}{2}$. The low-frequency source series will have positive autocorrelation

[3]Rasmussen (2002) is an unpublished Master's thesis written in Danish. It can be obtained from the web page www.icecores.dk, publications, scientific thesis, or directly at http://www.nbi.ku.dk/research/page95689.htm.

[4]Note that the symbol τ is used for the depth offset or depth-lag, and not as usual in the literature for the more conventional time-lag.

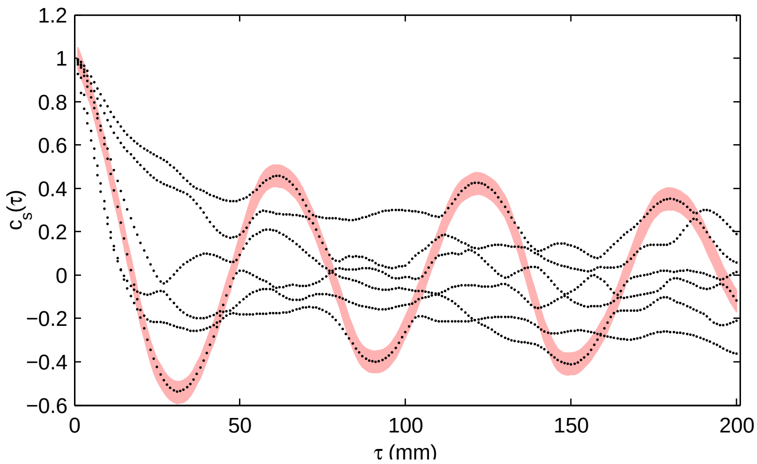

Figure 2.10: Values of the source autocorrelation functions $c_{s_j}(\tau)$ for $\tau = 1, \ldots, 200$ (black points) obtained by applying Dynamical Decorrelation to NGRIP data from 1452 – 1453.65 m depth. The autocorrelation function of the source series containing the annual series will have local minima at $\tau = \frac{\lambda_{\text{mean}}}{2}, \frac{3\lambda_{\text{mean}}}{2}, \frac{5\lambda_{\text{mean}}}{2}$ and local maxima at $\tau = \lambda, 2\lambda, 3\lambda$. This signature is clearly recognized in the calculated $c_{s_j}(\tau)$ values (marked by the red shaded band).

values as long as τ is small compared to the average period of the oscillations, and the high-frequency source series will have autocorrelation values close to zero except for very small values of τ. It is thus likely that the autocorrelation value of s_k will be numerically large and negative, and that no other source series will have similar negative autocorrelation values, for $\tau = \frac{\lambda_{\text{mean}}}{2}$. The ability to identify a τ value with this property is the main prerequisite for the DD method. Specifically, if a value of τ can be chosen so that the source series have mutually distinct autocorrelation values $c_{s_i}(\tau) \neq c_{s_j}(\tau), i, j \in [1, M], i \neq j$, the source series can be calculated from the measured data X as described in Rasmussen et al. (2002). However, when only the extraction of the source series containing the annual signal (s_k) is important, it is sufficient to require that the autocorrelation value of this series is distinct from that of the remaining series, $c_{s_k}(\tau) \neq c_{s_j}(\tau), j \in [1, M]$ for the given value of τ.

Autocorrelation values for $\tau = 1, \ldots, 200$ obtained by applying DD to a 1.65 m section of NGRIP data are shown in Fig. 2.10 to illustrate this effect. The values have been computed for each value of τ, and are plotted as black dots. The expected characteristic pattern of minima and maxima described above are recognized, and has been accentuated using the red shaded band. The source series containing the annual signal can thus be isolated by calculating the source series for $\tau = 31$ mm and choosing the source series with the lowest autocorrelation value.

Extracting the annual signal

Using the approach described above, the source series containing the annual signal can be extracted from all the available data series. Prior to the analysis, the data series are normalized

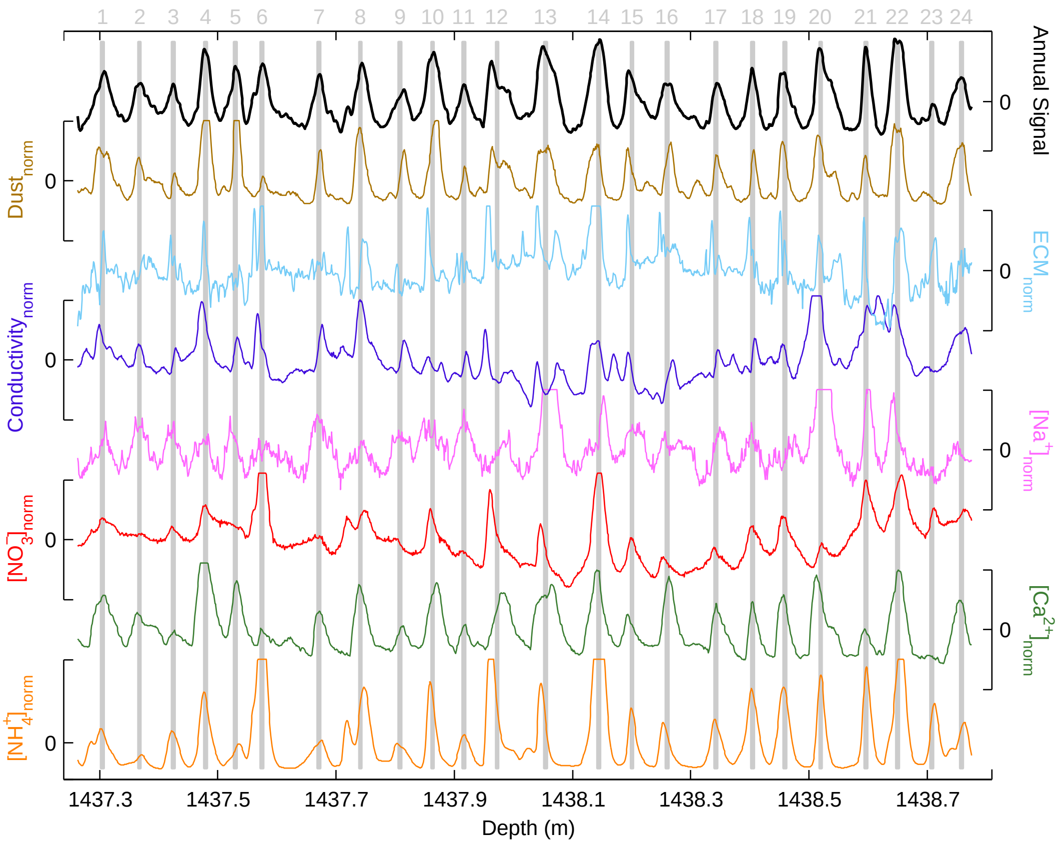

Figure 2.11: The annual signal obtained by applying Dynamical Decorrelation to a 1.65 m section of Holocene NGRIP CFA data (upper panel). The lower 7 panels show the synchronized and normalized data series, and the grey bars mark the annual layers according to the GICC05 time scale of Rasmussen et al. (2006). The extracted annual signal is less ambiguous than the original data series (see e.g. peaks no. 8 and 23). Also, the peak size vary less, and the extracted annual signal contains no peaks that are not interpreted as annual layers, making e.g. automatic annual layer detection mores simple.

to zero mean and unit variance, exceptionally high peaks are truncated, and the series are shifted relative to each other to ensure that the annual signal of the different species is in phase. The details about the data preprocessing procedure can be found in Rasmussen (2002). An example of the annual signal extracted from a 1.65 m sequence of NGRIP Holocene data is shown in Fig. 2.11 together with the normalized and phase-shifted data series used for the calculations.

For the presented data section, the annual signal is clear in most of the data series. The majority of the annual layers are presented by peaks in most of the series, but the peak heights vary by more than a magnitude, and most series contain small additional peaks or shoulders not related to the annual signal. In contrast to this, the extracted annual signal contains one peak major peak per annual layer, and the peak heights vary less. Identification of annual layers is much easier using the extracted annual signal due to the rather constant peak size and the fact that only one series has to be considered.

Direct determination of the mean annual layer thickness

The method presented above has the disadvantage that the annual peaks of the extracted annual signal still have to be identified and counted. In Rasmussen et al. (2002) the layers are identified by a simple threshold method, but automated method like those of Pohjola et al. (2002) or Taylor et al. (2004) can also be applied. However, most automated methods need a (presumably manually constructed) annual layer sequence, a so-called *training set*, for calibration. The estimated precision of multi-parameter annual layer identification by visual inspection is typically in the 1 – 5% range, and if this precision is to be met by an automated method, the training set must contain at least hundred years from each climatic period, and several hundred if a 1% precision is required. In the late glacial oscillation where the climatic conditions change frequently, the need for a training set from each climatic period means that a significant part of the total data set will have to be manually dated and used as training sets, and the usefulness of an automated method involving peak detection is therefore limited. A new application of the DD method is presented here, where the mean annual layer thickness in a data section is estimated without the need of identifying each annual layer. The concept somewhat resemble that of a Fourier analysis, in which the mean annual layer thickness is determined by calculating the dominating frequencies present in the data, although the method presented here is non-spectral and based on simultaneous analysis of multiple series.

The estimate is based on the source series autocorrelation values calculated as described in Rasmussen (2002) and shown in Fig. 2.10. The first local minimum of the curve is generated because the source signal containing the annual signal anti-autocorrelates for depth lag $\tau = \frac{\lambda_{\text{mean}}}{2}$. In Fig. 2.10, the minimum is located at $\tau = 31$ mm, which means that the mean annual layer thickness is approximately 62 mm. The location of this minimum can be determined directly from the autocorrelation values, but as the τ values are discrete with 1 mm resolution, the estimated annual layer thickness will only take on even millimeter values. In the example shown in Fig. 2.10, this means that the true value of λ_{mean} can be anywhere in the $[61, 63]$ mm interval, corresponding to a 1.5% error margin. The precision problem has been solved by determining the location of the minimum by interpolation between the discrete millimeter-values shown in Fig. 2.10. The τ value closest to the minimum is determined, and a parabola is fitted to the autocorrelation values of this τ value and its two neighbours. The exact location of the minimum is then determined as the abscissa of the vertex of the parabola. The procedure is illustrated in Fig. 2.12.

Autocorrelation functions and power spectra are closely related, as they represent the same information in the time domain and frequency domain, respectively. The advantage of the presented method over ordinary spectrum analysis is that it uses the values of the autocorrelation function of the source series, and not the data series. When performing a spectral analysis of ice cores data series, the annual peak is sometimes not present and otherwise often

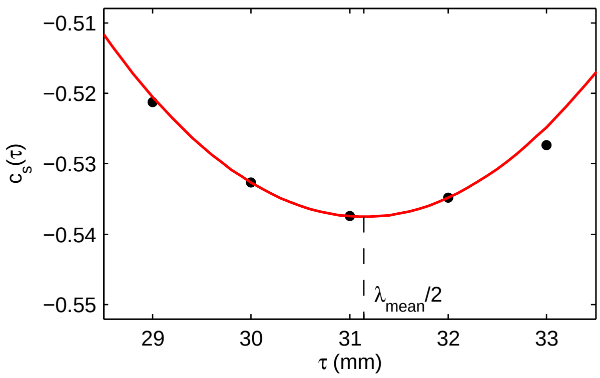

Figure 2.12: From the source series autocorrelation values of Fig. 2.10 (black points), $\frac{\lambda_{\text{mean}}}{2}$ is determined as the abscissa of the vertex of a parabola fitted to the point with lowest autocorrelation value and its two neighbours. In this example, the parabola (red) is fitted to the $\tau = 30$, $\tau = 31$, and $\tau = 32$ points, and $\frac{\lambda_{\text{mean}}}{2} = 31.15$ mm.

rather broad, and the exact frequency is therefore difficult to determine both because of the width of the annual peak and because of the frequency resolution of the spectrum (Pohjola et al., 2002). The latter problem can in theory be handled using Singular Spectrum Analysis, Maximum Entropy Method frequency calculation, or other frequency-adaptive methods, but the DD autocorrelation minimum method provides a much more direct estimate of the mean annual layer thickness with a theoretical precision well below one millimeter. This precision is related only to the determination of the location of the autocorrelation function minimum, and is not an error estimate of the time scale that can be derived from the λ_{mean} estimate, which depends on many other factors. Assuming that the source series with the annual signal contains exactly one peak per year, the number of years in the analyzed section of length L can be determined directly as $\frac{L}{\lambda_{\text{mean}}}$. The mean annual layer thickness changes with depth due to changes in the annual accumulation rate and changing flow-induced thinning, and the analysis must therefore be carried out for data sections small enough to ensure that the λ_{mean} does not change significantly over the length of the data section, and long enough to ensure numerical stability of the DD method.

The 1.65 m length of a NGRIP CFA run meets the above-mentioned requirements, except when a run contains an abrupt climatic transition. Fig. 2.13 shows the results of applying the DD autocorrelation minimum method to the climatically rather stable early Holocene section (data from the depth interval 1405.8 – 1489.95 m are used, excluding the last meters around the Younger Dryas-Preboreal transition). The mean annual layer thickness is determined for each run and converted to a number of years (blue). The result is compared to the annual layer count of Rasmussen et al. (2006), marked in red. For a single run, the source series autocorrelation values do not exhibit a clear minimum as exemplified in Fig. 2.10. The results from this run have been excluded from the comparison, seen in Fig. 2.10 as a gap in the blue curve at depth 1476 m. Differences are observed between the two curves, but for more

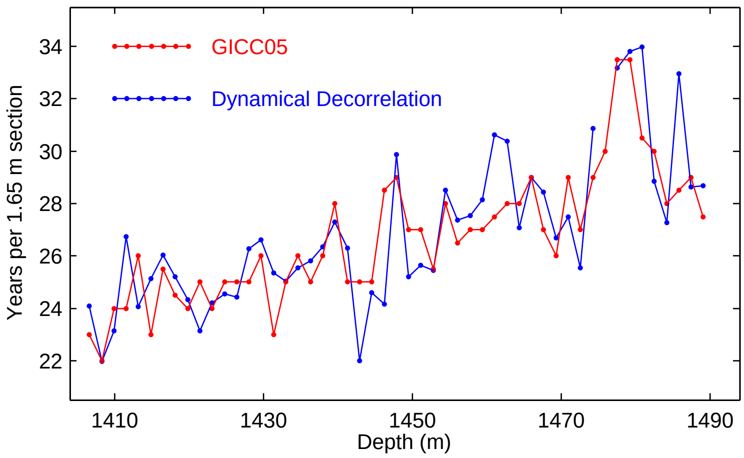

Figure 2.13: The number of annual layers in each 1.65 m section of the Holocene II part of the NGRIP ice core calculated by the Dynamical Decorrelation autocorrelation minimum approach (blue). The results are compared to the number of annual layers in GICC05 time scale (red). Over the entire period, the difference is 13 annual layers, corresponding to 1%. For a single run (depth ~1476 m), no clear minimum is found in the autocorrelation values, and results from this run have been excluded.

than half of the runs, the difference is less than one year, and some of the differences occur because an annual layer mark is located right at the inception point of two runs, and thus is counted as belonging to different runs by the different methods. The DD autocorrelation minimum method yields a total number of annual layers which is 13 years higher than in the GICC05 time scale, corresponding to an increase of just below 1%. The maximum counting error of the GICC05 time scale is 1% in the early Holocene, and the DD autocorrelation method thus produces results in agreement with the results of the visual inspection dating effort in this section.

In the Younger Dryas and Allerød periods, the data resolution is closer to being marginal, and even when using the resolution enhancement method of Rasmussen et al. (2005), a significant fraction of the annual layers is represented in the data series as shoulders on neighbouring peaks or as double peaks containing two annual layers. This means that the basic assumption of the DD method that the annual signal anti-autocorrelates for depth lag $\frac{\lambda_{\text{mean}}}{2}$ does not hold. In the coldest periods, this is reflected in the source series autocorrelation values, where no clear minimum is observed near the expected value of $\frac{\lambda_{\text{mean}}}{2}$. In slightly warmer periods (e.g. the warmer parts of Allerød) a minimum is observed for most data runs, but comparison with the GICC05 annual layer thicknesses shows that the DD autocorrelation minimum method overestimates the annual layer thickness, corresponding to the autocorrelation minimum arising from the well-resolved the annual layers only.

The method has also been tested under glacial conditions, where annual layers have been identified based primarily on conductivity, ECM, and visual stratigraphy data (Andersen et al., submitted). Two sections around 1792 m and 1806 m are identified representing the typical minimum and maximum annual layer thicknesses observed in MIS 2, 15 and 25 mm, respectively. For each section, the method has been tested twice, using all data series and the three well-resolved series only, to determine the effect of including the data series that do not apparently resolve the annual layers. Surprisingly, the autocorrelation values have the most clear minima when all data series are included in the analysis, indicating that the method successfully detects the annual signal even in data series that do not resolve the annual layers well enough for visual detection of annual layers. Occasionally, the method produces mean annual layer thickness estimates that are consistent with the GICC05 time scale, but for about two thirds of the runs, the mean annual layer thickness estimates are significantly different from those of the GICC05, indicating that the DD autocorrelation minimum approach cannot be successfully applied in sections where the annual layers are not well-resolved by most of the data series.

2.3 Conclusion

Different types of multi-parameter dating methods have been applied to the NGRIP data set. The one-at-a-time approach described in section 2.1 is based on detection of annual peaks by many investigators using one data series at a time and subsequent combination of the peak markings. From a technical point of view, the method successfully combines the many independent annual peak profiles to an annual layer sequence by first combining the marks of the different investigators, and then combining the marks set in the different data series, but the results show that too few annual layers are detected. Compared to the GICC05 time scale of Rasmussen et al. (2006), the method detects 2%, 31%, 12%, and 7% fewer layers in the early Holocene, Younger Dryas, Allerød, and Bølling periods, respectively. It is seen that the shortfall anti-correlates with the data resolution, so that almost every third year fails to be detected in the Younger Dryas where the data resolution is lowest. A better match can be obtained by increasing the weight assigned to uncertain peaks and lowering the probability mass threshold for a peak to be counted as an annual layer, but the discrepancies relative to the GICC05 time scale are still more than 15% in the Younger Dryas and about 5% in the Bølling interstadial, indicating that the fundamental problem not is the way the marks are combined, but that the investigators fail to detect a significant number of annual layers when using only one data series at a time. No consistent differences are observed between the number of peaks identified in each of the data series, and the problem can thus not be solved by attributing more weight to certain data series either.

As a result, the dating of the GRIP and NGRIP ice cores has been based on a synchronous multi-parameter approach where the availability of data allows it. As described in section 2.2.1, the layers have been identified by several investigators by visual inspection using all data series containing an annual signal. Using the data sets of both GRIP and NGRIP, the new GICC05 time scale provides a consistent GRIP-NGRIP chronology for the early Holocene in continuation of the δ^{18}O-based chronology of Vinther et al. (2006). Across the late glacial

Bølling–Allerød–Younger Dryas oscillation the GICC05 chronology continues based on NGRIP data. The GICC05 time scale and constitutes the first deep ice core time scale from Greenland which has been constructed independently from other dating methods. Across the entire section in question, frequent changes are observed in how the annual signal is represented in the data, and in order for an automated dating method to be successful, it must either involve an annual layer detection algorithm with adaptive criteria, or obtain a depth-age relation without the need of actual peak detection.

In section 2.2.2 the Dynamical Decorrelation method is reviewed, and it is shown that the method successfully extracts the annual signal from the multi-parameter data set. The annual layers can be identified from the extracted signal using an appropriate peak detection method, which must take into account the varying mean annual layer thickness and peak characteristics. Although the peaks still need to be detected, the task is much simpler because the peak detection is based on one data series only. The method must be calibrated for each climatic period using training data sets, and it is likely that annual layer detection by visual inspection will be necessary across climatic transitions due to the rapidly changing conditions in these intervals. The Dynamical Decorrelation autocorrelation minimum method presented on page 48 provides an efficient alternative to this approach. Based on the presented results and the performed tests it can be concluded that the location of the minimum in the source series autocorrelation values can be used to estimate the mean annual layer thicknesses in ice core data with excellent precision. However, the success of the method depends critically on the resolution of the data. When data series where almost all annual layers are resolved by most of the data series are available, the method produces annual layer thickness estimates that are consistent with the results of the GICC05 visual inspection annual layer count. It is important to note that the method is unsupervised in the sense that it does not need a training set of manually identified annual layers, and that it is very fast compared to annual layer detection by visual inspection. The main drawbacks of the method are that only the *mean* annual layer thickness is determined, and that the method produces no "warning messages" when marginally resolved data are used. When the resolution is much too low, no minimum is observed in the source series autocorrelation values, but for marginally resolved data the method produces erroneous results that are hard to detect if independent data are not available for validation. In the case of NGRIP CFA data, the method overestimates the mean annual layer thickness by several tens of percent in the Allerød period, while the method performs within a few percent of the GICC05 results using Bølling data just 10 meters further down the core. However, the results from these two sections are apparently equally convincing, and the discrepancies are only detected by comparison with the GICC05 results. The method should thus only be applied when it has been independently verified that the resolution is sufficiently high. The verification of data resolution does not necessarily imply visual annual layer counting. For NGRIP CFA data, it has been shown in Rasmussen et al. (2005) that the data resolution can be estimated directly from the data series, and by comparison to annual layer thickness estimates from flow modelling, it can be determined in which sections the annual layers are likely to be resolved by the data. Under these limitations, the Dynamical Decorrelation autocorrelation minimum method provides an efficient and unsupervised determination of the annual layer thickness profile. In addition, the good correspondence of the results with the GICC05 time scale supports that the rules used for annual layer identification in the construction of the GICC05 time scale are correct and unbiased.

Part 3

Interpreting the dated ice core records

This part of the thesis presents work on the analysis of dated ice core records with emphasis on the added value of studying records from multiple cores on a common time scale. The new GICC05 time scale described in the previous section has been applied to records from several ice cores, either by dating the cores in parallel or by synchronizing the records using climate-independent events. By making the records from several Greenland cores available on the same time scale, additional information on common variations and regional-scale climatic events can be identified and separated from more local effects, thereby widening our understanding of the climatic processes and mechanisms. The regional-scale Greenland signal extracted from multiple cores is also ideal for correlation with palaeoclimate records from e.g. ocean and lacustrine sediment cores or terrestrial records. Most of these records originate from locations far from Greenland, and can often not a priori be assumed to correlate better with one specific ice core than with any other core. In this case, comparison with a regional-scale signal less influenced by local phenomena will provide more robust correlation. The approach of interpreting multiple records on a common time scale is applied to three different time periods: the most recent 1800 years, the early Holocene, and the late part of the last glacial (14.9 – 32.45 ka b2k). The amount of information that can be extracted from the records and the level of detail of the analysis obviously differ markedly between these time periods due to the differences in synchronization precision and data availability and resolution, but the three studies share the concept of simultaneous investigation of multiple records on a common time scale.

For the most recent 800 years, annually resolved and synchronized records from five Greenland ice cores are available on the GICC05 time scale, and three of these go back 1800 years. Geographically, the cores cover a substantial part of Greenland, and provide a valuable record of the precipitation amount over Greenland. In section 3.1 it is discussed how the regional Greenland accumulation signal can be extracted from the annual layer sequences. The presented model forms the basis of the paper Andersen et al. (in press), in which the model is presented and the results are compared to other proxy data and archaeological evidence.

During the early Holocene, The North Atlantic area experienced a couple of climatic anomalies, or *events*, of which the most widely known is the 8.2 ka cold event. The DYE-3, GRIP, and NGRIP records provide a detailed view of the early Holocene climate and the synchronization makes it possible to assess how the climatic anomalies are reflected in different cores. The common isotope and accumulation signatures of the anomalies are presented in Rasmussen et al. (accepted) and the results are summarized in section 3.2.1.

Prior to 11.7 ka b2k, the GICC05 is based on NGRIP data only. As discussed in Rasmussen et al. (2006) and section 2.2.1, the GISP2 time scale of Meese et al. (1997) and Alley et al. (1997b) agrees with the GICC05 almost to the year at the Younger Dryas-Preboreal transition. However, large time scale differences are observed across the late glacial transition (Rasmussen et al., 2006) and in the glacial (Svensson et al., submitted). The differences between the GICC05, the ss09/ss09sea model time scales of GRIP, and the GISP2 time scale of Meese et al. (1997) means that the records of the three cores cannot readily be compared in detail, and in order to facilitate a detailed analysis of the similarities and differences of the records, the three cores have been matched back to about 32 ka b2k. The DYE-3 record is not included in this work because no data usable for synchronization are available in the glacial. A dedicated tool for synchronization of ice core records has been developed, and is presented in section 3.3 together with an approach for validating the synchronization of ice core records. The analysis of the synchronized NGRIP, GRIP, and GISP2 records is the topic of Rasmussen et al. (submitted), which is summarized in section 3.3.1.

3.1 Extracting the common Greenland accumulation signal from multiple annual layer profiles

The annual layer thickness profile obtained from an ice core drilled at a site without significant melting represents a record of the net precipitation amount at the place where the ice was formed, and if the flow pattern at the drill site is known, quantitative information about past annual accumulation rates can be derived directly from the annual layer thickness profile. For the NGRIP and GRIP ice cores, the corrections for flow-induced strain are relatively simple, while the situation is more complicated e.g. for the DYE-3 core, which is affected by upstream accumulation gradients (Reeh, 1989). Under the assumption that appropriate corrections for upstream accumulation gradients and flow-induced strain have been applied, the layer thickness profile is a record of the annual accumulation rate at the drill site. The mean annual accumulation rate obtained from an ice core profile is the local time- and area-averaged accumulation rate, but due to measurement noise and small-scale fluctuations in annual accumulation rate, the thicknesses of single annual layers are not representative of the local area-averaged values. Annual layer thicknesses are usually defined from the distance between adjacent maxima or minima in e.g. δ^{18}O or impurity data, and the true location of the minimum or maximum is obscured by the effect of discrete sampling and measurement noise. If the location of a maximum or minimum is artificially offset, the thickness of one annual layer will increase and the neighbouring layer will become thinner. In addition, drifting snow induces what is known as *glaciological noise*: if a certain annual layer in an ice core consists of more snow than the year's local area-averaged annual accumulation rate (due to e.g. snow drift), the snow forms a little rise on the surface, and to compensate for this it is likely that the next annual layer will be slightly thinner than average. Both effects mean that the noise on the thicknesses of neighbouring annual layers anti-correlates, giving rise to so-called blue noise (Fisher et al., 1985). The annual layer thickness noise related to small offsets in the minima and maxima locations only anti-correlates with the neighbouring layer, and the glaciological noise must be expected to have a correlation time of a few years at the most, as every period with snowdrift and every precipitation event will have a tendency to level out any irregularities. The blue noise can therefore efficiently be eliminated by temporal averaging, with an averaging time of a few years.

Even when the blue noise has been removed by averaging, the signal-to-noise ratio of single ice cores records is in general low (Fisher et al., 1985). This is especially true if the "signal" is defined as a regional precipitation signal and cores from different parts of the Greenland ice sheet are considered. In this case, different local meteorological conditions influence the individual records, and often cores from different sides of the ice divide will be affected by different air masses. Nevertheless it is assumed that the records share a common regional signal, representing periods of generally arid or humid conditions in Greenland. In the following, a model aiming at extracting this common signal from multiple accumulation records will be described. The model forms the basis of the work presented in Andersen et al. (in press), which is summarized in section 3.1.1.

Observations from Greenland cores show that sites with high mean accumulation rates also exhibit a high degree of variability in annual layer thickness. In other words, the variability scales with the amplitude. This observation is a cornerstone in the model, as it suggests that the common signal $x(t)$ is represented in each of the measured annual layer thickness profiles with a factor proportional to the mean annual layer thickness at each site. Therefore a model is proposed in which each of the different accumulation records $x_i(t)$ is generated from the common signal $x(t)$ according to

$$x_i(t) = \alpha_i x(t) + \sigma_i \eta_i(t) \tag{3.1}$$

The mean of the common signal is by definition unity, and α_i is thus closely related to the mean annual accumulation rate at site i. The σ_i terms are so-called *residual amplitudes*, and $\eta_i, i = 1, \ldots, N$ are mutually independent, spectrally white, zero-mean, unit-variance residual terms containing noise and the influence of local-scale meteorological phenomena.

The assumption of white noise is reasonable because the blue noise has been removed by temporal averaging as described above.

When denoting the temporal mean by $\langle\cdot\rangle$, and defining σ^2 as the variance of $x(t)$:

$$\sigma^2 = \langle x^2 \rangle - \langle x \rangle^2 = \langle x^2 \rangle - 1 \tag{3.2}$$

the following equations can be obtained by calculating the mean values of the measured profiles and their cross-correlations:

$$\begin{aligned} \langle x_i \rangle &= \alpha_i \langle x \rangle = \alpha_i & (3.3) \\ \langle x_i x_j \rangle &= \alpha_i \alpha_j \langle x^2 \rangle + \delta_{ij}\sigma_i^2 = \alpha_i \alpha_j \left(\sigma^2 + 1\right) + \delta_{ij}\sigma_i^2 & (3.4) \end{aligned}$$

where δ_{ij} is the delta function, $\delta_{ij} \equiv 1$ for $i = j$ and $\delta_{ij} \equiv 0$ otherwise. For N records, $2N + 1$ parameters have to be determined (one α_i and one σ_i per record, plus σ of the common signal). Eq. 3.3 yields N independent equations, and Eq. 3.4 another $N + \frac{N}{2}(N-1)$, totalling $\frac{N}{2}(N+3)$ independent equations, and the problem is thus overdetermined for $N \geq 3$. Optimal estimates of the parameters $(\widetilde{\alpha}_i)_{i=1,\ldots,N}$, $(\widetilde{\sigma}_i)_{i=1,\ldots,N}$ and $\widetilde{\sigma}$ have therefore been computed by determining the values that minimize the misfit function M, which is derived by taking the difference between right-hand and left-hand sides of Eqs. 3.3 and 3.4:

$$M = w_1 \sum_{i=1}^{N} |\widetilde{\alpha}_i - \langle x_i \rangle|^p + w_2 \sum_{i=1}^{N} \sum_{j=i}^{N} \left| \widetilde{\alpha}_i \widetilde{\alpha}_j (\widetilde{\sigma}^2 + 1) + \widetilde{\sigma}_i^2 \delta_{ij} - \langle x_i x_j \rangle \right|^p \tag{3.5}$$

The parameters have been obtained using standard least-squares minimization, that is $p = 2$ and $w_1 = w_2$. The sensitivity of the results has been tested using different starting values for the optimization algorithm, by varying the weights so that $w_1 \neq w_2$, and by replacing $p = 2$ with $p = 1$. The tests show that consistent parameter estimates are produced as long as realistic start values are used for the minimization.

The next step is to isolate the imprint of the common signal $x(t)$ in the individual records. It is assumed that the common accumulation signal estimate $\widetilde{x}(t)$ can be obtained as a linear combination of the individual measured records:

$$\widetilde{x}(t) = \sum_{i=1}^{N} \gamma_i x_i(t) = \sum_{i=1}^{N} \gamma_i \left(\alpha_i x(t) + \sigma_i \eta_i\right) \tag{3.6}$$

Under this assumption, the coefficients $(\gamma_i)_{i=1,\ldots,N}$ should be determined such that $\widetilde{x}$ gets the largest possible relative contribution from the common signal part $\sum_{i=1}^{N} \gamma_i \alpha_i x(t)$. To quantify this, the *signal-to-residual* (S/R) variance ratio is defined in analogy with the well-known signal-to-noise ratio as the variance of the total signal divided by the variance of the residual. For any linear combination of the form in Eq. 3.6 the residual is $r = \sum_{i=1}^{N} \gamma_i \sigma_i \eta_i$, and the S/R ratio becomes

$$\mathrm{S/R} \quad = \quad \frac{\langle \widetilde{x}^2 \rangle - \langle \widetilde{x} \rangle^2}{\langle r^2 \rangle - \langle r \rangle^2} \tag{3.7}$$

$$= \frac{\left(\sum_{i=1}^{N} \gamma_i \alpha_i\right)^2 \langle x^2 \rangle + \sum_{i=1}^{N} (\gamma_i \sigma_i)^2 - \left(\sum_{i=1}^{N} \gamma_i \alpha_i\right)^2}{\sum_{i=1}^{N} (\gamma_i \sigma_i)^2} \tag{3.8}$$

$$= \frac{\left(\sum_{i=1}^{N} \gamma_i \alpha_i\right)^2 \sigma^2}{\sum_{i=1}^{N} (\gamma_i \sigma_i)^2} + 1 \tag{3.9}$$

where the definition of σ^2 in Eq. 3.2 has been used in the simplification from Eqs. 3.8 to 3.9. The set of coefficients $(\gamma_i)_{i=1,\ldots,N}$ are determined by maximizing the S/R expression in Eq. 3.9. The details of the calculation are given in Andersen et al. (in press), where the coefficients are determined as $\gamma_i = \widetilde{\alpha}_i/\widetilde{\sigma}_i^2$. The optimal estimate of the common accumulation signal is thus calculated as

$$\widetilde{x}(t) = \sum_{i=1}^{N} \frac{\widetilde{\alpha}_i}{\widetilde{\sigma}_i^2} x_i(t) \tag{3.10}$$

Because of the signal-to-residual ratio maximization requirement, the obtained common signal $\widetilde{x}(t)$ is a better estimate of the common signal than what can be obtained by e.g. averaging the records (regardless of which weights are used) or performing a principal component analysis, as these methods also perform linear combinations of the measured series. The model is applied to data from a number of Greenland ice cores in Andersen et al. (in press), which will be summarized below.

3.1.1 Summary of Andersen et al. (in press)

The study presents data from five Central Greenland ice cores: the South Greenland DYE-3 core, the GRIP and Crête cores drilled close to the summit of the ice cap, the western Milcent core, and the northwestern NGRIP core. The GICC05 time scale is used as the common time scale for all the cores, and the cores are synchronized with close to annual precision throughout the period with the use of volcanic reference horizons and δ^{18}O annual cycle counting. Annually synchronized records from DYE-3, GRIP, and NGRIP are available back to AD 187, while the Crête and Milcent record lengths are limited by the length of the cores. The Crête record reaches back to AD 552, while the Milcent record only goes back to AD 1174 due to the high accumulation rates at the Milcent drill site. The records have been corrected for the effect of flow-induced thinning using a combined firnification model and Dansgaard-Johnsen flow model.

A numerical experiment has been performed to determine on which time scales the blue noise must be considered. When calculating the cross-correlation between records from different cores, the correlation depends on the resolution of the data. If the data are averaged over intervals of increasing length L, the cross-correlation is expected to rise, because the influence of the noise is reduced and the longer-term common variations thus get more weight. Possible synchronization errors where one record is offset one year relative to the other record lead to a similar rise in the cross-correlation with increasing L. Fig. 3.1 presents the cross-correlation coefficients between the four longest records as a function of the averaging length L. The

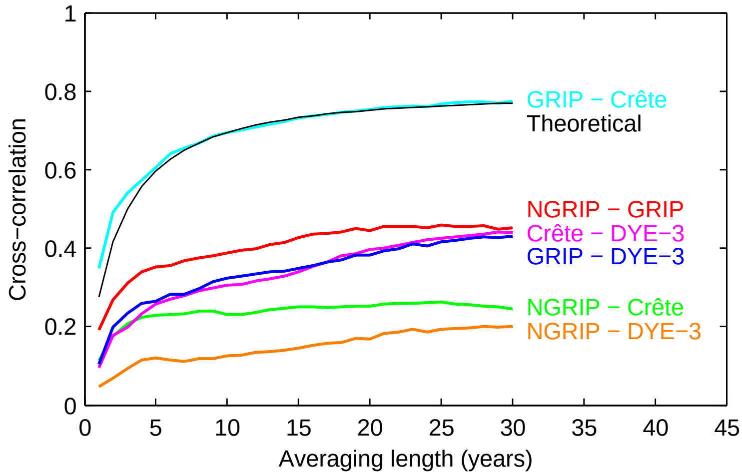

Figure 3.1: Cross-correlation between annual layer profiles from different ice cores as a function of averaging length calculated from measured data (coloured lines) and theoretical considerations (black line). The theoretical curve has been scaled to fit the uppermost measured curve (NGRIP - Crête). From Andersen et al. (in press).

black curve shows how the cross-correlation is theoretically expected to rise with L under the assumption that the data are influenced by white noise with an autocorrelation time of 10 years. The cross-correlation curves obtained from measurements seem to rise more steeply than the theoretical curve for L up to $3-5$ years, indicating that the blue noise and effects of synchronization errors are eliminated by averaging the records in 5 year intervals.

The common accumulation signal is extracted using the model of section 3.1 with 5-year averaged data from three, four, and five cores, respectively. When using all five cores, the resulting accumulation record covers the period AD 1973-1174, while the record reaches back to AD 187 when only three cores are used. It is illustrated how the common accumulation signal based on data from only three cores captures all prominent maxima and minima observed in the profile obtained using data from four or five records. The common accumulation signal obtained using data from DYE-3, GRIP, and NGRIP is presented in Fig. 3.2 together with the average δ^{18}O signal of the three cores, presented as the deviation from the mean value over the entire section.

The correlation between the optimal accumulation record and the δ^{18}O profile of Fig. 3.2 is 0.31, which is significant at the 99% level, and several examples of coinciding prominent minima and maxima are observed in the two records. Examples in the early part of the record are seen in AD 289 and AD 433, while the very strong δ^{18}O minimum in AD 530 probably is connected to a volcanic horizon found by Vinther et al. (2006) in AD 529. Many short periods with dry conditions are observed in the optimal accumulation record, and longer periods with unusually low accumulation are located approximately AD $1004-1075$ and in the first part of the 13th century. These findings are compared with results from sea sediment studies from Southern Greenland and are discussed in an archaeological context, because the timing of

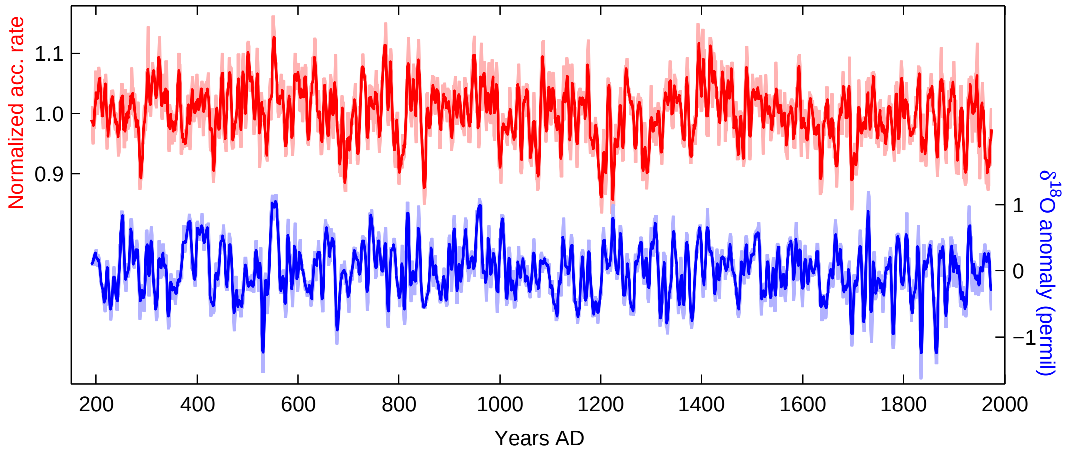

Figure 3.2: The optimal accumulation record over the period AD 191 to AD 1974 (red curve). The curve has been constructed from the 5-year averaged accumulation records from DYE-3, GRIP, and NGRIP. For every year the curve is the average value of the results obtained when using the five possible averaging bins (e.g. 1969 – 73, 1968 – 72, etc., respectively). The highest and lowest values found for every year are indicated by the pale red envelope in order to illustrate the model variability associated with the different binning. The corresponding δ^{18}O record from the three sites is displayed below in blue. The δ^{18}O curve has been constructed by making 5 year binned values, taking the average of the three records, and subtracting the mean. As for the accumulation data, the blue shade shows the range of values obtained when choosing different 5 year binning intervals. Modified slightly from Andersen et al. (in press)

these dry spells roughly coincide with the time where the Norse population disappeared in Greenland. It is argued that the reason for the decline of the Norse settlements very well could have been increased dryness rather than cooling, because the population would have had difficulties adapting to fast reductions in precipitation amount.

The records have been analyzed using the Multi-taper analysis toolbox of Ghil et al. (2002), and a significant and numerical robust spectral peak is found at 11.9 year periodicity, indicating a possible connection with the sunspot cycle. Cross-wavelet analysis has been performed using the method of Grinsted et al. (2004), but it has not been possible to establish proof of coherency of the 11.9 oscillation in the AD 1700 – 1974 period where observational sunspot data are available (Waldmeier, 1961).

3.2 Detection of climate events in the early Holocene

A short period of exceptionally low δ^{18}O values approximately 8.2 ka ago was discovered during analysis of the Camp Century and DYE-3 isotope profiles. Although presented for the first time by Hammer et al. (1986), the work of Alley et al. (1997a) is the first thorough study of the event, which has been known under the standard name *the 8.2 ka event*. Alley et al. (1997a) suggested that the event is a response to a massive fresh water pulse, and this idea has been substantiated by both geological evidence (e.g., Klitgaard-Kristensen et al., 1998; Barber

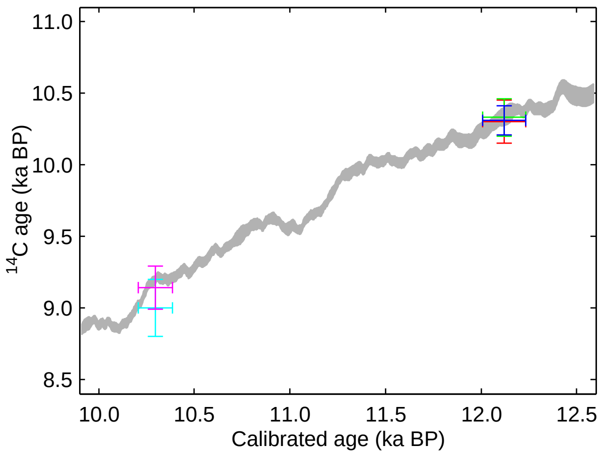

Figure 3.3: Comparison of the GICC05 ice core time scale with the IntCal04 terrestrial radiocarbon age calibration curve of Reimer et al. (2004). The crosses show the GICC05 age and maximum counting error estimates (horizontal) and the corresponding ^{14}C dates and 2σ-uncertainty estimates (vertical). See Rasmussen et al. (accepted) for ^{14}C dates, uncertainty estimates, and data sources. The GICC05 time scale is seen to be consistent with the IntCal04 curve both at the time of the Saksunarvatn eruption (left data points) and at the time of the Vedde eruption (right data points). Conventional BP ages (before 1950) are used in this figure. Figure from Rasmussen et al. (accepted).

et al., 1999) and model studies (Renssen et al., 2001, 2002; Wiersma and Renssen, 2006, and references therein). The event constitutes an analogy to future scenarios of increased fresh water flux to the North Atlantic, which has motivated numerous recent studies as summarized in the two review papers of Alley and Ágústdóttir (2005) and Rohling and Pälike (2005), and an extensive model-data comparison paper by Wiersma and Renssen (2006). Although the literature focuses on the 8.2 ka event, other climatic events or anomalies have been detected in early Holocene climate proxies, most notable a cold event in the time interval 9.2 – 9.5 ka b2k (e.g. Bond et al., 1997; von Grafenstein et al., 1999; McDermott et al., 2001), and the so-called Preboreal Oscillation in the first centuries after the termination of the Younger Dryas (Björck et al., 1997).

However, there is no clear consensus on what defines an event with regard to amplitude and duration, and the different time scales of the different archives yield different age estimates of the events. The advent of the GICC05 time scale has solved the dating consistency problem for the DYE-3, GRIP and NGRIP cores, and differences relative to the GISP2 core are small (20 – 40 years) and vary only slowly in the 8 – 10 ka b2k interval. However, the different records show no consistent picture with regard to the shape of the anomalies, and the anomaly onset and end points are not clearly defined. This is especially problematic because the 8.2 ka and 9.3 ka events are often used for indirect dating of other palaeoclimatic records by visual correlation to the Greenland δ^{18}O records.

In order to establish the ice core signature of the early Holocene climate event and to provide a template for comparison with data from other archives, data from DYE-3, GRIP, and NGRIP have been compiled. The results are presented in Rasmussen et al. (accepted) and are summarized below. This study employs an objective, yet simple, criterium for defining an event, while more sophisticated methods are briefly reviewed in section 3.2.2.

3.2.1 Summary of Rasmussen et al. (accepted)

The aim of the paper is to characterize the early Holocene climate anomalies as they are recorded in Greenland ice cores. The paper presents the isotope and annual layer thickness profiles of the DYE-3, GRIP and NGRIP ice cores (Dansgaard et al., 1982; Johnsen et al., 1997, 2001; NGRIP members, 2004) on the GICC05 time scale. The paper presents the GICC05 time scale for the 0 – 14.8 ka b2k time interval by briefly reviewing the results of Rasmussen et al. (2006) and Vinther et al. (2006). In addition, a comparison of GICC05 with the IntCal04 terrestrial radiocarbon age calibration curve of Reimer et al. (2004) is included. The comparison is made using the Saksunarvatn and Vedde tephra layers, which have been identified in the Greenland ice cores as well as in ^{14}C-dated archives. By comparing the GICC05 age of the volcanic deposits to the IntCal04-calibrated ^{14}C age estimates obtained by ^{14}C-dating material found adjacent to the tephras, an independent validation of the GICC05 time scale can be made. Fig. 3.3 shows the comparison, using Saksunarvatn age estimates from Jóhansen (1975) and Björck et al. (2001) and Vedde age estimates from Bard et al. (1994), Wastegård et al. (1998), and Birks et al. (1996). The GICC05 time scale is shown to be fully consistent with the IntCal04 curve, as the different age estimates fit well within the respective error margins. The good correspondence indicates that the maximum counting error of the GICC05 time scale across the late glacial oscillation with good reason can be interpreted as the total uncertainty of the GICC05 time scale.

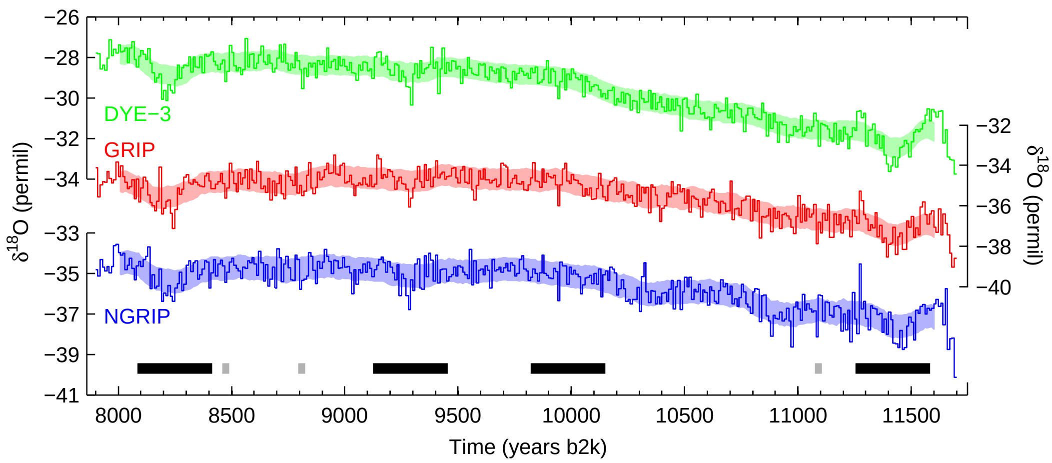

Figure 3.4: The DYE-3, GRIP and NGRIP δ^{18}O profiles in the 7.9 – 11.7 ka b2k interval, presented in 10 year resolution on the GICC05 time scale. The shaded envelopes are the regions that are within one standard deviation from the 210 year running mean of the individual profiles. The black lines at the bottom indicate the position of the sections shown in Fig. 3.5. Figure from Rasmussen et al. (accepted).

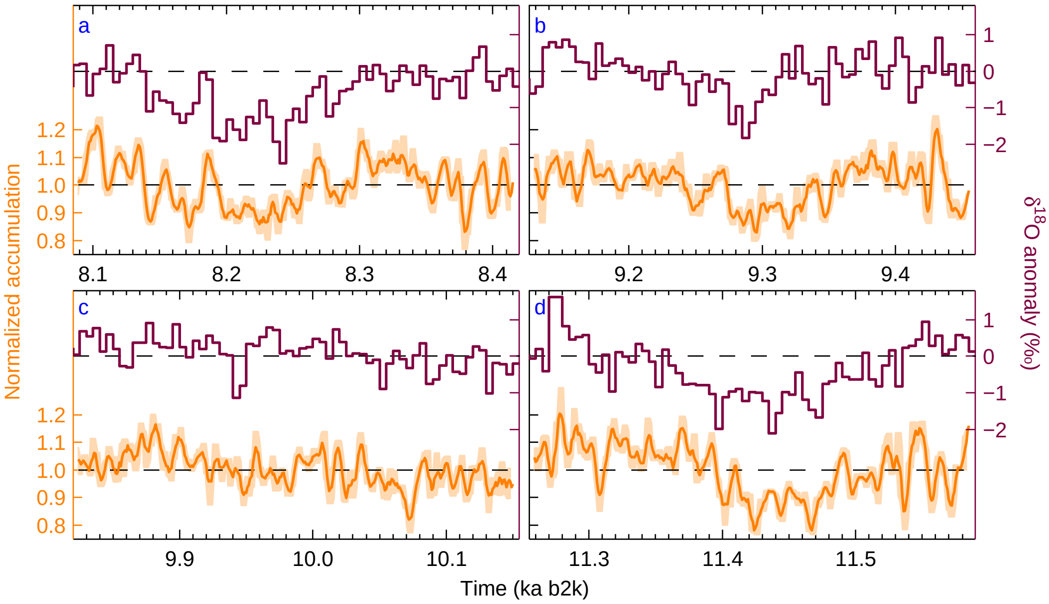

Figure 3.5: Modelled accumulation rates and mean δ^{18}O curves (5 year resolution) across the 8.2 ka event (a, top left), the 9.3 ka event (b, top right), the 9.95 ka δ^{18}O anomaly (c, bottom left) and the Preboreal Oscillation (d, bottom right). The shaded bands indicate the uncertainty intrinsic to the accumulation model of Andersen et al. (in press). Figure from Rasmussen et al. (accepted).

In order to be able to analyze the DYE-3 records on the GICC05 time scale in the early Holocene where annual layers cannot be identified in DYE-3 based on the available data series, the GICC05 time scale has been transferred to the DYE-3 core by matching ECM peaks common to the three cores with an estimated precision of a couple of years. The synchronized δ^{18}O profiles are shown in Fig. 3.4 with 10 year resolution. As a simple indicator of which features in the isotope profiles are common to the three records, the places where all three profiles simultaneously deviate more than one standard deviation from their respective running means are identified. Each of the shaded bands around the isotope profiles in Fig. 3.4 represents plus/minus one standard deviation from the 210 year running mean. The exact choice of averaging length is arbitrary, but the value must be larger than the typical duration of the expected (decadal-scale) anomalies, and small enough for the running mean curve to capture the gradual trends observed in the 10 – 11.7 ka b2k section. Any value in the 100 – 300 year interval give essentially identical results.

It is seen that the three profiles only have strong common features deviating from the $\pm 1\sigma$ variation band at the 8.2 ka event, at 9.3 ka b2k, and at 11.4 – 11.5 ka b2k, while small deviations are found around 8.5, 8.8, 9.95 and 11.1 ka b2k. The annual layer profiles are analyzed to check if simultaneous anomalous values are observed. To do this, the three annual layer records are used as input to the accumulation model described in section 3.1. The results show that accumulation anomalies are observed only for the 8.2 ka event, the 9.3 ka event, and for the Preboreal Oscillation, while an accumulation anomaly is observed about

120 years offset from the 9.95 ka δ^{18}O anomaly. The common accumulation signal from the model and average δ^{18}O anomalies across these four intervals are shown in Fig. 3.5. The 9.95 ka anomaly and the accumulation anomaly at 10.07 ka b2k are located too far away to be ascribed to the same climatic event, and it is thus concluded that the only significant simultaneous δ^{18}O and accumulation anomalies in the early Holocene recorded in the DYE-3, GRIP, and NGRIP records are the 8.2 ka event, 9.3 ka event, and the Preboreal Oscillation. It is seen that the mean δ^{18}O profiles show strong correlation with the modelled accumulation signal across both the 8.2 and 9.3 ka events. This correlation is much stronger than when comparing the δ^{18}O and annual layer thickness profiles of the individual records, supporting the supposition that the profiles of Fig. 3.5 better represent the Greenland signature of the geographically widespread climatic events. The analysis also shows that the 9.3 ka event is shorter but otherwise rather similar to the 8.2 ka event in that the central part of the anomaly consists of a 2 ‰ δ^{18}O minimum and accumulation rates about 15% below the level outside the event. The data presented here thus indicate that that the 8.2 ka event from a Greenland point of view is not as unique as suggested in many studies. With regard to the dating of the event, it is concluded that the event durations are not well-defined as they depend critically on which criteria are used to define the end and onset points.

3.2.2 Defining climatic events and transitions

The criterium used in Rasmussen et al. (accepted) to discriminate between climatic anomalies and insignificant deviations from the rather stable early Holocene climate does not assess the problem of how to define the start and end points of the events. For example, as can be seen in Fig. 3.5a, the onset and end points of the 8.2 ka event are not obvious, and the determination of the age and duration of the event is therefore not straight-forward. In the following, some approaches dealing with the question of how to define climatic anomalies and transitions are discussed. The methods are introduced by application to data from the 8.2 ka event.

The most direct way of defining a climatic transition is to look through the available records for the first sign of changing conditions. As an example, the transition depths used to define the onsets of the Bølling, Allerød, and Preboreal periods in the work of Rasmussen et al. (2006) have been obtained from analysis of the combined set of impurity and isotope records (J. P. Steffensen, pers. comm.). At each of these transitions, the deuterium excess d, defined as $d = \delta\text{D} - 8 \cdot \delta^{18}\text{O}$, is observed to change abruptly before any other record starts to change, and it is thus reasonable to assume that the deuterium excess signal is connected to the physical process that drives the transition. In this case, the transition can be defined by visual identification of the first sign of change because the transition is very abrupt. In many other cases, however, the definition of a transition is not as evident, and an objective criterium for the definition of a transition or climatic anomaly will be useful. An objective definition is also important to the study of the mechanisms of climatic transitions, for example because differences in the timing of the transition as observed in different records can be quantitatively assessed.

In general, a transition from one climatic state to another can be defined by first assuming that the conditions some distance away on each side of the transition are stable and can be characterized e.g. by certain mean values and standard deviations. Using the statistical properties of the two states, the point that most likely separates the two states can be calculated. A similar approach has been developed in the work of Mudelsee (2000), in which a transition ramp has taken the place of the transition point mentioned above. The basis of the method is to fit a ramp function $x_{\text{fit}}(t)$ to the data profile $x(t)$, $x_{\text{fit}}(t)$ being given as

$$x_{\text{fit}}(t) = \begin{cases} x_1, & t < t_1 \\ x_1 + (t - t_1)\frac{x_2 - x_1}{t_2 - t_1}, & t_1 \leq t < t_2 \\ x_2, & t_2 \leq t \end{cases} \tag{3.11}$$

The problem is thus to find the inflexion points (t_1, x_1) and (t_2, x_2). It is assumed that the data $x(t)$ follow the underlying ramp function shape according to the expression

$$x(t) = x_{\text{fit}}(t) + \epsilon(t) \tag{3.12}$$

where the residual term ϵ is characterized by a standard deviation σ which in itself can be described by a ramp function or a constant value. The residual term ϵ is allowed to be first order autoregressive, that is, the value of ϵ correlates with the value of ϵ at the nearest previous data point. This representation of the data is very general, and must be considered one of the strong points of the method, because most climate data are autoregressive (e.g., Thejll and Schmith, 2005). A rather sophisticated method for determining the best values of t_1, t_2, x_1 and x_2 is given in Mudelsee (2000) based on user-supplied σ values. The software package described in Mudelsee (2000)[1] includes different diagnostic tools in order to help the user obtain reasonable values of σ, but the fact that σ cannot be estimated as a part of the calculations is one of the major drawbacks of the method. In addition to σ, the user must supply search intervals that narrow down where the program searches for t_1 and t_2, but these intervals can be specified to be very wide and thus do not limit the usefulness of the method.

The ramp fitting approach has been applied to the optimal accumulation record across the 8.2 ka event (Fig. 3.5a). Only data from the period 8.15 – 8.40 b2k are used, corresponding to the period just before the event, the onset slope, and the central part of the event. A similar analysis could be applied to the slope at the end of the event, and the two ramps could then be used to define the duration of the event (see Mudelsee, 2000, Fig. 16, for an analogous example). The onset of the 8.2 ka event in the accumulation profile consist of a positive anomaly followed by two steep sections of negative slope separated by a peak (8.24 – 8.27 and 8.28 – 8.30 ka b2k, respectively). To test the sensitivity of the ramp fitting method to the length of the input data, the method has been applied twice with similar settings to the

[1] The RAMPFIT program can be obtained from http://www.uni-leipzig.de/~meteo/MUDELSEE/

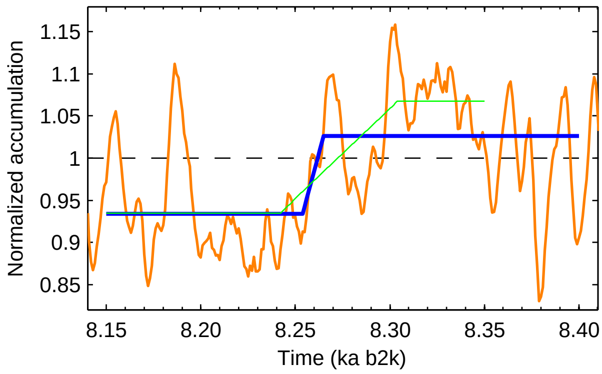

Figure 3.6: The optimal accumulation signal of Fig. 3.5a covering the onset of the 8.2 ka event (orange curve) and the ramp functions fitted to the curve using the approach of Mudelsee (2000). The blue curve is the resulting ramp function when using input data from the 8.15 – 8.4 ka b2k interval, while the green ramp is obtained when only the 8.15 – 8.35 ka b2k data interval is used.

8.15 – 8.4 and 8.15 – 8.35 ka b2k sections, respectively. For both tests, a σ value of 0.07 has been used, determined using the included tools for σ estimation, and the search intervals for t_1 and t_2 are given as 8.15 – 8.3 and 8.2 – 8.35 ka b2k, respectively. The results are presented in Fig. 3.6, and show that the method is sensitive to which data sections are used. Basically, the ramp fitting results resemble that of a visual inspection, namely that the transition can be placed at two different points, depending on whether the interval with accumulation values around 1.1 centered at 8.32 ka b2k is regarded as a part of the pre-event baseline, or a positive anomaly prior to the event onset.

The ramp fitting method has the advantage that the inflexion points are calculated from objective criteria, but according to the model assumptions formulated in Eqs. 3.11 and 3.12, the ramp fitting approach implies that the climatic conditions on each sides of the ramp are stable, which is often not the case. If, for example, the 8.2 ka event was caused by a partial breakdown of the thermohaline circulation in the North Atlantic due to massive freshwater influx, the climatic conditions during the central part of the event can not be assumed to be constant, but rather characterized by a fast onset and a subsequent slow return to normal Holocene conditions with hardly no stable period in between. This is exemplified by the δ^{18}O profile across the 8.2 ka event shown in Fig. 3.5a, which indeed contains a pronounced minimum with a duration of a century or more, but with no central period of low stable δ^{18}O values with duration of more that a few decades. It is thus problematic to apply the ramp fitting approach to this profile because the data delimitation indirectly implies a certain interpretation of what is considered the central part of the event and what is considered to be a part of the slope. For events like the 8.2 ka event, the slopes leading into the event and back to normal conditions are therefore more characteristic for the event than the central part of the event. By visual inspection of the accumulation and δ^{18}O profiles of Fig. 3.5a it is clear that both the onset and end slopes are long and irregular, and that several points could be chosen as the onset and end points, respectively. Also, the appearance of the slopes, and thus where the onset and end points are placed, will depend on the resolution of the data. The so-called *Significance of Zero crossings of derivatives* (SiZer) approach of Chaudhuri and Marron (1999) takes this fact into account and determines which sections of the curve have significant slopes irrespective of the data resolution[2]. The name SiZer comes from the fact that maxima and minima occur at the places where the first derivative changes sign (crosses zero), and SiZer is thus conceptually related to the peak detection algorithm of Pohjola et al. (2002), although the latter approach uses the sign change of the second derivative and thus identifies mid-points of slopes rather than minima and maxima.

The basic concept behind SiZer is to identify the sections of a curve which have significant slope for a large number of smoothed versions of the data, and then present the results graphically in a easily comprehensible way. The theoretical work upon which SiZer relies is extensive, and it is beyond the scope of this work to provide an adequate introduction to the methodology. Interested readers are referred to Chaudhuri and Marron (1999) for an introduction and Hannig and Marron (2006) for a discussion of how the slope significance is calculated. In the present work, the significance level is chosen to 95%, and the interval of significant slopes has been computed using the method recommended by Hannig and Marron (2006). The results of applying SiZer analysis to the 8.2 ka event profiles are shown in Fig. 3.7 (accumulation data above and δ^{18}O data below). The raw data profiles (orange and purple curves in the "Overlay of smooth curves" panels, respectively) are smoothed by convolution with a kernel function (here of Gaussian shape), whose width is parameterized by the so-called *bandwidth* parameter h. Small values of h corresponds to very little smoothing and vice versa. For each level of smoothing (32 levels are used in Fig. 3.7), it is determined which parts of the curve have significant nonzero slopes. Areas with significant positive, significant negative, and insignificant slopes are marked in the so-called "SiZer slope map" as a function of time and bandwidth h with the colours blue, red, and purple, respectively. Slopes that are significant for many values of h appear in the SiZer slope map as unbroken vertical areas of one colour (marked by white arrows in Fig. 3.7). The determination of the location of these areas is not performed by the SiZer algorithm, but is manually determined from the SiZer slope map.

The SiZer analysis of the 8.2 ka event data shows that neither the onset nor the end of the event can be uniquely defined from the shape of the curves, as both onset and end slopes contain two distinct periods with prominent and basically equally significant slopes. The most prominent slopes into the event are centered at 8.295 and 8.26 ka b2k, while the most likely endpoints are around 8.195 and 8.14 k2 b2k. According to the analysis, it is therefore a matter of definition whether the 8.2 ka event should be assigned a duration of 65, 100, 120,

[2]The SiZer software used for this work has been supplied by J. S. Marron and co-workers and has been downloaded from http://www.stat.unc.edu/postscript/papers/marron/Matlab6Software/Smoothing/.

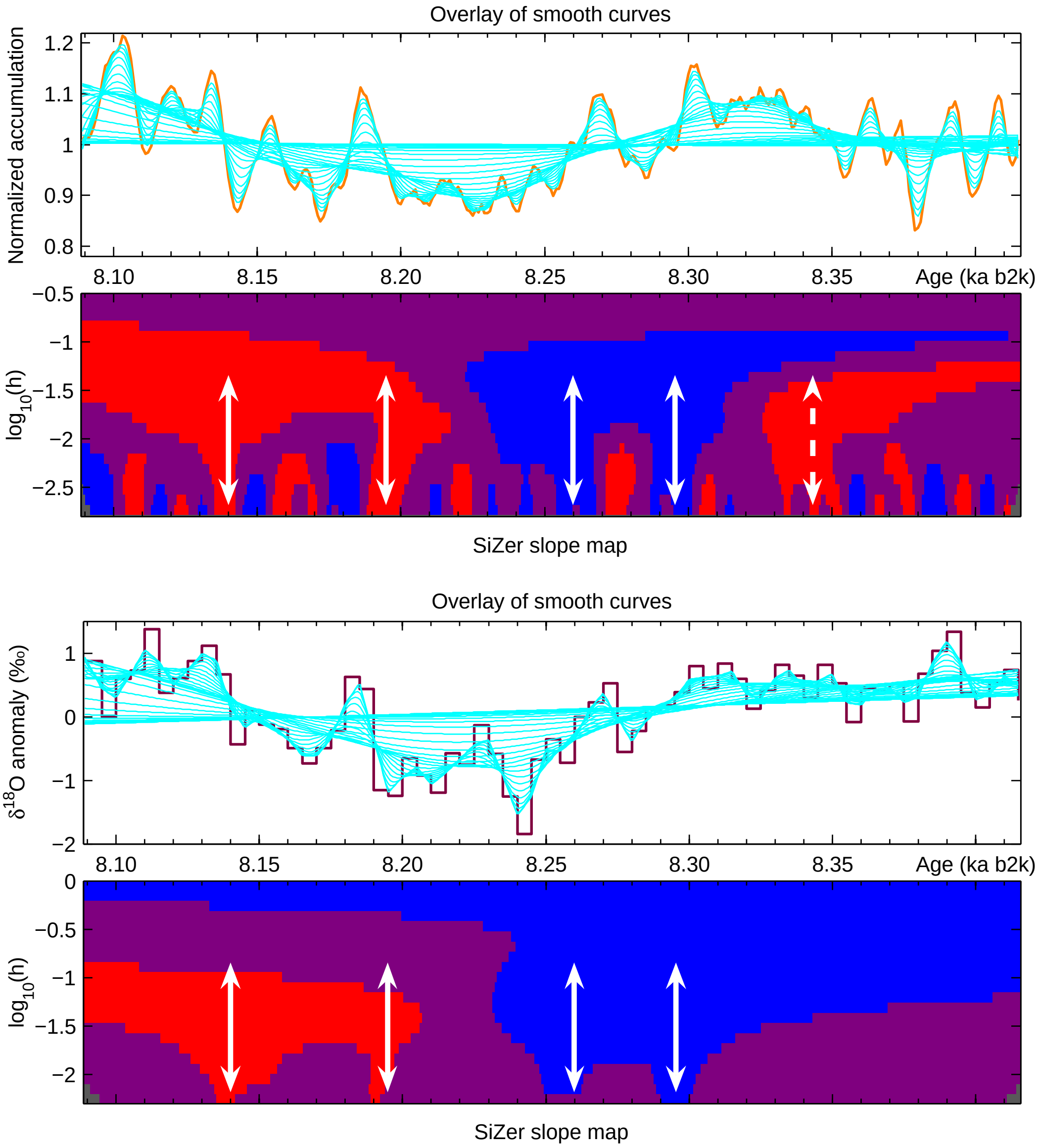

Figure 3.7: Results of SiZer analysis of the accumulation profile (upper panels) and δ^{18}O profile (lower panels) of the 8.2 ka event as presented in Fig. 3.5a. The "Overlay of smooth curves" panels show the input data (orange/purple curves) and smoothed versions hereof (cyan curves). Each level of smoothing corresponds to a horizontal line in the "SiZer slope maps" below, where the red colour are areas of significant negative slope and blue areas are areas of significant positive slope (note that the definition of positive and negative slopes follow normal mathematical usage, which due to the reversed time axis of the plot is opposite the physical meaning). Purple is used for areas with zero or insignificant slope. The bandwidth h on the axis of ordinates is a measure of the smoothness of the curve (see text for details), where the largest values of $\log_{10}(h)$ correspond to the most heavily smoothed curves. The large blue and red areas of the SiZer slope maps that are present for all values of h (marked by white arrows) show that the accumulation and δ^{18}O profiles agree on the location of significant slopes: the onset of the event consist of two equally prominent slopes centered at 8.26 and 8.295 ka b2k, respectively, while the end of the event in a similar way consists of prominent slopes centered at 8.14 and 8.195 ka b2k. The accumulation signal also contain a significant slope prior to the onset of the 8.2 ka event, centered around 8.34 ka b2k (dashed arrow).

or 155 years[3]. Although the analysis thus does not unambiguously identify the onset and end points, the results of the SiZer analysis are useful when correlation the ice core records with less well-resolved records. The SiZer slope map shows which slopes of the records are robust to averaging, or equivalently, which slopes would also be present if the data resolution was lower. If, for example, the 8.2 ka event signature curves of Fig. 3.5a are matched with a sediment profile with a temporal resolution of, e.g., a decade or two, only the features that are insensitive to smoothing according to the SiZer slope maps should be used for the matching.

Neither the SiZer approach nor that of Mudelsee (2000) takes into account that the data used are time series, as the result are indifferent to inversion of the time scale. It can be argued that the onset of the 8.2 ka event must be defined as 8.3 ka b2k because this is the age of the beginning of the first of the two slopes leading into the event according to the SiZer analysis, and also the age of the first kink in the ramp function fitted to the 8.35 – 8.15 ka b2k accumulation data (Fig. 3.6). However, from a purely statistical point of view, it has been demonstrated that both the SiZer approach and the ramp fitting method fail to uniquely identify a convincing onset point of the 8.2 ka event, but that they are able to produce objective and quantitative estimates of the points of transition when applied to well-chosen data sets. In this respect, they complement transition detection by visual inspection, but the results of either analysis do not reduce the importance of the interpretation. Specifically when using accumulation data, the onset point of the 8.2 ka event depends on the interpretation of the period of high accumulation values just prior to the onset of the 8.2 ka event (see e.g. Fig. 3.6). If the period of high accumulation values is considered to be a part of the variability of the stable Holocene climate, the onset of the 8.2 ka event can be defined as any of the two slopes centered around 8.295 ka b2k or 8.26 ka b2k, respectively. However, the period of high accumulation can also be interpreted as a part of an accumulation oscillation together with the slope centered around 8.295 ka b2k, in which case the onset of the 8.2 event is most naturally defined as the slope centered around 8.26 ka b2k. This ambiguity is reflected by the results of the ramp fitting approach, which identifies one or the other slope to be most significant depending on which data excerpt is used for the analysis, and also by the SiZer analysis, which identifies all three slopes as significant. The main advantage of the SiZer and ramp fitting approaches is thus that the location of the most significant transitions and slopes are determined objectively, but the data sections used should not be chosen uncritically, and the sensitivity of the results to data delimitation should be carefully investigated.

[3]Similar results are obtained for the 9.3 ka event, but are not shown. Here the onset slope is centered around 9360 and 9330 ka b2k, while the end slope is located around 9275 and 9240 ka b2k, giving event durations of 55, 85, 90, or 120 years.

3.3 Synchronization of ice core records

The GICC05 time scale currently reaches back to 42 ka b2k. The most recent 7.9 ka have been dated by identification of the annual cycle in δ^{18}O data from DYE-3, GRIP (back to 2.8 ka b2k), and NGRIP (back to 1.8 ka b2k) as described in Vinther et al. (2006). As was discussed in section 2.2.1, CFA impurity data from GRIP and NGRIP are used to extend the GICC05 time scale through the late glacial oscillation (7.9 – 14.8 ka b2k). Below this period, only the NGRIP visual stratigraphy, ECM profile, and electrolytical conductivity profile fully resolve the annual layers, and the annual layer identification has thus been based mainly on these three parameters with support from the remaining impurity records in the interstadials where the accumulation is roughly double that of the stadials (Andersen et al., submitted). In summary, the GICC05 time scale is based on data from all three cores down to 7.9 ka b2k, on GRIP and NGRIP data down to the onset of the Holocene at 11.7 ka b2k, and only NGRIP data below this. When the NGRIP records on the GICC05 time scale are compared with the GRIP records on the ss09sea time scale of Johnsen et al. (2001) and the GISP2 records on the time scale of Meese et al. (1997) and Alley et al. (1997b), the differences between the time scales severely limit the possibility of making detailed comparisons, and in addition the precision of the time scales cannot be directly compared because the uncertainties are not reported using the same conventions. For example, the dates of the rapid climate shifts in the glacial (the so-called *Dansgaard-Oeschger events*, or D-O events) differ by several centuries according to the GICC05 time scale and the GISP2 time scale, respectively (Svensson et al., submitted), which is the same order of magnitude as the duration of the D-O events. In addition to the absolute time scale differences, the number of years within some stadials and interstadials deviates with more than 30% between the two time scales (Svensson et al., submitted), making detailed comparison of the records virtually impossible.

In order to investigate in detail e.g. how climate shifts are recorded in the different ice cores records and to assess possible leads and lags in the climate system, it is essential to be able to compare the records from different cores on a much finer scale than these different time scales allow. Optimally, the records must be available on a common time scale. The most direct way of achieving this is to match the records of the cores using synchronous horizons or wiggle matching. If coarse-scale synchronization is sufficient and only cores from the same hemisphere are considered, the cores can be matched by aligning e.g. the stadial-interstadial variations in the δ^{18}O profiles of the cores, assuming that e.g. D-O events are recorded simultaneously in different cores. By doing this, any information about relative timing of climate change in the different records is lost, so if relative timing issues are to be considered, or the records are to be compared in detail, the matching of the cores must be performed using climate independent horizons.

Few methods exist for performing climate independent synchronization of ice core records. Variations in the atmospheric methane content can be used to synchronize ice cores from any part of the world, because the atmosphere has a mixing time of the order of one year, which is much shorter than the atmospheric lifetime of methane. Synchronization is performed using measurements of the methane content in air bubbles in the ice (e.g. Blunier et al., 1998; Blunier and Brook, 2001), and if the synchronization is to be used for records that are derived from measurements directly on the ice (e.g. δ^{18}O and impurity records), a correction for the bubble-ice age difference must be performed. This correction is nontrivial and the uncertainty of the correction is considerable, especially close to climatic transitions (Blunier and Schwander, 2000). Also, methane measurements require large samples of ice, and decadal or coarser resolution is therefore typical. Taking these difficulties into consideration, methane-based synchronization can most often not be used on time scales shorter than a century.

For high-resolution synchronization of ice records, the use of volcanic deposits is the most direct and well-understood method (Wolff et al., 1999; Udisti et al., 2004; Bay et al., 2006). Recent work by Robert Rohde (pers. comm., 2006) and colleagues indicates that the volcanic matching can be complemented by matching the visual stratigraphy records obtained by in-hole visual logging tools (Bay et al., 2001). However, the method needs further development and validation before it can be applied in general, and matching of volcanic event thus remains the best available method for synchronization of records from different ice cores. Deposits from a certain eruption are not guaranteed to be present all over Greenland, because meteorological factors influence the geographical distribution of the deposits. Indeed, many volcanic deposits are found in one of the two Central Greenland GRIP and GISP2 cores, located about 30 km apart, and not in the other. A study of recent volcanic deposits in Antarctica shows that the sulphate peaks typically start 1 – 3 years after the eruption and has a similar duration (Palmer et al., 2001). The maximum difference in arrival times and peak maximum location between two Greenland sites must therefore be considered to be one year, and when the deposits from a certain eruption are found in two cores, the layer thus constitutes a horizon that is close to being simultaneous in the two cores. Explosive volcanic eruptions emit large amounts of tephra and gases into the atmosphere. Oxidation and gas-to-particle conversion is responsible for SO_2 being converted into sulfuric acid (H_2SO_4), which is transported and precipitated onto the ice sheet. The most direct way of detecting a volcanic layer is therefore to measure the concentration of sulphate in the ice, but high-resolution sulphate measurements are often not available. Instead, the volcanic layers are identified from their acid content, which gives rise to peaks in the ECM signal and in the record of dielectric properties of the core (DEP). When tephra is found in the ice core, the composition of glass shards in the tephra can be analyzed in order to identify the source of the layer (Mortensen et al., 2005; Grönvold et al., 1995). However, often sulphate and acidity peaks in the ice core are not accompanied by detectable amounts of tephra, and an unambiguous match to volcanic layers in other cores cannot be made. In this case, the matching relies on matching of characteristic patterns of acidic peaks found in several cores. In Rasmussen et al. (2006), the NGRIP-based GICC05 time scale is transferred to GRIP and GISP2 depths using 48 common ECM match points in the time period 11.7 – 14.8 ka b2k, of which only one, the Vedde ash at 12,171 b2k, has been identified in several cores and thus constitute a perfectly certain match point. The depths of the 48 ECM peaks are shown in Fig. 2.9, and the acidic peaks form a pattern which is recognized from one core to the next. The sulphate arrives in Greenland up to a year after the eruption, and the acidity peak shapes vary between the cores, leading to a possible mismatch of two individual cores by one or two years. Uncertainty in the depth assignment during ECM data processing (typically some centimeters) adds to the total uncertainty, which is estimated to a few years. This uncertainty estimate is based upon the assumption that the correct peaks are matched between the records, which is reasonable because there are many clear match points across the late glacial oscillation. Between the match points the time scale is transferred by linear interpolation, adding slightly to the uncertainty of the match. Even in the sections farthest away from match points, the maximum total mismatch is estimated to less than a decade and the matching thus greatly improves the potential for studying the similarities and differences of the NGRIP, GRIP and GISP2 climate records.

Essentially the same approach has been used to synchronize the NGRIP, GRIP, and GISP2 records back to about 32 ka b2k, but in this work also peaks in the [NH_4^+] profile, probably originating from biomass burning events, have been used for the matching. The work is described in Rasmussen et al. (submitted) and summarized in section 3.3.1. The match points are in general more sparse prior to 15 ka b2k than in the 10 – 15 ka b2k section, and there are two sections longer than a millennium without any match points. This makes the pattern-matching approach employed in Rasmussen et al. (2006) more difficult and increases the risk of matching horizons that are not synchronous in the cores. Systematic validation has therefore been necessary to ensure that the performed match is robust. As a first step, match points set independently by several investigators are compared. Non-consistent match points are observed in a few sections with very sparse match points, but in general the independent match point sequences confirm each other, and are also corroborated by the observation that all major features of the δ^{18}O and [Ca^{2+}] profiles of the three cores line up when the records are synchronized using the match points. In the absence of independent data sources for validation, it is therefore assumed that the overall matching is correct. Under this assumption, different tests have been used to identify single erroneous match points or small groups of erroneous match points. The most straightforward test of a stratigraphic match is to plot the depths of the match points $d_1, ..., d_N$ and $D_1, ..., D_N$ in two cores against each other and look for points that deviate from the general trend. The slope of the (d, D)-graph is the ratio between the annual layer thicknesses in the two cores. It is reasonable to assume that the ratio between the accumulation rates at the two drill sites only changes abruptly at climatic transitions, and that the thinning factor due to ice flow only changes slowly with depth. The ratio between the annual layer thicknesses in the two cores must therefore be expected to change slowly, corresponding to that the (d, D)-graph has little or no curvature, although the slope is likely to change from one climatic period to another due to changing precipitation patterns. Single match points or small groups of match points that do not represent synchronous events will be offset from the curve, but if the mismatch is small, the offset may not be clearly visible on a graph covering several hundred meters of core. Two other ways of representing the same information are therefore used:

- The depth differences $d_i - D_i$ are plotted versus d_i for all i. Essentially this corresponds to the (d, D)-graph with most of the trend removed, which makes it easier to detect points that are offset from the curve.

- The depth difference ratios $r_i = (D_{i+1} - D_i)/(d_{i+1} - d_i)$ are plotted versus d_i for $i = 1, ..., N-1$. This corresponds to plotting the slopes of the (d, D)-graph between each pair of points. An erroneous match point will be visible as a neighbouring pair of unusually low and high slope values.

Although a certain layer observed in two or more cores represents a truly synchronous event, the location of the match point can be offset slightly due to a number of factors. For example, volcanic events often give rise to ECM peaks that are 5 – 10 cm wide and contain multiple maxima, and the peak shapes are often not similar from one core to another. The differences are likely to be caused by a combination of differences in transport paths and accumulation conditions at the different drill sites. Also problems with the depth control of the different data series mean that the peaks observed in the SO_4^{2-} and ECM profiles can be offset by a few centimeters. The estimated total uncertainty on the location of a match point is about 10 cm. For two closely spaced match points, 10 cm is a large relative difference and a match point can thus appear to be offset in the depth difference ratio graph even though the match is correct. The point will, however, not be offset significantly in the depth difference plot because of the small absolute offset, and simultaneous inspection of the depth difference and depth difference ratio plots is therefore a useful approach for detection of erroneous match points. The three ways of visualizing the match point depths are illustrated in Fig. 3.8. It is seen that both depth difference plots and depth difference ratio plots must be used in order to detect significant offsets without getting "false alarms" from close points that are only offset a few centimeters due to the above-mentioned causes.

A specialized tool, *Matchmaker*, has been developed as part of the thesis work to facilitate efficient matching of records from two or more ice cores, incorporating the above-mentioned validation approach. Matchmaker makes it possible to browse through all available data series from the cores, to scale the data series freely, and to set match points with a mouse click. Different match point types are available for match points of different degrees of certainty, and marks are available for marking special features for later scrutinizing. The program allows simultaneous matching of three or more cores and handles the case where a match point not is found in all cores. The depth difference plots and depth difference ratio plots are generated in a separate window and are updated every time a match point is moved. The program has been

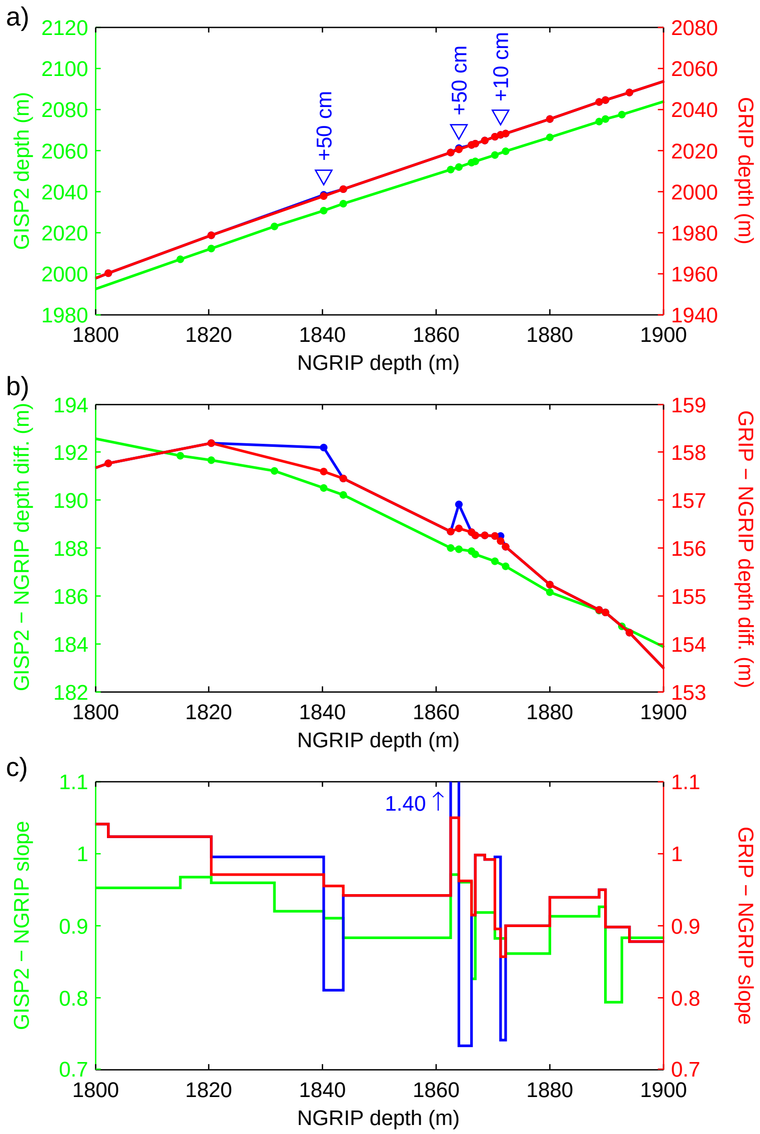

Figure 3.8: Examples of different ways of plotting match points to reveal dubious matches when synchronizing three cores. The data from Rasmussen et al. (submitted) show match points obtained when matching GRIP and GISP2 records to the NGRIP records. In order to demonstrate the sensitivity to erroneous matching of the different match point plots, three NGRIP-GRIP match points (marked by blue triangles) have been offset by 50 cm, 50 cm, and 10 cm, respectively. The 50 cm offsets represent realistic, but rather small, matching errors, while the 10 cm offset is the maximum total uncertainty of the location of match points. In panel (a), the GRIP/GISP2 match point depths are plotted versus NGRIP depths. When showing match points covering 100 meters of core, the offsets (blue curve) are hardly discernible from the correct match points (red curve). In the depth-difference plot in panel (b) the 50 cm offsets are clearly visible: the error at 1864 m stands out clearly, while the error at 1840 m is less obvious due to larger match point spacing. Only in the depth difference ratio plot in panel (c) all offsets are clearly visible as pairs of increased/decreased slope values. Note how the 10 cm offset imposed on the 1871 m match point to the right shows up clearly in the depth difference ratio plot (c) but is insignificant in the depth difference plot (b). Simultaneous inspection of depth difference and depth difference ratio plots is a sensitive way of detecting significant offsets, while depth-versus-depth plot are of little use except when very short sections are considered. The results of the matching are discussed in section 3.3.1.

used to match the NGRIP, GRIP, and GISP2 records in the 14.9 – 32.45 ka b2k time interval. This synchronization is the basis of the work presented in Rasmussen et al. (submitted), which is summarized below[4].

3.3.1 Summary of Rasmussen et al. (submitted)

The aim of the work is to synchronize the NGRIP, GRIP, and GISP2 records using climate-independent horizons with the purpose of comparing the climate records of the cores on a sub-centennial scale. Volcanic deposits (as recorded by the ECM, DEP, and SO_4^{2-} profiles) and peaks in the NH_4^+ concentration are used for the synchronization. The study covers the 14.9 – 32.45 ka b2k time interval, which is a period where the $\delta^{18}O$ records of the three cores even before synchronization can be seen to be significantly different. The matching has been performed in the following steps:

- The three ice cores are matched on a coarse scale using the stadial-interstadial shifts observed in the $\delta^{18}O$ and $[Ca^{2+}]$ records.
- Characteristic peaks and patterns of peaks are located in the ECM, DEP, and $[SO_4^{2-}]$ profiles and are used to define the match points. The selected match points are often supported by smaller features of both volcanic and non-volcanic origin, such as small neighbouring ECM/DEP peaks or characteristic patterns of $[NH_4^+]$ peaks, but these secondary match points are not used for the synchronization itself. A few very strong individual $[NH_4^+]$ peaks are used as match points.

  When wide peaks are encountered, the sharpest peak or the steepest flank in the data series with highest resolution available is chosen to define the match point. The maximum uncertainty of the synchronization is in general estimated to be 10 cm, with a few exceptions due to strange unusual peak shapes or limitations in data resolution.
- Individual match point locations are validated by inspection of the depth difference and depth difference ratio plots as illustrated in Fig. 3.8.
- The overall synchronization is validated by letting several investigators independently set match points in the same data sections, and by repeating the matching starting from the other end of the depth interval considered. Differences of 10 – 20 cm (the same order of magnitude as the match point location uncertainty) are handled by adjusting match point locations slightly, while sections with larger discrepancies have been re-matched independently by at least two investigators. In case of persistent discrepancies, no match points are accepted in the section in question. A single exception from this

[4]The manuscript uses the Greenland Stadial (GS) and Greenland Interstadial nomenclature of Björck et al. (1998) and Walker et al. (1999) and the numbering therein, although a change of numbering has recently been suggested by Rousseau et al. (in press).

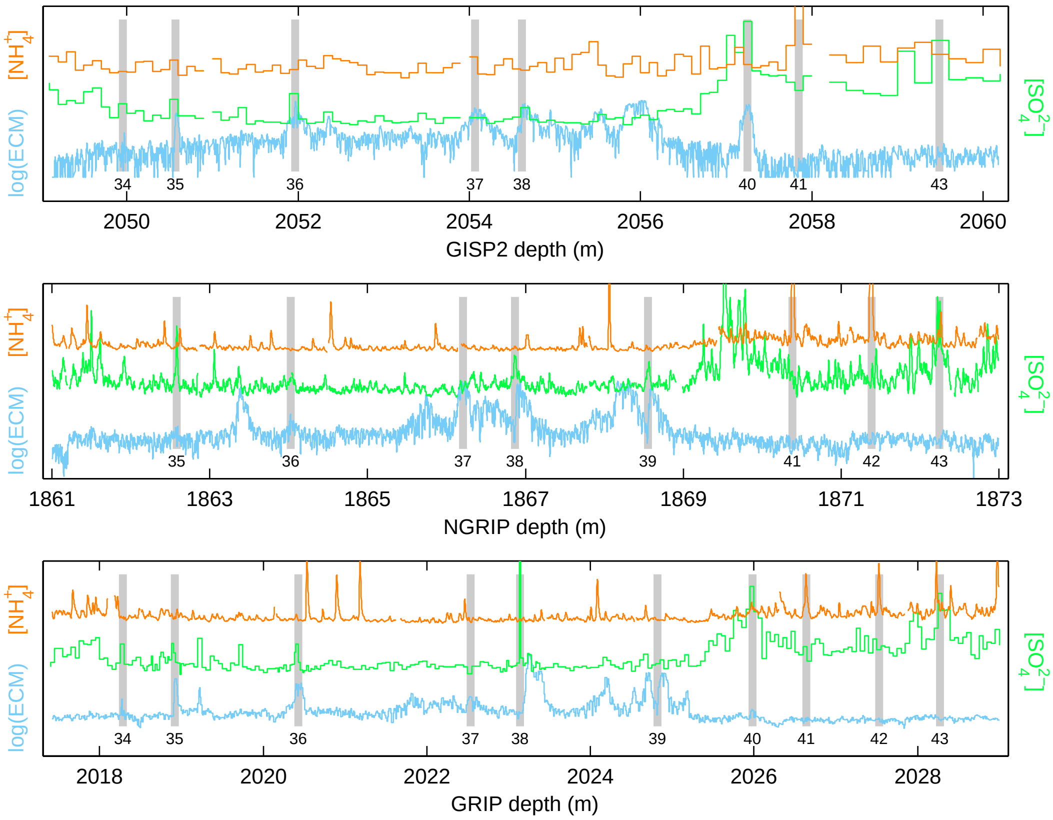

Figure 3.9: Synchronized section of the three cores. The ECM, [SO_4^{2-}], and [NH_4^+] data series are shown together with the match points. The ECM peaks appear less well-defined because of the logarithmic axis. Match point 34 has only been found in the GRIP and GISP2 records, and match points 40 in NGRIP and 39 in GISP2 have not been set because their positions within the wide [SO_4^{2-}]/ECM peaks are uncertain. Number 42 cannot be set in GISP2 because it is based on [NH_4^+] data, which are not available for the GISP2 core in sufficient resolution.

rule has been made in the time interval 22.2 – 23.8 ka b2k, where the synchronization presented is less certain than in other intervals, but still considered much more likely than the alternatives.

The result is 66 match points in the 14.9 – 32.45 ka b2k section, some of which are valid for two cores only. An example of a synchronized section is shown in Fig. 3.9. The match points are unevenly distributed with a minimum spacing of 10 yrs / 0.3 m and a maximum spacing of 2 kyrs / 40 m, and are all shown on a depth difference plot in Fig. 3.10. The shape of the GRIP-NGRIP depth difference curve (green curves) has positive slope in the top of the core because the GRIP drill site receives more accumulation than the NGRIP site, but at a depth of 1820 m, this is balanced by the more rapid thinning at GRIP, resulting in the annual layers of the NGRIP core being thicker than those of the GRIP core below 1820 m depth. This flow effect is also seen in the GISP2-NGRIP and GISP2-GRIP depth difference curves (orange curves), but the trend is disturbed in the 16.5 – 18.3 ka b2k interval (grey shaded areas, 1646 – 1688 m NGRIP depth, 1797 – 1841 m GRIP depth), across which the

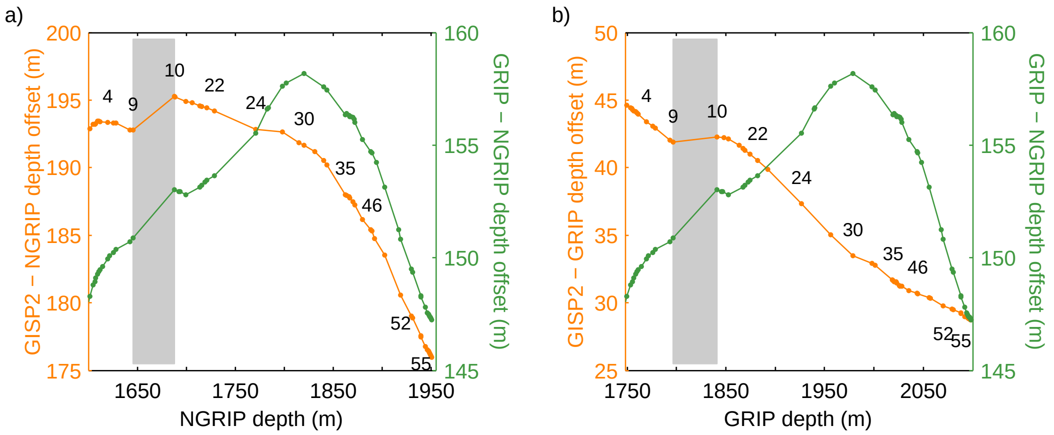

Figure 3.10: Depth differences between the match points in the three cores plotted versus NGRIP depth (a) and GRIP depth (b). The grey shaded areas mark an interval in which the GISP2-NGRIP and GISP2-GRIP depth difference curves (green curves) have an unexpected shape.

depth difference curves make a surprising kink. There are no match points in this 1.8 ky long period, and the behaviour of the depth difference curves inside the interval can therefore not be assessed. Just outside the anomaly, the GISP2 annual layers are 2.5 – 3% thinner than those in the NGRIP core (slope between −0.03 and −0.025), while the mean slope is 0.060 inside the anomaly. The GISP2 annual layers are thus on average about 9% thicker during the anomaly compared to the average value outside this period. When the same analysis is performed using the GISP2-GRIP synchronization, the corresponding slopes are −0.057 outside the interval and 0.009 inside, reflecting a 6 – 7% increase in mean GISP2 annual layer thickness within the anomaly period. The NGRIP-GRIP curve also has a small kink to the right of the grey shaded area, but the amplitude of this kink is only 0.2 m, and thus hardly represent a significant anomaly. Also, the average slope of the NGRIP-GRIP depth difference curve across the 16.5 – 18.3 ka b2k section does not deviate from the trend in the 1600 – 1800 m NGRIP depth interval, so the GRIP and NGRIP sites receive proportional amounts of precipitation within the 16.5 – 18.3 ka b2k section and outside this section, respectively. The most likely cause of the anomaly is thus that the GISP2 accumulation rates are rased by 7 – 9% on average in the 16.5 – 18.3 ka b2k interval. The anomaly could be caused by migration of the ice divide, as location of a drill site relative to an ice divide is known to have a large impact on the accumulation rate.

Using the match points of this work in conjunction with those of Rasmussen et al. (2006), the GICC05 timescale of Andersen et al. (submitted) has been applied to the GRIP and GISP2 cores. Between match points, the time scale has been interpolated linearly. Fig. 3.11 presents the position of the match points and 50 year average values of the δ^{18}O and [Ca^{2+}] records from the NGRIP, GRIP and GISP2 cores on the GICC05 time scale. In general, the [Ca^{2+}] profiles are very similar and anti-correlate with the δ^{18}O values (note the reversed

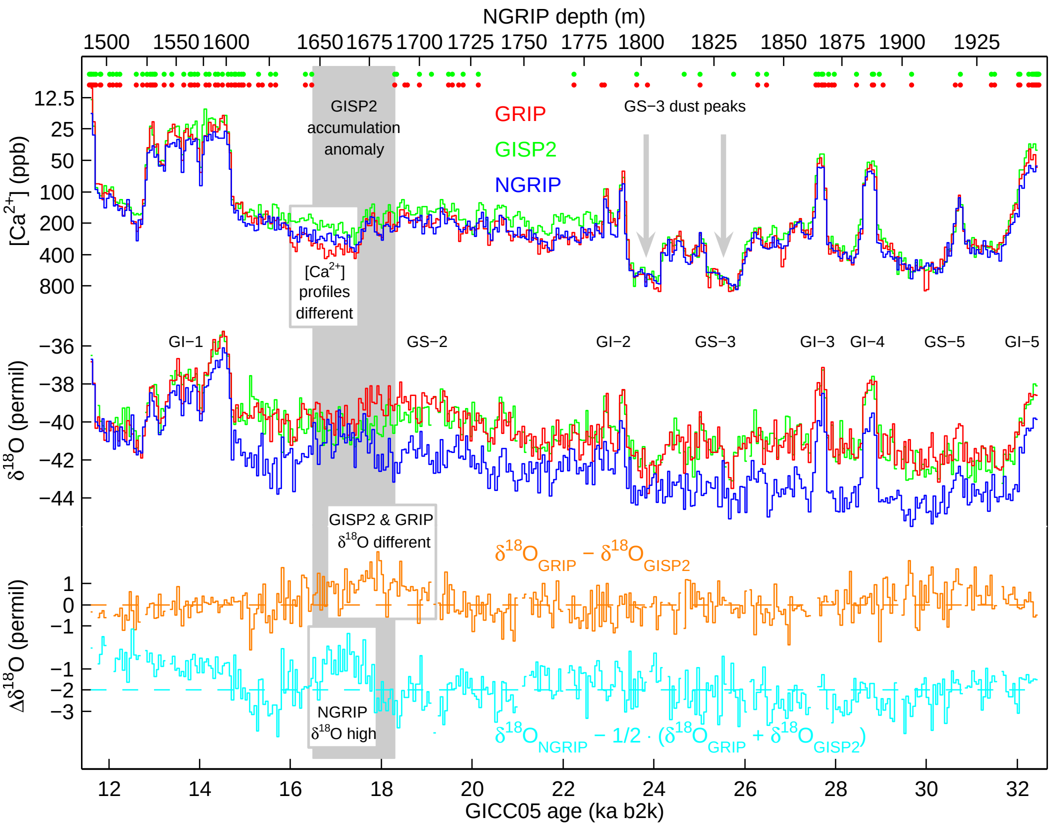

Figure 3.11: 50 year average values of δ^{18}O and [Ca^{2+}] on the GICC05 time scale (GRIP in red, GISP2 in green, NGRIP in blue). The dots in the top show the position of the match points used to synchronize the NGRIP ice core with the GRIP (red dots) and GISP2 (green dots) cores. In the bottom of the plot, differences between the isotope curves are shown. The shaded interval marks the GISP2 accumulation anomaly also shown in Fig. 3.10, and the three boxes indicate the position of areas of anomalous δ^{18}O values and [Ca^{2+}] values (see text for a discussion of these anomalies).

logarithmical [Ca^{2+}]-scale). The exceptions from this relationship are the two very distinct dust peaks in GS-3 first reported by Hammer et al. (1985). The agreement of the individual δ^{18}O profiles is less good on the centennial scale, but the profiles agree very well on amplitude and timing of the larger variations. However, a number of differences are observed roughly contemporaneous with the GISP2 accumulation anomaly (marked by grey shade in Fig. 3.11). These differences are described below and are marked by boxes in Fig. 3.11.

- In general, the NGRIP δ^{18}O values are offset in the glacial by about 2 permil relative to the GRIP and GISP2 values. However, in the period 16.4 – 17.9 ka b2k the NGRIP δ^{18}O values are on the same level as the GRIP/GISP2 δ^{18}O values. To emphasize this, the offset of the NGRIP δ^{18}O curve from the mean of the GRIP and GISP2 curves is plotted in below the isotope profiles of Fig. 3.11 (cyan curve).

- In the period 16.8 – 19.2 ka b2k the GRIP and GISP2 δ^{18}O curves deviate over a longer section, contrary to the normal situation in the entire section studied. This is seen most clearly in the curve showing the difference between GRIP and GISP2 δ^{18}O values (orange curve).

- The [Ca^{2+}] values are slightly elevated and the three profiles agree less well in the 16 – 17.5 ka b2k interval.

The anomalies are all located within the same 3 ky long period, indicating that they a likely to be related. The causes of these anomalies are unknown, but it must be concluded that the climatic conditions in this period are different from those of the preceding millennia. The results indicate that the atmospheric circulation patterns are different in this period, and that the air masses reaching the different drill sites originate from other source areas than what characterizes the common glacial situation.

3.4 Conclusion

The results presented in Andersen et al. (in press), Rasmussen et al. (accepted), and Rasmussen et al. (submitted) are all based on the advent of the GICC05 time scale and exploits the fact that several cores are available, or can be made available, on a common time scale. The work demonstrates that development of a common chronological framework for multiple ice cores brings along new possibilities for the study of the climate of the past. The most immediate of these is the chance to separate the regional climatic signal from the effects of phenomena only affecting single cores. A model has been developed to extract the regional accumulation signal from parallel accumulation records from the Holocene, and the results show a much improved correlation with the mean δ^{18}O profile than what is observed in the records from single cores. The extracted profiles represent more representative records of past Greenland climate, and are obvious candidates for correlation with records from other archives.

Although annual scale synchronization of the NGRIP, GRIP, and GISP2 records is not possible in the glacial, the concept of a common chronological framework can be successfully applied by matching the volcanic deposits in the cores. This synchronization is important because most existing ice core time scales differ significantly and in addition are difficult to compare directly due to lack of a generally accepted convention for reporting uncertainties. The uncertainty problem has not in itself been solved by the GICC05 time scale, because a fully adequate uncertainty estimate cannot be constructed without the availability of precise and independent age estimates, or an independent verification of the rules used for annual layer identification. However, the approach of synchronizing different ice cores using time scale independent horizons offers an alternative where the records of different cores can be compared in detail regardless of the incommensurability of the individual time scales and uncertainty estimates. The synchronized records show remarkable similarity over most of the time period investigated, but significant differences of unknown origin in both accumulation rates, δ^{18}O values, and Ca^{2+} concentrations are observed in the late glacial 16 – 19 ka b2k time interval.

The work demonstrates that even though the different Greenland ice core records at a first glance tell the same story, there are significant differences between the records that can only be detected and investigated using a high-resolution synchronization of the cores, and that the records contain information that can only be extracted using simultaneous investigation of multiple records. The results thus emphasize that reliable dating as well as precise synchronization of ice core records are essential elements in the analysis of the palaeoclimate and in the understanding of the dynamics of the climate system.

Concluding remarks and outlook

Precise dating of ice core records is the backbone of the study of the palaeoclimate, because reliable time scales are a prerequisite for mapping out past climate changes and perform comparison of records from different archives. Independent time scales are particulary valuable when investigating the relative timing of climate changes as recorded in different records, especially if the uncertainty of the time scale can be quantified. For most Greenland and some Antarctic ice cores, independent time scales can be constructed by identification and counting of annual layers in at least parts of the cores. The identification of annual layers is most often tackled by visual inspection of selected data profiles, or by semi-automated methods that reproduce the results of visual annual layer identification. As described in section 2.2.1, the new GICC05 time scale has been constructed in this way and is a fully independent time scale. With regard to the uncertainty, a novel approach has been introduced with the aim of providing a consistent estimate of the interpretation uncertainty based on the clarity of the annual signal. Although the problem of insufficient assessment of the uncertainty thus is partly handled for the GICC05 time scale, automated ways of annual layer identification would allow greater objectiveness in the annual layer identification procedure and thus further improve the time scale consistency and uncertainty estimation.

This thesis presents some advances in this direction by introducing two fundamentally different automated approaches to the problem of defining annual layers based on multi-parameter data. The first method is an attempt to mimic the way annual layers are defined by visual inspection of multi-parameter data sets. In this approach, which is described in section 2.1, peaks are identified and marked in one series at a time, and then combined to form an annual layer sequence using objective criteria. Only the combination of the marks has been automated in the work presented here, but the method can be combined with automated single-species peak detection algorithms to form a fully automated approach. Some calibration and tuning of the method is necessary, but the sensitivity of the result to the calibration procedure can be evaluated objectively by varying the values of the control parameters of the method. The second method extracts the common annual signal from sequences of multi-parameter data by identifying the signature of the annual signal in a Dynamical Decorrelation decomposition of the data. The extraction algorithm is unsupervised, and thus requires no calibration, and can either extract a data series containing the annual signal or determine the mean annual layer thickness directly (section 2.2.2). In the first case, the annual layers still have to be identified using a peak detection algorithm, but the complexity of the problem is greatly reduced as only one data series needs to be considered. When used to determine mean annual layer thicknesses, the method is fully objective and requires no calibration or training sets as long as the resolution of the data is sufficient.

The automated methods presented in the thesis are all sensitive to insufficient data resolution. While investigators identifying annual layers by visual inspection to a large degree can adapt to marginal and varying data resolution, the results show that the automated methods presented here only work well when most of the series in the multi-parameter data set resolve the annual layers. For future projects, this calls for advance planning to ensure sufficient measurement resolution if automated dating methods are going to be applied, and for existing records the need for resolution optimization is emphasized. Two independent methods for enhancing the resolution of NGRIP CFA data are presented. The methods are inherently different, as one is spectral and based on measured analysis system characteristics (section 1.1), while the other method estimates the amount of smoothing using a Monte Carlo approach (section 1.2). While the spectral approach has been routinely applied to long sections of data that have been used for dating, the Monte Carlo approach has only been applied to short sections of data for development and evaluation purposes. Despite their methodical differences, the two methods produce consistent results, and can be applied to essentially all types of data that have undergone some kind of smoothing or diffusion, thereby improving data quality and increasing the usability of the data for dating purposes. However, for the GRIP and NGRIP records the resolution improvement obtainable by the spectral method is not sufficient to allow application of the automated dating methods to pre-Holocene records. Further development of the Monte Carlo resolution enhancement approach into an operational method and the application of this method to long data sets will show whether the resolution can be improved sufficiently to allow automated dating of pre-Holocene records.

Equally important as reliable time scales is the establishment of chronological frameworks for studying multiple records on common time scales. The concept applies to all types of records, but is here applied to ice core data only. Where data resolution and availability allow it, several cores can be dated in parallel, greatly increasing the reliability of the resulting time scale and providing unique possibilities for annual-scale comparison of the records. In cases where annual layer identification is not possible in all the records, the records can be synchronized using simultaneous horizons, making the application of one time scale to all records possible. In either case the synchronized records can be used to investigate the relation between the parallel records and to extract common features that are obscured by noise and the effect of local phenomena in the individual records. This is exemplified in sections 3.1 and 3.2, where regional isotope and accumulation patterns are extracted from multiple Holocene records, and in section 3.3, where detailed synchronization of the GRIP, NGRIP, and GISP2 records permits identification of periods with anomalous δ^{18}O and accumulation conditions.

The synchronization of the GRIP, NGRIP, and GISP2 records can be extended back in time based on robust matching of common features of mainly volcanic origin. However, the match points are in some sections rather sparse, which limits the resolution of the subsequent analysis of the synchronized records. In contrast to this, matching of records using data from optical logging tools holds the potential for high-resolution matching, but lacks precise depth control due to elastic cable stretching and other technical issues. An integrated approach combining the matching approach presented here with tephra match point validation and the use of data from optical logging tools can possibly provide a detailed and precise matching of the entire undisturbed records. The synchronized records will allow pin-pointing of periods of atypical climate conditions, detailed assessment of issues related to timing of past climate change, and identification of periods with increased spatial differences between the records. In this way, improved methods for dating and synchronization of ice cores can unravel the mechanisms of past climate change and widen our understanding of the climate of the last glacial cycle.

Bibliography

Alley, R., Ágústdóttir, A., 2005. The 8k event: cause and consequences of a major Holocene abrupt climate change. Quaternary Science Reviews 24, 1123–1149.

Alley, R., Mayewski, P., Sowers, T., Stuiver, M., Taylor, K., Clark, P., 1997a. Holocene climatic instability: A prominent widespread event 8200 yr ago. Geology 25, 483–486.

Alley, R. B., Shuman, C. A., Meese, D. A., Gow, A. J., Taylor, K. C., Cuffey, K. M., Fitzpatrick, J. J., Grootes, P. M., Zielinski, G. A., Ram, M., Spinelli, G., Elder, B., 1997b. Visual-stratigraphic dating of the GISP2 ice core: Basic, reproducibility, and application. Journal of Geophysical Research 102 (C12), 26367–26381.

Andersen, K. K., Ditlevsen, P. D., Rasmussen, S. O., Clausen, H. B., Johnsen, S. J., Steffensen, J. P., in press. Retrieving a common accumulation record from Greenland ice cores for the past 1800 years. Journal of Geophysical Research, doi: 10.1029/2005JD006765.

Andersen, K. K., Svensson, A., Johnsen, S., Rasmussen, S. O., Bigler, M., Röthlisberger, R., Ruth, U., Siggaard-Andersen, M.-L., Steffensen, J. P., Dahl-Jensen, D., Vinther, B. M., Clausen, H. B., submitted. The Greenland Ice Core Chronology 2005, 15–42 kyr. Part 1: Constructing the time scale, Quaternary Science Reviews.

Barber, D., Dyke, A., Hillaire-Marcel, C., Jennings, A., Andrews, J., Kerwin, M., Bilodeau, G., McNeely, R., Southon, J., Morehead, M., Gagnon, J.-M., 1999. Forcing of the cold event of 8,200 years ago by catastrophic drainage of Laurentide lakes. Nature 400, 344–348.

Bard, E., Arnold, M., Mangerud, M., Paterne, M., Labeyrie, L., Duprat, J., Mélières, M. A., Sonstegaard, E., Duplessy, J. C., 1994. The North Atlantic atmosphere-sea surface ^{14}C gradient during the Younger Dryas climatic event. Earth and Planetary Science Letters 126, 275–287.

Bay, R. C., Bramall, N. E., Price, P. B., Clow, G. D., Hawley, R. L., Udisti, R., Castellano, E., 2006. Globally synchronous ice core volcanic tracers and abrupt cooling during the last glacial period. Journal of Geophysical Research 111, D11108.

Bay, R. C., Price, P. B., Clow, G. D., Gow, A. J., 2001. Climate logging with a new rapid optical technique at Siple Dome. Geophysical Research Letters 28 (24), 4635–4638.

Bigler, M., 2004. Hochauflösende Spurenstoffmessungen an polaren Eisbohrkernen: Glaziochemische und klimatische Prozessstudien, Ph.D. dissertation, University of Bern, Switzerland.

Birks, H., Gulliksen, S., Haflidason, H., Mangerud, J., Possnert, G., 1996. New radiocarbon dates for the Vedde Ash and the Saksunarvatn Ash from Western Norway. Quaternary Research 45 (2), 119–127.

Björck, S., Muscheler, R., Kromer, B., Andresen, C., Heinemeier, J., Johnsen, S., Conley, D., Koç, N., Spurk, M., Veski, S., 2001. High-resolution analyses of an early Holocene climate event may imply decreased solar forcing as an important climate trigger. Geology 12, 1107–1110.

Björck, S., Rundgren, M., Ingólfsson, Ó., Funder, S., 1997. The Preboreal oscillation around the Nordic Seas: terrestrial and lacustrine responses. Journal of Quaternary Science 12, 455–465.

Björck, S., Walker, M. J. C., Cwynar, L. C., Johnsen, S., Knudsen, K.-L., Lowe, J. J., Wohlfarth, B., INTIMATE Members, 1998. An event stratigraphy for the Last Termination in the North Atlantic region based on the Greenland ice-core record: a proposal by the INTIMATE group. Journal of Quaternary Science 13 (4), 283–292.

Blunier, T., Brook, E. J., 2001. Timing of millennial-scale climate change in Antarctica and Greenland during the last glacial period. Science 291, 109–112.

Blunier, T., Chappellaz, J., Schwander, J., Dällenbach, A., Stauffer, B., Stocker, T., Raynaud, D., Jouzel, J., Clausen, H., Hammer, C., Johnsen, S., 1998. Asynchrony of Antarctic and Greenland climate change during the last glacial period. Nature 394, 739–743.

Blunier, T., Schwander, J., 2000. Gas enclosure in ice: Age difference and fractionation. In: Hondoh, T. (Ed.), Physics of Ice Core Records. Hokkaido University Press, Sapporo, pp. 307–326.

Bond, G., Showers, W., Cheseby, M., Lotti, R., Almasi, P., deMenocal, P., Priore, P., Cullen, H., Hajdas, I., Bonani, G., 1997. A pervasive millennial-scale cycle in North Atlantic Holocene and glacial climates. Science 278 (5341), 1257–1266.

Chaudhuri, P., Marron, J., 1999. SiZer for exploration of structures in curves. Journal of the American Statistical Association 94 (447), 807–823.

Dansgaard, W., Clausen, H., Gundestrup, N., Hammer, C., Johnsen, S., Kristinsdottir, P., Reeh, N., 1982. A new Greenland deep ice core. Science 218, 1273–1277.

Dansgaard, W., Johnsen, S., Clausen, H., Dahl-Jensen, D., Gundestrup, N., Hammer, C., Hvidberg, C., Steffensen, J., Sveinbjörnsdottir, A., Jouzel, J., Bond, G., 1993. Evidence for general instability of past climate from a 250-kyr ice-core record. Nature 364 (6434), 218–220.

Fisher, D. A., Reeh, N., Clausen, H. B., 1985. Stratigraphic noise in time series derived from ice cores. Annals of Glaciology 7, 76–83.

Ghil, M., Allen, R. M., Dettinger, M. D., Ide, K., Kondrashov, D., Mann, M. E., Robertson, A., Tian, Y., Varadi, F., Yiou, P., 2002. Advanced spectral methods for climatic time series. Reviews of Geophysics 40 (1), 1001.

Grinsted, A., Moore, J. C., Jevrejeva, S., 2004. Application of the cross wavelet transform and wavelet coherence to geophysical time series. Nonlinear Processes in Geophysics 11, 561–566.

Grönvold, K., Óskarsson, N., Johnsen, S. J., Clausen, H. B., Hammer, C. U., Bond, G., Bard, E., 1995. Ash layers from Iceland in the Greenland GRIP ice core correlated with oceanic and land sediments. Earth and Planetary Science Letters 135, 149–155.

Grootes, P. M., Stuiver, M., 1997. Oxygen 18/16 variability in Greenland snow and ice with 10^{-3} to 10^{5}-year time resolution. Journal of Geophysical Research 102, 26455–26470.

Hammer, C., 1989. Dating by physical and chemical seasonal variations and reference horizons. In: Oeschger, H., Langway, C.C., J. (Eds.), Dahlem Konference: The Environmental Record in Glaciers and Ice Sheets. Physical, Chemical, and Earth Sciences Research Report 8. John Wiley, New York, pp. 99–121.

Hammer, C., Clausen, H., Dansgaard, W., Neftel, A., Kristinsdottir, P., Johnson, E., 1985. Continuous impurity analysis along the Dye-3 deep core. In: Langway, C.C., J., Oeschger, H., Dansgaard, W. (Eds.), Greenland Ice Core: Geophysics, Geochemistry, and the Environment. Geophys. Monogr. Ser., vol. 33. American Geophysical Union (AGU), Washington, D.C., pp. 90–94.

Hammer, C. U., Clausen, H. B., Langway, Jr., C. C., 1994. Electrical conductivity method (ECM) stratigraphic dating of the Byrd Station ice core, Antarctica. Annals of Glaciology 20, 115–120.

Hammer, C. U., Clausen, H. B., Tauber, H., 1986. Ice-core dating of the Pleistocene/Holocene boundary applied to a calibration of the ^{14}C time scale. Radiocarbon 28, 284–291.

Hannig, J., Marron, J. S., 2006. Advanced distribution theory for SiZer. Journal of the American Statistical Association 101 (474), 484–499.

Hansen, L. K., Larsen, J., Kolenda, T., 2000. On independent component analysis for multimedia signals. In: Guan, L., Kung, S. Y., Larsen, J. (Eds.), Multimedia Image and Video Processing. CRC Press, Ch. 7, pp. 175–199.

Hyvärinen, A., Karhunen, J., Oja, E., 2001. Independent Component Analysis. John Wiley & Sons.

Jóhansen, J., 1975. Pollen diagrams from the Shetland and Faroe Islands. New Phytologist 75, 369–387.

Johnsen, S., Dahl-Jensen, D., Dansgaard, W., Gundestrup, N., 1995. Greenland palaeotemperatures derived from GRIP bore hole temperature and ice core isotope profiles. Tellus 47B, 624–629.

Johnsen, S. J., Andersen, N., 1978. On power estimation in maximum entropy spectral analysis. Geophysics 43, 681–690.

Johnsen, S. J., Clausen, H. B., Dansgaard, W., Fuhrer, K., Gundestrup, N., Hammer, C. U., Iversen, P., Jouzel, J., Stauffer, B., Steffensen, J. P., 1992. Irregular glacial interstadials recorded in a new Greenland ice core. Nature 359, 311–313.

Johnsen, S. J., Clausen, H. B., Dansgaard, W., Gundestrup, N. S., Hammer, C. U., Andersen, U., Andersen, K. K., Hvidberg, C. S., Dahl-Jensen, D., Steffensen, J. P., Shoji, H., Sveinbjörnsdóttir, Á. E., White, J., Jouzel, J., Fisher, D., 1997. The δ^{18}O record along the Greenland Ice Core Project deep ice core and the problem of possible Eemian climatic instability. Journal of Geophysical Research 102 (C12), 26397–26410.

Johnsen, S. J., Dahl-Jensen, D., Gundestrup, N., Steffensen, J. P., Clausen, H. B., Miller, H., Masson-Delmotte, V., Sveinbjörnsdottir, A. E., White, J., 2001. Oxygen isotope and palaeotemperature records from six Greenland ice-core stations: Camp Century, Dye-3, GRIP, GISP2, Renland and NorthGRIP. Journal of Quaternary Science 16, 299–307.

Klitgaard-Kristensen, D., Sejrup, H.-P., Haflidason, H., Johnsen, S., Spurk, M., 1998. A regional 8200 cal. yr BP cooling event in northwest Europe, induced by final stages of the Laurentide ice-sheet deglaciation? Journal of Quaternary Science 13 (165–169).

McDermott, F., Mattey, D. P., Hawkesworth, C., 2001. Centennial-scale Holocene climate variability revealed by a high-resolution speleothem δ^{18}O record from SW Ireland. Science 294 (5545), 1328–1331.

Meese, D. A., Gow, A. J., Alley, R. B., Zielinski, G. A., Grootes, P. M., Ram, M., Taylor, K. C., Mayewski, P. A., Bolzan, J. F., 1997. The Greenland Ice Sheet Project 2 depth-age scale: Methods and results. Journal of Geophysical Research 102 (C12), 26411–26423.

Molgedey, L., Schuster, H., 1994. Separation of independent signals using time-delayed correlations. Physical Review Letters 72 (23), 3634–3637.

Mortensen, A., Bigler, M., Grönvold, K., Steffensen, J., Johnsen, S., 2005. Volcanic ash layers from the Last Glacial Termination in the NGRIP ice core. Journal of Quaternary Science 20 (3), 209–219.

Mosegaard, K., Tarantola, A., 1995. Monte Carlo sampling of solutions to inverse problems. Journal of Geophysical Research. 100 (B7), 12,431–12,447.

Mudelsee, M., 2000. Ramp function regression: a tool for quantifying climate transitions. Computers & Geosciences 26, 293–307.

NGRIP members, 2004. High-resolution record of Northern Hemisphere climate extending into the last interglacial period. Nature 431, 147–151.

Palmer, A. S., van Ommen, T. D., Curran, M. A. J., Morgan, V., Souney, J. M., Mayewski, P. A., 2001. High-precision dating of volcanic events (A.D. 1301 – 1995) using ice cores from Law Dome, Antarctica. Journal of Geophysical Research 106 (D22), 28,089–28,095.

Parrenin, F., Jouzel, J., Waelbroeck, C., Ritz, C., Barnola, J., 2001. Dating the Vostok ice core by an inverse method. Journal of Geophysical Research 106 (D23), 31,837–31,851.

Pohjola, V. A., Moore, J. C., Isaksson, E., Jauhiainen, T., van de Wal, R. S. W., Martma, T., Meijer, H. A. J., Vaikmäe, R., 2002. Effect of periodic melting on geochemical and isotopic signals in an ice core from Lomonosovfonna, Svalbard. Journal of Geophysical Research 107 (D4), 1–14.

Qi, Y., Minka, T. P., Picard, R. W., 2002. Bayesian spectrum estimation of unevenly sampled nonstationary data. In: Proceedings of the IEEE International Conference on Acoustics, Speech, and Signal Processing. Vol. 2. pp. 1473–1476.

Rasmussen, S. O., 2002. Dynamisk dekorrelation anvendt til iskernedatering, Master thesis, University of Copenhagen.

Rasmussen, S. O., Andersen, K. K., Johnsen, S. J., Bigler, M., McCormack, T., 2005. Deconvolution-based resolution enhancement of chemical ice core records obtained by Continuous Flow Analysis. Journal of Geophysical Research 110, D17304.

Rasmussen, S. O., Andersen, K. K., Siggaard-Andersen, M.-L., Clausen, H. B., 2002. Extracting the annual signal from Greenland ice-core chemistry and isotopic records. Annals of Glaciology 35, 131–135.

Rasmussen, S. O., Andersen, K. K., Svensson, A. M., Steffensen, J. P., Vinther, B., Clausen, H. B., Siggaard-Andersen, M.-L., Johnsen, S. J., Larsen, L. B., Dahl-Jensen, D., Bigler, M., Röthlisberger, R., Fischer, H., Goto-Azuma, K., Hansson, M., Ruth, U., 2006. A new Greenland ice core chronology for the last glacial termination. Journal of Geophysical Research 111, D06102.

Rasmussen, S. O., Seierstad, I. K., Andersen, K. K., Bigler, M., Dahl-Jensen, D., Johnsen, S. J., submitted. Synchronization of the NGRIP, GRIP, and GISP2 ice cores across MIS 2 and palaeoclimatic implications, Quaternary Science Reviews.

Rasmussen, S. O., Vinther, B. M., Clausen, H. B., Andersen, K. K., accepted. Early Holocene climate oscillations recorded in three Greenland ice cores, Quaternary Science Reviews.

Reeh, N., 1989. Dating by ice flow modeling: A useful tool or an exercise in applied mathematics? In: Oeschger, H., Langway, Jr., C. C. (Eds.), Dahlem Konference: The Environmental Record in Glaciers and Ice Sheets. Physical, Chemical, and Earth Sciences Research Report 8. John Wiley, New York.

Reimer, P. J., Baillie, M. G. L., Bard, E., Bayliss, A., Beck, J. W., Bertrand, C. J. H., Blackwell, P. G., Buck, C. E., Burr, G. S., Cutler, K. B., Damon, P. E., Edwards, R. L., Fairbanks, R. G., Friedrich, M., Guilderson, T. P., Hogg, A. G., Hughen, K. A., Kromer, B., McCormac, G., Manning, S., Ramsey, C. B., Reimer, R. W., Remmele, S., Southon, J. R., Stuiver, M., Talamo, S., Taylor, F. W., van der Plicht, J., Weyhenmeyer, C. E., 2004. Radiocarbon calibration from 0–26 cal kyr BP. Radiocarbon 46 (3), 1029–1058.

Renssen, H., Goosse, H., Fichefet, T., 2002. Modeling the effect of freshwater pulses on the early Holocene climate: the influence of high frequency climate variability. Paleoceanography 17 (2), 1020.

Renssen, H., Goosse, H., Fichefet, T., Campin, J.-M., 2001. The 8.2 kyr BP event simulated by a global atmosphere-sea-ice-ocean model. Geophysical Research Letters 28, 1567–1570.

Rohling, E., Pälike, H., 2005. Centennial-scale climate cooling with a sudden cold event around 8,200 years ago. Nature 434, 975–979.

Röthlisberger, R., Bigler, M., Hutterli, M., Sommer, S., Stauffer, B., Junghans, H., Wagenbach, D., 2000. Technique for continuous high-resolution analysis of trace substances in firn and ice cores. Environmental Science and Technology 34 (2), 338–342.

Rousseau, D., Kuklac, G., McManus, J., in press. What is what in the ice and the ocean? Quaternary Science Reviews.

Ruth, U., Wagenbach, D., Steffensen, J., Bigler, M., 2003. Continuous record of microparticle concentration and size distribution in the central Greenland NGRIP ice core during the last glacial period. Journal of Geophysical Research. 108, 4098.

Sigg, A., 1990. Wasserstoffperoxid-Messungen an Eisbohrkernen aus Grönland und der Antarktis und ihre atmosphärenchemische Bedeutung, Ph.D. dissertation, University of Bern, Switzerland.

Stuiver, M., Grootes, P. M., 2000. GISP2 Oxygen isotope ratios. Quaternary Research 53, 277–284.

Svensson, A., Andersen, K. K., Bigler, M., Clausen, H. B., Dahl-Jensen, D., Davies, S. M., Johnsen, S. J., Muscheler, R., Rasmussen, S. O., Röthlisberger, R., Steffensen, J. P., Vinther, B. M., submitted. The Greenland Ice Core Chronology 2005, 15–42 kyr. Part 2: Comparison to other records, Quaternary Science Reviews.

Taylor, K. C., Alley, R. B., Meese, D. A., Spencer, M. K., Brook, E. J., Dunbar, N. W., Finkel, R. C., Gow, A. J., Kurbatov, A. V., Lamorey, G. W., Mayewski, P. A., Meyerson, E. A., Nishiizumi, K., Zielinski, G. A., 2004. Dating the Siple Dome (Antarctica) ice core by manual and computer interpretation of annual layering. Journal of Glaciology 50 (170), 453–461.

Thejll, P., Schmith, T., 2005. Limitations on regression analysis due to serially correlated residuals: Application to climate reconstruction from proxies. Journal of Geophysical Research 110, D18103.

Udisti, R., Becagli, S., Castellano, E., Delmonte, B., Jouzel, J., Petit, J. R., Schwander, J., Stenni, B., Wolff, E. W., 2004. Stratigraphic correlations between the European Project for Ice Coring in Antarctica (EPICA) Dome C and Vostok ice cores showing the relative variations of snow accumulation over the past 45 kyr. Journal of Geophysical Research 109, D08101.

Vinther, B. M., Clausen, H. B., Johnsen, S. J., Rasmussen, S. O., Andersen, K. K., Buchardt, S. L., Dahl-Jensen, D., Seierstad, I. K., Siggaard-Andersen, M.-L., Steffensen, J. P., Svensson, A. M., Olsen, J., Heinemeier, J., 2006. A synchronized dating of three Greenland ice cores throughout the Holocene. Journal of Geophysical Research 111, D13102.

von Grafenstein, U., Erlenkeuser, H., Brauer, A., Jouzel, J., Johnsen, S. J., 1999. A Mid-European decadal isotope-climate record from 15,500 to 5000 years B.P. Science 284 (5420), 1654–1657.

Waldmeier, M., 1961. The sunspot-activity in the years 1610–1960. Schulthess & Co AG, Zürich, data (updated to 2004) available from ftp://ftp.ngdc.noaa.gov.

Walker, M. J. C., Björck, S., Lowe, J. J., Cwynar, L. C., Johnsen, S., Knudsen, K.-L., Wohlfarth, B., 1999. Isotopic 'events' in the GRIP ice core: a stratotype for the Late Pleistocene. Quaternary Science Reviews 18 (10–11), 1143–1150.

Wastegård, S., Björck, S., Possnert, G., Wohlfarth, B., 1998. Evidence for the occurrence of Vedde Ash in Sweden: radiocarbon and calendar age estimates. Journal of Quaternary Science 13, 271–274.

Wiersma, A., Renssen, H., 2006. Model-data comparison for the 8.2 ka BP event: Confirmation of a forcing mechanism by catastrophic drainage of Laurentide Lakes. Quaternary Science Reviews 25 (1–2), 63–88.

Wolff, E. W., Basile, I., Petit, J.-R., Schwander, J., 1999. Comparison of Holocene electrical records from Dome C and Vostok. Annals of Glaciology 29, 89–93.

Co-author statements

Co-authors statements signed by all co-authors have been collected in a folder and has been handed over to the chairman of the evaluation committee. The text is reproduced below.

Rasmussen et al. (2005) co-author statement

The undersigned co-authors hereby recognise that this paper is used as a part of the PhD dissertation of Sune Olander Rasmussen.

SOR had a leading role in the development of the mathematical technique. He performed most of the numerical analysis, and was the leading author in the preparation of the manuscript text and illustrations.

Rasmussen et al. (2006) co-author statement

The undersigned co-authors hereby recognise that this paper is used as a part of the PhD dissertation of Sune Olander Rasmussen.

SOR developed the tools used for the annual layer counting procedure, and was among the group of people doing the bulk part of the counting. He coordinated and performed much of the evaluation and analysis of the results, and was the leading author in the preparation of the manuscript text and illustrations.

Andersen et al. (in press) co-author statement

The undersigned co-authors hereby recognise that this paper is used as a part of the PhD dissertation of Sune Olander Rasmussen.

SOR participated in the development of the model and was responsible for most of the numerical modelling work. He made significant contributions to the illustrations and the manuscript text.

Rasmussen et al. (accepted) co-author statement

The undersigned co-authors hereby recognise that this paper is used as a part of the PhD dissertation of Sune Olander Rasmussen.

SOR had a leading role in the numerical work and analysis, and was the leading author in the preparation of the manuscript text and illustrations.

Rasmussen et al. (submitted) co-author statement

The undersigned co-authors hereby recognise that this paper is used as a part of the PhD dissertation of Sune Olander Rasmussen.

SOR was among the three authors making the synchronization upon which the work is based. SOR made significant contributions to the analysis and discussion of the results and was the leading author in the preparation of the manuscript text and illustrations.

Deconvolution-based resolution enhancement of chemical ice core records obtained by continuous flow analysis

S. O. Rasmussen, K. K. Andersen, and S. J. Johnsen
Ice and Climate Research, University of Copenhagen, Copenhagen, Denmark

M. Bigler[1]
Climate and Environmental Physics, Physics Institute, University of Bern, Bern, Switzerland

T. McCormack
British Antarctic Survey, Cambridge, UK

Received 20 December 2004; revised 8 April 2005; accepted 14 June 2005; published 13 September 2005.

[1] Continuous flow analysis (CFA) has become a popular measuring technique for obtaining high-resolution chemical ice core records due to an attractive combination of measuring speed and resolution. However, when analyzing the deeper sections of ice cores or cores from low-accumulation areas, there is still need for further improvement of the resolution. Here a method for resolution enhancement of CFA data is presented. It is demonstrated that it is possible to improve the resolution of CFA data by restoring some of the detail that was lost in the measuring process, thus improving the usefulness of the data for high-resolution studies such as annual layer counting. The presented method uses deconvolution techniques and is robust to the presence of noise in the measurements. If integrated into the data processing, it requires no additional data collection. The method is applied to selected ice core data sequences from Greenland and Antarctica, and the results demonstrate that the data quality can be significantly improved.

Citation: Rasmussen, S. O., K. K. Andersen, S. J. Johnsen, M. Bigler, and T. McCormack (2005), Deconvolution-based resolution enhancement of chemical ice core records obtained by continuous flow analysis, *J. Geophys. Res.*, *110*, D17304, doi:10.1029/2004JD005717.

1. Introduction

[2] Chemical ice core records contain a wealth of information about the composition of the past atmosphere and provide information about large-scale changes of circulation patterns and climatic conditions in both the source regions and on the polar ice sheets [*Legrand and Mayewski*, 1997]. If the depth resolution of the measurement is sufficient even annual layers and events on a subannual timescale can be resolved. Examples include deposits from volcanic eruptions [e.g., *Bigler et al.*, 2002], biomass burning events [e.g., *Fuhrer et al.*, 1996], and the identification and counting of annual layers, which is of paramount importance for the precise dating of ice cores [*Hammer et al.*, 1978; *Meese et al.*, 1997; *Alley et al.*, 1997].

[3] In recent years, the use of Continuous Flow Analysis (CFA) systems has become increasingly popular for chemical ice core analysis [*Sigg et al.*, 1994; *Anklin et al.*, 1998; *Röthlisberger et al.*, 2000; *McConnell et al.*, 2002]. Continuously melted subsections of the ice core provide a steady sample flow which is immediately analyzed by means of fluorescence and absorption spectrophotometric detection methods. CFA stands out because good resolution, high measuring speed, and the elimination of time-consuming sample cleaning is combined, without compromising analytical accuracy [*Littot et al.*, 2002]. However, because many meters of ice core have to be analyzed in order to provide long, continuous data sets the trade-off between measuring speed and resolution is still an important issue. The resolution is mainly limited by the geometry of the melting device and by how much turbulent mixing takes place in small volumes within the setup (inside, e.g., the debubbler, pump tubes, reaction columns, and flow cells). Although cycles with short wavelengths are obliterated by this mixing some of the lost details can be restored using deconvolution techniques. In this paper a method of restoring CFA data to optimize their potential for example for annual layer counting is presented. The method is mathematically similar to the method used for correcting the effect of the diffusion in the ice of the stable isotopes [*Johnsen*, 1977; *Johnsen et al.*, 2000]. However, the information

[1]Now at Ice and Climate Research, University of Copenhagen, Copenhagen, Denmark.

0148-0227/05/2004JD005717$09.00

needed to correct for diffusion of stable isotopes has to be obtained from diffusion and firnification models whereas in this study the correction can be derived directly from calibration measurements. The method can be integrated in the data processing work line so that only a little extra work is needed. How much the resolution can be improved depends on the signal-to-noise ratio, and at the same time the resolution enhanced data series are filtered in an optimal manner. Although the method is applied only to CFA chemistry data here, it can be used for any liquid-based continuous measurement or sampling system where the sample undergoes mixing before or during the measurement.

2. Data

[4] Two data sources have been used in this work. The method has been developed using data from the North Greenland Ice Core Project (NGRIP) ice core [*NGRIP Members*, 2004], and the method has also been applied to data from the upper part of the ice core from Berkner Island, inside the Filchner-Ronne Ice Shelf, Antarctica, to illustrate that the method is generally applicable and robust.

[5] During the NGRIP field season in year 2000, measurements were performed on the NGRIP deep ice core using a Continuous Flow Analysis (CFA) setup [*Röthlisberger et al.*, 2000]. For the depth interval from 1404.7 to 2930.4 m a 3 cm $\times$ 3 cm cross section of ice was cut from the main core in 1.65 m pieces and continuously melted for CFA measurements at a speed of 3–4 cm min^{-1}. The analysis systems measured, among other parameters, the concentrations of NH_4^+, Ca^{2+}, NO_3^-, Na^+, and SO_4^{2-} and the electrolytical conductivity of the meltwater [*Bigler*, 2004]. Although the data collection resolution is around one millimeter, the actual data resolution only allows identification of cycles with wavelengths down to between one and two centimeters. The presented resolution enhancement method is applied to the NGRIP [NH_4^+], [Ca^{2+}], and conductivity data series only, but could be applied in a similar way to the other NGRIP CFA data series. The resolution enhanced data series from NGRIP are currently being used for interpretation of the NGRIP chemistry record for dating purposes (S. O. Rasmussen et al., A new Greenland ice core chronology for the last glacial termination, submitted to *Journal of Geophysical Research*, 2005).

[6] The CFA setup at the British Antarctic Survey used to analyze ice cores from Berkner Island is in principle similar to the NGRIP setup although fewer parameters are measured. Because of the low impurity content in the Holocene part of the ice core, and the fact that Antarctic ice cores in general contain less impurities than Greenland ice cores, the signal-to-noise ratio is significantly worse than for the NGRIP data, especially for the Ca^{2+} subsystem. The resolution enhancement method is applied to a 1 m long section of Berkner Island [Ca^{2+}] data from 27 m depth in order to demonstrate how the method deals with noisy data. It should be pointed out that the quality of the presented data section is not representative of the general Berkner Island data quality. The processing of the first season of Berkner Island data is ongoing, for which reason the data are presented in uncalibrated units and on a measurement timescale rather than on a depth scale.

3. Resolution Enhancement

[7] The sample flow from the melting device passes through a debubbler and is split up to feed the different CFA analysis subsystems where it is continuously mixed with reagents that allow fluorescent or absorbent complexes to form. The amount of complex is measured with spectrophotometric detectors, producing a voltage signal which is related to the concentration of the relevant species. In order to convert the voltage signal to concentration, ultrapure water (blank) is passed through the system before and after the sample to establish the baseline, and standard solutions are measured at regular intervals. The flow of sample, standard solution and blank is illustrated in Figure 1. When the valves switch for example from blank to standard the measured voltage rises from the baseline level and approaches a stable level. This level is used to determine the calibration curve. However, the shape and steepness of the measured curve contains additional information about the nature of the mixing and the relevant time constants in the subsystem. For the Ca^{2+}, NH_4^+, and conductivity subsystems in the NGRIP setup, blank-standard and standard-blank responses are used to estimate the strength of the mixing. The blank-standard and standard-blank response curves must be converted from voltage to concentration before they are used in the analysis. This conversion is straightforward for the NH_4^+ and Ca^{2+} subsystems because the measured voltage from the photomultiplier is linearly related to the concentration. The same holds for the conductivity series which is a direct measurement. This is the reason why these three data series were chosen for the pilot study.

[8] It should be noted that the restoration of the signals presented here is based on response curves obtained from standard measurements. Only the mixing that takes place in the analysis system (the shaded area in Figure 1) is considered while the mixing of the sample that takes place in the melting system and the debubbler unit is excluded. In order to estimate the total mixing, the system's response to blank-standard and standard-blank shifts could be measured by melting a block of clean ice followed by a block of ice with uniform (nonzero) concentration. However, in practice this procedure is not readily performed. First, obtaining ice with evenly distributed impurities is not trivial. Such ice is not available from natural sources, and freezing a standard solution will not produce ice with uniform concentration. Second, the ice should have a clean air content similar to that of glacier ice so that the sample-to-air ratio in the segmented flow from the melting device to the debubbler unit is representative of the real measurement conditions. For these reasons, measurements of the total system's response were only carried out by pouring liquid standard and blank solutions directly onto the melting device, but as the conditions were not representative of the real measurement conditions, they have not been used for the resolution enhancement. Consequently only the mixing in the analysis subsystem will be considered. This means that the restoration performed here only accounts for a part of the total mixing, and that additional details possibly could have been

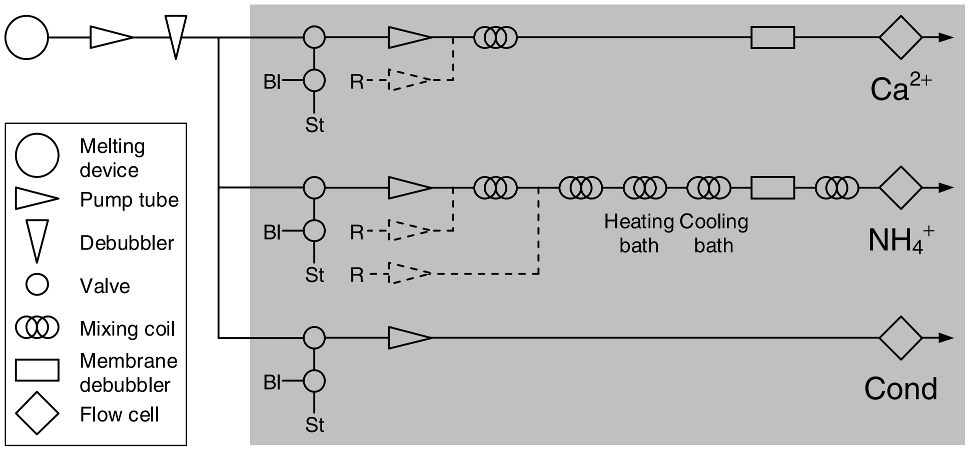

Figure 1. Simplified flowchart of the CFA setups for Ca^{2+}, NH_4^+, and electrolytical meltwater conductivity. Sample water from continuously melted ice is pumped to the warm lab, debubbled and split into substreams to feed the different analysis subsystems, where specific reagents (R) are added. Valves allow switching between sample, blank (Bl) or standard solution (St), which are used to establish baselines and to calibrate the measurements. The total system comprises a set of different mixing volumes (tubing, debubbler, mixing coils, and flow cells as listed in the legend). However, in this work, only the part of the mixing that takes place within the grey shaded area is considered. Dashed lines indicate the parts of the setup which do not contribute to the mixing.

restored if good estimates of the total mixing strength had been available.

4. Restoration Filter Design

[9] Restoration of details lost due to mixing can be efficiently handled by deconvolution techniques, operating in either the time domain or the spectral domain. A time domain approach was tested by *Sigg* [1990] in order to improve the resolution of CFA [H_2O_2] measurements. The resolution enhancement method presented here is a spectral method where the problem of performing the restoration becomes a question of determining the effect of the mixing as a spectral filter. The spectral approach has the important advantage that it allows a consistent treatment of the noise. The rest of this section is a description of how the filters are constructed from data and calibration measurements. A less mathematical oriented summary can be found in the caption of Figure 2 where the deconvolution filters and the results of the resolution enhanced NGRIP data are exemplified.

[10] Assume that the valves switch from blank to standard or vice versa at $t = 0$. The incoming, unmixed signal $S(t)$ can then be represented by a step function going from one constant concentration to another. Without loss of generality, the situation can be scaled so that the initial level is zero and that the final level is unity. The incoming signal can thus be represented by the Heaviside function

$$S(t) = \begin{cases} 0 & t < 0 \\ 1 & t \geq 0 \end{cases} \tag{1}$$

but the measured system response to $S(t)$ will be a smooth curve $s(t)$ because mixing has blurred the sharp shift in concentration. In a convolution formulation this corresponds to convolution of $S(t)$ with a mixing response function $M(\tau)$

$$s(t) = \int_{-\infty}^{\infty} S(\tau)M(t-\tau)d\tau \tag{2}$$

In the spectral domain, convolution is merely multiplication, so the mixing is described by

$$\tilde{s} = \tilde{S}\tilde{M} \tag{3}$$

where the tilde denotes Fourier transformation. When differentiating equation (2) with respect to time the mixing filter $M(\tau)$ is unaffected and equation (3) becomes

$$\tilde{s}' = \tilde{S}'\tilde{M} = \tilde{M} \tag{4}$$

where the last equality comes from the fact that the derivative of a Heaviside step function is the delta function, and that the Fourier transform of the delta function is unity. Thus the mixing filter $\tilde{M}$ can be determined by measuring the system response to a step function, differentiating, and performing a Fourier transformation.

[11] During a measuring campaign the characteristics of the mixing will change. When for example tubes or columns in the setup are changed then the mixing filter will change as well. The mixing filter for the NGRIP NH_4^+ subsystem at the depth 1622 m is shown in Figure 2b (brown curve) as an example. It is seen that the very long wavelengths ($\lambda >$ 100 mm) are hardly affected, while the amplitude of a cycle with $\lambda = 10$ mm will be reduced to about 10^{-2} of its original amplitude.

[12] The effect of the mixing can also be illustrated by looking at $s'(t)$ in the time domain. Because s' is the

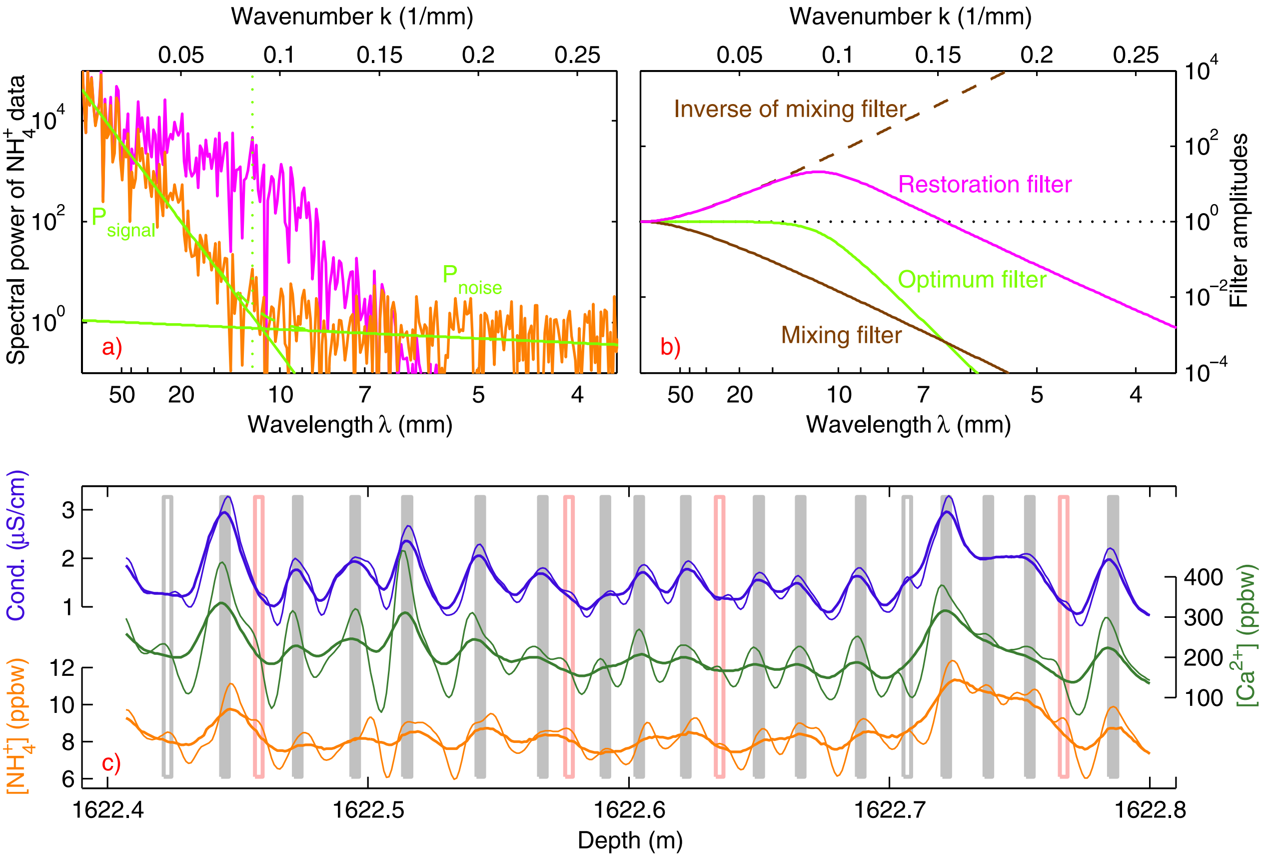

Figure 2. (a, b) Data used to construct the deconvolution filters needed for signal restoration and (c) examples of the restored signals. The spectral power of a one meter NH_4^+ data section from about 1622 m depth (Figure 2a, orange) has distinct signal and noise parts, P_{signal} and P_{noise} (Figure 2a, light green lines). This separation of the data spectral power into signal and noise parts defines the optimum filter (Figure 2b, light green line) that allows restoration of the original signal without blowing up the noise. The strength of the mixing in the analysis system is estimated from the response curves (Figure 2b, brown line). The inverted mixing filter (Figure 2b, dashed brown line) is combined with the optimum filter (Figure 2b, light green line), forming the restoration filter (Figure 2b, magenta line). It is seen that the effect of the restoration is amplification of wavelengths down to 6–7 mm and that the maximum amplification is applied to wavelengths of about 11 mm. The spectral power of the restored signal is also shown (Figure 2a, magenta line). For a data sequence from the Oldest Dryas, about 15 ka, the original data (Figure 2c, heavy lines) and restored signals (Figure 2c, thin lines) are shown together with suggested annual layers markings. See section 4 for additional details.

measured response to S' which is a pulse of "delta function shape", s' is called the pulse response. The pulse responses of the three analysis subsystems are illustrated in Figure 3. The curves have been shifted to remove the different time lags introduced by the CFA subsystems, and thus only the shape of the curves should be considered. It is apparent from the width of the curves that the mixing in the conductivity measurement subsystem is much weaker than the mixing in the NH_4^+ and Ca^{2+} subsystems. In the latter, an infinitely sharp pulse is spread out to become an approx. 20 mm wide peak, while the peak produced by the conductivity subsystem is only roughly half as wide. The difference is expected because the conductivity measurement system contains less tubing and no mixing or reaction coils. Because the conductivity measurement subsystem does not contain large mixing volumes, the mixing inferred from the conductivity pulse response can also be regarded as an estimate of the maximum mixing taking place in the melting and debubbling part of the system.

[13] When sample is passed through the analysis system the mixing processes are unchanged. Let D be the unmixed signal entering the analysis system, and d the measured signal. In analogy with equation (3), the original and measured signals are related by

$$\tilde{d} = \tilde{D}\tilde{M} \tag{5}$$

where $\tilde{M}$ is the same filter as in equation (4). Once the mixing filter $\tilde{M}$ has been determined using the procedure described above the unmixed signal D can then in theory be restored by inverse Fourier transform of $\tilde{D}$, where

$$\tilde{D} = \tilde{d}\tilde{M}^{-1} \tag{6}$$

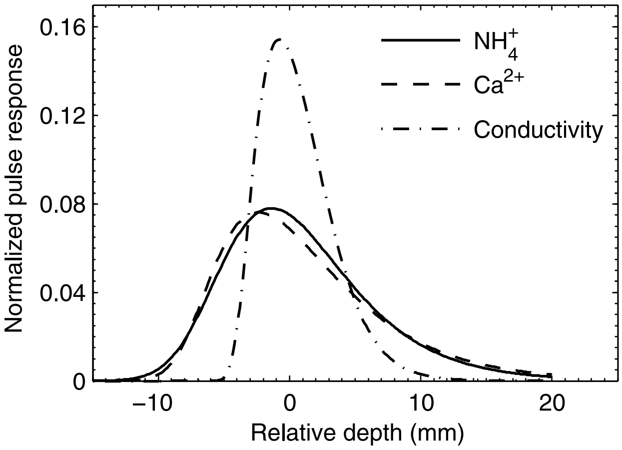

Figure 3. Response curves for the NGRIP NH_4^+, Ca^{2+}, and conductivity subsystems, showing the measured response to a delta function pulse at zero depth. For the NH_4^+ and Ca^{2+} subsystems, the pulse is spread out to become ~20 mm wide peaks, while the conductivity subsystem has a more narrow response curve corresponding to less mixing.

Cycles with short wavelengths are almost entirely obliterated by the mixing and when the signal is restored using equation (6) the amplitudes of these cycles are consequently heavily amplified. In the presence of noise on the measurements, heavily amplified high-frequency noise will dominate the restored signal. Handling this problem by removing the short wavelengths will in turn remove some of the signal and may cause ringing effects. The optimal trade-off between retaining as much signal as possible without amplifying the noise too much is accomplished by constructing an optimum filter $\widetilde{F}$, or Wiener filter, which for each wave number k is defined as:

$$\widetilde{F}(k) = \frac{P_{\text{signal}}}{P_{\text{signal}} + P_{\text{noise}}} \quad (7)$$

where P denotes the spectral power of the measured signal and noise, respectively [*Johnsen*, 1977]. Determining P_{signal} and P_{noise} is in general not straightforward, but in this work, P_{signal} and P_{noise} are estimated from the spectral power of the measurements P_{measured} as illustrated in Figure 2a. Each of the light green lines (P_{signal} and P_{noise}) is determined as a least squares fit to P_{measured} (orange curve) above and below a certain noise-signal cutoff wavelength (dotted light green line), respectively. The best value of the noise-signal cutoff wavelength is determined by minimizing the total RMS difference between the sum $P_{\text{signal}} + P_{\text{noise}}$ (dashed green line) and P_{measured} (orange curve) and is 11.6 mm in the presented example. The two light green lines represent the best estimates of the signal and noise parts of the spectral power and $\widetilde{F}(k)$ is calculated according to equation (7) from these estimates (Figure 2b, light green line). In this example, the filter amplitude is close to unity for wavelengths down to 15 mm, while the noise spectral power is about 4 orders of magnitude larger than the remaining signal power for the λ = 6 mm oscillations.

[14] The optimum filter $\widetilde{F}$ is multiplied with the inverse of the mixing filter $\widetilde{M}^{-1}$ to form the restoration filter $\widetilde{R}$ (Figure 2b, magenta curve), which is used to calculate the best possible estimate of the original data, D_{est}:

$$\widetilde{D_{est}} = \widetilde{d}\,\widetilde{F}\,\widetilde{M}^{-1} \equiv \widetilde{d}\,\widetilde{R} \quad (8)$$

The restored signal D_{est} can now be determined by inverse Fourier transformation of $\widetilde{D_{est}}$. Alternatively, the restoration filter $\widetilde{R}$ can be transformed back to a time domain filter $R(\tau)$, which is then used to determine D_{est} from

$$D_{est}(t) = \int_{-\infty}^{\infty} d(\tau)\,R(t-\tau)d\tau \quad (9)$$

without the need of Fourier transforming the data.

5. Results and Discussion

[15] Examples of original (thick lines) and restore (thin lines) NGRIP data are shown in Figure 2c. The selected data section comes from a depth of 1622 m corresponding to the Oldest Dryas (age about 15 ka). From the preliminary NGRIP model timescale [*NGRIP Members*, 2004] the mean annual layer thickness is expected to be about 2 cm. The P_{signal} and P_{noise} curves intersect at $\lambda \approx 11$ mm, suggesting that an annual layer with thickness 11 mm or less will be so heavily weakened by the mixing that it is indistinguishable from the noise. By applying the restoration filter (2b, magenta curve), wavelengths around this critical wavelength are amplified, thus pushing the limit of how thin layers can safely be detected in the data. The resolution improvement is illustrated by the difference between the spectral amplitudes of the original and restored signals (orange and magenta curves in Figure 2a, respectively). Whereas the P_{signal} and P_{noise} curves intersect at $\lambda \approx 11$ mm for the original data, the signal part of the enhanced data spectrum intersect P_{noise} at $\lambda \approx 7$ mm.

[16] A preliminary annual layer count illustrates the usefulness of the method. Using all the available CFA series, the annual layers have been identified. These layers are marked by grey, vertical bars in Figure 2c. The open grey bars indicate features that are possible annual layers, but that are less clearly identifiable. The restored signals support these uncertain annual layers as actual annual layers because peaks or clear "shoulders" are visible in all three restored data series at each of these depths. Also entirely new features appear in the restored series. The open magenta bars in Figure 2c mark annual layers present only in the restored series. It is not clear from the presented data series alone whether these features represent annual layers. A final decision will thus have to await cross checks with additional data. By applying the method to the full length of the CFA profiles, and by applying the method to all species, it is hoped that the uncertainty of annual layer counting in

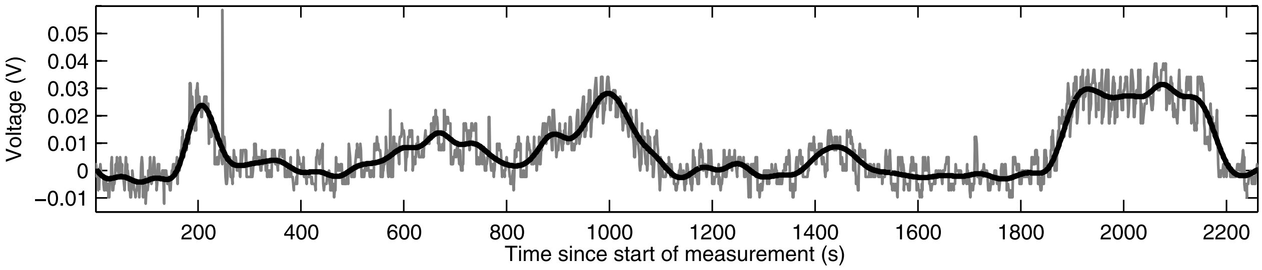

Figure 4. Example of the results of the resolution enhancement method (black curve) when applied to a 1 m long raw [Ca^{2+}] data sequence (grey curve) from the shallow part of the Berkner Island ice core. The presented sequence has a poor signal-to-noise ratio, but the method accounts for this via the optimum filter. Note how the spurious peak at 250 s (probably originating from an air bubble in the system) is removed by the filtering, easing the subsequent data processing.

the deeper parts of the NGRIP core can be significantly reduced due to the increased resolution.

[17] An application of the method on a 1 m section of [Ca^{2+}] data from the Berkner Island ice core is illustrated in Figure 4. Because of a poor signal-to-noise ratio the method cannot safely restore much of the lost detail. This is due to the optimum filter $\widetilde{F}$ dropping below unity at higher wavelengths and decreasing more steeply than the inverse mixing filter $\widetilde{M}^{-1}$ rises. The resulting restoration filter $\widetilde{R}$ thus resembles the optimum filter $\widetilde{F}$ and the effect of the resolution enhancement is almost the same as using the optimum filter alone. In this case, little is gained from resolution enhancement point of view. However, from a data processing and interpretation point of view the produced signal is improved because of the included filtering. An important point is that the filtering is performed without manually choosing a low-pass filter cutoff frequency because the optimum filter in equation (7) automatically accommodates the signal-to-noise ratio of the data section in question.

[18] The method will thus automatically improve the resolution as much as possible given the level of noise in the measurements and can therefore safely be applied to any data series as long as the (inverse) mixing filter is well determined. As the mixing filter reflects the combined mixing characteristics of the setup the mixing filter cannot be expected to remain unchanged when parts of the system are replaced, or when for example the melt speed is changed. Experiences obtained from both the NGRIP and Berkner Island measurements indicate that slow changes in the mixing characteristics due to wear take place with time but without affecting the results significantly. In contrast, changes in mixing characteristics due to replacement of tubing, columns, and flow cells or changes in melt speed are significant and the mixing filter must be modified to account for this. It is therefore advisable to integrate the mixing filter determination in the calibration operation so that a mixing filter is generated from every set of calibration measurements. By integrating the collection of calibrated blank-standard and standard-blank response curves in the data processing tools, most of the data needed for resolution enhancement can be gathered without much additional work. As an additional benefit, a comparison of the mixing characteristics from one measurement to the next gives a fast check on the system stability. The combination of system stability check and resolution enhancement means that the usefulness and reliability of the produced data can be significantly improved by the use of the presented method.

[19] **Acknowledgments.** This work is a contribution of the Copenhagen Ice Core Dating Initiative, which is supported by a grant from the Carlsberg Foundation. S.O.R. gratefully acknowledges Robert Mulvaney, British Antarctic Survey, for financial support during a visit to BAS from August to October 2004.

References

Alley, R. B., et al. (1997), Visual-stratigraphic dating of the GISP2 ice core: Basic, reproducibility, and application, *J. Geophys. Res.*, *102*(C12), 26,367–26,381.

Anklin, M., R. C. Bales, E. Mosley-Thompson, and K. Steffen (1998), Annual accumulation at two sites in Northwest Greenland during recent centuries, *J. Geophys. Res.*, *103*(D22), 28,775–28,783.

Bigler, M. (2004), Hochauflösende Spurenstoffmessungen an polaren Eisbohrkernen: Glaziochemische und klimatische Prozessstudien, Ph.D. dissertation, Univ. of Bern, Bern, Switzerland.

Bigler, M., D. Wagenbach, H. Fischer, J. Kipfstuhl, H. Miller, S. Sommer, and B. Stauffer (2002), Sulphate record from a northeast Greenland ice core over the last 1200 years based on continuous flow analysis, *Ann. Glaciol.*, *35*, 250–256.

Fuhrer, K., A. Neftel, M. Anklin, T. Staffelbach, and M. Legrand (1996), High-resolution ammonium ice core record covering a complete glacial-interglacial cycle, *J. Geophys. Res.*, *101*(D2), 4147–4164.

Hammer, C. U., H. B. Clausen, W. Dansgaard, N. Gundestrup, S. J. Johnsen, and N. Reeh (1978), Dating of Greenland ice cores by flow models, isotopes, volcanic debris, and continental dust, *J. Glaciol.*, *20*(82), 3–26.

Johnsen, S. J. (1977), Stable isotope homogenization of polar firn and ice, in *Proceedings of Symposium on Isotopes and Impurities in Snow and Ice, IUGG XVI, General Assembly, Grenoble Aug./Sept. 1975*, *IAHS AISH Publ.*, *118*, 210–219.

Johnsen, S. J., H. B. Clausen, K. M. Cuffey, G. Hoffmann, J. Schwander, and T. Creyts (2000), Diffusion of stable isotopes in polar firn and ice: The isotope effect in firn diffusion, in *Physics of Ice Core Records*, edited by T. Hondoh, pp. 121–140, Hokkaido Univ. Press, Sapporo, Japan.

Legrand, M., and P. Mayewski (1997), Glaciochemistry of polar ice cores: A review, *Rev. Geophys.*, *35*(3), 219–243.

Littot, G. C., et al. (2002), Comparison of analytical methods used for measuring major ions in the EPICA Dome C (Antarctica) ice core, *Ann. Glaciol.*, *35*(1), 299–305.

McConnell, J. R., G. W. Lamorey, S. W. Lambert, and K. C. Taylor (2002), Continuous ice-core chemical analyses using inductively coupled plasma mass spectrometry, *Environ. Sci. Technol.*, *36*, 7–11.

Meese, D. A., A. J. Gow, R. B. Alley, G. A. Zielinski, P. M. Grootes, M. Ram, K. C. Taylor, P. A. Mayewski, and J. F. Bolzan (1997), The Greenland Ice Sheet Project 2 depth-age scale: Methods and results, *J. Geophys. Res.*, *102*(C12), 26,411–26,423.

North Greenland Ice Core Project Members (NGRIP) (2004), High-resolution record of Northern Hemisphere climate extending into the last interglacial period, *Nature*, *431*, 147–151.

Röthlisberger, R., M. Bigler, M. Hutterli, S. Sommer, B. Stauffer, H. Junghans, and D. Wagenbach (2000), Technique for continuous high-resolution analysis of trace substances in firn and ice cores, *Environ. Sci. Technol.*, *34*(2), 338–342.

Sigg, A. (1990), Wasserstoffperoxid-Messungen an Eisbohrkernen aus Grönland und der Antarktis und ihre atmosphärenchemische Bedeutung, Ph.D. dissertation, University of Bern, Bern, Switzerland.

Sigg, A., K. Fuhrer, M. Anklin, T. Staffelbach, and D. Zurmühle (1994), A continuous analysis technique for trace species in ice cores, *Environ. Sci. Technol.*, *28*, 204–210.

K. K. Andersen, M. Bigler, S. J. Johnsen, and S. O. Rasmussen, Ice and Climate Research, Niels Bohr Institute, University of Copenhagen, Juliane Maries Vej 30, DK-2100 Copenhagen, Denmark. (olander@gfy.ku.dk)

T. McCormack, British Antarctic Survey, High Cross, Cambridge CB3 0ET, UK.

A new Greenland ice core chronology for the last glacial termination

S. O. Rasmussen,[1] K. K. Andersen,[1] A. M. Svensson,[1] J. P. Steffensen,[1] B. M. Vinther,[1]
H. B. Clausen,[1] M.-L. Siggaard-Andersen,[2,3] S. J. Johnsen,[1] L. B. Larsen,[1]
D. Dahl-Jensen,[1] M. Bigler,[3,4] R. Röthlisberger,[4,5] H. Fischer,[2] K. Goto-Azuma,[6]
M. E. Hansson,[7] and U. Ruth[2]

Received 13 April 2005; revised 22 November 2005; accepted 19 December 2005; published 21 March 2006.

[1] We present a new common stratigraphic timescale for the North Greenland Ice Core Project (NGRIP) and GRIP ice cores. The timescale covers the period 7.9–14.8 kyr before present and includes the Bølling, Allerød, Younger Dryas, and early Holocene periods. We use a combination of new and previously published data, the most prominent being new high-resolution Continuous Flow Analysis (CFA) impurity records from the NGRIP ice core. Several investigators have identified and counted annual layers using a multiparameter approach, and the maximum counting error is estimated to be up to 2% in the Holocene part and about 3% for the older parts. These counting error estimates reflect the number of annual layers that were hard to interpret, but not a possible bias in the set of rules used for annual layer identification. As the GRIP and NGRIP ice cores are not optimal for annual layer counting in the middle and late Holocene, the timescale is tied to a prominent volcanic event inside the 8.2 kyr cold event, recently dated in the DYE-3 ice core to 8236 years before A. D. 2000 (b2k) with a maximum counting error of 47 years. The new timescale dates the Younger Dryas-Preboreal transition to 11,703 b2k, which is 100–150 years older than according to the present GRIP and NGRIP timescales. The age of the transition matches the GISP2 timescale within a few years, but viewed over the entire 7.9–14.8 kyr section, there are significant differences between the new timescale and the GISP2 timescale. The transition from the glacial into the Bølling interstadial is dated to 14,692 b2k. The presented timescale is a part of a new Greenland ice core chronology common to the DYE-3, GRIP, and NGRIP ice cores, named the Greenland Ice Core Chronology 2005 (GICC05). The annual layer thicknesses are observed to be log-normally distributed with good approximation, and compared to the early Holocene, the mean accumulation rates in the Younger Dryas and Bølling periods are found to be 47 ± 2% and 88 ± 2%, respectively.

Citation: Rasmussen, S. O., et. al. (2006), A new Greenland ice core chronology for the last glacial termination, *J. Geophys. Res.*, *111*, D06102, doi:10.1029/2005JD006079.

1. Introduction

[2] A wealth of information about paleoclimate can be extracted from polar ice cores, but the full potential of these data can be exploited only with a reliable depth-age relation. Especially when studying the dramatic climatic transitions of the past, accurate age estimates are of great importance because the relative timing of climate changes around the globe gives indications of the causes and mechanisms for rapid climatic changes [*Bond et al.*, 1993; *Blunier et al.*, 1998]. Much effort has therefore been put into developing timescales for ice cores, based either on identification and counting of annual layers or modeling the depth-age relationship [*Hammer et al.*, 1978; *Hammer*, 1989]. Greenland ice cores can be dated by annual layer counting when the accumulation rate is sufficient to resolve annual layers, and the timescales of different ice cores can be matched and validated using volcanic layers and other independently dated stratigraphic markers [*Clausen et al.*, 1997; *Anklin et al.*, 1998]. The DYE-3 and GRIP ice cores were dated about 8 kyr back by counting annual layers in the stable isotope and electrical conductivity measurement profiles [*Hammer et al.*, 1986; *Hammer*, 1989; *Johnsen et al.*, 1992]. Below this,

[1]Ice and Climate, Niels Bohr Institute, University of Copenhagen, Copenhagen, Denmark.
[2]Alfred-Wegener-Institute for Polar and Marine Research, Bremerhaven, Germany.
[3]Now at Ice and Climate, Niels Bohr Institute, University of Copenhagen, Copenhagen, Denmark.
[4]Climate and Environmental Physics, Physics Institute, University of Bern, Bern, Switzerland.
[5]Now at British Antarctic Survey, Cambridge, UK.
[6]National Institute of Polar Research, Tokyo, Japan.
[7]Department of Physical Geography and Quaternary Geology, Stockholm University, Stockholm, Sweden.

0148-0227/06/2005JD006079$09.00

annual layers were identified using GRIP chemistry data as well. In the glacial part of GRIP, discontinuous annual layer counting was used as input for ice flow modeling (*Dansgaard et al.* [1993], *Johnsen et al.* [1995] (ss09 timescale), *Johnsen et al.* [2001] (ss09sea timescale)), while the GISP2 ice core was dated using stratigraphic methods also in the glacial, relying primarily on the visual layers in the ice [*Alley et al.*, 1997; *Meese et al.*, 1997]. As discussed by *Southon* [2004], the different timescales of GRIP and GISP2 are up to several thousand years offset in parts of the glacial, and there are significant differences in the Holocene as well.

[3] Drilling of the NGRIP ice core was completed successfully in 2003 [*Dahl-Jensen et al.*, 2002; *North Greenland Ice Core Project* (*NGRIP*) *Members*, 2004]. Liquid water was found when the drill penetrated the ice sheet, revealing melting point temperatures at the bedrock. The melting at the base limits the age of the ice in the NGRIP ice core to be $\sim$123 ky old [*NGRIP Members*, 2004]. The combination of moderate accumulation rates (19 cm of ice equivalent per year in present time) and bottom melting results in a different flow pattern than that of GRIP and GISP2, and the annual layers are thus more than 5 mm thick over the entire length of the NGRIP core. This means that in the middle and early part of the glacial the annual layers are thicker than those observed in the GRIP and GISP2 ice cores [*NGRIP Members*, 2004; *Dahl-Jensen et al.*, 1993; *Johnsen et al.*, 2001; *Meese et al.*, 1997]. This fact, and the development of new high-resolution impurity measurement techniques, makes the NGRIP ice core ideal for stratigraphic dating purposes, and has motivated the initiation of the Copenhagen Ice Core Dating Initiative, with the construction of a new stratigraphic timescale for the GRIP and NGRIP ice cores as one of the main objectives. Here we present a stratigraphic timescale for the period 7.9–14.8 kyr before A. D. 2000 (b2k), using multi-parameter data from both the GRIP and NGRIP ice cores. The datum of the presented timescale is a readily recognizable volcanic event inside the characteristic 8.2 kyr cold event, dated using data from the DYE-3 ice core. In the section 7.9 – 10.3 kyr before present, the timescale is based on new annual layer counting using existing impurity records from the GRIP ice core [*Fuhrer et al.*, 1993, 1996, 1999]. From 10.3 kyr b2k and back also NGRIP impurity records are available, and down to the Younger Dryas – Preboreal transition (henceforth named the YDPB transition) the timescale is based on the combined GRIP-NGRIP data set. For NGRIP, the timescale continues through the Younger Dryas, Allerød and Bølling periods back to 14.8 kyr before present. The new timescale is named the Greenland Ice Core Chronology 2005, or GICC05.

[4] In order to be able to refer to the different sections of the presented timescale in a short and unambiguous way, the names Holocene I, Holocene II, Younger Dryas, Allerød, Bølling, and Oldest Dryas are used as illustrated in Figure 1, although this use does not comply with the formal bio-stratigraphic definitions of the periods. The transition depths used to define the onset and end of the Bølling and Younger Dryas periods are derived from deuterium excess data (the deuterium excess is defined as $\delta D - 8\delta^{18}O$). In each of these transitions, the deuterium excess changes abruptly, and the change occurs prior to, or simultaneously with, changes in all other climate proxies. As changes in the deuterium excess are connected to changes in the moisture sources [*Jouzel and Merlivat*, 1984; *Johnsen et al.*, 1989; *Taylor et al.*, 1997; *Masson-Delmotte et al.*, 2005a, 2005b], the abrupt shifts in deuterium excess indicate that dramatic reorganizations of the atmospheric circulation took place at the onset of these transitions, followed by more gradual changes in temperature and ice core impurity content. A discussion of the implications of these observations is beyond the scope of this work, but it should be stressed that the timing of the transitions as defined by the deuterium excess must be expected to precede changes in temperature and vegetation recorded in other archives.

[5] All ages in this work are reported in calendar years relative to the year A. D. 2000. Unfortunately the BP notation has in several instances been used with reference to other years than the conventional A. D. 1950 when reporting ice cores results. To avoid further confusion, and to underline the independency from radiocarbon-based dating, the notation b2k is introduced, being both short and unambiguous.

2. Data

[6] For NGRIP, Continuous Flow Analysis (CFA) data of soluble ions were used for identification of annual layers [*Bigler*, 2004; *Röthlisberger et al.*, 2000]. The resolution of the [NH_4^+], [Ca^{2+}], and conductivity series has been enhanced as described in the work of *Rasmussen et al.* [2005], by correcting for the effect of dispersion in the CFA system using deconvolution techniques. The correction method uses the measured smooth response to a sudden concentration jump, obtained from calibration measurements, to estimate the mixing strength and restores as much as possible of the high-frequency part of the signal taking into account the presence of measurement noise. Moreover, CFA dust data (the number concentration of particles with diameter larger than 1.0μm) of *Ruth et al.* [2003] were used. Electrical conductivity measurement (ECM) data representing the acidity of the ice were used [*Dahl-Jensen et al.*, 2002]. All ECM profiles are shown as [H^+] in μequiv./kg. The visual stratigraphy (VS) grey-scale refraction profile of *Svensson et al.* [2005] were also included, but as the raw VS data contain many close, thin layers representing sub-annual variations, we used a profile smoothed by applying a Gaussian filter with s = 4 mm.

[7] The ice core drill got stuck in 1997 during the NGRIP drilling operation and a new core had to be drilled. The two cores are referred to as NGRIP1 and NGRIP2, respectively. Measurements have been performed on the NGRIP1 core down to a depth of 1372 m, while measurements on the NGRIP2 core start at a depth of 1346 m (corresponding to approximately 9.5 kyr b2k). In the zone of overlap the mean offset between NGRIP1 and NGRIP2 is 0.43 m, with the same feature appearing at greater depths in the NGRIP1 core than in the NGRIP2 core [*Hvidberg et al.*, 2002]. All depths are NGRIP2 depths unless noted otherwise, and thus NGRIP1 data have been shifted 0.43 m to fit the NGRIP2 depth scale.

[8] From the GRIP ice core, ECM data and the CFA records of [NH_4^+], [H_2O_2], and [Ca^{2+}] obtained by *Fuhrer et al.* [1993, 1996, 1999] were used.

[9] Table 1 lists the data series and the estimated effective resolution of each of the data series used. The effective resolution is defined for each series as the shortest cycle that can be identified in that series.

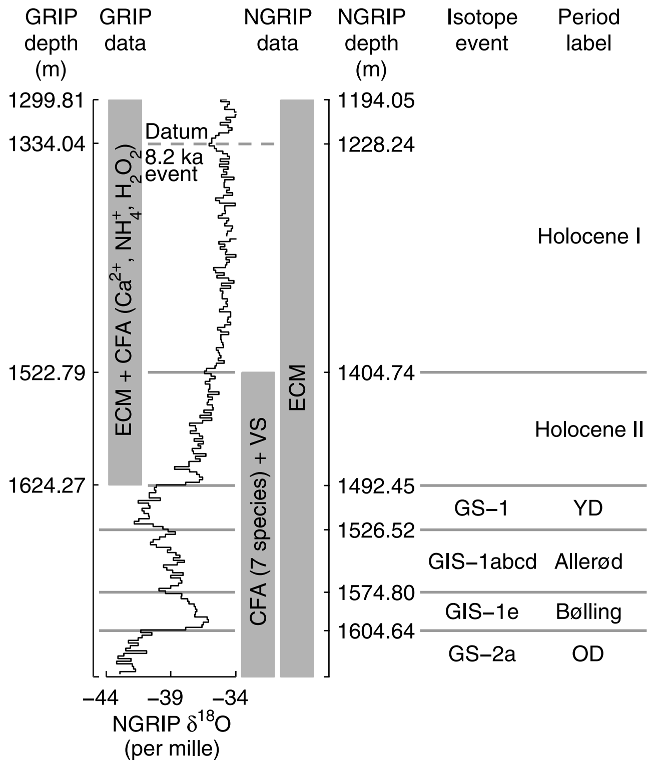

Figure 1. Overview of the data series used for the different parts of the GRIP and NGRIP ice cores. VS refers to the visual stratigraphy data, and ECM refers to electrical conductivity measurement data. The period labels are the names used throughout this work to identify the different time periods. YD and OD refer to the Younger Dryas and Oldest Dryas, respectively. The isotope event names refer to those of *Björck et al.* [1998].

[10] Model estimates of mean annual layer thicknesses in the NGRIP ice core [*Johnsen et al.*, 2001; *NGRIP Members*, 2004] are above 5 cm in the Holocene, around 3 cm in the Younger Dryas, about 4 cm in Bølling and Allerød, and 2–3 cm in the Oldest Dryas. The resolution of the CFA, ECM, and VS data thus allows identification of annual layers in the ice from the Holocene and back through the transition, while the resolution of the CFA data becomes marginal below the transition into the Bølling interstadial. Preliminary results show that the CFA data quality improves at greater depths, and it is thus possible to use CFA data for the identification of annual layers within most interstadials, where the accumulation is roughly twice that of the stadials. During the cold stadials annual layer identification has to rely mostly on VS and ECM.

3. Observed Seasonality

[11] Many of the impurity records obtained from Greenland ice cores exhibit annual variations [*Beer et al.*, 1991; *Whitlow et al.*, 1992; *Fischer and Wagenbach*, 1996]. The CFA, ECM, and VS data from GRIP and NGRIP are so highly resolved that the intra-annual timing of the different species is clearly detected at all depths. In the relatively warm periods (the Holocene, the Bølling and part of the Allerød period) the different species peak at different times of the year. The relative timing of the species resembles that observed for recent times [*Whitlow et al.*, 1992; *Laj et al.*, 1992; *Steffensen*, 1988; *Anklin et al.*, 1998; *Fuhrer et al.*, 1993; *Bory et al.*, 2002]. A typical annual layer is characteristic by having the sea salt dominated [Na^+] peaking in late winter. The VS record generally contains much more than one peak per year and is not easy to interpret, but in general there are layers of high refraction (cloudy bands) at springtime, coinciding with high dust content, high [Ca^{2+}] and dips in the [H_2O_2] curve. Summer is characterized by high concentration of [NH_4^+], [NO_3^-], and sometimes of [SO_4^{2-}]. In general, dips in the ECM correlate with peaks in [NH_4^+] and [Ca^{2+}], while the electrolytical conductivity (henceforth just called the conductivity) is related to the total content of ions present in the meltwater and thus contains several peaks per year due to the different seasonality of the individual species. In the colder periods, the differences in seasonality almost vanish and most series peak simultaneously, making the conductivity record useful for identification of annual layers. The [NH_4^+] signal does not consistently show clear annual cycles in the cold periods. In the colder periods, the annual signal in VS becomes more prominent, but the VS record still contains more than one peak per year on average.

[12] It should be noted that although there is an annual [H_2O_2] signal present in recently formed snow, this signal has been erased by diffusion at the depths in question in this work. However, because [H_2O_2] is only preserved in ice with low dust levels [*Fuhrer et al.*, 1993], the dips in the [H_2O_2] curve indicate high dust content. As the GRIP [H_2O_2] measurements have significantly higher resolution than the corresponding [Ca^{2+}] measurements, details obscured by

Table 1. Data Sets Used in the Construction of the Presented Timescale

Ice Core	Species	Depth Interval, m	Sampling Resolution, mm	Estimated Effective Resolution,[a] mm
NGRIP2	CFA: NH_4^+, Ca^{2+}, conductivity (resolution enhanced)	1404–1607	1	10–15[b]
	CFA: NO_3^-, Na^+, SO_4^{2-}, dust	1404–1607	1	15–25[b]
	visual stratigraphy	1404–1607	<1	~3
	ECM	1346–1607	1	4
NGRIP1	ECM	1195–1372	10	40
GRIP	CFA: NH_4^+, H_2O_2	1300–1624	2	~20[c]
	CFA: Ca^{2+}	1300–1624	2	~50[c]
	ECM	1300–1624	10	40

[a]The effective resolution is the shortest wavelength that can be identified from the data.
[b]The resolution varies with depth due to changing experimental conditions.
[c]Approximate values obtained from inspection of the data. *Fuhrer et al.* [1993] report the resolution defined as the *e*-folding scale as 7, 12, and 35 mm for the NH_4^+, H_2O_2, and Ca^{2+} subsystems, respectively.

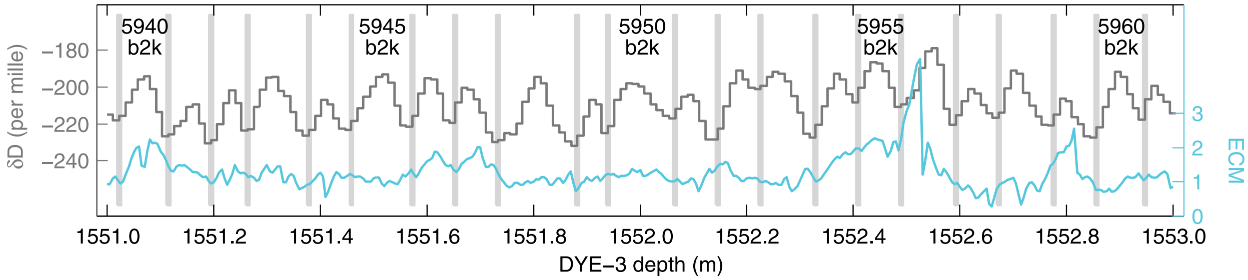

Figure 2. A section of new δD data used for the revision of the DYE-3 timescale (dark gray), together with the ECM data (blue) used in the construction of the former DYE-3 timescale of *Hammer et al.* [1986]. The annual layer markings of the revised timescale are shown by light gray vertical bars (dates are relative to A.D. 2000, denoted b2k).

the low resolution of the [Ca^{2+}] resolution are often resolved by the [H_2O_2] data.

4. Identification of Annual Layers

[13] Identification and subsequent counting of annual layers in ice cores has been performed in various ways. The most direct, practically as well as conceptually, is to base the identification on a single parameter, which is known to exhibit annual cycles. *Langway* [1967], used visible features to establish one of the first stratigraphic timescales for a Greenland ice core, ranging a few hundred years back, but most often $\delta^{18}O$ data are used where the accumulation rate is sufficiently high. The $\delta^{18}O$ parameter is the obvious choice because the close connection between $\delta^{18}O$ and temperature makes it highly probable that the observed cycles actually represent annual layers. Mainly using $\delta^{18}O$ measurements, a timescale for the last 8 kyr was constructed by counting of annual layers in the DYE-3 ice core [*Hammer et al.*, 1986]. Another prominent example of a single parameter stratigraphic timescale is that of the Byrd ice core, which was dated some 50,000 years back in time primarily using ECM data containing clear annual cycles [*Hammer et al.*, 1994]. When more parallel data series with sufficient resolution are available from the same segment of an ice core, it is obviously preferable to base the identification of annual layers on all the available data [*Johnsen et al.*, 1992; *Meese et al.*, 1997; *Alley et al.*, 1997; *Anklin et al.*, 1998]. This is especially true when the available data series cannot be guaranteed to be pure annual signals, but contain contributions from other processes than those generating the annual pattern. For example, the concentration of NH_4^+ in the Greenland ice cores exhibits clear annual variations in the Holocene and in the Bølling interstadial, but the annual signal is occasionally obscured by high peaks originating from, e.g., biomass burning events. The use of multiple data series thus improves the quality of the timescale produced by making the identification of annual layers more robust. However, multi-parameter data sets with a resolution sufficient for annual layer counting are sparse, and are seldom available from the brittle part of ice cores, where internal cracks in the ice make it virtually impossible to obtain uncontaminated continuous measurements of the impurities in the ice. This is one of the main reasons why multi-parameter CFA measurements have only been carried out below the depth of 1300 m in the GRIP core and below 1400 m in the NGRIP core. Because of the relatively low accumulation rate at the NGRIP drill site, $\delta^{18}O$ data from NGRIP are not optimal for identification of annual layers, while for the GRIP core, $\delta^{18}O$ measurements are not available with sufficient resolution to allow identification of annual layers in the 4–8 kyr part of the core.

[14] Owing to the relatively high accumulation rate at DYE-3, stable isotope ratios from the DYE-3 ice core thus remain, in the opinion of the authors, the best ice core data available for dating the most recent 8 kyr. However, at the time when the DYE-3 timescale of *Hammer et al.* [1986] was constructed, highly resolved stable isotope ratios had only been measured continuously down to 5.9 kyr b2k, and the timescale was therefore to some degree based on interpolation and on ECM measurements below this [*Hammer*, 1989]. However, the highly resolved DYE-3 isotope ratio profile has recently been completed [*Vinther et al.*, 2006]. Using the complete DYE-3 isotope data set together with GRIP $\delta^{18}O$ data in the 0–3.8 kyr b2k interval and NGRIP $\delta^{18}O$ data in the 0–1.9 kyr b2k interval, a new and much more robust cross-validated timescale for the DYE-3, GRIP, and NGRIP ice cores reaching just beyond the 8.2 kyr cold event has been constructed [*Vinther et al.*, 2006]. Figure 2 shows one of the new sections of DYE-3 δD data from around 6 kyr b2k together with the corresponding ECM data initially used to construct the DYE-3 timescale. It is seen that the annual layers are clearly identifiable from the δD data without diffusion correction, and it is apparent that the counting error is reduced significantly compared with the uncertainty of the previous dating. The most recent 1.9 kyr have been dated with no cumulated uncertainty as the reference horizon of Vesuvius (A.D. 79) is dated accurately from historical records. In the 1.9–3.8 kyr b2k section the GRIP and DYE-3 records were matched using common ECM events, and the annual layers were identified from the combined records. The maximum counting error is therefore very small, estimated to about 0.25%. In the 3.8–8.3 kyr b2k section the timescale is based on DYE-3 stable isotope ratios, as illustrated in Figure 2. In the 3.8–6.9 kyr b2k part, the estimated maximum counting error is 0.5%. At the DYE-3 drill site, diffusion of the oxygen isotopes in the ice affects the annual signal when the annual layer thickness is below 6 cm. Owing

Table 2. Depth of the ECM Double Peak Inside the 8.2 kyr Event in Selected Greenland Ice Cores[a]

Ice Core	Depth, m
NGRIP1	1228.67
NGRIP2	1228.24[b]
GRIP	1334.04
DYE-3	1691.06
GISP2	1392.66

[a]The peak serves as the datum of the presented timescale and is assigned the age 8236 b2k with a maximum counting error of 47 years [*Vinther et al.*, 2006].

[b]Estimated using the calculated offset of 0.43 m between NGRIP1 and NGRIP2 as described in section 2.

to ice-flow induced thinning, the mean annual layer thickness is reduced to about 6 cm at a depth of 1625 m (corresponding to 6.9 kyr b2k). From 6.9 to 8.3 kyr b2k the maximum counting error therefore increases to 2%, because the annual signal gradually is weakened by diffusion in the ice. In this way, the new timescale reaches beyond the 8.2 kyr cold event with a cumulated maximum counting error of about 50 years. The maximum counting error has been estimated from the number of potential annual layers that were hard to interpret, and does not include a possible bias in the annual layer identification process. The concept of maximum counting error will be discussed further in section 5.1.4.

[15] A prominent ECM double peak is found close to the deepest part of the δ^{18}O-minimum of the 8.2 kyr cold event [*Hammer et al.*, 1986]. The layer is characterized by a high fluoride content, and can thus most likely be attributed to an Icelandic volcano. Because of the special timing of the ECM double peak inside the δ^{18}O minimum, this stratigraphic horizon can be uniquely identified in all central Greenland ice cores, and has thus been chosen as the datum of the presented timescale. According to the revised DYE-3 timescale [*Vinther et al.*, 2006], the annual layer inside the ECM double peak has been dated to 8236 b2k with a maximum counting error of 47 years. Any future changes in the dating of this horizon will propagate to the presented GICC05 timescale. The depths of this horizon in the central Greenland deep ice cores are listed in Table 2.

4.1. Multiparameter Annual Layer Counting in the GRIP Ice Core (Holocene I Section)

[16] Below 8.3 kyr b2k, the resolution of the DYE-3 isotope signal becomes insufficient for annual layer identification due to flow-induced thinning of the layers, and the GRIP isotope signal is so severely dampened by diffusion that identification of annual layers from the isotope profile alone is dubious. Instead, annual layers were identified from the CFA data set of *Fuhrer et al.* [1993, 1996, 1999], which has already provided the GRIP core with a stratigraphic timescale covering the period from 7.9 kyr b2k to the YDPB transition [*Johnsen et al.*, 1992]. An initial comparison of this timescale with the new NGRIP data (see below) indicate that the existing GRIP timescale is missing a significant number of annual layers in the Holocene II section, and a new GRIP chronology has therefore been constructed using the [NH_4^+], [H_2O_2], and [Ca^{2+}] series obtained by *Fuhrer et al.* [1993, 1996, 1999], ECM data, and short sections of high-resolution isotope data (5 meter of data for every 50 meters).

[17] In general the [Ca^{2+}] series has fewer peaks than the [NH_4^+] series, which at least partially arises from the fact that the [Ca^{2+}] measurements have a significantly lower resolution (see Table 1). When originally marking the annual layers in the GRIP core, the [Ca^{2+}] series was believed to be the most reliable for annual layer identification, while the [NH_4^+] series was considered to contain additional peaks not related to the annual signal. If on the other hand all significant peaks in the [NH_4^+] signal are counted as years, the number of annual layers increase by about 7%. The approach used here is based on the different seasonality of the series as described in section 3: the spring is characterized by high dust content leading to high [Ca^{2+}] and dips in the [H_2O_2] curve, while the [NH_4^+] has summer maxima and corresponding ECM minima. The annual layers have been defined as matching pairs of these spring and summer indicators, which is supported by the high-resolution δ^{18}O data where available. One of these sections is shown in Figure 3. The fact that the dust-rich spring is observed in both the [Ca^{2+}] and [H_2O_2] curves, while the summers are seen in both the [NH_4^+] and ECM curves reduces the counting error significantly as measurement-related problems and resulting data gaps often affect only one series at a time. When either the spring or summer indication is weak, or when the relative timing of the spring and summer indicators is unusual, an "uncertain layer mark" has been placed. From the start it was agreed between the investigators that the uncertain marks should be regarded and counted as "half years," and the uncertain marks have therefore been set with this in mind. The validity of the applied criteria has been tested by marking annual layers in the Holocene II section using GRIP data only, and subsequently cross-validating with the NGRIP annual layer sequence. Differences smaller than 1% were observed, and the criteria used in the GRIP and NGRIP parts are therefore considered to be consistent.

[18] In practice, the timescale was constructed by first letting three investigators (BMV, JPS, and SOR) independently place annual layer marks. The three annual layer profiles were different in around 200 places in the 2.4 ky long section, but the total number of annual layer marks in the three profiles agreed within 1.5%. Each point of disagreement was subsequently reviewed with a fourth investigator (HBC) acting as arbitrator. The resulting timescale represents a compromise between the three initial versions, using uncertain layer marks to mark points where unanimity could not be reached, or where either the spring or summer indicators are not clear. The resulting timescale contains about 1.5% more annual layers than the previous counted GRIP scale in the Holocene I section [*Johnsen et al.*, 2001].

4.2. Multiparameter Annual Layer Counting in the NGRIP Ice Core

[19] The NGRIP data set comprises an extensive set of measurements, where a clear annual signal is present in up to 9 parallel data series. As an initial approach, three investigators (KKA, AMS, and JPS) made independent annual layer counts based on all available NGRIP data series. In the Holocene, Allerød, and Bølling periods, the

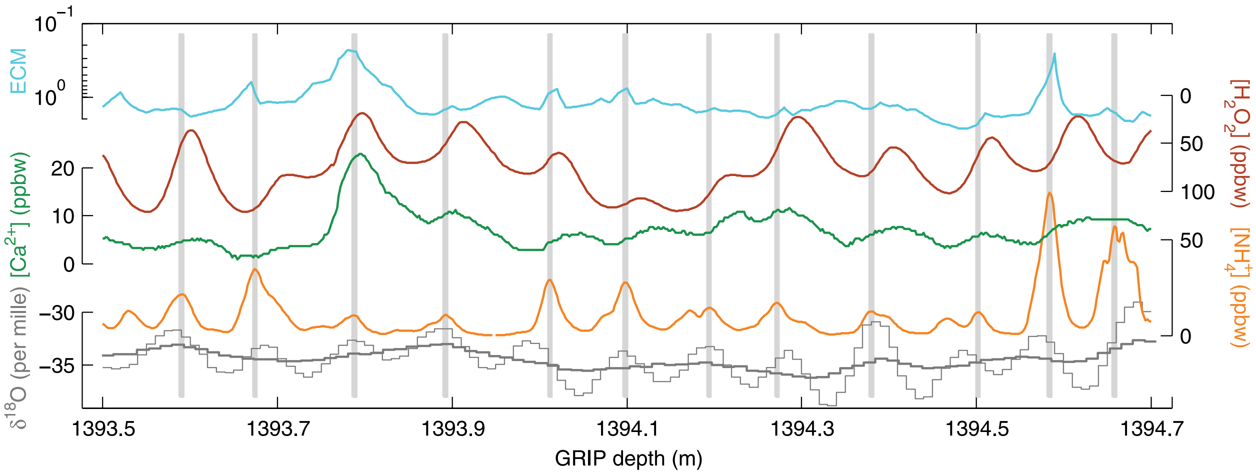

Figure 3. Example of 1.2 m of GRIP data and annual layer markings (gray vertical bars) from about 8.8 kyr b2k. The annual layers are identified as matching pairs of spring and summer indicators: spring is characterized by high dust content, leading to peaks in $[Ca^{2+}]$ and dips in the $[H_2O_2]$ curve, while summer is characterized by high $[NH_4^+]$ and corresponding minima in the ECM curve. Note that the ECM and $[H_2O_2]$ curves are plotted on reversed scales. In this section the annual layer identification procedure is supported by high-resolution $\delta^{18}O$ data, corrected for diffusion using the method of *Johnsen* [1977] and *Johnsen et al.* [2000] (raw data, thick line; diffusion corrected data, thin line).

investigators agreed within a few percent on the number of annual layer marks, and in many century-long sections they agreed on every year, but in the Younger and Oldest Dryas discrepancies of up to 5% and 10%, respectively, were observed. The differences were most pronounced in the coldest periods where thin annual layers begin to appear as shoulders on neighboring peaks, and around sharp transitions. Again the three initial timescales were reviewed with a fourth investigator (SOR) acting as arbitrator, thereby producing a timescale where every annual layer marking was acceptable by all investigators. Ambiguous features and points, where unanimity could not be reached, were marked by uncertain layer marks.

4.2.1. Holocene II Section, NGRIP Depth 1404.7–1492.45 m

[20] In the Holocene, the series show strong and different seasonality as described in section 3 and illustrated in the upper part of Figure 4. Slightly different relative timing of the different species is often observed for one or two years, most often related to apparent merging of successive seasons, where, e.g., winter and spring peaks or spring and summer peaks occur simultaneously as observed in Figure 4, where the $[Na^+]$ winter peak and the following $[Ca^{2+}]$ and dust spring peaks occur at the same depth of 1464.87 m. The fact that the different series have different seasonality makes it highly improbable that full years are missing in the data set due to post-depositional processes or missing precipitation, and also makes the identification of annual layers very robust. Of the 1436 annual layers marked in this section, only 23 marks, or 1.6%, were marked as uncertain layers. Of these 23 marks, 20 are placed where some series indicate that an annual layer is present, while other series do not have evidence of a layer. The remaining 3 uncertain layers are caused by data gaps or short sections with data quality problems.

[21] GRIP CFA data are also available in the Holocene II section, and the GRIP and NGRIP cores can be matched on an annual basis by first using major ECM horizons to provide a low-resolution stratigraphic matching of the two records and then by matching the $[NH_4^+]$ profiles of the two cores year by year in between the fix points. In Figure 4, the NGRIP data (upper nine panels) are presented together with the corresponding $\delta^{18}O$, $[NH_4^+]$, $[Ca^{2+}]$, $[H_2O_2]$, and ECM series from GRIP (lower five panels). In order to be able to asses the possible bias of the annual layer counting procedure, two investigators (BMV and HBC) constructed a timescale for the Holocene II period using the combined data set of CFA and ECM data from both NGRIP and GRIP independently from the four-investigator NGRIP timescale described above. The question of possible bias will be discussed further in section 5.1.4.

4.2.2. Younger Dryas Section, Depth 1492.45–1526.52 m

[22] During cold periods like the Younger Dryas, those series showing annual cycles mostly peak simultaneously. This supports the conclusions of *Werner et al.* [2000] that point to that central Greenland receives only little winter precipitation under glacial conditions. Although there is roughly one $[NH_4^+]$ peak per year on average, the $[NH_4^+]$ signal was not in general regarded as being reliable for annual layer identification in the Younger Dryas. Also the ECM signal becomes very hard to interpret in some sections. In the Younger Dryas, the expected mean annual layer thickness derived from flow modeling is less than twice the wavelength of the shortest cycle that can be resolved by the CFA measurements. Thus thin annual layers may be poorly resolved or in exceptional cases vanish. When identifying the annual layers, special consideration was put into identifying features that could represent two almost merged layers. In Figure 5 the usable data series (original and resolution enhanced) are shown together with the annual layer markings. The uncertain layer at depth 1502.39 m could possibly be a thin annual layer that cannot be fully

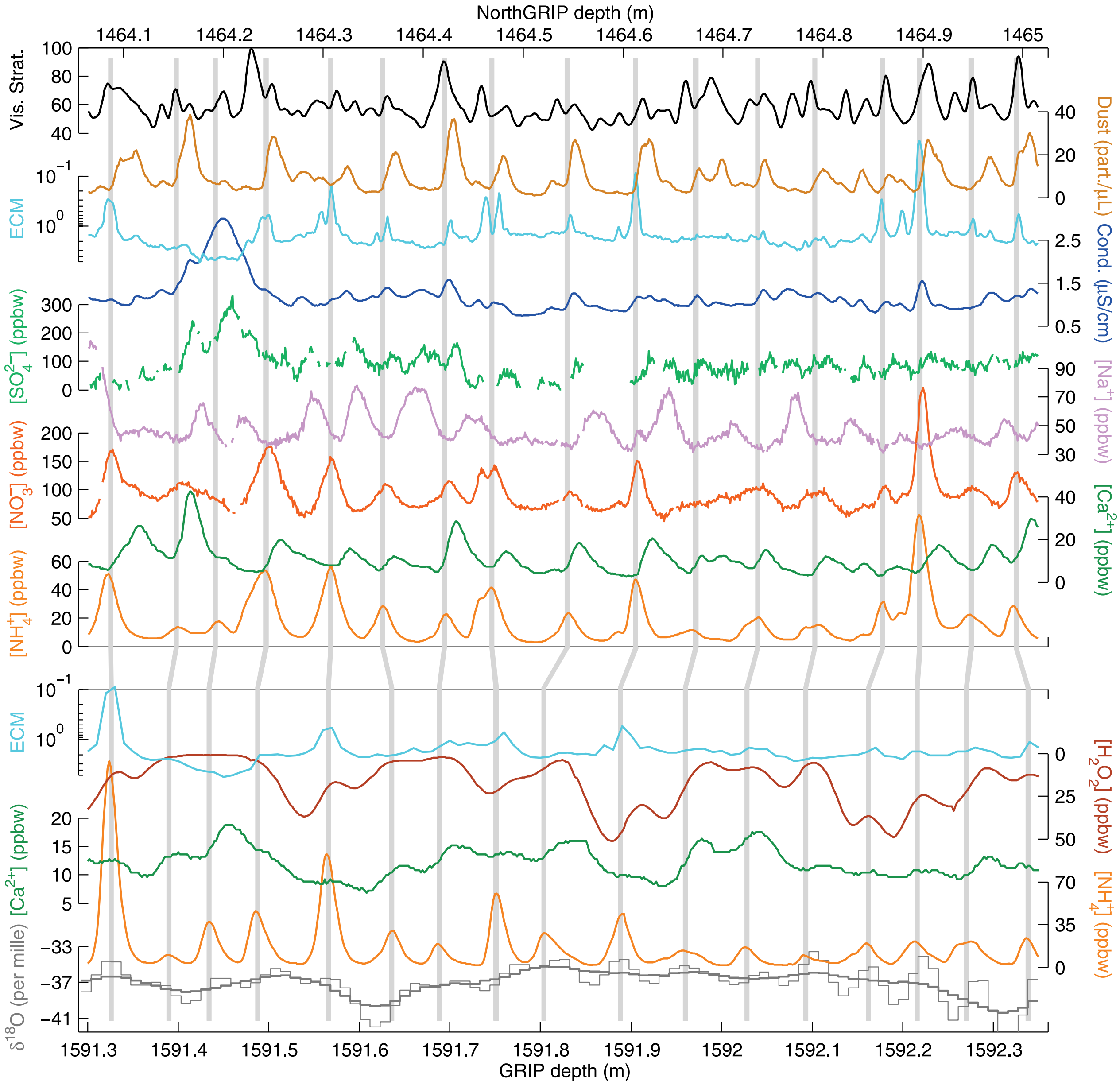

Figure 4. Example of data and annual layer markings (gray vertical bars) from the early Holocene. The upper nine panels show a 0.95-m-long section of NGRIP data, and the lower five panels show the corresponding 1.05-m section in the GRIP data set. The annual layers are marked at the summer peaks, which are defined by high [NH_4^+] and [NO_3^-]. The spring is characterized by high dust mass, leading to peaking [Ca^{2+}] and dips in the [H_2O_2] profile, while the [Na^+] peaks in late winter. The visual stratigraphy profile does not contain clear annual layers but contains peaks corresponding to almost every dust peak. The ECM (note the reverse logarithmic scale) anticorrelates strongly with the largest peaks in [NH_4^+] but does not itself allow safe identification of annual layers. The lower four panels show the same time interval in the GRIP core, from which [Ca^{2+}] and [NH_4^+] measurements exist [*Fuhrer et al.*, 1993, 1996, 1999]. The similarity of the [NH_4^+] records (and consequently also to some degree the ECM records) from NGRIP and GRIP allows a close stratigraphic matching of the two cores. The annual layer identification has been based on impurity data only but is supported by comparison with high-resolution δ^{18}O data that are available for a few short sections in the Holocene. The δ^{18}O data have been corrected for diffusion using the method of *Johnsen* [1977] and *Johnsen et al.* [2000] (raw data, thick line; diffusion corrected data, thin line).

resolved, but may also just arise from unusually shaped annual peaks.

[23] 1232 annual layers are marked in the Younger Dryas, of which 78 are uncertain. The uncertain layers fall in two categories: layers that are only supported by evidence in some of the series (type I), and as the one illustrated, shoulders, wide peaks, or double peaks that could represent two thin annual layers not fully resolved or one annual layer

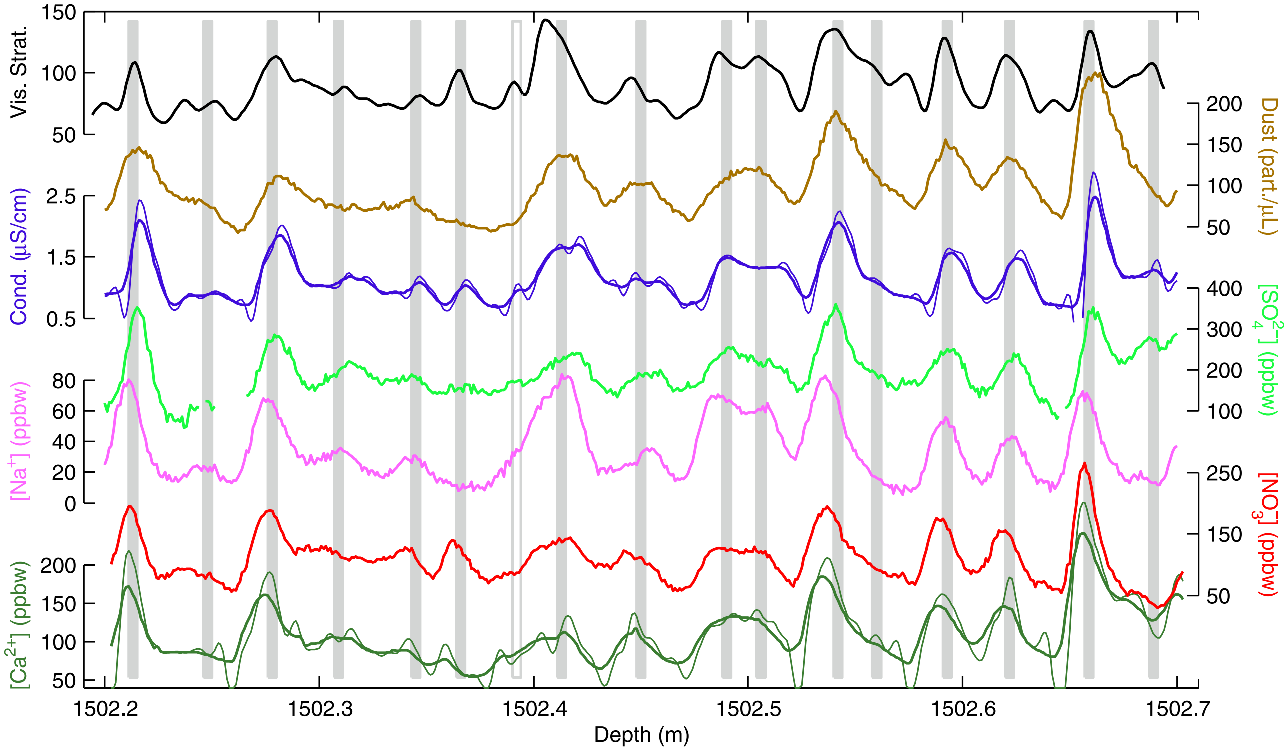

Figure 5. Example of data (heavy lines), resolution-enhanced data (thin lines), and annual layer markings (gray bars) from the Younger Dryas. The different series peak almost simultaneously, and peaks in the VS profile are seen to be connected closely to the annual layers. However, too many layers could easily be counted if the counting was based on VS data alone, emphasizing the importance of using multiple data series for annual layer counting. The uncertain layer (open gray bar) at 1502.39 m is a potential thin annual layer, not fully resolved by the measurements.

represented by peaks with unusual shapes (type II). Type II layers account for almost 3/4 of the uncertain layers in the Younger Dryas.

4.2.3. Bølling and Allerød Sections, Depth 1526.52–1604.64 m

[24] The Bølling and Allerød sections proved to be the most challenging sections to date, due to the very changeable nature of the data (and climate) in this time interval. Stable isotope data show that climatic conditions generally change from a rather warm climate at the beginning of the Bølling to a much cooler climate at the end of the Allerød, but also that the temperature changes abruptly toward both cooler and warmer conditions several times during this period. This variability is clearly observed in all data series. The seasonality of the series changes rapidly several times; from conditions similar to those in the Younger Dryas, where all series peak simultaneously, to Holocene-like conditions where the series have different seasonality. These changes do not always happen synchronously with changes in the concentration levels, isotopic values, or observed annual layer thickness. A detailed study of the different timing of the changes in the different data series can increase the understanding of the physical processes governing the climate system, but this is beyond the scope of this work. However, the observed changes of the properties of the data make the identification of annual layers difficult, even when all data series are available.

[25] In the warmer parts of Bølling and Allerød, the [NH_4^+] series proves useful for dating, as observed in the Holocene. The VS and conductivity series show clear annual cycles in the sections where most series peak simultaneously. The [NH_4^+] and [NO_3^-] series are observed to have a peculiar tendency to contain additional simultaneous summer peaks not present in the other series, a phenomenon not encountered elsewhere in the data used in this work. In Figure 6, a section from a relatively cold part of Allerød is shown. It is apparent that the relative timing of the different series is less constant than in the Holocene and Younger Dryas. Note also how the [NH_4^+] and [NO_3^-] series have roughly the same number of peaks as the other series, but without exhibiting a clear annual cycle, and that the dust mass series only barely resolves the annual cycle. The ECM does not show clear annual cycles, and there are substantially more peaks in VS than those associated with the annual layers. A section at the boundary between Bølling and Allerød (inside MIS-1d) is shown on Figure 7. It is also a relatively cold period, having δ^{18}O-values only slightly higher than those in the Allerød section in Figure 6. The dust and [NH_4^+] series have been excluded, as they do not show annual cycles, while the [NO_3^-] and ECM series again are showing clear annual cycles. Note also how the series peak almost simultaneously, and that the annual layers can be placed based almost on the ECM and VS series alone. The sections in Figures 6 and 7 would be expected to be rather similar from their isotopic values alone, but the differences clearly illustrate the challenges of identifying annual layers in periods with highly variable climatic conditions.

[26] Of the 1843 annual layer markings in the Bølling and Allerød, 94 are uncertain layers. About 10 are placed to

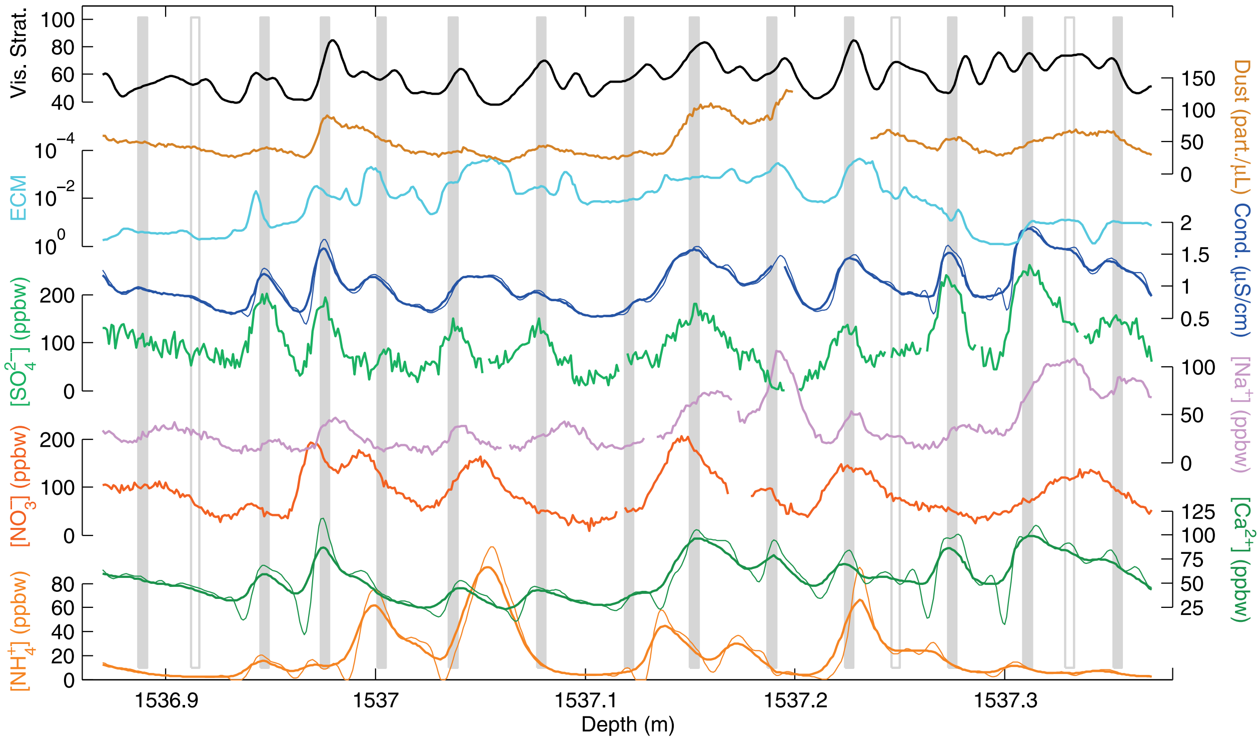

Figure 6. Example of data (heavy lines), resolution-enhanced data (thin lines), and annual layer markings (gray bars) from a cold period in Allerød. In this section the [NH$_4^+$] and [NO$_3^-$] series do not show clear annual cycles, while the other series peak almost simultaneously. The open gray bars indicate uncertain layers. The annual layer marks have been set in the annual peaks of [Ca^{2+}].

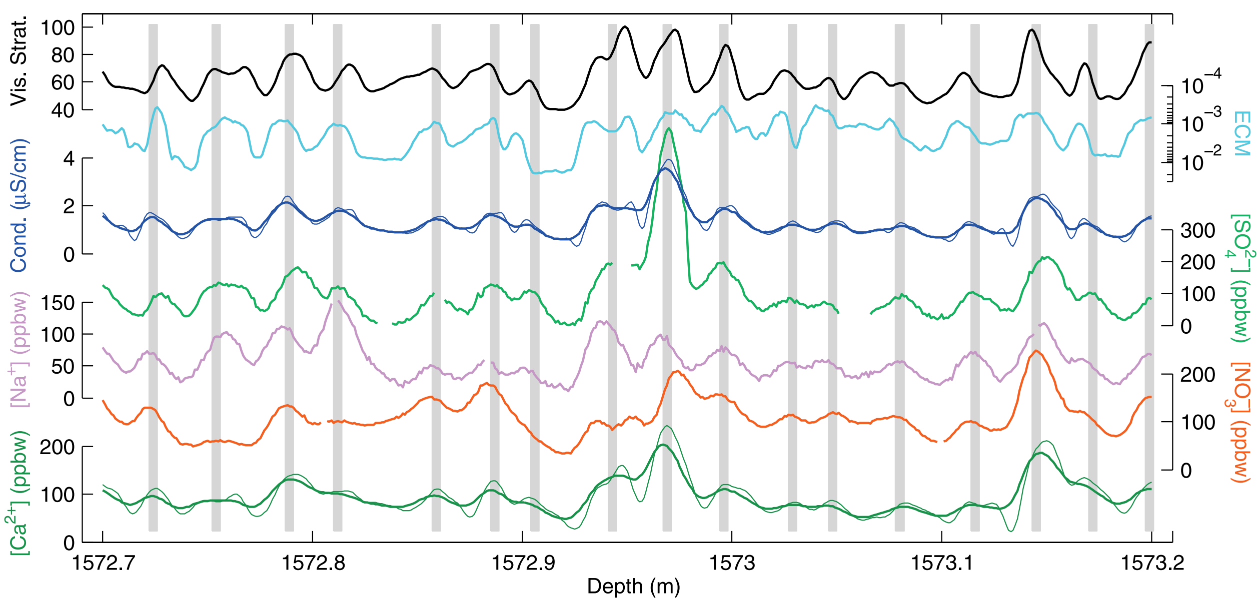

Figure 7. Example of data (heavy lines), resolution-enhanced data (thin lines), and annual layer markings from the cold period between Bølling and Allerød (MIS-1d), with δ^{18}O values close to that of the section shown in Figure 6. However, in this section all series peak simultaneously, and there are no variations in seasonality. The [NO$_3^-$] and ECM series show clear annual cycles, and the annual layers could be identified with reasonable certainty based on the ECM and VS series alone. The [NH$_4^+$] signal is not shown, as it does not exhibit a clear annual signal.

mark layers that are uncertain because of data quality problems and data gaps, and the rest are equally divided between the two types defined in section 4.2.2.

4.2.4. Oldest Dryas Section, Depth 1604.64 m and Below

[27] In the Oldest Dryas, the phasing of the series is similar to the phasing observed in the Younger Dryas. When comparing the data resolution with estimated model annual layer thicknesses from the ss09sea model of *NGRIP Members* [2004], it is apparent that the resolution is marginal in the Oldest Dryas. An inspection shows that the data series do indeed contain many double peaks, wide peaks, and shoulders suspected to contain additional annual layers. As the initial approach, we use the same criteria as in the Younger Dryas, marking the most prominent of these features with two annual layer markings and the less pronounced with an annual layer marking plus a type II uncertain layer marking. However, it is clear that many weak indications remain in the data that could possibly represent additional annual layers. Because of the marginal resolution of the CFA data, more emphasis has to be put on the highly resolved VS and ECM data series, and only the last few meters of the Oldest Dryas before the transition into Bølling have therefore been included in the presented timescale. The timescale for these few meters is slightly less reliable, but because of the shortness of the section (87 marks, of which 7 are uncertain), and the fact that the isotope values (and thus the expected annual layer thickness) do not attain full glacial values, the problem is of minor importance.

5. Constructing the Final Timescale

[28] As described in section 4, the datum of the presented timescale is the volcanic horizon inside the 8.2 kyr cold event dated in the DYE-3 ice core to 8236 b2k with a maximum counting error of 47 years. In the Holocene I section, the revised timescale based on GRIP CFA data is used. The GRIP timescale has been transferred to NGRIP by matching the ECM signals of GRIP and NGRIP. The GRIP [NH_4^+] series contains clear annual peaks, and because peaks in the [NH_4^+] series lead to minima in the ECM signal, it is possible to match the two series on an annual scale. The matching can be ambiguous, but for every few tens of years better fix points are supplied by strong ECM peaks, primarily related to volcanism, or by recognizable patterns in the [NH_4^+] and ECM curves. The mismatch is estimated to be maximum one year at fix points and maximum 3 years in long sections without fix points. The result is a common Holocene I timescale for GRIP and NGRIP starting with the year 7903 b2k (GRIP depth 1299.82 m, NGRIP depth 1194.05 m), leading up to the year 10,276 b2k (GRIP depth 1522.79 m, NGRIP depth 1404.71 m) after which the NGRIP CFA data start.

[29] In the Holocene II section, the four-investigator timescale based on NGRIP data and the two-investigator timescale based on both GRIP and NGRIP data have been combined. The latter is constructed without uncertain layer markings, while the first one contains 23 uncertain marks. On top of the uncertain layers only present in the 4-investigator timescale, the number of years found in one but not the other timescale amounts to 9 and 7 annual layer markings, respectively. In order to reach a common result, the two timescales were compared and combined by one investigator from each group. It was agreed how to interpret the combined GRIP and NGRIP data in each of the 39 points of disagreement. The use of uncertain layer markings has been adopted for this combined timescale, and the uncertain layers were counted as 0.5 year in the construction of the final timescale. The resulting Holocene II timescale is valid for both cores, covering the age interval 10,277–11,703 b2k, and contains 6.6% more annual layers than the existing GRIP timescale [*Johnsen et al.*, 1992]. Finally, the timescale of the Holocene I and II periods was transferred to DYE-3 depths using the same ECM-based matching procedure, making the GICC05 timescale valid for all three cores.

[30] The annual layer counting in NGRIP continues back to a depth of 1607 m, reaching a few meters below the Oldest Dryas - Bølling transition, which is found at a depth of 1604.64 m, corresponding to an age of 14,692 b2k. As above, the uncertain marks have been counted as 0.5 year.

[31] Below the YDPB transition, matching of the GRIP and NGRIP series becomes more difficult as the GRIP CFA fails to resolve the annuals in the Younger Dryas, and the annual cycles in the ECM signal become hard to identify. The timescale obtained from the NGRIP CFA data can therefore not readily be transferred on a year-by-year basis to the GRIP core below the YDPB transition. Work by *Seierstad et al.* [2006] focuses on the possibility of matching the GRIP and NGRIP records at greater depths, and on identifying annual layers based on high-resolution δD data within the Bølling-Allerød period in the GRIP core, and future progress in this work will hopefully extend the time range where GRIP data is available on the GICC05 timescale.

5.1. Assessing the Uncertainty

[32] Contributions to the uncertainty of a stratigraphic ice core timescale include problems with the core stratigraphy, core loss during drilling and handling, data loss during sampling and measurements, insufficient measuring resolution, and misinterpretation of the annual layer record [*Alley et al.*, 1997].

5.1.1. Uncertainty From Imperfect Core Stratigraphy

[33] The basic assumption that the ice core comprises an unbroken sequence of precipitation from the past can be erroneous due to missing precipitation or due to post-depositional processes like re-deposition or melting. The relatively high accumulation rates and small surface slopes make loss of full years due to missing precipitation or wind scouring unlikely [*Fisher et al.*, 1983], and melt events are known to occur only extremely rarely at the GRIP and NGRIP drill sites. In the 1400 year long Holocene II section where both GRIP and NGRIP CFA data exist, the records were matched year to year, and no indication of missing years was found when comparing the records, substantiating the assumption of the ice cores being unbroken annual layer sequences. This is also supported by the discussion in section 6. In cold periods with lower accumulation, and possibly more stormy conditions, this may not be true, but the uncertainty contribution from imperfect core stratigra-

phy is considered to be insignificant in the time periods spanned by this work.

5.1.2. Uncertainty From Data Gaps

[34] In the depth interval considered in this work, core loss is nonexistent, and only very short sections of the NGRIP core could not be sampled for the CFA measurements. Around irregular core breaks, the ends of the CFA sample pieces had to be trimmed, resulting in a few centimeters of missing CFA data, but VS and ECM measurements are often available across these short CFA data gaps. Most of the gaps are less than a centimeter long, not causing ambiguities in the process of annual layer identification. Longer data gaps of 2–10 cm (corresponding to about once or twice the mean annual layer thickness) occur on average every five meters or so, but using the ECM and VS data, it is usually possible to place the annual layer markings without significant uncertainty. In addition to the short sections where all CFA data are missing, one or more of the CFA series are sometimes missing over longer intervals due to problems with one or more of the analysis subsystems. In the cases where annual layer identification has been difficult due to missing data series, the uncertainty has been indicated by using uncertain layer marks. The total uncertainty due to missing data is thus estimated to be around ten years out of the 4000–5000 years spanned by the NGRIP data in this work, and most of the uncertainty is accounted for by the use of uncertain layer markings.

[35] In the GRIP Holocene I section there are occasional CFA data gaps affecting one or two of the series, totalling about 10 m, plus a number of smaller gaps which do not cause problems for the annual layer identification. Most of the longer gaps contain 2–4 annual layer marks, but the uncertainty contribution is small because all species are not missing at the same time, and because ECM data are available across the CFA data gaps. The estimated total uncertainty contribution from data gaps is a few per mille, of which the major part is accounted for via the use of uncertain layer marks.

5.1.3. Uncertainty From Insufficient Measuring Resolution

[36] The combined CFA, ECM, isotope, and VS data set is believed to resolve the annual layers well in the Holocene and in the warm parts of the Bølling and Allerød, while extraordinarily thin annual layers may show up only faintly or be lost in the Younger Dryas and in the coldest parts of the Allerød period.

[37] In the Holocene section, only a couple of features that could represent poorly resolved layers were identified. These were marked with uncertain layer marks. It is not considered to be likely that a significant number of years have vanished completely due to insufficient resolution.

[38] Double peaks suspected to contain more than one year are much more common in the Younger Dryas section. In addition, a small number of years may have been lost altogether due to insufficient resolution at the end of Allerød and in the Younger Dryas. Special care was taken not to miss thin layers represented as poorly separated double peaks or shoulders on neighboring peaks. Depending on the amount of evidence present, these features were marked as two layers or as a layer and an uncertain layer. The upper limit of the number of lost layers is estimated to be a few tens of years in the section comprising the Younger Dryas and the end of Allerød, corresponding to about 1% of the section's annual layers.

5.1.4. Uncertainty From Erroneous Interpretation of the Annual Layer Record

[39] The vast majority of annual layers stand out clearly in all data series, but uncertainty is introduced when an annual layer is backed up by evidence only in some of the data series, or when a certain well-resolved feature is suspected to contain more than one annual layer. Also, the basic assumption that the annual layers in ice cores are represented by peaks in almost all the individual data series may not be perfectly true. This uncertainty contribution is the dominant part of the total uncertainty, but can only be partially assessed quantitatively. The cases of ambiguity in the annual layer identification process have been identified using the uncertain layer markings, but in addition one must expect that there can be a bias in the annual layer identification process. This is clearly illustrated by the result of the revision of the GRIP Holocene timescale. As described in section 4.1 and 5, the number of annual layers in the Holocene I and II sections have increased by 1.5% and 6.6% from the old to the new GRIP timescale, respectively. These differences reflect a change in the way data are interpreted, rather than counting errors, which is reflected by the fact that the increase in the number of annual marks in the Holocene II section is 4–5 times larger than the number of uncertain layer marks in the same section.

[40] The comparison of the 2-investigator and the 4-investigator timescales of the Holocene II section constitutes the only place where we can make an independent bias magnitude estimate. The two timescales were made using partially the same data, but the two groups of investigators worked independently of each other. The differences are described in section 5, and indicate a bias level of 1% or less in the Holocene II section. Below the YDPB transition, we do not have the opportunity of checking the timescale with independent ice core data, and thus only aim at estimating the maximum counting error, which we derive from the number of uncertain layer marks. Over the total depth interval in question here, 294 of 7021 annual layer marks (corresponding to 4.2%) were of the uncertain type. As the uncertain layer marks are regarded as 0.5 ± 0.5 year in the final timescale, the number of years in the section is 6874 with a maximum counting error of 147 years assuming that the counting errors are correlated. In Table 3, the number of layer markings within each climatic period are listed together with the maximum counting error derived from the number of uncertain layer markings in this way. The counting error derived from the uncertain layer markings heavily depends on whether the uncertainties are assumed to be correlated or uncorrelated, and consequently on which error summation procedure should be applied. If the counting errors are assumed to be fully uncorrelated, the errors should be summed in a quadratic sense, producing a maximum counting error estimate of $\sqrt{\left(\frac{1}{2}\right)^2 + \ldots + \left(\frac{1}{2}\right)^2} = \sqrt{294\left(\frac{1}{2}\right)^2} = \frac{\sqrt{294}}{2} \approx 9$. Using the more reasonable assumption that the errors are fully correlated within each climatic period and uncorrelated from one period to the other, the maximum error estimate becomes $\sqrt{48^2 + 10^2 + 39^2 + 31^2 + 17^2 + 4^2} = 72$, using the period division from Figure 1. This approach was also used

Table 3. Estimated Maximum Counting Error Excluding Possible Bias in the Annual Layer Identification Process for the Different Climatic Periods

Section	NGRIP Depth, m	Number of Annual Layers		Duration, years	Maximum Counting Error	
		Certain	Uncertain		Absolute, years	Relative
Holocene I	1194.05–1404.74[a]	2326	96	2374	48	2.0%
Holocene II	1404.74–1492.45	1418	19	1427	10	0.67%
Younger Dryas	1492.45–1526.52	1154	78	1193	39	3.3%
Allerød	1526.52–1574.80	1147	61	1178	31	2.6%
Bølling	1574.80–1604.64	602	33	618	17	2.7%
End of Oldest Dryas	1604.64–1607.00	80	7	84	4	~4%
Total		6727	294	6874	147	2.1%

[a]Timescale based on GRIP CFA data, corresponding GRIP depths: 1299.81–1522.75 m.

when deriving counting error estimates for the previous GRIP timescale, but has the obvious disadvantage that the maximum counting error estimate depends on the choice of which periods are considered independent. If for example the Allerød period is considered to consist of 4 independent periods (corresponding to the GIS1a-e of *Björck et al.* [1998]), the 61 uncertain layer marks only result in a maximum counting estimate of $\sqrt{\left(\frac{9}{2}\right)^2+\left(\frac{10}{2}\right)^2+\left(\frac{38}{2}\right)^2+\left(\frac{4}{2}\right)^2} \approx 20$ years instead of 31 years if Allerød is considered to be one period. Recognizing that the counting errors in reality are neither uncorrelated nor fully correlated, we adopt the simple and conservative approach, summing up the uncertainties as if they were correlated. The counting error estimates presented here are thus highly conservative, and as the maximum counting error dominates over the sources of uncertainty associated with imperfect stratigraphy and data gaps by about an order of magnitude, only the maximum counting error is given. The uncertainty from bias in the annual layer identification process can by the nature of the problem not be estimated without the existence of independent data sources, and is thus not included in the error estimates presented.

6. Distribution of Annual Layer Thicknesses

[41] Figure 8 shows the annual layer thickness profile derived from the NGRIP core using the GICC05 timescale. The uncertainty band indicated in the figure is derived from the uncertain layer marks, and thus represents the part of the uncertainty that arise from features in the data that the investigators found ambiguous. The strain correction has been performed using a first-order flow model, where the strain ϵ at depth z is given as $\epsilon = 1 - \frac{z}{z_0}$. The value z_0 = 2680 m is used, whereby ϵ closely resembles the strain history derived from the ss09sea model [*NGRIP Members*, 2004] in the 1200–1600 m depth interval. As the ss09sea model timescale is significantly different from the GICC05 timescale in this interval, the absolute accumulation rate values should therefore be regarded as preliminary. However, the ratios between the accumulation rates in the Holocene II, Younger Dryas, and Bølling periods are robust to a wide range of reasonable z_0 values.

[42] Distributions of strain corrected observed annual layer thicknesses within three selected periods are shown in Figure 9 (note the logarithmic scale). To ensure that the climatic conditions are rather constant within each period, the variable Allerød period has been excluded, and a few meters at each end of the periods have been removed to ensure that the transitions between the individual periods do not influence the distributions. It is apparent from the figure that the annual layer thicknesses to a good approximation are log-normally distributed, and that the variability of the annual layer thicknesses is by far smallest in the Holocene II section, and roughly identical for the Younger Dryas and Bølling sections. If the conclusion that annual layer thicknesses are log-normally distributed holds in general, mean and standard deviation values of accumulation rates should be calculated from logarithmic transformed data rather than from the observed annual layer thicknesses, contrary to common usage, because the notion of standard deviation makes more sense when calculated for data that are approximately symmetrically distributed. Using the mean accumulation rate values derived from the fitted log-normal curves

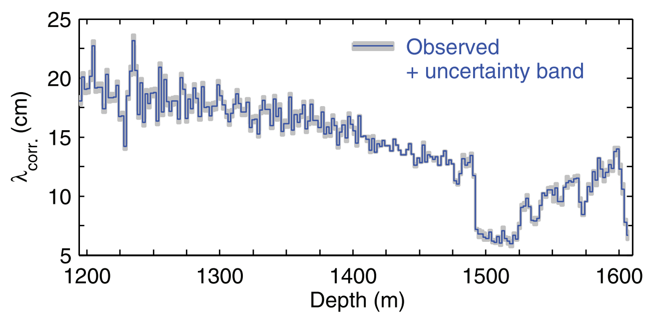

Figure 8. Observed annual accumulation rates after strain correction, λ_{corr}, averaged over 2-m sections. The shaded uncertainty band is derived from the uncertain annual layer marks (in the Holocene II and glacial parts) and thus represents only the part of the uncertainty that is related to ambiguous features in the data set. In the Holocene I section a constant 2% uncertainty band is used. The high variability of λ_{corr} in the Holocene I section is likely to be caused by a combination of two effects: (1) at smaller depths, each 2-m interval contains fewer annual layers, resulting in increased scatter around the mean value; and (2) the transfer of the GRIP databased timescale to NGRIP depths using common ECM fix points introduces an uncertainty in the number of annual layers in each 2-m interval, and thus in the derived accumulation rates, although the total number of annual layers remains accurate. The accumulation rates are sensitive to how the strain correction is performed and should be regarded as preliminary results.

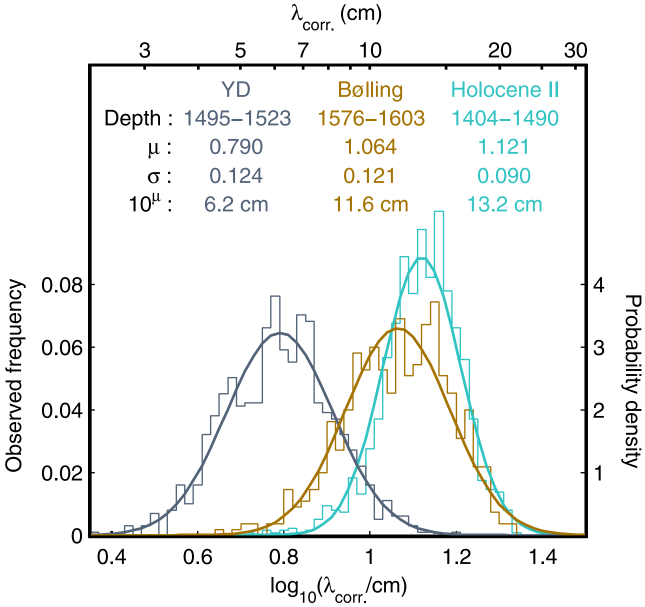

Figure 9. Distribution of strain corrected annual layer thicknesses λ_{corr} in the Holocene II, Younger Dryas, and Bølling periods (thin lines). The distributions of $\log(\lambda_{corr})$ in each of the three periods are close to Gaussian distributions (thick lines). The coefficients of the fitted Gaussian curves are listed. The annual layer thickness is thus seen to have a log-normal distribution, and the chances of encountering an annual layer with half and double the mean thickness, respectively, are thus equal (see section 6). The mean accumulation rates (the 10^{μ} values) derived from the fitted curves are sensitive to how the strain correction is performed and should be regarded as preliminary results.

of Figure 9, the accumulation rate in the Younger Dryas and Bølling periods are 47% and 88% of the Holocene II value, respectively, or 48% and 89% of the Holocene II values if ordinary mean values are used. These ratios are robust within ±1% for $z_0 \in [2580, 2780]$m. Although the strain profile derived from the ss09sea model is not fully consistent with the GICC05 timescale, the inaccuracy of the strain profile is regarded to be smaller than the effect of varying z_0 within the bounds described, and we thus regard the accumulation rate ratios presented to be precise at least within ±2%. The ratios indicate a smaller contrast between the stadial and interstadial accumulation rates than those observed in the GISP2 ice core where the similar ratios are approximately 43% and 97% [*Alley et al.*, 1993; *Cuffey and Clow*, 1997].

[43] Being log-normally distributed, annual layers with, e.g., double and half the mean annual thickness λ_{mean}, respectively, will occur with equal probabilities. Using the fitted distributions, the probability of a random annual layer being either thicker than $2\lambda_{mean}$ or thinner than $\lambda_{mean}/2$ can be estimated to be below 0.1% for the Holocene II section, 1.5% for the Younger Dryas, and 1.3% for Bølling. When compared with the resolution of the data used in this work, the distribution of the annual layer thicknesses for the Holocene II section indicates that it is extremely unlikely that any annual layers have been missed in the Holocene parts of this work due to insufficient resolution, and that the problem also should be negligible in the Bølling section.

7. Discussion and Conclusions

[44] The GICC05 timescale across the last termination (7,903 – 14,776 b2k) has been constructed by identifying and counting annual layers using multi-parameter data sets from the GRIP and NGRIP ice cores. The ages of the onset and end of the Younger Dryas, Bølling and Allerød periods can be found in Table 4 along with the ages of the Saksunarvatn and Vedde volcanic ash layers. In Figure 10, 20 year mean values of NGRIP δ^{18}O data are shown on the GICC05 timescale. For comparison, the same δ^{18}O data are shown on the previously used timescales: the existing counted timescale for the Holocene part and the ss09sea model timescale below the YDPB transition [*Johnsen et al.*, 1992, 2001]. The GRIP isotope profile is not displayed, as the ss09sea timescale is common to the GRIP and NGRIP cores [*NGRIP Members*, 2004]. The 20 year resolution GISP2 isotope profile of *Grootes and Stuiver* [1997] and *Stuiver and Grootes* [2000] is presented on the timescale of *Meese et al.* [1997]. The differences between the timescales are apparent in Figure 11, where the differences in the dating of 46 selected ECM horizons in the three timescales are shown.

[45] At the datum of the GICC05 timescale (8236 b2k), the existing NGRIP timescales yield ages that are about 20 years younger than the GICC05, but the difference grows increasingly fast toward the YDPB transition. The transition has been dated to 11,703 b2k with a maximum counting error of 99 years, pushing the YDPB transition about 150 years back relative to the previous GRIP and NGRIP age estimates. The difference increases slowly to

Table 4. Age and Maximum Counting Error Estimates for Selected Horizons[a]

Horizon	NGRIP Depth, m	Age, b2k	Total Maximum Counting Error, years
Upper limit of presented timescale	1194.05	7,903	41
Timescale datum (8.2 kyr cold event)	1228.24	8,236	47
Saksunarvatn volcanic layer	1409.83	10,347	89
YD-Preboreal transition	1492.45	11,703	99
Vedde volcanic layer (Z1)	1506.14	12,171	114
Onset of Younger Dryas	1526.52	12,896	138
End of Bølling	1574.80	14,075	169
Onset Bølling	1604.64	14,692	186
Lower limit of presented timescale	1606.96	14,776	190

[a]The total maximum counting error consists of a maximum counting error derived as described in section 5.1.4 plus the 41-year maximum counting error from the dating of the upper 7.9 kyr in the DYE-3 ice core but does not include possible bias in the annual layer identification process. All ages are reported relative to A.D. 2000 (b2k).

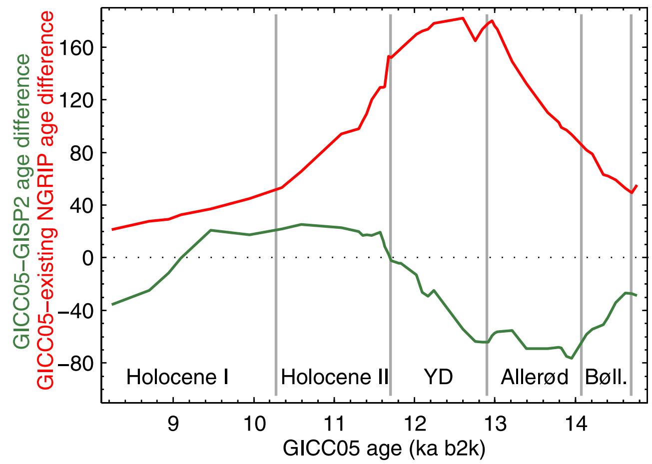

Figure 11. Detailed comparison of the GICC05 timescale with the existing NGRIP/GRIP timescales (specified in the caption of Figure 10) and the GISP2 timescale of *Meese et al.* [1997] using the dates of 46 common ECM events in the NGRIP, GRIP, and GISP2 cores (see Figure 10). Positive values indicate that an event is older according to the GICC05 timescale.

about 180 years at 12.5 kyr b2k, and then monotonically decreases again through the Allerød and Bølling periods until the onset of Bølling, where the difference has been reduced to about 50 years. The differences between the former and new timescales in the Holocene part reflect the new interpretation of the GRIP data, while the differences below the YDPB transition indicate that the relationship between δ^{18}O and accumulation used to construct the model timescales [*Johnsen et al.*, 1995; *Dahl-Jensen et al.*, 1993; *Johnsen et al.*, 2001] needs improvement in the Bølling and Allerød periods.

[46] In general, the GICC05 timescale agrees better with the GISP2 timescale than the former GRIP and NGRIP timescales. At the 8.2 kyr event the GISP2 timescale yields dates that are 36 years older than the corresponding GICC05 ages, but the main difference between the GICC05 and GISP2 timescales in the Holocene is the number of annual layers in the 8.2–9.5 kyr b2k section, where the GISP2 timescale lacks about 60 years, or 5%, relative to the GICC05. It should be noted that the investigators producing the GISP2 timescale did not agree on the number of years in the GISP2 1371–1519 m depth interval (GISP2 age

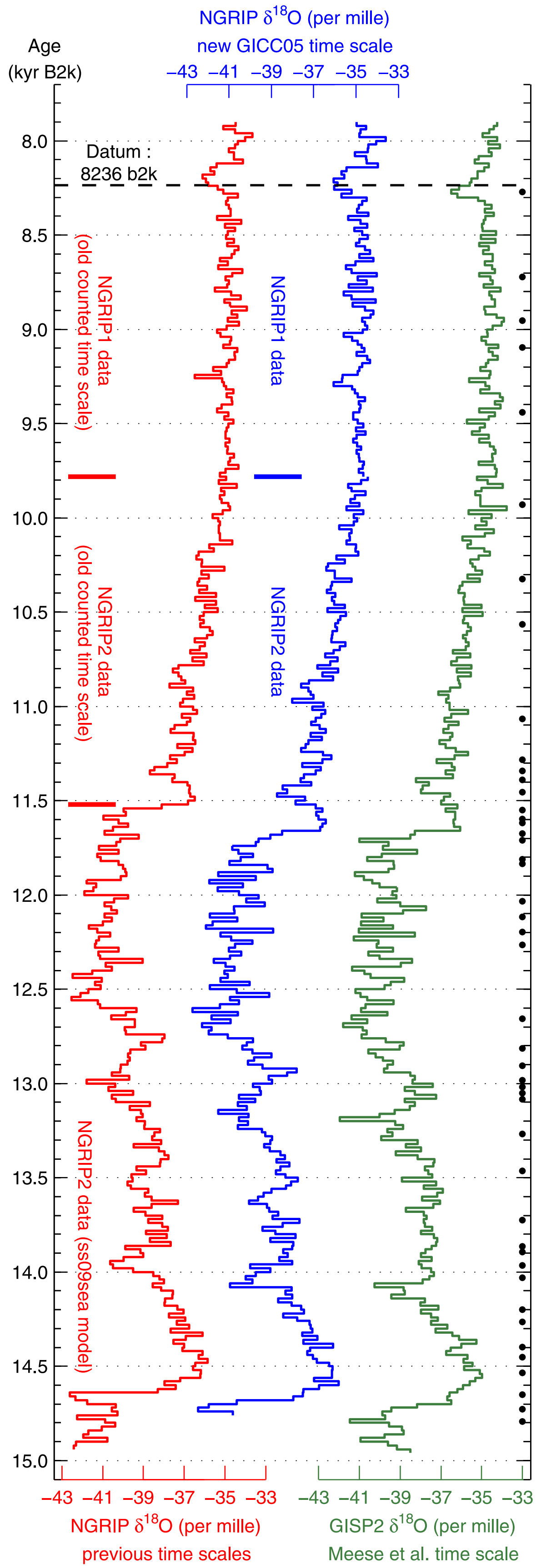

Figure 10. Stable isotope profiles from NGRIP and GISP2 of the entire sections covered by the presented timescale. The red curve shows 20-year mean values of NGRIP δ^{18}O data on the existing counted timescale (Holocene part) and ss09 sea model timescale (glacial part). The blue curve shows the same data on the new GICC05 timescale. The difference between the shape of the blue and red curves is a consequence of different 20-year averaging intervals, as the underlying δ^{18}O data are the same. The green curve show GISP2 δ^{18}O data on the timescale of *Meese et al.* [1997]. The black bullets to the right are the fix points used for the comparison in Figure 11, shown relative to the GISP2 curve.

8070 - 9424 b2k), where R. B. Alley counted 72 years more than the number of years in the official GISP2 timescale after the ice core had been stored for a few years [*Alley et al.*, 1997, Table 2]. The GICC05 and GISP2 timescales have roughly the same number of years in the 9.5–11.5 kyr b2k section, and agree within a few years on the age of the YDPB transition when the transition depth is defined using deuterium excess data (T. Popp, personal communication, 2005). However, the difference grows rapidly in the Younger Dryas section. In the 11.5–12.9 kyr b2k section, corresponding to the Younger Dryas and the first 2 centuries of the Preboreal, the GISP2 timescale contains 84 years, or 6%, more years than the GICC05. In the Allerød the two scales agree fairly well again, while GISP2 has about 40, or 6%, years less in the Bølling period relative to the GICC05. Significant differences which cannot be attributed to counting uncertainty thus remain between the GICC05 and GISP2 timescales.

[47] As previously mentioned, the GICC05 timescale has not been transferred to the GRIP depth scale on a year-to-year basis below the YDPB transition due to marginal data resolution, but common features in the ECM signal allow for matching of the two cores. Interpolation is used between fix points, leading to an estimated maximum matching error of 5 years. *Björck et al.* [1998] defines the Younger Dryas as the GRIP depth interval 1623.6–1661.5 m and gives the duration as 1150 ± 50 years. The matching of the GRIP and NGRIP ECM records makes it possible to identify the corresponding depth interval in the NGRIP core, and according to GICC05 the duration of the Younger Dryas is evaluated to be 1186 years (maximum counting error 44 years). The deviation from the duration given in Table 3 arises from the different definitions of onset and end depths. The GICC05 timescale thus agrees well with the INTIMATE duration estimate of *Björck et al.* [1998], even though the onset and termination of the Younger Dryas are 150–200 years older according to GICC05. In the same way, the total duration of the Bølling – Allerød period (GIS-1a through 1e) is given as 2050 ± 50 years by *Björck et al.* [1998] (GRIP depth 1661.5–1753.4 m), while the corresponding duration is only 1818 (maximum counting error 53 years) according to the GICC05 timescale. The combination of the Bølling – Allerød being 200–250 years shorter and the YDPB transition being 150 years older in the GICC05 compared to *Björck et al.* [1998], means that the age of 14,750 ± 50 b2k for the onset of Bølling given by *Björck et al.* [1998] agrees fairly well with the GICC05 age of 14,692 b2k (maximum counting error 186 years).

[48] It should be emphasized that the maximum counting errors given here reflect a conservative estimate of the maximum error associated with interpretation of ambiguous features in the data, data gaps, and marginal resolution in accordance with the discussion in section 5.1.4, but does not include uncertainty contributions from possible bias in the annual layer identification process, that can not be quantitatively assessed without independent data.

[49] The relative phasing of the different impurity data series is observed to be different during cold and warm conditions, indicating that the annual distribution of precipitation changes rapidly both at the climate transitions and within the Bølling and Allerød periods. The annual layer thicknesses are observed to be log-normally distributed with good approximation, and the ratios of the mean accumulation rates of Younger Dryas and Bølling to that of the early Holocene are 47 ± 2% and 88 ± 2%, respectively.

[50] The work with the new Greenland Ice Core Chronology continues, and the timescale presented here will be both extended further back in time and compared and validated by comparison with results from independent dating strategies. Only by providing the ice cores with reliable timescales, the full value of the records extracted from the ice cores can be appreciated and used in conjunction with other paleoclimatic data, thereby assessing essential questions about the timing of past climatic changes.

8. Online Data Access

[51] The 20-year mean values of GRIP and NGRIP $\delta^{18}O$ data on the GICC05 timescale (as shown for NGRIP in Figure 10) can be downloaded from http://www.icecores.dk.

[52] **Acknowledgments.** This work is a contribution of the Copenhagen Ice Core Dating Initiative which is supported by a grant from the Carlsberg Foundation. NGRIP is directed and organized by the Ice and Climate Research Group at the Niels Bohr Institute, University of Copenhagen, Denmark. It is supported by funding agencies in Denmark (SNF), Belgium (FNRS-CFB), France (IPEV and INSU/CNRS), Germany (AWI), Iceland (RannIs), Japan (MEXT), Sweden (SPRS), Switzerland (SNF) and the USA (NSF, Office of Polar Programs). SOR gratefully acknowledges Robert Mulvaney, and British Antarctic Survey, for support during a visit to BAS from August to October 2004. We thank Eric Wolff for comments during review that greatly improved the quality of the uncertainty discussion.

References

Alley, R., et al. (1993), Abrupt increase in Greenland snow accumulation at the end of the Younger Dryas event, *Nature*, *362*(6420), 527–529.

Alley, R. B., et al. (1997), Visual-stratigraphic dating of the GISP2 ice core: Basic, reproducibility, and application, *J. Geophys. Res.*, *102*(C12), 26,367–26,381.

Anklin, M., R. C. Bales, E. Mosley-Thompson, and K. Steffen (1998), Annual accumulation at two sites in Northwest Greenland during recent centuries, *J. Geophys. Res.*, *103*(D22), 28,775–28,783.

Beer, J., et al. (1991), Seasonal variations in the concentrations of ^{10}Be, Cl^-, NO_3^-, SO_4^{2-}, H_2O_2, ^{210}Pb, ^3H, mineral dust, and $\delta^{18}O$ in Greenland snow, *Atmos. Environ.*, *25*(19), 899–904.

Bigler, M. (2004), Hochauflösende Spurenstoffmessungen an polaren Eisbohrkernen: Glaziochemische und klimatische Prozessstudien, Ph.D. dissertation, University of Bern, Bern, Switzerland.

Björck, S., M. J. C. Walker, L. C. Cwynar, S. Johnsen, K.-L. Knudsen, J. J. Lowe, B. Wohlfarth, and INTIMATE Members (1998), An event stratigraphy for the Last Termination in the North Atlantic region based on the Greenland ice-core record: A proposal by the INTIMATE group, *J. Quat. Sci.*, *13*(4), 283–292.

Blunier, T., et al. (1998), Asynchrony of Antarctic and Greenland climate change during the last glacial period, *Nature*, *394*, 739–743.

Bond, G., W. Broecker, S. Johnsen, J. McManus, L. Labeyrie, J. Jouzel, and G. Bonani (1993), Correlations between climate records from North Atlantic sediments and Greenland ice, *Nature*, *365*(6442), 143–147.

Bory, A.-M., P. Biscaye, A. Svensson, and F. Grousset (2002), Seasonal variability in the origin of recent atmospheric mineral dust at NorthGRIP, Greenland, *Earth Planet. Sci. Lett.*, *196*, 123–134.

Clausen, H., C. Hammer, C. Hvidberg, D. Dahl-Jensen, J. Steffensen, J. Kipfstuhl, and M. Legrand (1997), A comparison of the volcanic records over the past 4000 years from the Greenland Ice Core Project and Dye3 Greenland ice cores, *J. Geophys. Res.*, *102*(C12), 26,707–26,723.

Cuffey, K., and G. Clow (1997), Temperature, accumulation, and ice sheet elevation in central Greenland through the last deglacial transition, *J. Geophys. Res.*, *102*, 26,383–26,396.

Dahl-Jensen, D., S. J. Johnsen, C. U. Hammer, H. B. Clausen, and J. Jouzel (1993), Past accumulation rates derived from observed annual layers in the GRIP ice core from Summit, central Greenland, in *Ice in the Climate System, NATO ASI Ser. I*, vol. 12, edited by R. W. Peltier, pp. 517–532, Springer, New York.

Dahl-Jensen, D., N. S. Gundestrup, H. Miller, O. Watanabe, S. J. Johnsen, J. P. Steffensen, H. B. Clausen, A. Svensson, and L. B. Larsen (2002), The NorthGRIP deep drilling programme, *Ann. Glaciol.*, *35*, 1–4.

Dansgaard, W., et al. (1993), Evidence for general instability of past climate from a 250-kyr ice-core record, *Nature*, *364*(6434), 218–220.

Fischer, H., and D. Wagenbach (1996), Large-scale spatial trends in recent firn chemistry along an east-west transect through central Greenland, *Atmos. Environ.*, *30*(19), 3227–3238.

Fisher, D., R. Koerner, W. Paterson, W. Dansgaard, N. Gundestrup, and N. Reeh (1983), Effect of wind scouring on climate records from ice-core oxygen-isotope profiles, *Nature*, *301*, 205–209.

Fuhrer, K., A. Neftel, M. Anklin, and V. Maggi (1993), Continuous measurements of hydrogen peroxide, formaldehyde, calcium and ammonium concentrations along the new GRIP ice core from Summit, central Greenland, *Atmos. Environ.*, *27A*(12), 1873–1880.

Fuhrer, K., A. Neftel, M. Anklin, T. Staffelbach, and M. Legrand (1996), High-resolution ammonium ice core record covering a complete glacial-interglacial cycle, *J. Geophys. Res.*, *101*(D2), 4147–4164.

Fuhrer, K., E. W. Wolff, and S. J. Johnsen (1999), Timescales for dust variability in the Greenland Ice Core Project (GRIP) ice core in the last 100,000 years, *J. Geophys. Res.*, *104*(D24), 31,043–31,052.

Grootes, P. M., and M. Stuiver (1997), Oxygen 18/16 variability in Greenland snow and ice with 10^{-3} to 10^{5}-year time resolution, *J. Geophys. Res.*, *102*, 26,455–26,470.

Hammer, C. (1989), Dating by physical and chemical seasonal variations and reference horizons, in *Dahlem Konferenc: The Environmental Record in Glaciers and Ice Sheets, Physical, Chemical, and Earth Sciences Research Report 8*, edited by J. Oeschger and J. Langway, pp. 99–121, John Wiley, Hoboken, N. J.

Hammer, C. U., H. B. Clausen, W. Dansgaard, N. Gundestrup, S. J. Johnsen, and N. Reeh (1978), Dating of Greenland ice cores by flow models, isotopes, volcanic debris, and continental dust, *J. Glaciol.*, *20*(82), 3–26.

Hammer, C. U., H. B. Clausen, and H. Tauber (1986), Ice-core dating of the Pleistocene/Holocene boundary applied to a calibration of the ^{14}C time-scale, *Radiocarbon*, *28*, 284–291.

Hammer, C. U., H. B. Clausen, and C. C. Langway Jr. (1994), Electrical conductivity method (ECM) stratigraphic dating of the Byrd Station ice core, Antarctica, *Ann. Glaciol.*, *20*, 115–120.

Hvidberg, C. S., J. P. Steffensen, H. B. Clausen, H. Shoji, and J. Kipfstuhl (2002), The NorthGRIP ice-core logging procedure: Description and evaluation, *Ann. Glaciol.*, *35*, 5–8.

Johnsen, S. J. (1977), Stable isotope homogenization of polar firn and ice, in *Proceedings of the Symposium on Isotopes and Impurities in Snow and Ice, I. U. G. G. XVI, General Assembly, Grenoble Aug./Sept., 1975 IAHS-AISH Publ. 118*, pp. 210–219, Int. Assoc. of Hydrol. Sci., Gentbrugge, Belgium.

Johnsen, S. J., W. Dansgaard, and J. White (1989), The origin of Arctic precipitation under present and glacial conditions, *Tellus, Ser. B*, *41*, 452–468.

Johnsen, S. J., et al. (1992), Irregular glacial interstadials recorded in a new Greenland ice core, *Nature*, *359*, 311–313.

Johnsen, S. J., D. Dahl-Jensen, W. Dansgaard, and N. Gundestrup (1995), Greenland palaeotemperatures derived from GRIP bore hole temperature and ice core isotope profiles, *Tellus, Ser. B*, *47*, 624–629.

Johnsen, S. J., H. B. Clausen, K. M. Cuffey, G. Hoffmann, J. Schwander, and T. Creyts (2000), Diffusion of stable isotopes in polar firn and ice: The isotope effect in firn diffusion, in *Physics of Ice Core Records*,edited by T. Hondoh. pp. 121–140, Hokkaido Univ. Press, Sapporo.

Johnsen, S. J., D. Dahl-Jensen, N. Gundestrup, J. P. Steffensen, H. B. Clausen, H. Miller, V. Masson-Delmotte, A. E. Sveinbjörnsdottir, and J. White (2001), Oxygen isotope and palaeotemperature records from six Greenland ice-core stations: Camp Century, Dye-3, GRIP, GISP2, Renland and NorthGRIP, *J. Quat. Sci.*, *16*, 299–307.

Jouzel, J., and L. Merlivat (1984), Deuterium and oxygen-18 in precipitation: Modeling of the isotopic effects during snow formation, *J. Geophys. Res.*, *89*(D7), 11,749–11,757.

Laj, P., J. M. Palais, and H. Sigurdsson (1992), Changing sources of impurities to the Greenland ice sheet over the last 250 years, *Atmos. Environ.*, *26A*(14), 2627–2640.

Langway, C. C., Jr. (1967), Stratigraphic analysis of a deep ice core from Greenland, *CRREL Res. Rep. 77*, pp. 1–130, Cold Reg. Res. and Eng. Lab., Hanover, N. H.

Masson-Delmotte, V., J. Jouzel, A. Landais, M. Stievenard, S. J. Johnsen, J. W. C. White, M. Werner, A. Sveinbjornsdottir, and K. Fuhrer (2005a), GRIP deuterium excess reveals rapid and orbital-scale changes in Greenland moisture origin, *Science*, *209*, 118–121, doi:10.1126/science.1108575.

Masson-Delmotte, V., et al. (2005b), Holocene climatic changes in Greenland: Different deuterium excess signals at Greenland Ice Core Project (GRIP) and NorthGRIP, *J. Geophys. Res.*, *110*, D14102, doi:10.1029/2004JD005575.

Meese, D. A., A. J. Gow, R. B. Alley, G. A. Zielinski, P. M. Grootes, M. Ram, K. C. Taylor, P. A. Mayewski, and J. F. Bolzan (1997), The Greenland Ice Sheet Project 2 depth-age scale: Methods and results, *J. Geophys. Res.*, *102*(C12), 26,411–26,423.

North Greenland Ice Core Project Members (2004), High-resolution record of Northern Hemisphere climate extending into the last interglacial period, *Nature*, *431*, 147–151.

Rasmussen, S. O., K. K. Andersen, S. J. Johnsen, M. Bigler, and T. McCormack (2005), Deconvolution-based resolution enhancement of chemical ice core records obtained by Continuous Flow Analysis, *J. Geophys. Res.*, *110*, D17304, doi:10.1029/2004JD005717.

Röthlisberger, R., M. Bigler, M. Hutterli, S. Sommer, B. Stauffer, H. Junghans, and D. Wagenbach (2000), Technique for continuous high-resolution analysis of trace substances in firn and ice cores, *Environ. Sci. Technol.*, *34*(2), 338–342.

Ruth, U., D. Wagenbach, J. Steffensen, and M. Bigler (2003), Continuous record of microparticle concentration and size distribution in the central Greenland NGRIP ice core during the last glacial period, *J. Geophys. Res.*, *108*(D3), 4098, doi:10.1029/2002JD002376.

Seierstad, I. K., S. J. Johnsen, B. M. Vinther, and J. Olsen (2006), The duration of the Bølling-Allerød period (Greenland Interstadial 1) in the GRIP ice core, *Ann. Glaciol.*, in press.

Southon, J. (2004), A radiocarbon perspective on Greenland ice-core chronologies: Can we use ice cores for ^{14}C calibration?, *Radiocarbon*, *46*(3), 1239–1260.

Steffensen, J. P. (1988), Analysis of the seasonal variation in dust, Cl^-, NO_3^-, and SO_4^{2-} in two Central Greenland firn cores, *Ann. Glaciol.*, *10*, 171–177.

Stuiver, M., and P. M. Grootes (2000), GISP2 Oxygen isotope ratios, *Quat. Res.*, *53*, 277–284, doi:10.1006/qres.2000.2127.

Svensson, A., S. W. Nielsen, S. Kipfstuhl, S. J. Johnsen, J. P. Steffensen, M. Bigler, U. Ruth, and R. Rthlisberger (2005), Visual stratigraphy of the North Greenland Ice Core Project (NorthGRIP) ice core during the last glacial period, *J. Geophys. Res.*, *110*, D02108, doi:10.1029/2004JD005134.

Taylor, K., et al. (1997), The Holocene-Younger Dryas transition recorded at Summit, *Greenland, Science*, *278*, 825–827.

Vinther, B. M., et al. (2006), A synchronized dating of three Greenland ice cores throughout the Holocene, *J. Geophys. Res.*, doi:10.1029/2005JD006921, in press.

Werner, M., U. Mikolajewicz, M. Heimann, and G. Hoffmann (2000), Borehole versus isotope temperatures on Greenland: Seasonality does matter, *Geophys. Res. Lett.*, *27*(5), 723–726.

Whitlow, S., P. A. Mayewski, and J. E. Dibb (1992), A comparison of major chemical species seasonal concentration and accumulation at the South Pole and Summit, Greenland, *Atmos. Environ.*, *26A*(11), 2045–2054.

K. K. Andersen, M. Bigler, H. B. Clausen, D. Dahl-Jensen, S. J. Johnsen, L. B. Larsen, S. O. Rasmussen, M.-L. Siggaard-Andersen, J. P. Steffensen, A. M. Svensson, and B. M. Vinther, Ice and Climate, Niels Bohr Institute, University of Copenhagen, Juliane Maries Vej 30, DK-2100 Copenhagen, Denmark. (olander@gfy.ku.dk)

H. Fischer and U. Ruth, Alfred-Wegener-Institute for Polar and Marine Research, Columbusstrasse, D-27568 Bremerhaven, Germany.

K. Goto-Azuma, National Institute of Polar Research, 1-9-10 Kaga, Itabashi-ku, Tokyo 173-8515, Japan.

M. E. Hansson, Department of Physical Geography and Quaternary Geology, Stockholm University, S-106 91 Stockholm, Sweden.

R. Röthlisberger, British Antarctic Survey, High Cross, Madingley Road, Cambridge CB3 0ET, UK.

JOURNAL OF GEOPHYSICAL RESEARCH, VOL. 111, XXXX, DOI:10.1029/2005JD006765,

Retrieving a common accumulation record from Greenland ice cores for the past 1800 years

K. K. Andersen, P. D. Ditlevsen, S. O. Rasmussen, H. B. Clausen, B. M. Vinther, S. J. Johnsen and J. P. Steffensen

Ice and Climate, Niels Bohr Institute, University of Copenhagen, Copenhagen, Denmark

Received 13 October 2005; revised 18 February 2006; accepted 24 April 2006.

Abstract. In the accumulation zone of the Greenland ice sheet the annual accumulation rate may be determined through identification of the annual cycle in the isotopic climate signal and other parameters that exhibit seasonal variations. On an annual basis the accumulation rate in different Greenland ice cores is highly variable, and the degree of correlation between accumulation series from different ice cores is low. However, when using multi year averages of the different accumulation records the correlation increases significantly. A statistical model has been developed to estimate the common climate signal in the different accumulation records through optimization of the ratio between the variance of the common signal and of the residual. Using this model a common Greenland accumulation record for the past 1800 years has been extracted. The record shows significant 11.9 years periodicity. A sharp transition to very dry conditions is found just before A. D. 1200 and very dry conditions during the 13th century together with dry and cold spells during the 14th century may have put extra strain on the Norse population in Greenland and have contributed to their extinction. Accumulation rates gradually decrease from a distinct maximum in A. D. 1394 to very dry conditions in the late 17th century, and thus reflect the Little Ice Age.

1. Introduction

The net precipitation rate in the accumulation zone of an ice sheet is recorded in the annual ice layer thickness profile which may be obtained from ice cores. However, due to local fluctuations and especially variations in the snow surface due to drift (sastrugies) the signal to noise variance ratio is rather poor, of the order 1–3, as established from comparisons of different shallow cores drilled close to one another [*Fisher et al.*, 1985]. The deep ice cores in Greenland are distributed mainly along the ice divide. As demonstrated by several authors these cores contain a common climatic signal over the large scale climatic changes during the last glacial period [e.g., *Johnsen et al.*, 2001]. In order to separate the common climatic information from local phenomena and noise for the shorter term variations during climatically stable periods it is however crucial to improve the signal to noise ratio. *Crüger et al.*, [2004] showed that it is problematic to assume a common signal in records from different sites on the Greenland ice sheet on short time scales, but we expect extreme features and long-term variations to be concurrent over large parts of Greenland.

2. Ice Cores and Ice Flow

In this work we compare the annual ice layer thickness profiles from five Greenland ice cores. The cores were chosen to ensure relatively long accumulation records of annual resolution over a common time period. The cores used in this study are the DYE-3 [*Dansgaard et al.*, 1982], the Milcent [*Hammer et al.*, 1978], the Crête [*Hammer et al.*, 1980], the GRIP [*Johnsen et al.*, 1992] and the NorthGRIP (NGRIP) [*Johnsen et al.*, 2001; *NorthGRIP members*, 2004] ice cores (Figure 1). Details about the location, accumulation rates of the cores and the length of the stratigraphies used for this study are given in Table 1. The NGRIP, GRIP and Crête ice cores are all located very close to the ice divide, GRIP and Crête in the center of the Greenland ice sheet and NGRIP 324 kilometers NNW of the GRIP drill site. Milcent is in the central part of Greenland, but about 260 km west of the ice divide, whereas the DYE-3 drill site is located on the southern part of the ice sheet, about 30 km east of the ice divide. The ice cores used for this study are thus rather widely spaced, and all sites are subject to local meteorological conditions. Moreover the cores derive from both sides of the ice divide, which is known to influence the recorded signal [*Clausen et al.*, 1988; *Rogers et al.*, 1998] as the sites are affected by different air masses. Nevertheless it is expected that to a first approximation these ice cores share a common climate signal on an annual to decadal scale, which we here wish to extract. The accumulation rates were determined by identifying and counting annual layers as determined from the high resolution δ^{18}O and Electrical Conductivity Measurement (ECM) records. In the case of NGRIP these records were supported by Ion Chromatographic (IC) measurements at 5 cm resolution over the upper 350m [*Vinther et al.*, 2006]. The stratigraphy of the single cores has been cross-checked using known volcanic horizons and ECM as also described by *Vinther et al.* [2006]. The dating uncertainty is estimated to be 1-2 years over the first millenium increasing to a few years at the end of the records used here.

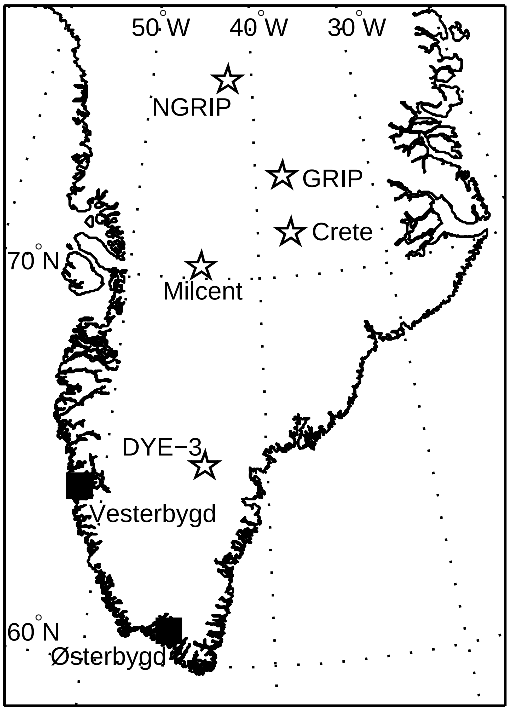

Figure 1. Location of sites in this study.

The stratigraphically dated records used in this study are of different lengths. The Crête and Milcent ice cores are intermediate length ice cores of about 400 m, and the length of the records presented is determined by the length of the cores. The DYE-3, GRIP and NGRIP ice cores are all deep ice cores reaching back through the last glacial period. The length of the used stratigraphies for NGRIP, GRIP and DYE-3 is given by the section where both high resolution deconvoluted δ^{18}O and IC measurements provide reliable annual layer identification for the NGRIP ice core, and all three cores thus could be independently dated as part of the new 'Greenland Ice Core Chronology 2005' (GICC05) [*Vinther et al.*, 2006]. The length of each stratigraphy is limited by the initial accumulation rate at the site determining the isotopic diffusion, together with the sampling resolution and the location of the brittle zone in the cores. The accumulation rate at the DYE-3 drilling site is high enough to preserve annual cycles in the isotopic signal throughout most of the Holocene. *Hammer et al.* [1986] used this fact to count annual layers continuously back to 5.9 ka BP and in sequences to about 8 ka BP. *Vinther et al.* [2006] refined the isotopic measurements and completed the DYE-3 stratigraphy back to 8.2 kyr BP. This together with the work of *Rasmussen et al.* [2006] comprises GICC05 throughout the Holocene period, combining and cross-dating the best available measurements from the NGRIP, GRIP and DYE-3 records.

In order to derive annual accumulation rates from the observed annual layer thicknesses, the data had to be corrected for densification and thinning of the ice layers due to ice flow. This was done by using a flow model [*Johnsen and Dansgaard*, 1992; *Johnsen et al.*, 1999] also accounting for firnification at the top of the ice. In this way we obtained cross-dated chronological time series of annual accumulation rates over the latest two millenia, with relative dating errors being at most a few years. The ice flow in the DYE-3 region is complicated by upstream surface undulations, and the obtained accumulation rate profile thus contains longer term variations of non-climatic origin [*Reeh*, 1989]. In order to remove these variations we have filtered the DYE-3 accumulation record with a Butterworth filter of order 3 with a cut-off frequency of 0.001 year^{-1}, eliminating the lowest frequency variations. The Milcent site is also slightly affected by upstream effects and the accumulation record has been linearly detrended. The obtained accumulation records are shown as five year average values in Figure 2.

The most commonly used climatic parameter obtained from Greenland ice cores is the δ^{18}O record, which is a proxy for the temperature at the location of formation of the precipitation. However as indicated by model simulations [e.g. *Werner et al.*, 2000] the δ^{18}O signal is modulated by the amount of precipitation formed at a given time and temperature. The amount of precipitation is thus in some aspects a more direct climate signal than δ^{18}O. Across large-scale climatic changes, like the Dansgaard Oeschger events, there is a clear correlation between δ^{18}O and accumulation rates [*Dahl-Jensen et al.*, 1993]. *Kapsner et al* [1995] and *Crüger et al* [2004] have however shown that both during the most recent Holocene and the transition out of the last glacial period atmospheric circulation had larger influence on accumulation than temperature. Figure 3 shows scatter plots of δ^{18}O versus the logarithm of the accumulation for the records used in this study. The δ^{18}O records of DYE-3 and Milcent have here been corrected in the same manner as the accumulation records. The correlations are rather weak, and thus confirm that different information may be obtained from the two records. As noted above the accumulation records are probably strongly influenced by atmospheric circulation.

3. Statistical Distribution of Annual Layer Thicknesses

The time series of annual accumulation rates obtained after correction for flow and compression are shown in Figure 2. It may be seen that the variance of each record roughly scales with the mean value (note the different axis scaling). This means that the amplitude of the local accumulation variability as well as the noise in a record is proportional to the mean accumulation rate. This fact is of importance for the model described here. The statistical distribution of annual layer thicknesses from each of the

Table 1. Location, annual accumulation rate (in meters of ice equivalent) and time span covered by the stratigraphically dated ice cores used for this study. Apart from NGRIP these are the same cores that were used by *Vinther et al.* [2003]. The stratigraphic dating of the GRIP and DYE-3 cores has recently been extended over most of the Holocene (*Vinther et al.*, 2006), but we here use them over their common period with NGRIP, back to A. D. 187.

Ice Core	Position	Acc. rate [m(i.e.)/yr]	Year drilled	Oldest year counted
NGRIP	75.10 °N 42.32 °W	0.19	1996	A. D. 187
GRIP	72.58 °N 37.64 °W	0.23	1993	
Crête	71.12 °N 37.32 °W	0.30	1974	A. D. 552
Milcent	70.30 °N 44.55 °W	0.53	1973	A. D. 1174
DYE-3	65.18 °N 43.83 °W	0.56	1979	

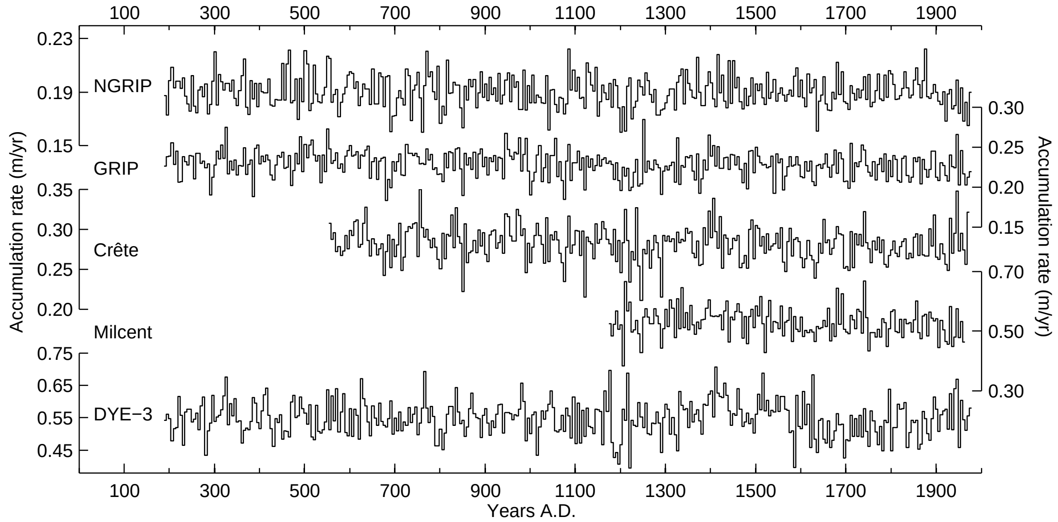

Figure 2. The flow corrected accumulation series used in this work. The data are shown as 5 year average values.

drill sites is shown in Figure 4. δ^{18}O sampling in the ice cores drilled in the 1970's (Crête, Milcent, and DYE-3) was done according to predicted timescales, such that 8 or 12 samples were cut per year. This means that the obtained accumulation rates from these cores take on discrete values, which is seen on the plots, especially for the shorter Crête and Milcent cores. The GRIP and NGRIP cores were cut in samples of constant size, and the discrete spectrum of layer thicknesses is changed into a continuous spectrum when correcting for the effect of layer thinning. The distributions of especially the longer cores are observed not to be symmetric around the mean. When plotted on a logarithmic accumulation axis the distributions become approximately symmetric, with a shape close to a normal distribution, as also observed by *Rasmussen et al.* [2006] for the accumulation record from the Early Holocene, Younger Dryas and Bølling sections of the NGRIP core. It may be expected that the accumulation rates follow Gamma distributions, as they are derived as the sum of positive independent precipitation events. Due to the discrete sampling rates and the limited number of annual layers in the records we can however not distinguish between this and a lognormal distribution. In the following we will for simplicity use the fact that the logarithm of the accumulation rates is approximately normally distributed.

4. Noise Model

From the set of available accumulation rate series we want to estimate a common accumulation record signifying the variability in the mean regional precipitation over the past millenia. This signal is denoted $x(t)$. As pointed out by e.g. *Fisher et al.* [1985] the variance in the accumulation is ascribable to temporal, regional areal and local areal variability. We are here only interested in the common temporal variability. The local variability due to blowing snow and heterogenous snowfall is considerably diminished through temporal averaging over intervals of a few years. The regional areal variability may be ascribed to varying atmospheric circulation and storm tracks together with orography [*Ohmura and Reeh*, 1991; *Dethloff et al.*, 2002; *Crüger et al.*, 2004].

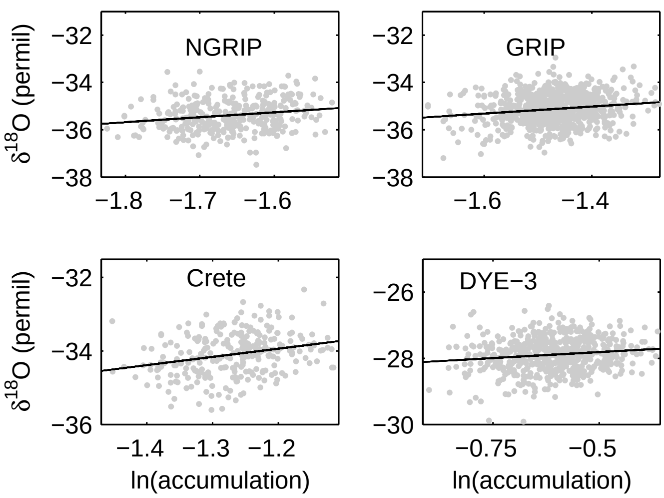

Figure 3. Scatter plots of the 5 year averaged logarithm of the accumulation rate and δ^{18}O for the whole length of the four longest series. The black lines indicate the best linear fits to the data with slopes of 1.71, 1.83, 2.1 and 0.44 for NGRIP, GRIP, Crête, and DYE-3, respectively. The lower dependence for DYE-3 may be due to problems in the correction for ice flow. Correlations between ln(accumulation) and δ^{18}O are 0.21, 0.17, 0.29 and 0.14, which are all significant at the 99% level.

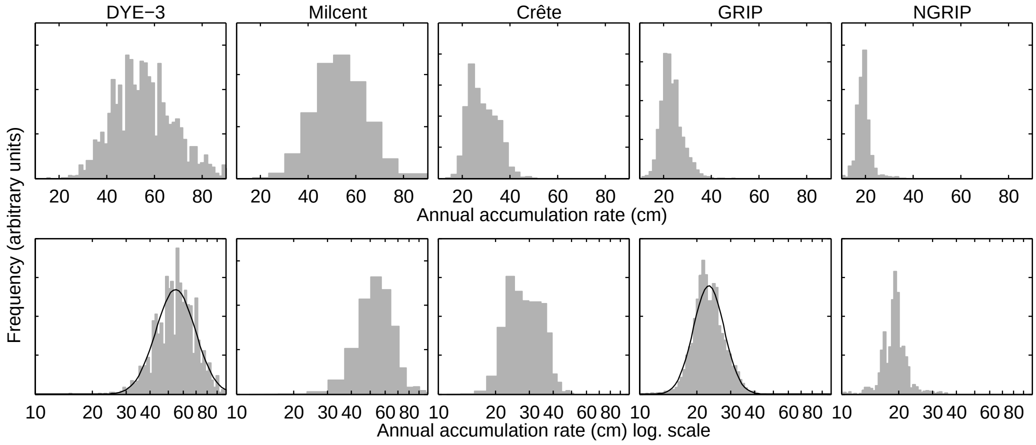

Figure 4. The distribution of annual accumulation rates. Discrete values of the accumulation rates are obvious, especially for the shorter Crête and Milcent cores, but also for NGRIP, where a very high frequency is found around 19 cm. Distributions are plotted both on a linear and a logarithmic scale, and the distributions are seen to be more symmetric on the logarithmic scale. The distributions from the DYE-3 and GRIP records have been fitted to normal distributions on the logarithmic scale.

4.1. Model

As a first approximation we can assume that the measured accumulation at site i, denoted $x_i(t)$, receives a contribution from the common signal $x(t)$ with some site specific scaling constant α_i. In addition, $x_i(t)$ may contain regional variability, but it is here treated as noise such that the measured signal is given as,

$$x_i(t) = \alpha_i x(t) + \sigma_i \eta_i(t). \tag{1}$$

The residual $\eta_i(t)$ is assumed have zero mean and unit variance such that σ_i^2 is the variance of the residual term. Further we will assume that the residual terms at two different sites i and j are uncorrelated; $\langle \eta_i \eta_j \rangle = \delta_{ij}$, where $\langle \cdot \rangle$ represents the temporal mean. As shown above the measured accumulation rates x_i are lognormally distributed. The noise as defined here consists of two main contributions, the larger scale variability from site to site, which as a first estimate can be regarded as white noise, and the glaciological noise which is blue noise for annually resolved records [*Fisher et al.*, 1985]. The blue noise may be ascribed to blowing snow (sastrugies) and discrete measurements sampling but it can efficiently be reduced by temporal averaging, and the assumption that $\eta_i(t)$ can be regarded as white noise is thus reasonable if we use accumulation data averaged over intervals large enough to remove the blue noise characteristics of the glaciological noise.

Even though we do not know to which extent $x(t)$ is a stationary stochastic process we will treat it as such and define the (unknown) signal variance,

$$\sigma^2 = \langle x^2 \rangle - \langle x \rangle^2. \tag{2}$$

4.2. Temporal Averaging

After having corrected for layer thinning and snow compression the annual layer thickness is a measure of the accumulated precipitation including noise attributable to drifting snow.

If the climate signal is auto correlated over times longer than the sampling time the noise can be reduced by temporal averaging of the signal. By doing that we of course lose information on the fluctuations of the climate signal on timescales faster than the averaging time. With only few noisy timeseries available some temporal averaging is however necessary in order to improve the signal to noise variance ratio. Consider two records $x_i(t)$ and $x_j(t)$ related according to (1). With $y_i \equiv x_i - \langle x_i \rangle$ and $y_j \equiv x_j - \langle x_j \rangle$ being the deviations from the average, the temporal average over any odd number m of points is,

$$\overline{y}_i(t) = \frac{1}{m} \sum_{k=-\mu}^{\mu} y_i(t+k),\ \mu = (m-1)/2. \tag{3}$$

The covariance between the series is then given by:

$$\langle \overline{y}_i \overline{y}_j \rangle = \frac{1}{m^2} \sum_{k=-\mu}^{\mu} \sum_{l=-\mu}^{\mu} \langle y_i(t+k) y_j(t+l) \rangle. \tag{4}$$

With the deviation from the climate signal being defined as $y = x - \langle x \rangle$ we have,

$$\begin{aligned} \langle y_i(t+k) y_j(t+l) \rangle &= \alpha_i \alpha_j \langle y(t+k) y(t+l) \rangle + \sigma_i^2 \delta_{ij} \delta_{kl} \\ &= \alpha_i \alpha_j c(k-l) + \sigma_i^2 \delta_{ij} \delta_{kl}, \end{aligned} \tag{5}$$

where we have introduced the autocovariance $c(\tau) = \langle y(t) y(t+\tau) \rangle$ for the climate signal. δ_{ij} is the Kronecker delta. By inserting this into (4) we obtain,

$$\begin{aligned} \langle \overline{y}_i \overline{y}_j \rangle &= \frac{1}{m} \alpha_i \alpha_j \left[c(0) + 2 \sum_{k=1}^{m-1} \frac{m-k}{m} c(k) + \frac{\sigma_i^2}{\alpha_i \alpha_j} \delta_{ij} \right] \\ &= \frac{1}{m} \alpha_i \alpha_j \left[I[c] + \frac{\sigma_i^2}{\alpha_i \alpha_j} \delta_{ij} \right], \end{aligned} \tag{6}$$

where $I[c] \equiv c(0) + 2 \sum_{k=1}^{m-1} c(k)(m-k)/m$. Finally we have the expression for the correlation coefficient,

$$\begin{aligned} C_{ij} &= \langle \overline{y}_i \overline{y}_j \rangle / \sqrt{\langle \overline{y}_i^2 \rangle \langle \overline{y}_j^2 \rangle} \\ &= \left[1 + \left(\frac{\sigma_i^2}{\alpha_i^2} + \frac{\sigma_j^2}{\alpha_j^2} \right) \frac{1}{I[c]} + \left(\frac{\sigma_i^2 \sigma_j^2}{\alpha_i^2 \alpha_j^2} \right) \frac{1}{I[c]^2} \right]^{-1/2}. \end{aligned} \tag{7}$$

If the climate signal is assumed to be a red noise signal with autocorrelation $c(t) = \sigma^2 \exp(-|t|/T)$, where T is the

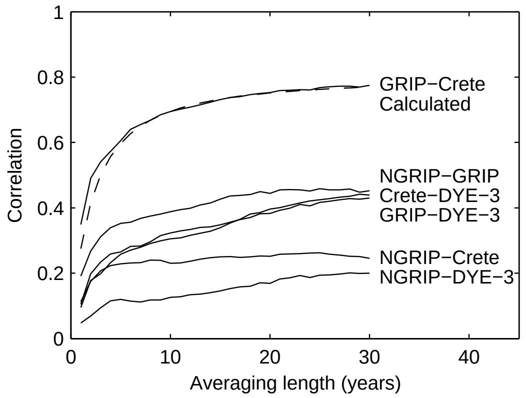

Figure 5. Correlation between the logarithm of the accumulation time series from the different ice cores. The correlation improves with averaging length as the noise decreases. The dashed line displays the correlation coefficient as calculated when using the estimated parameters for GRIP and Crête in (7) and assuming a correlation time of 10 years. The increase in correlation between the cores observed for averaging lengths below 5 years grows faster than for the theoretical result. This is probably due to the removal of blue noise, and an averaging time of 5 years was used in this work.

correlation time, then by approximating the sum with an integral we obtain,

$$I[c] = 2\sigma^2 T \left[1 + \frac{T}{m}(\exp(-m/T) - 1)\right]. \qquad (8)$$

Figure 5 shows the correlation coefficients between all pairs of records used for this study, when averaging over an increasing number of years. Based on the findings in Section 3 the averages have been taken over the logarithm of the data. The maximum correlation of 0.77 is obtained between the GRIP and the Crête ice cores when averaging over 30 years. The correlations between the cores are generally significant at the 99% level, except for NGRIP-DYE-3 and NGRIP-Crête. The significance level for NGRIP-Crête is around 90 %. A correlation time of about 10 years may be anticipated, and a comparison with the result obtained from (7) using T=10 years agrees well with the ice core data for longer term averages (dashed curve in Figure 5). For short term averages the correlation coefficients between ice core records increase faster than the theoretical result of (7) in agreement with the blue noise spectrum observed by *Fisher et al.* [1985], while the curves mostly follow the shape of the theoretical result for averaging lengths above 3-5 years. We thus conclude that the major part of the blue noise has been removed when averaging over 5 year intervals, and apply this averaging approach in the rest of this work, assuming that the residual term $\eta_i(t)$ can be regarded as white noise.

5. Determination of Model Parameters

With accumulation series from n ice cores we have to determine $2n+1$ unknown parameters, namely (α_i, σ_i) for $i = 1, ..., n$ and σ. The overall magnitude of the climate signal is arbitrary, and we set $\langle x \rangle = 1$. The variance of the climate signal (2) then becomes $\sigma^2 = \langle x^2 \rangle - 1$. Equations for the signal scaling parameters α_i may be estimated from averaging (1) over the whole length of the series,

$$\langle x_i \rangle = \alpha_i \langle x \rangle = \alpha_i. \qquad (9)$$

Further equations can be derived from the covariance matrix. Assuming that the signals $x_i(t)$ are stationary processes the covariance c_{ij} between two signals may be calculated as

$$\begin{aligned} c_{ij} &= \langle x_i x_j \rangle = \langle (\alpha_i x + \sigma_i \eta_i)(\alpha_j x + \sigma_j \eta_j) \rangle \\ &= \alpha_i \alpha_j \langle x^2 \rangle + \sigma_i^2 \delta_{ij} \\ &= \alpha_i \alpha_j (\sigma^2 + 1) + \sigma_i^2 \delta_{ij}. \qquad (10) \end{aligned}$$

The set of equations from (9) and (10) is overdetermined and is solved by finding the set of estimated parameters $\widetilde{\alpha}_i$, $\widetilde{\sigma}_i$, and $\widetilde{\sigma}$ that minimizes the total misfit M defined as

$$\begin{aligned} M &= \sum_{i=1}^{n} (\widetilde{\alpha}_i - \langle x_i \rangle)^2 \\ &+ \sum_{i=1}^{n} \sum_{j=i}^{n} \left(\widetilde{\alpha}_i \widetilde{\alpha}_j (\widetilde{\sigma}^2 + 1) + \widetilde{\sigma}_i^2 \delta_{ij} - \langle x_i x_j \rangle \right)^2. \qquad (11) \end{aligned}$$

For the minimalization, the initial guesses were $\widetilde{\alpha}_i = \langle x_i \rangle, \widetilde{\sigma}_i = 0.8 \cdot std(x_i)$ and $\widetilde{\sigma}^2 = 0.002$, but the estimated parameter values are insensitive to the choice of initial guesses, as long as reasonable values are used.

Table 2. The values of α_i, σ_i, γ_i and the model signal to residual variance ratio, F_i, for the five records, when averaging over five year intervals for the period A. D. 1176-1965.

Ice core	α_i	σ_i	γ_i	F_i
NGRIP	0.19	0.98e-2	0.333	1.68
GRIP	0.23	1.06e-2	0.337	1.82
Crête	0.28	1.45e-2	0.225	1.68
Milcent	0.53	3.49e-2	7.33e-2	1.42
DYE-3	0.54	5.43e-2	3.13e-2	1.18

6. Optimal Climate Signal

We now want to use the results of the presented model to calculate an estimate $\tilde{x}(t)$ of the common climate signal $x(t)$ extracting maximum information on the common climate variability in the records. The method applied finds the linear combination of the individual records which optimizes the ratio between the variance of the common signal and the variance of the residual, as estimated from the model.

6.1. Accumulation Reconstruction

Based on the model given in (1), equations (9) and (10) may be combined to give the expression for the variance of any of the measured series x_i

$$\langle x_i^2 \rangle - \langle x_i \rangle^2 = \alpha_i^2 \sigma^2 + \sigma_i^2. \qquad (12)$$

With the presented model the ratio, F_i, between the total variance of a record and the variance of the residual is given as

$$F_i = \text{variance of record / variance of residual} = (\alpha_i \sigma / \sigma_i)^2 + 1. \qquad (13)$$

The estimate $\tilde{x}(t)$ of the common climate signal will be constructed such that the model based ratio between the variance of the total signal and the residual is maximized. The linear combination is expressed as

$$\tilde{x}(t) = \sum_i \gamma_i x_i, \qquad (14)$$

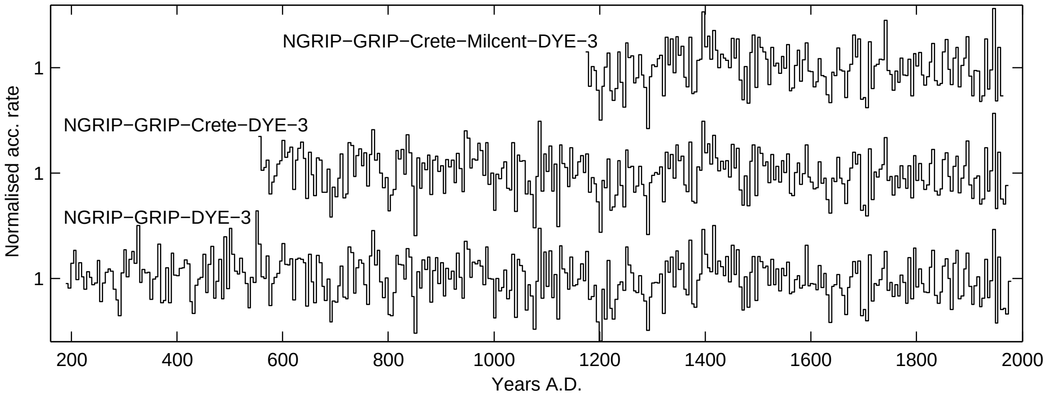

Figure 6. The optimal accumulation records based on three, four, and five cores, depending on the length of the records. The different reconstructions are highly correlated over the common interval A. D. 1178-1973.

with the coefficients γ_i being determined such that $\tilde{x}(t)$ represents $x(t)$ as closely as possible. We can do this in two different ways which lead to the same result. Firstly the linear combination which maximizes $F_{\tilde{x}}$ may be found directly. Combining (1) and (14) one gets $\tilde{x}(t) = \sum_i(\gamma_i\alpha_i x(t) + \gamma_i\sigma_i\eta_i(t))$. The signal to residual variance ratio $F_{\tilde{x}}$ for any linear combination of x_i's may be expressed as

$$F_{\tilde{x}} = \frac{(\sum_i \gamma_i\alpha_i)^2\sigma^2}{\sum_i(\gamma_i\sigma_i)^2} + 1, \qquad (15)$$

from which we have,

$$\frac{\partial F_{\tilde{x}}}{\partial \gamma_k} = \frac{2\sigma^2\sum_i\gamma_i\alpha_i}{(\sum_i(\gamma_i\sigma_i)^2)^2}\left[\alpha_k\sum_j(\gamma_j\sigma_j)^2 - \gamma_k\sigma_k^2\sum_j\gamma_j\alpha_j\right]. \qquad (16)$$

By redefining $\tilde{\gamma}_j = \gamma_j\sigma_j^2/\alpha_j$ we get,

$$\frac{\partial F_{\tilde{x}}}{\partial \gamma_k} = 0 \Rightarrow \sum_j(\tilde{\gamma}_j - \tilde{\gamma}_k)\Big(\frac{\alpha_j}{\sigma_j}\Big)^2\tilde{\gamma}_j = 0, \qquad (17)$$

with the solution $\tilde{\gamma}_j = \tilde{\gamma}$ for all j, where $\tilde{\gamma}$ is an arbitrary constant. From the definition above we thus get $\gamma_j = \alpha_j/\sigma_j^2$. As an alternative to maximizing the signal to residual variance ratio we can simply determine $\tilde{x}(t)$ by minimizing the root mean square error between a linear combination of the series $x_i(t)$ and (the unknown) $x(t)$. This results in the same linear combination as above. The estimated optimal climate record can thus be represented as,

$$\begin{aligned}\tilde{x}(t) &= \sum_i\left(\frac{\alpha_i}{\sigma_i^2}\right)x_i(t)\\ &= \sum_i\left(\left(\frac{\alpha_i}{\sigma_i}\right)^2 x(t) + \left(\frac{\alpha_i}{\sigma_i}\right)\eta_i(t)\right). \qquad (18)\end{aligned}$$

The estimated model parameters determined for the five ice core records over the common time interval, A. D. 1176-1965 are given in Table 2. The values for α_i found by the minimalization procedure agree well with the accumulation rates given in Table 1, although those are averages over recent years, whereas the α_i's correspond to long term averages. As expected high σ_i's are found for the high accumulation sites. The model assumption that the residual signals are

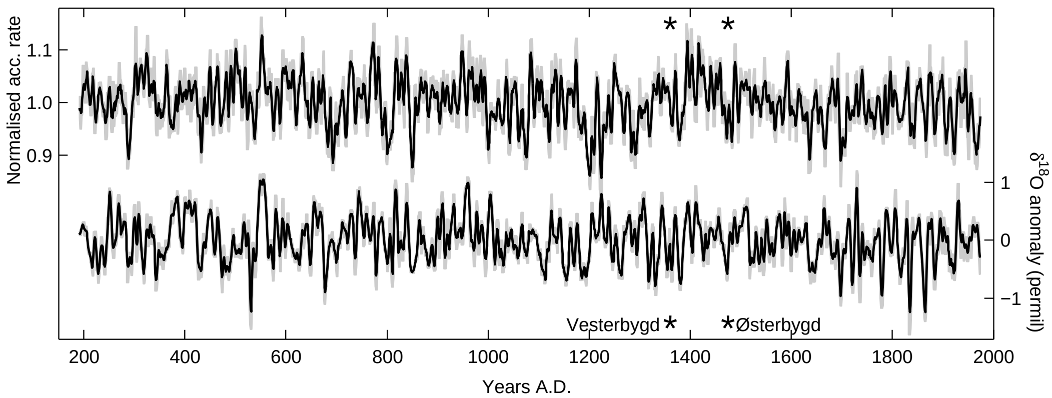

Figure 7. The optimal accumulation record over the period 191 A. D. to 1974 A. D. The curve has been constructed from the 5 year averaged accumulation records from DYE-3, GRIP and NGRIP. For every year the curve shown here is the average value of the results obtained when using five different averaging bins. The highest and lowest values found for every year are indicated by the grey envelope in order to illustrate the model variability associated with the different binning. The corresponding curve for the $\delta^{18}O$ records from the three sites is displayed below. The $\delta^{18}O$ curve was constructed by simple stacking of the three records, and binning of the resulting record. The years A. D. 1360 and 1475 when the norse settlements in Greenland were deserted have been marked on the plot.

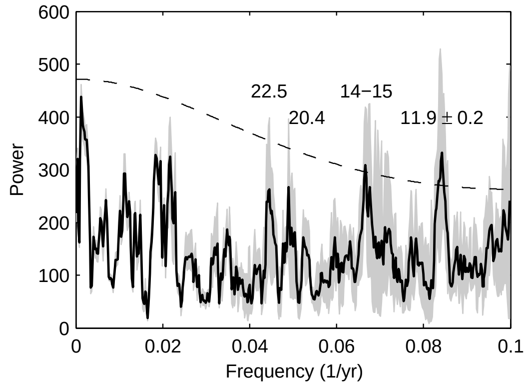

Figure 8. MTM Spectral analysis of the longest reconstructions based on the NGRIP, GRIP and DYE-3 records. The analysis has been carried out for all five possible binnings. The range of values obtained is shown as the grey shaded area, while the mean of the five spectra is shown as the black line. The dashed line indicates the 99 % significance level. The same major spectral peaks arise when using data averaged over three and four years wide bins.

mutually uncorrelated was checked with the estimated series, and is largely confirmed. We find comparable modeled signal to residual variance ratios for all cores investigated here, meaning that the variability from all cores has comparable influence on the common signal. DYE-3 has the lowest ratio, which probably reflects the fact the DYE-3 is located east of the ice divide and considerably further south than the other ice cores included in this study. The DYE-3 site receives a larger proportion of its precipitation from cyclonic activity associated with the Icelandic low than the other cores [*Hutterli et al.*, 2005]. Moreover as mentioned earlier the DYE-3 accumulation record had to be corrected for ice flow at the site. When comparing the signal to residual ratios in this study with the signal to noise ratio estimates by *Fisher et al.* [1985] their values, especially for DYE-3, are considerably higher than what is found here (note that the definition of their ratios correspond to equation (13) minus 1). *Fisher et al.* [1985] in their study investigated the local signal to noise variance ratio by comparing the noise in a number of ice cores drilled close to another, whereas we here aim at the common signal over Greenland, considering everything else as the residual. The definition of noise in the two studies is thus inherently different and can not readily be compared.

6.2. Sensitivity of the Reconstruction

From the five cores we have calculated three estimates of the common accumulation curve as shown in Figure 6. The three curves are constructed by using the three, four, and five longest records over their common period, respectively. The three resulting curves show convincing agreement over their common periods, and all major minima and maxima recur in all curves. The correlation over the common interval is 0.94 between the reconstructions from three and four ice cores, 0.90 between the three and five cores reconstructions and 0.98 between the four and five cores reconstructions. The best agreement is thus found for the reconstructions with the most cores, but all three curves are highly correlated. We will in the following discuss the longest record, based on NGRIP, GRIP and DYE-3 as a common accumulation rate reconstruction.

When estimating the model parameters for the optimal climate curve, the original accumulation data are first averaged over discrete five year bins. These bins can of course be constructed in five different ways, and Figure 7 illustrates the variability associated with the choice of bins. Although differences are obvious, choosing a different set of bins does not significantly change the location of prominent maxima and minima.

6.3. Spectral Analysis

Spectral analysis has been carried out on the longest reconstructed accumulation records with the five different binnings using the MTM method [*Gihl et al., 2002*]. With 358 data points and three tapers a significance level of 99% has been used. Very little long-term variation is contained in the record, and significant peaks occur in the spectra of the single reconstructions with periods of 22.5, 20.4, 14-15, and 11.9 years. When averaging the spectra for the five different binnings it may be seen that only the peak at 11.9 years is robust, whereas the peak around 14-15 years is weakly defined and only marginally significant (Figure 8). The sharp peak at 11.9 years could indicate a relationship with the 11-year sunspot cycle [e.g. *Stuiver and Braziunas*, 1993], however this could not be confirmed in a coherence analysis carried out with sunspot data covering the period A. D. 1700-1974 [*Waldmeier, 1961*]. Further investigations of the possible connection between the accumulation record and solar forcing should be carried out, but are beyond the scope of this paper.

7. Other Reconstructions of a Common Accumulation Record

In order to test the robustness of our results we also calculated a common accumulation record using several other methods. Besides the model presented in this paper we computed the simple stack of the available accumulation series, the "α-stacked" series and the first principal component derived using the five accumulation records averaged over 5 years for the period A. D. 1176 to A. D. 1965.

7.1. Stacking the Records

As an obvious choice the optimal record has been compared to a simple stack

$$x_s(t) = \frac{1}{n}\sum_i x_i(t) \tag{19}$$

of the original records. A probably more appropriate method is what we here call the "α-stack",

$$x_{as}(t) = \frac{1}{n}\sum_i \frac{x_i(t)}{\alpha_i} \tag{20}$$

where all records are scaled down by their mean accumulation rate before stacking. As discussed here and in *Fisher et*

Table 3. The first three EOFs based on the five accumulation series averaged over 5 years for the period A. D. 1176-1965. On average over the five possible sets of bins the carried variances are 46.9%, 27.2% and 11.7%.

Ice core	EOF1	EOF2	EOF3
NGRIP	0.20	0.25	0.77
GRIP	0.40	0.28	-0.21
DYE-3	0.71	-0.69	0.08
Crête	0.37	0.33	-0.55
Milcent	0.40	0.53	0.20
Variance (%)	47.8	26.3	11.8

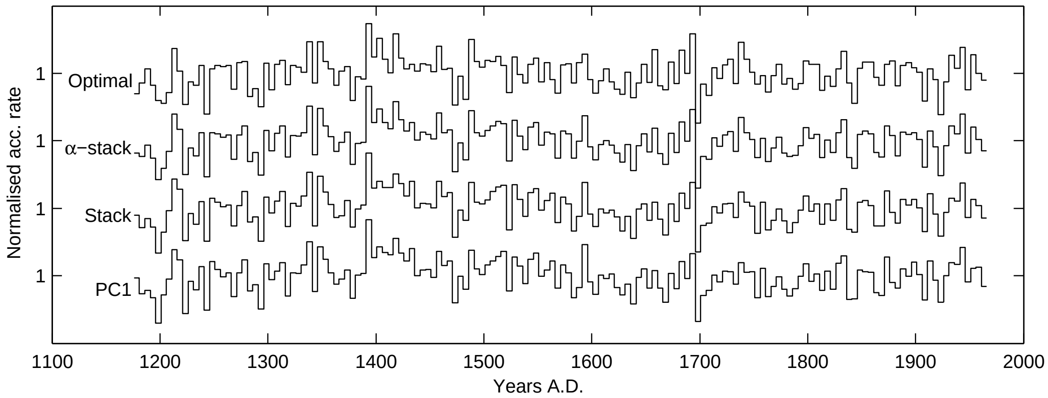

Figure 9. The resulting accumulation profiles over the period A. D. 1176-1965 using different methods as described in Sections 6 and 7. The parameters and the signal to residual ratios calculated for the different climate series are given in Tables 2 and 4.

al. [1985] the variance of individual accumulation records is approximately proportional to the average annual accumulation rate, which makes this approach very reasonable.

7.2. Principal Component Analysis

A third comparison was made performing a Principal Component Analysis (PCA) on the accumulation data. In the same way as for the other reconstructions the PCA analysis was performed on the 5 year logarithmically averaged accumulation data in order to avoid the blue noise. In analogy with the α-stack each series was hereafter divided by its mean value, whereafter all series were centered around zero for the analysis, i. e. $z_i(t) = x(t) + (\sigma_i/\alpha_i)\eta_i(t) - 1$

Table 3 displays the weights on the first three EOFs. The first EOF carries 48% of the variance and is a strong signal of the common variance in the accumulation records. The weight of DYE-3 on EOF1 is strongest, and NGRIP is weakest. EOF2 carries 26% of the variance, and DYE-3 has strong negative weight on this pattern. DYE-3 has almost no weight on EOF3, which is most strongly influenced by NGRIP and Crête.

The first principal component, PC1, is displayed in Figure 9 together with the records obtained by the accumulation, the stacking and the α-stacking of the five ice core records averaged over 5 year bins for the period A. D. 1176 to A. D.1965 .

7.3. Evaluation of the Different Reconstructions

The four different reconstructions displayed in Figure 9 are quite similar, and highly correlated with each other. However important differences may be noted. All reconstructions are formed as linear combinations of the five ice core records. The simple stacking puts equal weight on each record, whereas DYE-3 has strongest weight on PC1 as seen in Table 3. In the model presented in this work, and the α-stack the coefficients in the linear combination are 'corrected' for the accumulation rate, such that high accumulation records have lower coefficients (Table 2), which in fact prevents over representation of these records. This is also displayed by the fact that the correlation between the model reconstruction and the α-stack is 0.96, whereas it is 0.89 and 0.87 for the correlation with the stack and PC1 respectively.

Based on the model presented here (1) signal to residual variance ratios may be calculated for the different reconstruction approaches. The signal to residual variance ratio of the optimal record is $F_{\tilde{x}} = \sum_i (\alpha_i/\sigma_i)^2\sigma^2 + 1$, where the signal to residual variance ratios of the individual records are $F_i = (\alpha_i/\sigma_i)^2\sigma^2 + 1$. Stacking the n records, $x_s(t) = 1/n\sum_i x_i(t)$, gives the signal to residual variance ratio, $F_s = \sum_i \alpha_i^2/\sum_i \sigma_i^2\sigma^2 + 1$, and the α-stack results in a signal to residual variance ratio $F_{as} = N^2\sigma^2/\sum_i(\sigma_i/\alpha_i)^2 + 1$.

As the principal components are linear combinations of the original data series the model signal to residual variance ratio may be calculated in the same manner as described in section 6.1. The series used for the PCA are $z_i(t) = x(t) + (\sigma_i/\alpha_i)\eta_i(t) - 1$, and the principal components are linear combinations $z_{pc} = \sum_i e_i z_i$ where e_i is the loading for z_i. This results in $F_{pc} = (\sum_i e_i)^2\sigma^2/\sum_i(\sigma_i e_i/\alpha_i)^2 + 1$

The estimated signal to residual variance ratios for the obtained reconstructions are given in Table 4. The model presented here gives significantly higher values than the other reconstructions, and α-stacking results in somewhat higher values than the principal component analysis and the simple stacking.

From these evaluations we conclude that the model presented here gives a more representative reconstruction of the common signal than the other methods, and that it should be superior in reconstructing the common climate variability.

8. Climatic Interpretation of the Reconstruction

Based on the analysis above the reconstructed accumulation record (Figure 7) is in the following discussed in terms of climate variability over the past 1800 years.

Table 4. Signal to residual variance ratios for the different calculated records. The values are averages of the five values obtained with different five year bin configurations. The ratios between the signal to residual variance ratios for the different methods are given below.

	F
Model	3.7
α-Stack	2.9
Stack	2.1
PC1	2.2
	F ratio
$\frac{Model}{\alpha-Stack}$	1.2–1.4
$\frac{Model}{Stack}$	1.5–2.0
$\frac{Model}{PC1}$	1.4–2.0

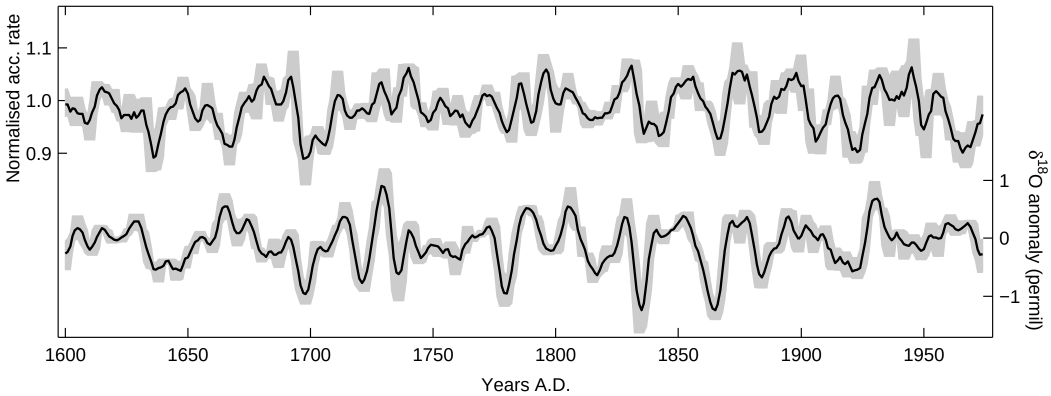

Figure 10. The same as Figure 7, but zoomed in on the latest centuries. Several coinciding minima between the two curves are found during this period.

8.1. Accumulation and the Isotopic Climate Records

The reconstructed accumulation curve is in Figure 7 displayed together with the corresponding $\delta^{18}O$ curve based on simple stacking of the individual records. As expected the two curves show only few similarities when compared over the past 1800 years. The correlation between the two is 0.31 which is significant at the 99 % level and higher than for most of the individual records (see caption for Figure 3). There are several occurrences of coinciding minima in the two records. In the early part of the record this applies for the years A. D. 289 and A. D. 433. The very strong minimum for $\delta^{18}O$ in A. D. 530 is probably connected to a strong volcanic horizon in A. D. 529 [*Vinther et al.*, 2006]. A minor minimum in accumulation is found in A. D. 537, and these two minima are followed by coinciding maxima in both curves around A. D. 551. Another strong minimum in $\delta^{18}O$ is found around A. D. 678, but the apparently corresponding minimum in accumulation is in fact not synchronous, it only occurs 15 years later, around A. D. 693.

Over the latest centuries the common accumulation and $\delta^{18}O$ curves are characterized by concordant fast variations, which tend to be in phase. The correlation between the two curves increases to 0.41 for the period A. D. 1700 to 1974, and synchronous minima are found around 1697, 1778, 1833, 1861, 1884 and 1921 (Figure 10).

All in all several occurrences of coinciding sharp minima and partly maxima are found over the 1800 years, but there is very little agreement in longer term variations.

8.2. Climatic Implications of the Common Accumulation Record

Focusing on the common accumulation record in Figure 7 some very interesting features may be noted. Several occurrences of very dry spells are found around A. D. 289, 433, 693, 801, 850, 1004, 1075, 1200, 1223, 1287, 1290, 1636, 1697, 1921, and 1965. Most of these are just dry spells of very short duration. However the period from A. D. 1004 to 1075 is generally arid with only a few years showing accumulation rates above average. This is followed by a moister century from A. D. 1081 to 1174. The 13th century was generally drier than average, especially the earliest part around the strong minima in 1200 and 1223 with only a short moister spell around A. D. 1215. Significantly moister than average conditions are not encountered before the accumulation rate abruptly increases to the peak value in A. D. 1394. Following this sharp increase in accumulation rates conditions gradually become drier again until the three minima in A. D. 1636, 1667 and 1697 (see also Figure 10). After these minima the accumulation rate over the latest centuries shows distinct short time variability but no clear trend.

The early part of the Greenland accumulation record presented here agrees well with findings from the Igaliku Fjord in the area of the Norse eastern settlement (Østerbygd) in Southern Greenland (Figure 1). *Jensen et al.* [2004] using sediment cores from southern Greenland reported cold and moist climate condition between A. D. 500 and 700. In our record the period between the two minima in 433 and 693 is generally moister than average with only a few short dry spells. The Medieval Warm Period between A. D. 800 and 1250 is reported to have been very variable with generally increased wind stress in the Igaliku Fjord. A cooling event is reported in A. D. 960-1140. This time period encompasses the very dry 11th century in the accumulation record. After the accumulation maximum in A. D. 1174 our accumulation record shows two centuries of extremely low to low values. As already noted by [*Dansgaard et al.*, 1975] climate conditions in this period must have been harsh and put extra strain on the Greenland population. The 13th century shows three deep accumulation minima, beginning with the minimum at A. D. 1200. Each of these represents five to ten year intervals with mean precipitation about 10 % lower than the long term mean. The mid-14th to early 15th century is the time when the Norse population disappeared in Greenland, and the Western Settlement (Vesterbygd) is believed to have lain waste around A. D. 1360 [*Lynnerup and Nørby*, 2004]. The last reports from the Eastern settlement (Østerbygd) are from a wedding in A. D. 1408, and it is believed to have been deserted around 1450-1500 as marked in Figure 7. The 14th century shows low $\delta^{18}O$ values with spells of dry conditions, most markedly around 1380 where both the accumulation and isotope records have a distinct minimum. After the abrupt accumulation increase in A. D. 1394 short dry periods recurred in A. D. 1470-1480. Unusually dry periods may thus very well have contributed to the demise of the Norse population. The sustainability of pasture and livestock was marginal even under 'normal conditions' [*McGovern*, 2000], and the Norse in the Eastern Settlement designed irrigation constructions directing water from high lakes into their fields. This laborious undertaking strongly indicates that precipitation and water supply was indeed critical for farming and grassing fields. The deep minimum in the record around A. D. 1200 also precedes a period where a shift towards a more marine diet (fish and seal) is observed [*Arneborg et al.*, 1999]. It is commonly assumed that the reason for the decline of the Norse settlements was the change to a colder climate in the Little Ice Age, however, this happened on a much longer time scale than the spells of very low precipitation. This means that we must expect that it was easier for Norse farmers to adapt to the change in temperature, and the drought could have initiated the Norse abandoning farming and their ultimate disappearance.

A sharp increase in accumulation occurs just before the peak value in A. D. 1394, with some of the highest values recorded over the whole period. This sudden increase in accumulation coincides with the abrupt increase in sea-salt concentration in the GISP2 ice core [*Kreutz et al.*, 1997] interpreted as increased meridional atmospheric circulation intensity at the onset of the Little Ice Age. In our reconstructed accumulation record, besides a shorter dry interval around A. D. 1470-1480, the accumulation rate slowly decreased until the second half of the 17th century, when minima of about 10 % lower than average accumulation rates are found between 1636 to 1697. The Little Ice Age period may thus be seen as a minimum in accumulation during the period from 1635 to 1700 in the common accumulation record presented here. This minimum could possibly be associated with the Maunder minimum in A. D. 1650-1715 [*Stuiver and Braziunas*, 1993].

9. Summary and Conclusion

A method has been presented to extract a common Greenland accumulation record over the past 1800 years. Annual accumulation records contain blue noise attributable to depositional effects, and this noise may be diminished by temporal averaging over a few years. We here used accumulation rate records from five Greenland ice cores which have been very thoroughly cross-dated. The common accumulation record was extracted by optimizing the ratio between the variance of the common signal and of the residual signal in all ice core records. The obtained signal has been compared to the stacked $\delta^{18}O$ record from the same cores, and besides episodic coinciding minima in both records very little agreement is found. The two records thus contain different climatic information and the accumulation record during this period is probably more related to atmospheric circulation changes than temperature variability.

The obtained record of the common accumulation rate is quite robust with regard to the number of ice cores included in the reconstruction. Comparable reconstructions based on other methods were made. All records are highly correlated but the method presented here results in the highest signal to residual variance ratio, and thus is superior in reconstructing the common climate signal.

The 1800 years accumulation record shows longer term variations in accumulation rate over Greenland with especially the 13th and 14th centuries being persistently drier that normal, and with several very dry periods and a lack of unusually wet periods. This may very well have put additional strain on the Norse population in Greenland, and thus have contributed to their extinction.

Spectral analysis of the record shows 11.9 years periodicity. This together with the low accumulation rates during the Maunder minimum indicates a possible solar influence which deserves further investigations.

Although accumulation rates over Greenland are highly dependent on local and regional features it has been demonstrated that a common Greenland accumulation record may be extracted from very precisely dated records. The noise in the obtained climate signal has been minimized by temporal averaging, and the local contribution was separated by the optimization procedure. The obtained record should thus be a more valuable input to hemispheric and global scale climate reconstructions than records from single ice cores.

10. Data Access

The reconstructed accumulation record is available from http://icecores.dk.

Acknowledgments. Discussions with David Fisher, Peter Thejll and Jette Arneborg are greatly appreciated. KKA was supported by the Danish National Science Foundation and the Carlsberg Foundation. This work is a contribution to the Copenhagen Ice Core Dating Initiative, which is supported by a grant from the Carlsberg Foundation.

References

Arneborg, J., J. Heinemeier, N. Lynnerup, H. L. Nielsen, N. Rud and A. E. Sveinbjörnsdottir (1999), Change of Diet of the Greenland Vikings determined form stable carbon isotope analysis and 14 C dating of their bones., *Radiocarbon 41(2),* 157–168.

Clausen, H. B., N. Gundestrup, S. J. Johnsen, R. Bindschadler, and J. Zwally (1988), Glaciological investigations in the Crête-area, Central Greenland. A search for a new deep-drilling site, *Annals of Glaciology, 10,* 10–15.

Crüger, T., H. Fischer, and H. von Storch, What do accumulation records of single ice cores in Greenland represent? (2004), *J. Geophys. Res., 109*, D21110, doi:10.1029/2004JD005014.

Dahl-Jensen, D., S. J. Johnsen, C. U. Hammer, H. B. Clausen and J. Jouzel (1993), Past Accumulation rates derived from observed annual layers in the GRIP ice core from Summit, Central Greenland, in *Ice in the climate system, NATO ASI Series*, vol. 12, edited by W. R. Peltier, pp. 517–532, Springer-Verlag Berlin Heidelberg.

Dansgaard, W., S. J. Johnsen, N. Reeh, N. Gundestrup, H. B. Clausen, C. U. Hammer (1975), Climatic Changes, Norsemen and modern man, *Nature 255*, 24–28.

Dansgaard, W., H. B. Clausen, N. Gundestrup, C. U. Hammer, S. J. Johnsen, P. M. Kristinsdottir and N. Reeh (1982), A New Greenland Deep Ice Core, *Science, 218*, 1273–1277.

Dethloff, K., M. Schwager, J. H. Christensen, S. Kiilsholm, A. Rinke, W. Dorn, F. Jung-Rothenhäusler, H. Fischer, S. Kipfstuhl, and H. Miller (2002), Recent Greenland accumulation estimated from regional climate model simulations and ice core analysis, *Journal of Climate, 15(19)*, 2821–2832.

Fisher, D. A., N. Reeh and H. B. Clausen (1985), Stratigraphic noise in time series derived from ice cores, *Annals of Glaciology, 7*, 76–83.

Ghil M., R. M. Allen, M. D. Dettinger, K. Ide, D. Kondrashov, M. E. Mann, A. Robertson, Y. Tian, F. Varadi, and P. Yiou (2002). Advanced spectral methods for climatic time series, Rev. Geophys., 40(1), pp.3.1-3.41.

Hammer, C. U. et al. (1978). Dating of Greenland ice cores by flow models, isotopes, volcanic debris, and continental dust, *Journal of Glaciology 20,* 3–26.

Hammer, C. U., H. B. Clausen and W. Dansgaard (1980), Greenland ice sheet evidence of post-glacial volcanism and its climatic impact, *Nature, 288*, 230–235.

Hammer, C. U., H. B. Clausen, and H. Tauber (1986), Ice-core dating of the Pleistocene/Holocene boundary applied to a calibration of the ^{14}C time scale, *Radiocarbon, 28(2A)*, 284–291.

Hutterli, M. A., Raible, C. C., and Stocker, T. F. (2005), Reconstructing climate variability from Greenland ice sheet accumulation: An ERA40 study, *Geophys. Res. Lett.,* 32, L23712, doi:23710.21029/22005GL024745.

Jensen, K. G., A. Kuijpers, N. Koç and J. Heinemeier (2004), Diatom evidense of hydrographic changes and ice conditions in Igaliku Fjord, South Greenland, during the past 1500 years, *the Holocene 14*, 2, 152–164.

Johnsen, S. J. and W. Dansgaard (1992), On flow model dating of stable isotope records from Greenland ice cores, in *The last Deglaciation: Absolute and Radiocarbon Chronologies, NATO ASI Series*, Vol. 12, edited by E. Bard and W. S. Broecker, pp. 13–24, Springer-Verlag Berlin Heidelberg.

Johnsen, S. J., H. B. Clausen, W. Dansgaard, K. Fuhrer, N. Gundestrup, C. U. Hammer, P. Iversen, J. Jouzel, B. Stauffer and J. P. Steffensen (1992), Irregular glacial interstadials recorded in a new Greenland ice core, *Nature, 359*, 311–313.

Johnsen, S. J., H. B. Clausen, J. Jouzel, J. Schwander, A. E. Sveinbjörnsdottir, and J. White (1999), Stable Isotope Records from Greenland Deep Ice Cores: The Climate Signal and the Role of Diffusion, in *Ice Physics and the Natural Environment, NATO ASI Series*, Vol. 156., edited by J. S. Wettlaufer et al, pp. 89–107, Springer Verlag.

Johnsen, S. J., D. Dahl-Jensen, N. Gundestrup, J. P. Steffensen, H. B. Clausen, H. Miller, V. Masson-Delmotte, A. E. Sveinbjörnsdottir, and J. White (2001), Oxygen isotope and palaeotemperature records from six Greenland ice-core stations: Camp Century, Dye-3, GRIP, GISP2, Renland and NorthGRIP, *Journal of Quaternary Science, 16(4)*, 299–307.

Kapsner, W. R., R. B. Alley, C. A. Shuman, S. Anandakrishnan, and P. M. Grootes (1995), Dominant influence of atmospheric circulation on snow accumulation in Greenland over the past 18,000 years, *Nature, 373(6509)*, 52–54.

Kreutz, K. J., P. A. Mayewski, L. D. Meeker, M. S. Twickler, S. I. Whitlow, and I. I. Pittalwala (1997), Bipolar changes in atmospheric circulation during the Little Ice Age, *Science, 277*, 1294–1296.

Lynnerup, N., S. Nørby, (2004), The Greenland Norse: bones, graves, computers, and DNA, *Polar Record 40 (213)*, 107–111.

McGovern, T. H. (2000), The Demise of Norse Greenland, in *Vikings the North Atlantic Saga.* edited by W.W. Fitzhugh and E.I. Ward, pp. 327–339, Smithsonian Press, Washington and London.

North Greenland Ice-Core Project (NorthGRIP) Members (2004), High resolution Climate Record of the Northern Hemisphere reaching into the last Glacial Interglacial Period, *Nature*, 431(7005), 147–151.

Ohmura, A., and N. Reeh, New precipitation and accumulation maps for Greenland (1991), *Journal of Glaciology, 37*, 125, 140-148.

Rasmussen, S. O., K. K. Andersen, A. M. Svensson, J. P. Steffensen, B. M. Vinther, H. B. Clausen, M.-L. S. Andersen, S. J. Johnsen, L. B. Larsen, M. Bigler, R. Röthlisberger, H. Fischer, K. Goto-Azuma, M. E. Hansson, and U. Ruth (2006), A new Greenland ice core chronology for the last glacial termination, *J. Geophys. Res., 111*, D06102, doi: 06110.01029/02005JD006079.

Reeh, N. (1989), Dating by ice flow modeling: A useful tool or an exercise in applied mathematics?, in *Dahlem Konferenzen: The Environmental Record in Glaciers and Ice Sheets,* edited by H. Oeschger and C. C. Langway Jr., pp. 141–159, John Wiley, Hoboken, N. J.

Rogers, J. C., J. F. Bolzan, V. A. Pohjola (1998), Atmospheric circulation variability associated with shallow-core seasonal isotopic extremes near Summit, Greenland, *J. Geophys. Res., D10*, 11,205-11,219.

Stuiver, M., and Braziunas, T. F. (1993), Sun, ocean, climate and atmospheric 14CO2: An evaluation of causal and spectral relationships, *Holocene*, 3, 289-305.

Vinther, B. M., Johnsen, S. J., Andersen, K. K., Clausen, H. B., and A. W. Hansen (2003), NAO signal recorded in stable isotopes of the Greenland ice cores, *Geophys. Res. Lett., 30,* No. 7, 1387, doi:10.1029/2002GL016193.

Vinther, B. M., Clausen, H. B., Johnsen, S. J., Rasmussen, S. O., Andersen, K. K., Buchardt, S. L., Seierstad, I. K., Siggaard-Andersen, M.-L., Steffensen, J. P., Svensson, A. M., Olsen, J., and J. Heinemeier (2006), A synchronized dating of three Greenland ice cores throughout the Holocene, *J. Geophys. Res., 111*, D13102, doi:10.1029/2005JD006921.

Waldmeier, M. (1961), The sunspot-activity in the years 1610–1960, Schulthess & Co AG, Zurich. Data (updated to 2004) available from ftp://ftp.ngdc.noaa.gov

Werner, M., U. Mikolajewicz, M. Heimann, G. Hoffmann (2000), Borehole versus isotope temperatures in Greenland: Seasonality does matter, *Geophys. Res. Lett.,* 27, 723–726.

K. K. Andersen, Ice and Climate, Niels Bohr Institute, University of Copenhagen, Denmark. (kka@gfy.ku.dk)

Early Holocene climate oscillations recorded in three Greenland ice cores

S. O. Rasmussen[1], B. M. Vinther, H. B. Clausen, K. K. Andersen

Ice and Climate Research, Niels Bohr Institute, University of Copenhagen, Juliane Maries Vej 30, DK-2100 Copenhagen, Denmark.

Accepted for publication in Quaternary Science Reviews.

Abstract

A new ice core chronology for the Greenland DYE-3, GRIP, and NGRIP ice cores has been constructed, making it possible to compare the δ^{18}O and accumulation signals recorded in the three cores on an almost annual scale throughout the Holocene. We here introduce the new time scale and investigate δ^{18}O and accumulation anomalies that are common to the three cores in the Early Holocene (7.9–11.7 ka before present). Three time periods with significant and synchronous anomalies in the δ^{18}O and accumulation signals stand out: the well known 8.2 ka event, an event of shorter duration but of almost similar amplitude around 9.3 ka before present, and the Preboreal Oscillation in the first centuries of the Holocene. For each of these sections, we present a δ^{18}O anomaly curve and a common accumulation signal that represents regional changes in the accumulation rate over the Greenland ice cap.

Key words: Early Holocene, GICC05, 8.2 ka event, 9.3 ka event, Preboreal Oscillation

1 Introduction

The study of Early Holocene climate variations has received much attention recently. The large amount of data collected and reviewed by Alley and Ágústdóttir (2005), Rohling and Pälike (2005), and Wiersma and Renssen (2006) clearly shows that the 8.2 ka event stands out in most North Atlantic Early Holocene climate records as the most prominent climate anomaly. The 8.2 ka event has been the subject of numerous

[1] Corresponding author, olander@gfy.ku.dk, Phone +45 3532 0590

investigations (e.g. Alley et al., 1997a, and the references above) since it was first pointed out in the Camp Century and DYE-3 δ^{18}O profiles by Hammer et al. (1986), and a detailed study of the ice core evidence has just been performed by Thomas et al. (submitted). In recent years the possible connection of the event with a massive fresh water pulse (Barber et al., 1999) has motivated further studies, because the 8.2 ka event provides a unique testing ground for climate models investigating the relationship between fresh water influx to the North Atlantic and the thermohaline circulation (Renssen et al., 2001; Wiersma and Renssen, 2006). Even though most attention has been directed to the 8.2 ka event, other anomalies are present in the Early Holocene climate proxies from the Central Greenland ice cores as well. Bond et al. (1997), von Grafenstein et al. (1999), and McDermott et al. (2001) all found a cold event in the time interval 9.2–9.5 ka before present, and the first centuries of the Holocene are dominated by the Preboreal Oscillation (Björck et al., 1997). Here we present the isotope and annual layer thickness profiles of the DYE-3, GRIP and NGRIP ice cores (Dansgaard et al., 1982; Johnsen et al., 1997, 2001; NGRIP members, 2004) on the new Greenland Ice Core Chronology 2005 time scale (GICC05) of Rasmussen et al. (2006). The GICC05 time scale is common to the three ice cores, and because the synchronization of the cores is precise down to a couple of years throughout the Holocene, the data from the three cores can be compared on an almost annual scale. From these profiles, the 8.2 ka event, the 9.3 ka event and the Preboreal Oscillation are identified as the only Early Holocene climate events on decadal scale that are common to all three cores and show both a significant δ^{18}O and annual layer thickness anomaly.

2 The Greenland Ice Core Chronology 2005

As a part of the Copenhagen Ice Core Dating Initiative, a new common time scale has been constructed for the DYE-3, GRIP, and NGRIP ice cores. The time scale is based on all available data series from the three ice cores that can be used to identify annual layers and has been named the Greenland Ice Core Chronology 2005 (GICC05). The construction of the GICC05 down to 7.9 ka before present is described in detail by Vinther et al. (2006), while the dating of the part from 7.9 ka before present to and including the Greenland Interstadial 1 (GI-1) is described by Rasmussen et al. (2006). The result of this dating effort will be summarized here. It should be noted that the GICC05 time scale reports ages relative to the year A.D. 2000, and that the notation b2k has been adapted to avoid confusion with the BP notation that has been used both with the conventional A.D. 1950 base year and other non-conventional base years when reporting ice core results. Also, it should be noted that the so-called *maximum counting errors* reported below are conservative estimates of the maximum error due to interpretation of ambiguous features in the data set, and not the total uncertainties of the time scale. The uncertainty contribution from data gaps and annual layers that have been removed from the sequence due to wind scouring or other post-depositional effects are negligible in the Holocene, but the criteria used for identifying the annual layers may be incorrect, introducing a possible bias in the dating.

In the upper section, the time scale has been constructed using stable isotope ratios. The advantage is that the δ^{18}O and δD profiles exhibit a clear annual cycle that allows reliable identification of annual layers, especially when several cores are dated in parallel. The individual profiles are matched using Electrical Conductivity Measurement (ECM) data that provide good match-points between the different profiles every 30–50 years on average. For the most recent 2 ka, annual layers have been identified using δ^{18}O data from DYE-3, GRIP, NGRIP, and a few additional shallow cores, and the time scale is considered to be exact at the volcanic layer of Vesuvius (A.D. 79), which has been uniquely identified from the tephras found in the ice core. In the 2–3.8 ka b2k section, δ^{18}O data from the GRIP and DYE-3 cores resolve the annual layers well, and the annual layers were identified from the combined matched records. The reproducibility of the annual layer count is very good, and the maximum counting error is estimated to be around 0.25%, corresponding to 5 years over the entire section. In the 3.8–7.9 ka b2k section the time scale is based on DYE-3 stable isotope ratios alone, and the uncertainty thus rises. In the 3.8–6.9 ka b2k part, the estimated maximum counting error is estimated to about 0.5%, rising to 2% in the 6.9–7.9 ka b2k section.

At greater depths, isotope ratios are not optimal for dating as the annual signal is obscured by progressing ice-flow-induced thinning of annual layers and diffusion smoothing, and the GICC05 time scale is therefore based on measurements of the impurity content of the ice below 7.9 ka b2k. The advantage of the impurity records is that they are not significantly affected by diffusion in the firn or ice, and are measured with high resolution. Also several parallel impurity records extracted from the same core can be used for annual layer identification, even though the annual signal can be less clear in the individual data series. ECM data and Continuous Flow Analysis (CFA) impurity records from GRIP (7.9–11.7 ka b2k section) (Fuhrer et al., 1993, 1996) and NGRIP (10.3–14.8 ka b2k section) have been used (Röthlisberger et al., 2000; Bigler, 2004). The maximum counting error is estimated to be 0.7–2% in the Holocene part and approximately 3% in the Greenland Stadial 1 (GS-1) and GI-1 periods.

The GICC05 time scale dates the termination of GS-1 (and thus the onset of the Holocene) to 11 703 b2k with a maximum counting error of 99 years, and the onset of GI-1e to 14 692 b2k with a maximum counting error of 186 years. The new GICC05 time scale agrees well with the GISP2 time scale (Meese et al., 1997; Alley et al., 1997b) at the termination of GS-1, thereby moving the transition some 150 years back relative to the existing GRIP and NGRIP time scales (Johnsen et al., 2001; NGRIP members, 2004). Although the different time scales thus agree well on the date of some of the major transitions, there are relative differences within Holocene, GS-1, and GI-1 periods of up to 7% between the number of years in the GICC05, GISP2 and former GRIP/NGRIP time scales, respectively.

The GICC05 is thus made by using different data series from the DYE-3, GRIP, and NGRIP ice cores in different sections, and patching these sections together into

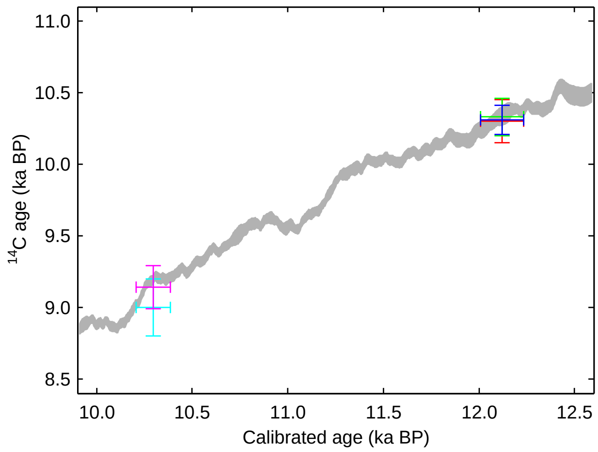

Fig. 1. By using tephras layers dated independently in the ice cores and by ^{14}C dating (crosses), the GICC05 ice core time scale can be compared with the IntCal04 terrestrial radiocarbon age calibration curve of Reimer et al. (2004), shown as the $\pm 2\sigma$ interval in grey shade. The horizontal error bars show the maximum counting error estimates of the GICC05 and the vertical error bars show the 2σ-uncertainty estimates of the ^{14}C dates (see text for ^{14}C dates and references). The GICC05 time scale is seen to be consistent with the IntCal04 curve both at the time of the Saksunarvatn eruption (left data points) and at age of the Vedde eruption (right data points). Conventional BP ages (before 1950) are used in this figure.

one consistent time scale, using at all times data from the core(s) that are optimal for that section. In this way it has also been possible to avoid basing the time scale on data from the brittle part of any of the cores. The cores have been matched throughout the Holocene so that the GICC05 here is a common time scale to the three ice cores, while the time scale in the glacial part presently is established only for the NGRIP core. In this work we focus on the Early Holocene section (7.9–11.7 ka b2k), where the time scale is based on impurity records.

Using the Saksunarvatn and Vedde tephra layers identified in the Greenland ice cores together with the corresponding ^{14}C age of the tephras, the GICC05 time scale can be directly compared with the IntCal04 terrestrial radiocarbon age calibration curve of Reimer et al. (2004). The Saksunarvatn tephra is dated to 10 347 b2k according to the GICC05, while the Vedde tephra is located at 12 171 b2k (with maximum counting errors of 89 and 114 years, respectively). The review paper of Grönvold et al. (1995) gives two estimates of the ^{14}C age of the Saksunarvatn tephra: 9140 BP from Jóhansen (1975) with an estimated 1σ-uncertainty of 75 years (Grönvold, pers. comm.), and 8900 BP from Björck et al. (1992). The latter has been changed to 9000 BP with an estimated uncertainty of 100 years by Björck et al. (2001). For the Vedde tephra, Bard et al. (1994) obtain 10 300 BP from 5 samples from two sites bracketing the tephra. From their data we estimate the 1σ-uncertainty to be around 75 years, being well in agreement with the estimates of 10330 ± 65 BP from Wastegård et al. (1998) and the 10310 ± 50 from Birks et al. (1996). The GICC05 and ^{14}C ages are shown in Fig. 1 together with the IntCal04 calibration curve of Reimer et al. (2004). The error bars show the maximum count-

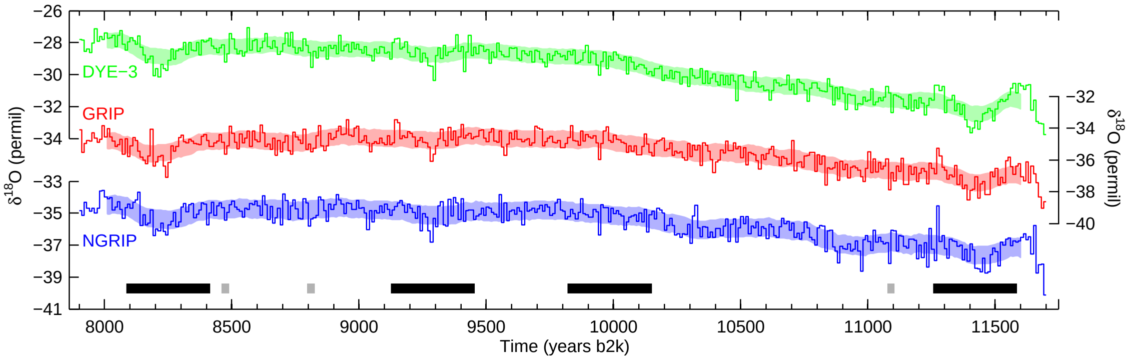

Fig. 2. The DYE-3, GRIP and NGRIP δ^{18}O profiles in the 7.9–11.7 KB b2k interval, resampled to 10 year resolution on the GICC05 time scale. The shaded envelopes are the regions that are within one standard deviation from the 210 year running mean of the individual profiles. The black lines at the bottom indicate the position of the sections shown in Fig. 4.

ing error estimates of the GICC05 time scale and the 2σ-uncertainty estimates of the ^{14}C dates. It it seen that that the GICC05 time scale is fully consistent with the IntCal04 curve, as the different age estimates fit well within the respective error margins.

3 The Early Holocene records

The 7.9–11.7 ka b2k part of the δ^{18}O profiles of DYE-3, GRIP, and NGRIP are shown on the GICC05 time scale in Fig. 2 as 10 year average values. It is seen that, in general, although the profiles agree on many details, there are also significant differences between the curves. As the distance between the DYE-3 and NGRIP drill sites is more than 1000 km, it is clear that the isotope signals cannot be expected to covary on short time scales, while the profiles are expected to contain common imprints of climatic events on regional or hemispheric scales. As a simple indicator of which features in the isotope profiles are common to the three records, we look at the places where all three profiles simultaneously deviate more than one standard deviation from their respective running means. Each of the shaded bands around the isotope profiles in Fig. 2 represent plus/minus one standard deviation from the 210 year running mean. The exact choice of averaging length is arbitrary, but the value should be larger than the typical duration of the expected (decadal-scale) anomalies, and small enough for the running mean curve to capture the gradual trends observed in the 10–11.7 ka b2k section. It is seen that the three profiles only have strong common features deviating from the $\pm 1\sigma$ variation band

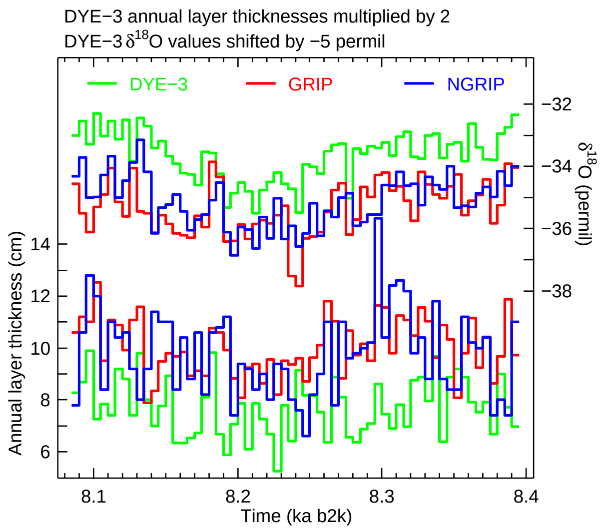

Fig. 3. Annual layer thicknesses (left axis) and δ^{18}O values (right axis) from the DYE-3, GRIP, and NGRIP ice cores around the 8.2 ka event, averaged to 5 year resolution. Note that the DYE-3 curves have been shifted vertically to fit the scale. While the three δ^{18}O curves agree on the overall shape of the event, the annual layer thickness profiles are less similar, and do not agree well with the shape of the δ^{18}O profiles.

at the well known 8.2 ka event, at 9.3 ka b2k, and in the Preboreal oscillation at 11.4–11.5 ka b2k, while a number of smaller features occur around 8.5, 8.8, 9.95 and 11.1 ka b2k. The anomalies in the δ^{18}O profiles can be attributed to temperature anomalies, but also to changing moisture sources and/or transport paths (Johnsen et al., 1989; Masson-Delmotte et al., 2005), and it is likely that these changes would also lead to changes in the annual accumulation at the drill sites. To determine whether the δ^{18}O anomalies are likely to represent larger scale features that are probably also observable outside Greenland, the obvious choice is to investigate whether simultaneously changes are observed in the annual layer thicknesses, reflecting changes in the amount of precipitation. The δ^{18}O profiles and the annual layer thickness profiles from the DYE-3, GRIP and NGRIP cores around the 8.2 ka event are shown in Fig. 3 averaged to 5 year resolution (note that the DYE-3 profiles have been shifted vertically to ease the comparison). It is seen that the annual layer thickness profiles have a negative anomaly coinciding with the δ^{18}O minimum, although the anomaly appears to have a longer duration and smaller amplitude in the DYE-3 profile. However it is clear that the amplitude of the common anomaly is comparable to, or smaller than, the amplitude of the short term variations in the individual annual layer thickness series. Although the δ^{18}O profiles agree better on the shape and amplitude of the anomaly than the accumulation profiles, significant differences can be found e.g. in the exact timing and amplitude of the deepest δ^{18}O minimum.

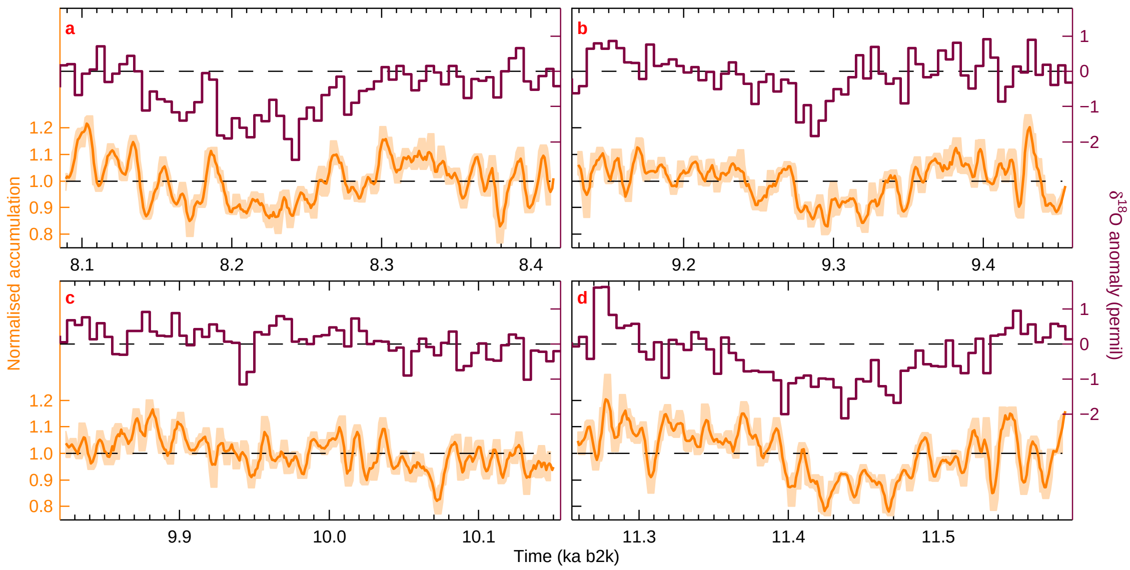

Fig. 4. Modelled accumulation rates and mean δ^{18}O curves across the 8.2 ka event (a, top left), the 9.3 ka event (b, top right), the 9.95 ka δ^{18}O anomaly (c, bottom left) and the Preboreal Oscillation (d, bottom right). The shaded bands indicate the uncertainty intrinsic to the accumulation model. For further explanation, refer to section 4.

4 Characterization of the Early Holocene climate events

Because of the differences between the individual accumulation and δ^{18}O profiles, we aim at producing a single accumulation and δ^{18}O anomaly curve that characterizes the general Greenland climate signal across the Early Holocene climate events. Masson-Delmotte et al. (2005) used a model and both δ^{18}O and deuterium excess data from GRIP and NGRIP to convert the isotope signals of the 8.2 ka event into site and source temperature anomalies, and found significant differences between the NGRIP and GRIP signals. Because well-calibrated deuterium excess data from the DYE-3 core are not available, and because the aim of this work is to present a mean regional signal rather than discussing differences between the individual Greenland ice cores, we refrain from converting the δ^{18}O anomaly into a temperature anomaly. Instead we have made a simple mean of the 5-year average δ^{18}O profiles from the three cores, as we do not expect features on shorter time scales to represent a regional climate signal. These profiles are shown in Fig. 4, presented as anomalies from the average values in the 100 year periods before and after each of the four events.

With regard to the accumulation signals, we have applied the model of Andersen et al. (in press) to extract a common accumulation signal across each of the Early Holocene climate events. The model aims at constructing a common accumulation signal from the three individual records by maximizing the signal-to-residual ratio (analogous to the signal-to-noise ratio). In this context, "signal" is the common regional accumulation signal and "residual" is everything else, including local climate phenomena, depositional noise, and measurement noise. The analysis has been

Period	8085–8415 b2k	9125–9455 b2k	9820–10150 b2k	11255–11585 b2k
DYE-3	1.33 ± 0.02	1.23 ± 0.08	1.08 ± 0.05	1.50 ± 0.11
GRIP	1.83 ± 0.18	1.73 ± 0.19	1.29 ± 0.22	2.02 ± 0.27
NGRIP	1.24 ± 0.03	1.33 ± 0.04	1.16 ± 0.09	3.11 ± 0.50
Model	2.39 ± 0.21	2.29 ± 0.28	1.52 ± 0.36	4.63 ± 0.62

Table 1
Signal-to-residual ratios for the individual records and the modelled common accumulation signals for the four sections shown in Fig. 4. It should be noted that the error intervals represent the uncertainty intrinsic to the accumulation model only, and do not include the uncertainty in the individual accumulation profiles.

performed on 5-year average values to reduce the spectrally blue noise found in accumulation data (Fisher et al., 1985). The 5-year average values were formed from logarithmical transformed data as Rasmussen et al. (2006) found the annual layer thicknesses to be roughly log-normally distributed. Strain correction has not been performed prior to the analysis, as the model is insensitive to scaling of the accumulation series. The difference between the strain correction that should be applied to the top and bottom of each of the sections, respectively, can be evaluated using a simple strain model (e.g. Rasmussen et al., 2006). The difference is 1–3% for the different sections and is considered negligible.

The modelled accumulation series across the 8.2 ka event, the 9.3 ka event, the 9.95 ka anomaly, and the Preboreal oscillation are shown in Fig. 4. The profiles are scaled so that the mean value over each interval is unity. The shaded envelopes around the accumulation model curves represent the uncertainty intrinsic to the model as described by Andersen et al. (in press) and does not take into account noise on the three original accumulation series or other factors contributing to the total uncertainty.

The signal-to-residual ratios of the individual records and the extracted common signal can be found in Table 1, which shows that a significant improvement of the signal-to-residual ratio is achieved. For the 8.5, 8.8, and 11.1 ka b2k anomalies, no significant accumulation anomalies are present in either the three individual accumulation records, or in the results of the accumulation model.

4.1 The 8.2 ka event

The 8.2 ka event stands out clearly in both the δ^{18}O and accumulation signals with an amplitude of 1–2 permil and 10%, respectively (Fig. 4a). The onset of the event is not well-defined, but is marked by a gradual decline in both δ^{18}O and accumulation anomalies starting around 8300 b2k. The end of the event is somewhat better defined around 8140 b2k, which gives a duration of 160 ± 10 years, which is in line with a recent estimate of Thomas et al. (submitted). While most of the decadal oscillations in the δ^{18}O curve synchronize rather well with those of the accumulation curve, the short period of very low δ^{18}O values around 8240-8245 ka b2k, that arises from a period of extremely low GRIP δ^{18}O values (Thomas et al., submitted), is not reflected in the accumulation signal at all.

4.2 The 9.3 ka event

Although the general appearance of the 9.3 ka event resembles that of the 8.2 ka event, there is a greater disagreement between the accumulation and δ^{18}O signals over the shape of the 9.3 ka event (Fig. 4b). The onset can be defined as 9350 b2k or 9310 b2k from the δ^{18}O, and the central part of the δ^{18}O minimum is about 40 year long, while the period of low accumulation values has a duration of about 70 years. The amplitude of both the δ^{18}O and accumulation anomalies are similar to those of the 8.2 ka event, and after the synchronous period of low values, both the δ^{18}O and accumulation values rise gently over a 100–150 year long period to values that are 1 permil and 8% above the general level, respectively. This contrasts with the sharp return to normal values observed at the end of the 8.2 ka event. The end of the 9.3 ka event is therefore hard to define, and the overall duration of the 9.3 ka event varies from 40 to more than 100 years depending on which criteria and which data series are used to define the onset and end.

4.3 The 9.95 ka anomaly

The 9.95 ka δ^{18}O anomaly and the corresponding accumulation model results are shown in Fig. 4c. The δ^{18}O anomaly of 9940-9950 b2k has no counterpart in the accumulation signal, but instead a clear accumulation anomaly is observed more than 100 years earlier, centered around 10 070 b2k. If the accumulation and δ^{18}O signals had been obtained from independent archives, or even from independently dated ice cores, one could have made the error of assuming synchronicity between these accumulation and δ^{18}O anomalies. This clearly illustrates the importance of good dating precision and underlines the dangers of wiggle-matching, when there is no independent evidence to suggest that the signals are synchronous events.

4.4 The Preboreal Oscillation

The Preboreal oscillation stands out clearly in both δ^{18}O and accumulation signals (Fig. 4d). The reference levels of the δ^{18}O and accumulation curves (dashed lines) are not well-established in this time interval due the absence of stable climatic conditions prior to the Preboreal Oscillation, but from Figs. 2 and 4d it is seen that the Preboreal oscillation consists of a short period of relatively high δ^{18}O values starting within the first 50 years after the termination of GS-1 followed by a period of low δ^{18}O values and low accumulation rates lasting for approximately 100 years, and ending with a period of moderate δ^{18}O values and relatively high accumulation rates. In the central part from 11.5 to 11.4 ka b2k, the δ^{18}O values are lowered by about 2 permil and the accumulation is reduced by $10 - 15\%$. The oscillation ends with a short period of very high δ^{18}O values around 11 270 – 11 280 b2k, about 400 years after the termination of GS-1.

5 Conclusions

We have presented synchronized δ^{18}O records from the DYE-3, GRIP, and NGRIP ice cores covering the Early Holocene on the GICC05 time scale. The new time scale dates the 8.2 ka event with an estimated maximum counting error of 47 years, the 9.3 ka event with an estimated maximum counting error of 70 years, and the Preboreal oscillation with an estimated maximum counting error of 97 years.
A comparison of the records across the 8.2 ka event shows that the profiles agree on the approximate duration and amplitude of the anomaly, but the differences between the three profiles indicate that the individual Greenland ice core records should not be regarded as a regional, let alone hemispherical, signal on time scales much shorter than 5–10 years. When correlating data from other archives with the Greenland ice core records it is essential to consider whether there is a reason for comparing with one specific ice core. Rogers et al. (2002) found that different ice cores that were retrieved from sites relatively close to each other but from East and West sides of the ice divide, respectively, recorded either Greenland East or West coast climate. In the same way the DYE-3 site may be much more influenced by storm tracks passing the Southern tip of Greenland than GRIP and NGRIP (Hutterli et al., 2005), and hence the DYE-3 climate record is thus the obvious choice for comparison with data from other climate archives in the South Greenland area. On the other hand, if no such preference can be assumed, and data from no specific ice core are preferable a priori, we propose that the common accumulation and isotope signals presented here are used as a representation of regional Greenland climate variability.
As illustrated in Figs. 2 and 4, the 8.2 ka event, the 9.3 ka event and the Preboreal oscillation have distinct δ^{18}O and accumulation anomalies, and these events are the only events in the 7.9–11.7 ka b2k interval that have significant synchronous δ^{18}O and accumulation anomalies that are common to the three cores. The central part of the events include a 1–2 permil lowering of the δ^{18}O value, corresponding to several degrees of cooling if the δ^{18}O anomaly is interpreted as a temperature signal, which agrees fairly well with the temperature reconstruction of the 8.2 ka event by Masson-Delmotte et al. (2005). The mean annual accumulation is about 10–15% below the normal level during each of the events, but the relative timing of the δ^{18}O minima and the accumulation anomalies is not the same for the three events, and there seems to be no general connection between the the deepest δ^{18}O

and accumulation minima, confirming that in the Holocene on short time scales other parameters than temperature are important in governing how much snowfall central Greenland receives (Crüger et al., 2004; Andersen et al., in press).

6 Data access

The construction of the GICC05 time scale in the Holocene is described in Vinther et al. (2006) and Rasmussen et al. (2006). The DYE-3, GRIP, and NGRIP $\delta^{18}O$ profiles are available on the GICC05 time scale at http://icecores.dk together with the $\delta^{18}O$ and accumulation model anomaly results presented in Fig. 4. Future extensions of the GICC time scale will also be posted here.

Acknowledgements

This work is a contribution of the Copenhagen Ice Core Dating Initiative which is supported by a grant from the Carlsberg Foundation.
NGRIP is directed and organized by the Ice and Climate Research Group at the Niels Bohr Institute, University of Copenhagen, Denmark. It is supported by funding agencies in Denmark (SNF), Belgium (FNRS-CFB), France (IPEV and INSU/CNRS), Germany (AWI), Iceland (RannIs), Japan (MEXT), Sweden (SPRS), Switzerland (SNF) and the USA (NSF, Office of Polar Programs).

References

Alley, R., Ágústdóttir, A., 2005. The 8k event: cause and consequences of a major Holocene abrupt climate change. Quaternary Science Reviews 24, 1123–1149.

Alley, R., Mayewski, P., Sowers, T., Stuiver, M., Taylor, K., Clark, P., 1997a. Holocene climatic instability: A prominent widespread event 8200 yr ago. Geology 25, 483–486.

Alley, R. B., Shuman, C. A., Meese, D. A., Gow, A. J., Taylor, K. C., Cuffey, K. M., Fitzpatrick, J. J., Grootes, P. M., Zielinski, G. A., Ram, M., Spinelli, G., Elder, B., 1997b. Visual-stratigraphic dating of the GISP2 ice core: Basic, reproducibility, and application. Journal of Geophysical Research 102 (C12), 26367–26381.

Andersen, K. K., Ditlevsen, P. D., Rasmussen, S. O., Clausen, H. B., Johnsen, S. J., Steffensen, J. P., in press. Retrieving a common accumulation record from Greenland ice cores for the past 1800 years. Journal of Geophysical Research, doi: 10.1029/2005JD006765.

Barber, D., Dyke, A., Hillaire-Marcel, C., Jennings, A., Andrews, J., Kerwin, M., Bilodeau, G., McNeely, R., Southon, J., Morehead, M., Gagnon, J.-M., 1999. Forcing of the cold event of 8,200 years ago by catastrophic drainage of Laurentide lakes. Nature 400, 344–348.

Bard, E., Arnold, M., Mangerud, M., Paterne, M., Labeyrie, L., Duprat, J., Mélières, M. A., Sonstegaard, E., Duplessy, J. C., 1994. The North Atlantic atmosphere-sea surface ^{14}C gradient during the Younger Dryas climatic event. Earth and Planetary Science Letters 126, 275–287.

Bigler, M., 2004. Hochauflösende Spurenstoffmessungen an polaren Eisbohrkernen: Glaziochemische und klimatische Prozessstudien, Ph.D. dissertation, University of Bern, Switzerland.

Birks, H., Gulliksen, S., Haflidason, H., Mangerud, J., Possnert, G., 1996. New radiocarbon dates for the Vedde Ash and the Saksunarvatn Ash from Western Norway. Quaternary Research 45 (2), 119–127.

Björck, S., Ingólfsson, Ó., Haflidason, H., Hallsdóttir, M., Andersson, N. J., 1992. Lake Torfadalsvatn: a high resolution record of the North Atlantic ash zone I and the last glacial-interglacial environmental changes in Iceland. Boreas 21, 15–22.

Björck, S., Muscheler, R., Kromer, B., Andresen, C., Heinemeier, J., Johnsen, S., Conley, D., Koç, N., Spurk, M., Veski, S., 2001. High-resolution analyses of an early Holocene climate event may imply decreased solar forcing as an important climate trigger. Geology 12, 1107–1110.

Björck, S., Rundgren, M., Ingólfsson, Ó., Funder, S., 1997. The Preboreal oscillation around the Nordic Seas: terrestrial and lacustrine responses. Journal of Quaternary Science 12, 455–465.

Bond, G., Showers, W., Cheseby, M., Lotti, R., Almasi, P., deMenocal, P., Priore, P., Cullen, H., Hajdas, I., Bonani, G., 1997. A pervasive millennial-scale cycle in North Atlantic Holocene and glacial climates. Science 278 (5341), 1257–1266.

Crüger, T., Fischer, H., von Storch, H., 2004. What do accumulation records of single ice cores in Greenland represent? Journal of Geophysical Research 109, D21110.

Dansgaard, W., Clausen, H., Gundestrup, N., Hammer, C., Johnsen, S., Kristinsdottir, P., Reeh, N., 1982. A new Greenland deep ice core. Science 218, 1273–1277.

Fisher, D. A., Reeh, N., Clausen, H. B., 1985. Stratigraphic noise in time series derived from ice cores. Annals of Glaciology 7, 76–83.

Fuhrer, K., Neftel, A., Anklin, M., Maggi, V., 1993. Continuous measurements of hydrogen peroxide, formaldehyde, calcium and ammonium concentrations along the new GRIP ice core from Summit, Central Greenland. Atmospheric Environment 27A (12), 1873–1880.

Fuhrer, K., Neftel, A., Anklin, M., Staffelbach, T., Legrand, M., 1996. High-resolution ammonium ice core record covering a complete glacial-interglacial cycle. Journal of Geophysical Research 101 (D2), 4147–4164.

Grönvold, K., Óksarsson, N., Johnsen, S. J., Clausen, H. B., Hammer, C. U., Bond, G., Bard, E., 1995. Ash layers from Iceand in the Greenland GRIP ice core correlated with oceanic and land sediments. Earth and Planetary Science Letters 135, 149–155.

Hammer, C. U., Clausen, H. B., Tauber, H., 1986. Ice-core dating of the Pleistocene/Holocene boundary applied to a calibration of the ^{14}C time scale. Radiocarbon 28, 284–291.

Hutterli, M. A., Raible, C. C., Stocker, T. F., 2005. Reconstructing climate variability from Greenland ice sheet accumulation: An ERA40 study. Geophysical Research Letters 32, L23712.

Jóhansen, J., 1975. Pollen diagrams from the Shetland and Faroe Islands. New Phytologist 75, 369–387.

Johnsen, S. J., Clausen, H. B., Dansgaard, W., Gundestrup, N. S., Hammer, C. U., Andersen, U., Andersen, K. K., Hvidberg, C. S., Dahl-Jensen, D., Steffensen, J. P., Shoji, H., Sveinbjörnsdóttir, Á. E., White, J., Jouzel, J., Fisher, D., 1997. The δ^{18}O record along the Greenland Ice Core Project deep ice core and the problem of possible Eemian climatic instability. Journal of Geophysical Research 102 (C12), 26397–26410.

Johnsen, S. J., Dahl-Jensen, D., Gundestrup, N., Steffensen, J. P., Clausen, H. B., Miller, H., Masson-Delmotte, V., Sveinbjörnsdottir, A. E., White, J., 2001. Oxygen isotope and palaeotemperature records from six Greenland ice-core stations:

Camp Century, Dye-3, GRIP, GISP2, Renland and NorthGRIP. Journal of Quaternary Science 16, 299–307.

Johnsen, S. J., Dansgaard, W., White, J., 1989. The origin of Arctic precipitation under present and glacial conditions. Tellus 41B, 452–468.

Masson-Delmotte, V., Landais, A., Stievenard, M., Cattani, O., Falourd, S., Jouzel, J., Johnsen, S. J., Dahl-Jensen, D., Sveinsbjornsdottir, A., White, J. W. C., Popp, T., Fischer, H., 2005. Holocene climatic changes in Greenland: Different deuterium excess signals at Greenland Ice Core Project (GRIP) and NorthGRIP. Journal of Geophysical Research 110, D14102.

McDermott, F., Mattey, D. P., Hawkesworth, C., 2001. Centennial-scale Holocene climate variability revealed by a high-resolution speleothem δ^{18}O record from SW Ireland. Science 294 (5545), 1328–1331.

Meese, D. A., Gow, A. J., Alley, R. B., Zielinski, G. A., Grootes, P. M., Ram, M., Taylor, K. C., Mayewski, P. A., Bolzan, J. F., 1997. The Greenland Ice Sheet Project 2 depth-age scale: Methods and results. Journal of Geophysical Research 102 (C12), 26411–26423.

NGRIP members, 2004. High-resolution record of Northern Hemisphere climate extending into the last interglacial period. Nature 431, 147–151.

Rasmussen, S. O., Andersen, K. K., Svensson, A. M., Steffensen, J. P., Vinther, B., Clausen, H. B., Siggaard-Andersen, M.-L., Johnsen, S. J., Larsen, L. B., Dahl-Jensen, D., Bigler, M., Röthlisberger, R., Fischer, H., Goto-Azuma, K., Hansson, M., Ruth, U., 2006. A new Greenland ice core chronology for the last glacial termination. Journal of Geophysical Research 111, D06102.

Reimer, P. J., Baillie, M. G. L., Bard, E., Bayliss, A., Beck, J. W., Bertrand, C. J. H., Blackwell, P. G., Buck, C. E., Burr, G. S., Cutler, K. B., Damon, P. E., Edwards, R. L., Fairbanks, R. G., Friedrich, M., Guilderson, T. P., Hogg, A. G., Hughen, K. A., Kromer, B., McCormac, G., Manning, S., Ramsey, C. B., Reimer, R. W., Remmele, S., Southon, J. R., Stuiver, M., Talamo, S., Taylor, F. W., van der Plicht, J., Weyhenmeyer, C. E., 2004. Radiocarbon calibration from 0–26 cal kyr BP. Radiocarbon 46 (3), 1029–1058.

Renssen, H., Goosse, H., Fichefet, T., Campin, J.-M., 2001. The 8.2 kyr BP event simulated by a global atmosphere-sea-ice-ocean model. Geophysical Research Letters 28, 1567–1570.

Rogers, J. C., Bolzan, J. F., Pohjola, V. A., 2002. Atmospheric circulation variability associated with shallow-core seasonal isotopic extremes near Summit, Greenland. Journal of Geophysical Research D10, 11,205–11,219.

Rohling, E., Pälike, H., 2005. Centennial-scale climate cooling with a sudden cold event around 8,200 years ago. Nature 434, 975–979.

Röthlisberger, R., Bigler, M., Hutterli, M., Sommer, S., Stauffer, B., Junghans, H., Wagenbach, D., 2000. Technique for continuous high-resolution analysis of trace substances in firn and ice cores. Environmental Science and Technology 34 (2), 338–342.

Thomas, E., Wolff, E., Mulvaney, R., Steffensen, J., Johnsen, S., Arrowsmith, C., White, J., Vaughn, B., Popp, T., submitted. The 8.2 kyr event from Greenland ice cores, Quaternary Science Reviews.

Vinther, B. M., Clausen, H. B., Johnsen, S. J., Rasmussen, S. O., Andersen, K. K., Buchardt, S. L., Dahl-Jensen, D., Seierstad, I. K., Siggaard-Andersen, M.-L., Steffensen, J. P., Svensson, A. M., Olsen, J., Heinemeier, J., 2006. A synchronized dating of three Greenland ice cores throughout the Holocene. Journal of Geophysical Research 111, D13102.

von Grafenstein, U., Erlenkeuser, H., Brauer, A., Jouzel, J., Johnsen, S. J., 1999. A Mid-European decadal isotope-climate record from 15,500 to 5000 years B.P. Science 284 (5420), 1654–1657.

Wastegård, S., Björck, S., Possnert, G., Wohlfarth, B., 1998. Evidence for the occurrence of Vedde Ash in Sweden: radiocarbon and calendar age estimates. Journal of Quaternary Science 13, 271–274.

Wiersma, A., Renssen, H., 2006. Model-data comparison for the 8.2 ka BP event: Confirmation of a forcing mechanism by catastrophic drainage of Laurentide Lakes. Quaternary Science Reviews 25 (1–2), 63–88.

Synchronization of the NGRIP, GRIP, and GISP2 ice cores across MIS 2 and palaeoclimatic implications

S. O. Rasmussen [1], I. K. Seierstad, K. K. Andersen, M. Bigler, D. Dahl-Jensen, S. J. Johnsen

Ice and Climate Research, Niels Bohr Institute, University of Copenhagen, Juliane Maries Vej 30, DK-2100 Copenhagen, Denmark.

Manuscript submitted to Quaternary Science Reviews.

Abstract

We here present a synchronization of the NGRIP, GRIP, and GISP2 ice cores based mainly on volcanic events over the period 14.9 – 32.45 ka b2k (before A.D. 2000), corresponding to MIS 2 and the end of MIS 3. The matching provides a means to apply the recent NGRIP-based Greenland Ice Core Chronology 2005 time scale to the GRIP and GISP2 ice cores, thereby making it possible to compare the synchronized palaeoclimate profiles of the cores in detail. The δ^{18}O and [Ca^{2+}] profiles of the three cores are presented on the common time scale and generally show excellent agreement across the stadial-interstadial transitions and across the two characteristic dust events in Greenland Stadial 3. However, large differences between the δ^{18}O and [Ca^{2+}] profiles of the three cores are seen in the 16 – 19 ka b2k interval, in which also the GISP2 accumulation rates are 7 – 9% higher than normal for the late glacial period. We conclude that changes of the atmospheric circulation are likely to have occurred in this period, increasing the spatial gradients in Greenland and resulting in larger variations between the records. It is also possible that the Central Greenland ice divide has migrated during this period.

---

[1] Corresponding author, olander@gfy.ku.dk

1 Introduction

Ice core data provide climate records of excellent resolution across the late glacial period, but detailed comparisons have been hampered by the lack of a common time scale. Comparisons of glacial ice core records have in general been made by assuming that the Greenland stadial-interstadial transitions as recorded by the δ^{18}O signals are synchronous, but this approach has a limited accuracy because the δ^{18}O transitions do not always look alike in different cores, and the assumption of simultaneous transitions means that possible leads and lags cannot be assessed (Bender et al., 1994). Synchronization of ice cores using gas records is also possible, but the determination of the ice age-gas age offset is not trivial, and smoothing takes place when the gas is enclosed in the bubbles of the ice (Blunier and Schwander, 2000). This makes the method less attractive for high-resolution synchronization of Greenland ice cores, while it has proved very successful for synchronizing Greenland and Antarctic records (Blunier and Brook, 2001). The situation is especially difficult during the millennia-long periods without abrupt climatic transitions in the late part of the glacial. In the very latest part of the glacial the δ^{18}O profiles of the Greenland ice cores are significantly different (e.g. NGRIP members, 2004; Johnsen et al., 2001; Svensson et al., submitted), making synchronization even more difficult.

As discussed by Southon (2004), the time scales of the GISP2 and GRIP ice cores differ significantly in the glacial period, which can be partially explained by the very different dating approaches applied. The glacial section of the GISP2 time scale was made by counting annual layers, identified mainly from visual inspection of the core stratigraphy (Alley et al., 1997; Meese et al., 1997), while the glacial part of the GRIP ice core was dated using an ice flow model incorporating an empirical δ^{18}O-accumulation relationship and two independently dated fix-points (Dansgaard et al., 1993; Johnsen et al., 1995), leading eventually to the improved ss09sea time scale (Johnsen et al., 2001). This time scale was transferred to NGRIP by using climatic transitions as observed in the δ^{18}O profiles and a number of prominent volcanoes as match points (NGRIP members, 2004).

Recently the DYE-3, GRIP, and NGRIP ice cores have been dated in parallel by annual layer counting in the Holocene as part of the Greenland Ice Core Chronology 2005 (GICC05) effort (Vinther et al., 2006; Rasmussen et al., 2006, accepted). Data from all three cores have been used to construct the common GICC05 time scale, and the cores are synchronized with a maximum offset of a few years. Below the Preboreal – Younger Dryas transition the GICC05 time scale is based on NGRIP data alone and currently reaches back to about 42 ka b2k (before the year A.D. 2000) (Andersen et al., submitted). The GICC05 agrees with the GISP2 time scale at the onset of Greenland interstadial 1 (GI-1) and the agreement is fairly good at the onsets of many of the interstadials. However, relative differences between the two time scales of about 10% and more than 30% are observed in the Bølling-

Allerød period and in some sections of the glacial, respectively (Rasmussen et al., 2006; Svensson et al., submitted).

Here we present a synchronization of the NGRIP, GRIP, and GISP2 ice cores from the onset of GI-1 to GI-5, 14.9 – 32.45 ka b2k, corresponding to Marine Isotope Stage 2 (MIS 2) and the end of MIS 3. The synchronization is based on identification of volcanic events that have been recorded in at least two of the three cores, similar to the method used to transfer the GICC05 time scale from NGRIP depths to GRIP depths across the last termination (11.7 – 14.8 ka b2k) (Rasmussen et al., 2006). In the present work we also match the records using peaks in the $[NH_4^+]$ profiles, probably originating from biomass burning (Fuhrer et al., 1996; Taylor et al., 1996). Volcanic and biomass burning events have been found because they represent distinct peaks that stand out from the climate-dependent background levels. Furthermore they are recorded almost simultaneously across the area where they are detected, while e.g. $\delta^{18}O$ cannot be assumed to change simultaneously across Greenland.

The obtained match points have been used to apply the GICC05 time scale to the GRIP and GISP2 ice cores, and the synchronization makes it possible to investigate regional differences between the three records and to determine the relative timing of climatic changes as recorded in the three ice cores.

2 Data

Explosive volcanic eruptions emit large amounts of tephra (e.g. ash) and gases (e.g. SO_2) into the atmosphere. Oxidation and gas-to-particle conversion transforms SO_2 to sulfuric acid (H_2SO_4). Volcanic events are therefore recorded in ice cores mainly as acidic peaks (Clausen et al., 1997; Hammer et al., 1980, 1997) and sulfate peaks (Zielinski et al., 1994; Zielinski, 2000; Bigler et al., 2002), although tephra particles also may be found (Mortensen et al., 2005; Grönvold et al., 1995). Electrical Conductivity Measurements (ECM), Dielectric Profiling (DEP), and $[SO_4^{2-}]$ measurements are the main data used for detection of volcanic events. The ECM profile is a measure of the $[H^+]$ of the ice and is obtained by moving a set of electrodes with a large voltage difference along a cleaned section of the core (Hammer, 1980). Also the dielectric properties of the core are effected by the acidity (Moore et al., 1989), but both volcanic ECM and DEP peaks can be weakened or even obliterated in sections with high dust level due to the increased alkalinity. The large peaks in the $[SO_4^{2-}]$ profile must thus be considered the most reliable indicator of volcanic activity in ice cores.

The data series used in this work are listed in Table 1 together with information on the resolution and data references. Measurements of $[SO_4^{2-}]$, $[NH_4^+]$, and $[Ca^{2+}]$ have been performed on melted samples of ice core, either as discrete samples used for ion chromatography (IC) or as Continuous Flow Analysis (CFA) measurements (Röthlisberger et al., 2000). [SO_4^{2-}] has only been measured within shorter sections of the GRIP core, but the other data profiles cover the entire section investigated. It should be noted that the depth resolution values given in Table 1 for the CFA data are the sampling resolution values, which are somewhat smaller than the shortest events that can be detected in the measured profiles. For the CFA data, the depth assignment has an uncertainty in the 1 – 2 cm range, while the GRIP and NGRIP ECM data can be offset from true depth by up to 5 cm due to less accurate depth control in the measurement setup.

3 Method

The use of volcanic deposits is the most direct and well-understood method for high-resolution synchronization of ice records (e.g., Wolff et al., 1999; Udisti et al., 2004; Bay et al., 2006). A study of recent volcanic deposits in Antarctica shows that the sulphate peaks typically start 1 – 3 years after the eruption and last 1 – 3 years (Palmer et al., 2001). In the construction of the GICC05 time scale, the DYE-3, GRIP, and NGRIP cores have been dated in parallel using $\delta^{18}O$ data back to 1814 b2k, and based on the experiences obtained in this interval, the maximum difference in arrival times and peak maximum location between two Greenland sites is estimated to one year. When volcanic fallout from a certain eruption is found in two or more cores, the layer can therefore be regarded as an almost simultaneous event. However, volcanic fallout is not distributed evenly, which is clearly seen by the fact that many volcanic layers are found in one of the two Central Greenland GRIP and GISP2 cores, located about 30 km apart, and not in the other.

The NGRIP, GRIP, and GISP2 cores have been matched by synchronizing volcanic signals in the section corresponding to the 14.9 – 32.45 kyr b2k time interval. A graphical Matlab application (”Matchmaker”) was designed to facilitate the matching procedure by allowing the user to scale and display the available data series for each core and align common features in an efficient way.

As a first step the three ice core records were matched on a coarse scale using the stadial-interstadial transitions observed in the climate profiles of e.g. $\delta^{18}O$ and [Ca^{2+}]. These first match points based on climatic events served only to align the curves before looking for potential synchronous volcanic events, appearing as peaks in profiles of ECM, DEP, [SO_4^{2-}] and at times [Ca^{2+}], and were not used for the final synchronization. Characteristic peaks observed in the data profiles were chosen manually to define match points (time-marker horizons) between the different cores, representing synchronous events. The selected match points were mainly volcanic events, but the synchronization was sometimes supported by features of non-volcanic origin, such as characteristic patterns of [NH_4^+] peaks appearing with similar spacing in two or three cores. These patterns of typically 3 – 5 adjacent peaks support

that the correct volcanic events have been matched, but they have not been used for the synchronization. However, a number of very strong individual $[NH_4^+]$ peaks have been chosen as match points.
To validate that the resulting match points do represent synchronous volcanic depositions, the depths of the match points $d_1, ..., d_N$ and $D_1, ..., D_N$ in two cores are plotted against each other. The slope of this curve is the ratio of the annual layer thicknesses in the two cores. This ratio depends on the ratio of the accumulation rates and the flow-related thinning rates at two drill sites, and must be expected to change only slowly except across stadial-interstadial transitions. If an event is matched incorrectly, this will be reflected in the slope of the curve, but if viewed over long sections, only very large discrepancies will be readily apparent due to the large range of values. If for example the match points span 200 – 300 m of ice core as is the case in this work, offsets of a few tens of centimeters will only be visible as minor wiggles on the curve. By plotting $d_i - D_i$ versus D_i a more sensitive quality check can be performed. The depth difference $d_i - D_i$ will vary smoothly under stable climatic conditions, and mismatched events will also here show up in the curve as kinks or sections with large curvature. However, due to the much smaller range of values taken on by $d_i - D_i$, the discrepancies will be much more easily visible when plotted. An even more sensitive approach is to calculate the ratio r_i of the distances between adjacent match points in one core relative to the other: $r_i = (D_{i+1} - D_i)/(d_{i+1} - d_i)$ for $i = 1, ..., N - 1$. Assuming that the accumulation rate at each site is rather constant within a climate period and that no abrupt changes in the flow pattern with depth occur, this ratio should remain constant or at least only change slowly. This will of course only be the case as long as the distance between adjacent match points is large enough to prevent that the results are seriously affected by problems with depth control, depositional noise, and short-range accumulation rate variability, which are important factors when the match point spacing is less than a few decades (Fisher et al., 1985). The latter two of the three validation methods have been used simultaneously while performing the synchronization in order to continuously evaluate the consistency of the match points. The results are here presented as plots of depth difference $d_i - D_i$ versus depth D_i. In these plots, the slope of the curves corresponds to the relative annual layer thickness deviation between the two cores, where a slope of e.g. 0.03 corresponds to the annual layers core in core d being 3% thicker than those of core D.

Typical volcanic peaks span a depth interval from a few millimeters to about 15 cm in the cores, and different data series from the same core may peak at slightly different depths across this interval. These differences are likely to be caused by a combination of differences in transport paths and accumulation conditions, and artificial offsets due to problems with precise co-registration of the signals in different data series as mentioned in section 2. The strategy applied here was to examine each volcanic event in detail and choose the most well-defined feature (e.g. the sharpest peak or the steepest flank) from the data series with highest possible resolution, at the same time checking that there is agreement between all other available data series. The precision of the synchronization is in general estimated to 10 cm or

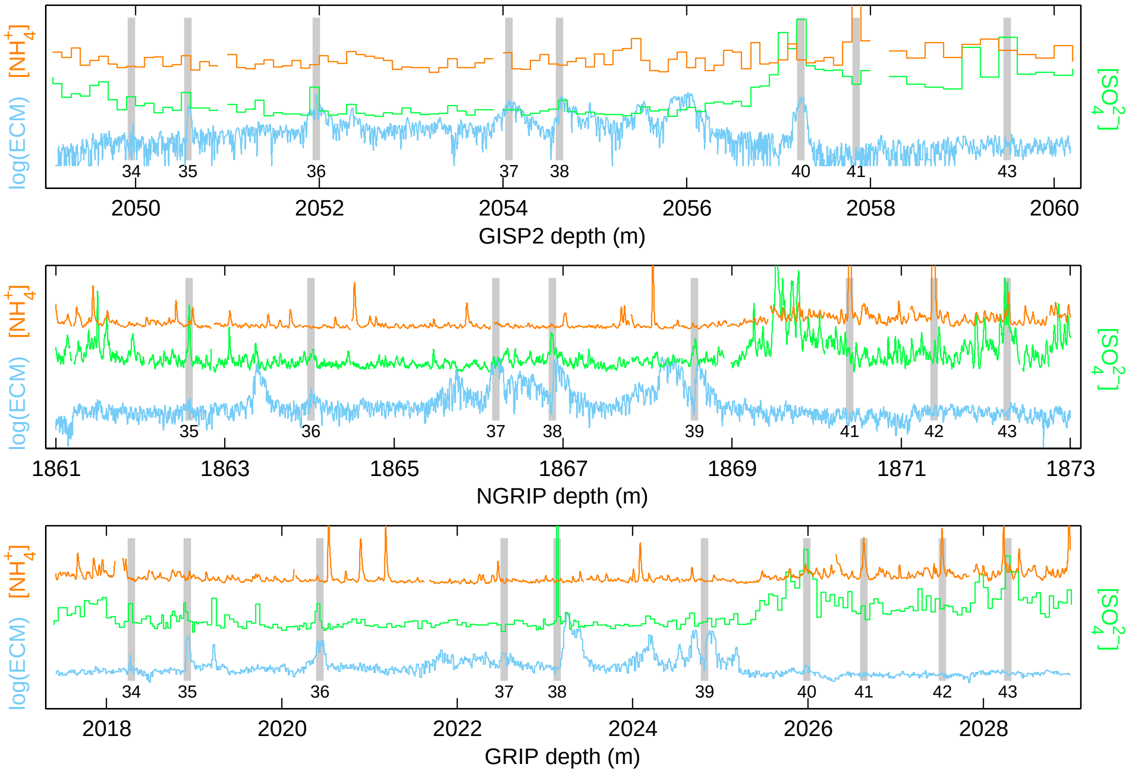

Fig. 1. Synchronized section of the three cores. The ECM, [SO_4^{2-}], and [NH_4^+] data series are shown together with the match points. The numbers refer to the match point numbers in Table 2. The ECM peaks appear less well-defined because of the logarithmic axis. Match point 34 has only been found in the GRIP and GISP2 records, and match point 40 in NGRIP / 39 in GISP2 have not been set because their positions within the wide [SO_4^{2-}]/ECM peaks are uncertain. Number 42 cannot be set in GISP2 because it is based on [NH_4^+] data, which are not available for the GISP2 core in sufficient resolution.

better. In some cases the peak shapes are wider or more offset between the cores, leading to less certain synchronization. Also the match points that have been based on GISP2 [SO_4^{2-}] and [NH_4^+] data are less certain as the data resolution is 20 cm.

The matching was performed both by having data from all three cores present at a time and also by matching the cores in pairs, i.e. GRIP-NGRIP, GRIP-GISP2 and GISP2-NGRIP. Three investigators performed the matching independently in order to validate the synchronization and check the reproducibility of the chosen match points. Match points identified by all investigators were accepted, and sections with discrepancies were revisited. In the case of discrepancies smaller than or about 10 cm, agreement was obtained by adjusting the exact positioning within the same volcanic event. Sections with larger discrepancies were re-matched independently by at least two investigators, and if the discrepancies remained, no match points were accepted in that section.

A synchronized section from the end of GI-3 is shown in Fig. 1 to illustrate how patterns of peaks can be recognized between cores and used for matching. It is also exemplified how some match points can only be used to synchronize two of the three cores because of ambiguous peak shapes and limited data resolution. It should be noted that the reliability of the individual match points cannot be adequately evaluated when showing 12 meters of data on a single plot because of the large dynamical range of the data values. The advantage of the Matchmaker application is indeed the opportunity to switch between detailed views of a certain peak and longer sequences of match points.

4 Results

Table 2 lists the match points between the NGRIP, GRIP, and GISP2 cores. 66 match points have been chosen within the 14.9 – 32.45 ka b2k section, corresponding to an average spacing of about 250 yrs. The match points are unevenly distributed across the section, with spacing ranging from approximately 10 yrs (distance about 0.3 m) to 2 kyrs (distance more than 40 m). The most dense distribution of distinct volcanic match points is observed from GI-3 and below (match points 34 – 66), and during the termination of GS-2 (match points 1 – 9). In the intermediate part, the number of distinct volcanic peaks is smaller and the distance between adjacent match points is thus greater. As described above, only match points that all investigators independently agreed upon have been included in the synchronization, apart from a single exception. In the depth interval bounded by match points 24 and 28 the matching is ambiguous. We believe that match points 25 – 27 represent by far the most likely synchronization, but acknowledge that other reasonable alignments of the cores are possible. In the middle of this section the matching may be an estimated 1 meter (or about 50 years) offset, although we find deviations of this magnitude to be unlikely.

Some match points are only found in two cores. This is especially the case for match points based on [NH_4^+] peaks, because the 20 cm resolution of the GISP2 [NH_4^+] data sometimes makes it difficult to make certain matches. This is both due to the fact that medium-size [NH_4^+] peaks that are only a few centimeters wide in the continuous GRIP and NGRIP records disappear when averaging over 20 cm sections, but also that matching of characteristic patterns of peaks is only possible in high-resolution data. Most of the match points that are only found in the NGRIP and GISP2 cores have not been set in the GRIP core due to the absence of [SO_4^{2-}] data, which sometimes are needed to confidently identify a certain volcanic event.

A somewhat surprising observation, given that the geographical distance between GRIP and GISP2 (28 km) is an order of magnitude smaller than the distance from GRIP/GISP2 to NGRIP (more than 300 km), is that the general similarity of the GRIP and GISP2 records is not significantly different from the similarity of the NGRIP and GRIP/GISP2 records.

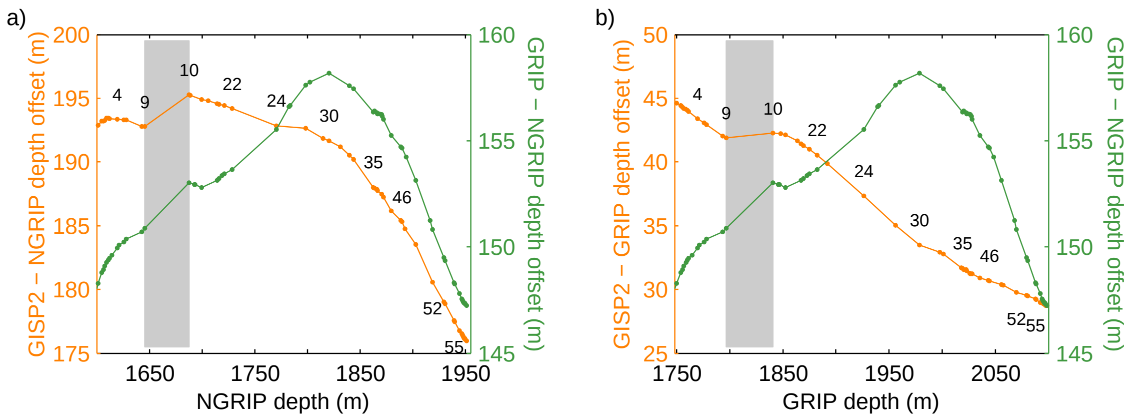

Fig. 2. Depth differences between the match points in the three cores plotted versus NGRIP depth (a) and GRIP depth (b). The numbers refer to the match point numbers in Table 2. The grey shaded area marks the interval between match points 9 and 10 (corresponding to 16.5 – 18.3 ka b2k) where the GISP2-NGRIP and GISP2-GRIP depth difference curves (orange curves) have an unusual shape.

Fig. 2 show the depth difference plots. In general the curves are smooth and have small curvature. Initially disregarding the grey shaded area between match points 9 and 10, the GISP2-GRIP depth difference (Fig. 2b, orange curve) is positive and monotonously decreasing with depth, because the slightly higher accumulation rates at GISP2 (Meese et al., 1997) are gradually compensated by more rapid flow-induced thinning of the layers. In a similar way, because NGRIP has a present-day annual accumulation rate of 19 cm (ice equivalent) (NGRIP members, 2004) while GRIP receives 23 cm (ice equivalent) per year (Johnsen et al., 1992), the GRIP-NGRIP depth difference curves (Fig. 2, green) are positive in the top of the core and increases until match point 30 (about 1820 m NGRIP depth, 1979 m GRIP depth), where the more rapid layer thinning at GRIP results in thinner annual layers in the GRIP core than in NGRIP, corresponding to negative slope of the depth difference curve. The same effect is seen for the GISP2-NGRIP depth difference (Fig. 2a, orange). Superimposed on this general trend an unexpected feature appears between match points 9 and 10 (grey shaded intervals). This 1.8 ky long interval is characterized by containing no clear match points, but as the match points in both ends are certain it is evident that the GISP2-NGRIP and GISP2-GRIP depth difference curves have bumps across this section. Just above match point 9 and below match point 10, the GISP2 annual layers are 2.5 – 3% thinner than those in the NGRIP core (slope between -0.03 and -0.025), while the mean slope is 0.060 between match point 9 and 10. The GISP2 annual layers are thus on average about 9% thicker in this period compared to the average value just outside this time period. When comparing GISP2 and GRIP, the corresponding slopes are -0.057 outside the interval and 0.009 inside, reflecting on average about 7% thicker annual layers in the GISP2 ice core. The NGRIP-GRIP depth difference curve shows a small anomaly just below the GISP2 annual layer thickness anomaly (match points 10 – 13), but the magnitude of this anomaly is only 20 cm.

It should be noted that the magnitude and location of the bumps in the GISP2-NGRIP and GISP2-GRIP depth difference curves are supported by an independent matching of the GRIP and GISP2 cores (pers. comm. R. Rohde, 2006) using data from an optical dust logging device (Bay et al., 2001).

5 Discussion

The match points in Table 2 and the match points of Rasmussen et al. (2006), covering in total the period from GI-5 to the onset of the Holocene, comprise a common stratigraphy of the three cores. Using this stratigraphy, the NGRIP-based GICC05 time scale can be applied to the GRIP and GISP2 cores, making the records of the three cores available on a common time scale. NGRIP depths corresponding to every 50 years from 11.6 to 32.45 ka b2k were obtained from the GICC05 depth-age relation (Rasmussen et al., 2006; Andersen et al., submitted). These depths were converted to GRIP and GISP2 depths using linear interpolation between the match point depths. In longer sections without match points the interpolation introduces a significant uncertainty in the calculated GRIP and GISP2 depths. We estimate that the maximum possible depth offset is 0.5 meter, corresponding to a shift of about 20 years. In Fig. 3 we present 50 year average values of the δ^{18}O and [Ca^{2+}] records from the NGRIP, GRIP and GISP2 cores on the GICC05 time scale, based on the data sets listed in Table 1. Note the reversed logarithmic scale of the [Ca^{2+}] curve. The records are shown over the 11.6 to 32.45 ka b2k period. The location of the NGRIP-GRIP (red dots) and NGRIP-GISP2 match points (green dots) used for the synchronization are shown in the top. The synchronization of the NGRIP, GRIP, and GISP2 records makes it possible to assess similarities and differences between these key records of the late glacial climate. The δ^{18}O and [Ca^{2+}] profiles of the three cores are seen to be very well aligned at all stadial-interstadial transitions. In contrast to the synchronicity of the onsets and terminations of interstadials, significant differences between the three δ^{18}O profiles are found within all climatic stages, probably reflecting variations in moisture transport to the Greenland ice cap. The most pronounced of these differences will be described in the following sections.

5.1 GISP2 accumulation anomaly

As described in the Results section, the depth difference curves derived from the match points of the synchronization show that the mean GISP2 annual layer thicknesses are unusually large in the 16.5 – 18.3 ka b2k interval compared to the annual layer thicknesses in the GRIP and NGRIP cores. The period is not characterized by stadial-interstadial transitions or other abrupt climatic shifts, and we are not aware of any flow phenomena that can produce such a short and abrupt annual layer thick-

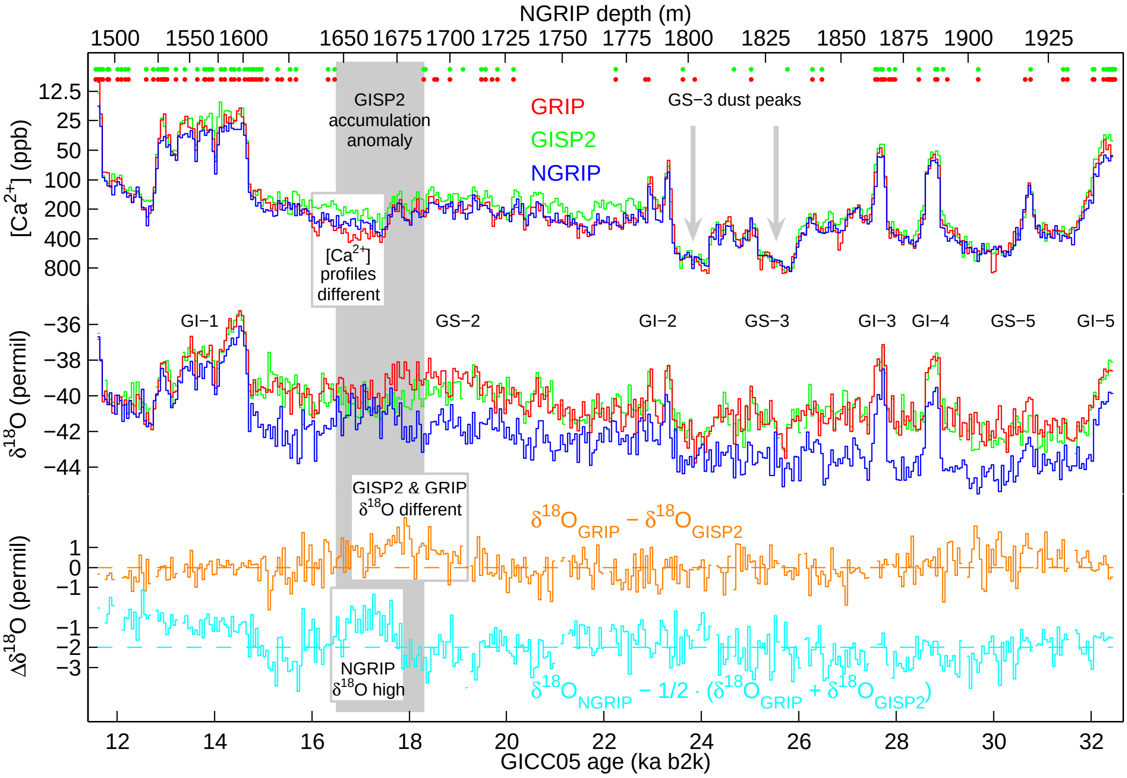

Fig. 3. 50 year average values of δ^{18}O and [Ca^{2+}] (see Table 1 for data sources) on the GICC05 time scale (GRIP (red), GISP2 (green), NGRIP (blue)). The dots in the top show the position of the match points used to synchronize the NGRIP ice core with the GRIP (red dots) and GISP2 (green dots) cores. In the bottom of the plot, the differences between the isotope curves are illustrated: the orange curve shows the difference between the δ^{18}O values in GRIP and GISP2, while the cyan curve shows the δ^{18}O offset between the NGRIP profile and the mean of the GRIP and GISP2 profiles. The shaded interval marks the GISP2 accumulation anomaly, and the three boxes indicate the position of areas of anomalous δ^{18}O values and [Ca^{2+}] values (see section 5 for further discussion of these anomalies). Greenland Stadials (GS) and Greenland Interstadials (GI) are numbered according to the convention of Björck et al. (1998) and Walker et al. (1999). A similar graph with 20 year resolution is available as supplementary information.

ness anomaly. The GRIP-NGRIP depth difference curve of Fig. 2 shows only a minor anomaly in this area, and in addition, the mean slope of the depth difference curve is similar in the 16.5 – 18.3 ka b2k period and in the neighbouring millennia. This means that the GRIP and NGRIP cores receive roughly proportional amounts of precipitation, and the anomaly is thus either caused by equally offset accumulation rates at both the GRIP and NGRIP drill sites, or anomalous accumulation rates at GISP2. No unusual annual layer thicknesses are observed in the NGRIP core in this interval (Andersen et al., submitted), and we thus consider it most likely that the annual layer thickness anomaly is caused by GISP2 receiving more precipitation than usual. The accumulation increase is 7 – 9% on average over the entire period, but the exact timing and duration of the anomaly cannot be determined due to lack of match points within the 16.5 – 18.3 ka b2k interval. If the duration of the period with elevated accumulation rates is shorter, the amplitude of the anomaly must have been correspondingly higher. The cause of the increased accumulation at GISP2 is not clear, but we speculate that it could be related to migration of the ice divide or differences in atmospheric circulation causing the NGRIP/GRIP and GISP2 drill sites to be influenced by air masses of different origin. Indeed, large accumulation differences have been observed near ice divides (Clausen et al., 1988; Fisher et al., 1983). The location of the GISP2 accumulation anomaly is marked in Fig. 3 with a grey shaded band.

5.2 The $\delta^{18}O$ profiles

In general the GRIP and GISP2 δ^{18}O profiles are very similar and agree on the shape and timing of the abrupt stadial-interstadial transitions. In contrast to this, the curves have significant differences on the centennial scale. The difference between the GRIP and GISP2 isotope profiles is presented in the lower part of Fig. 3 (orange curve, dashed curve marks the zero level), and show that the GRIP and GISP2 δ^{18}O values in each 50 year interval typically differ by 1 – 2 permil, but that there are no persistent differences apart from in the 16.8 – 19.2 ka b2k interval, in which the GRIP δ^{18}O values are 1 – 2 permil higher than the GISP2 values. This period is marked by a box in Fig. 3.

The NGRIP δ^{18}O values are in general about 2 permil lower than the GRIP and GISP2 values in the glacial as also reported by NGRIP members (2004). An exception is found around 17 ka b2k, where the NGRIP δ^{18}O values rise to the same level as the GRIP and GISP2 δ^{18}O values. The difference is seen most clearly from the cyan curve in Fig. 3, where the offset of the NGRIP δ^{18}O profile relative to the average GRIP-GISP2 values is shown (2 permil offset indicated by dashed cyan line). The offset is around 1.5 permil in the oldest part of the section investigated here and gently increases to about 2 – 3 permil around 28 ka b2k. In the 16.4 – 17.9 ka b2k section, the NGRIP δ^{18}O values are elevated to GRIP/GISP2 levels (marked by a box in Fig. 3), followed by a period with 2 – 3 permil offset before the offset again disappears during the warmer GI-1 period.

Using the accumulation rate-δ^{18}O relationship of the ss09sea model, the NGRIP δ^{18}O anomaly would imply an increase in modelled annual layer thicknesses of about 20%. Investigators counting annual layers in the NGRIP ice core found no significant changes in mean annual layer thicknesses in this section, and it is therefore concluded that the accumulation rates and δ^{18}O are decoupled in this section (Andersen et al., submitted; Svensson et al., submitted).

5.3 The [Ca^{2+}] profiles

The Ca^{2+} content of the different cores clearly anti-correlates with the $\delta^{18}O$ profiles (note the reversed logarithmical scale) as has generally been noted for Greenland ice cores (e.g. Fuhrer et al., 1999). The [Ca^{2+}] concentration in the GISP2 cores tends to be somewhat lower than in the other cores, most notably during the cold GS-2 period. The largest differences between the three dust profiles is seen in the 16 – 17.5 ka b2k interval, in which the [Ca^{2+}] values also are slightly increased relative to the rest of GS-2. This period is marked with a box in Fig. 3.

A special feature of the [Ca^{2+}] profiles is the two very distinct events in GS-3 first reported by Hammer et al. (1985), in which the dust levels increase by a factor of 3 in the NGRIP core (Ruth et al., 2003), and the [Ca^{2+}] content in all three cores increases from about 200 – 300 to 700 – 800 ppb. When the onsets and terminations are defined as the midpoints of the slopes in 20 year averaged [Ca^{2+}] data, the events date to $(23,380 \pm 20)$ – $(24,150 \pm 10)$ b2k and $(25,140 \pm 20)$ – $(25,980 \pm 60)$ b2k in GICC05, respectively, where the quoted uncertainty arises from the fact that the onsets and terminations are not instantaneous and well-defined. The absolute GICC05 maximum counting error at this depth is about 700 years (see Table 1 and Andersen et al. (submitted)), but from the difference in maximum counting error the uncertainty in the number of years across each of the events is less than 50 years. Adding up the uncertainties is not straightforward, but the event durations are approximately 770 years for the younger event and 840 years for the older with an estimated precision of a century or better. From Fig. 3 it is also apparent that the termination of the younger dust peak coincides with the onset of GI-2.

Generally, the three [Ca^{2+}] profiles show a consistent picture and display strong and synchronous climatic variations. Only short sporadic [Ca^{2+}] peaks connected to volcanic events were occasionally used as match points, and the close agreement between the profiles is therefore not implicit from the matching. The synchronicity of the profiles shows that if a volcanic match cannot be performed, [Ca^{2+}] is a better parameter for matching than $\delta^{18}O$, as the [Ca^{2+}] profiles of the three cores in general agree better than the $\delta^{18}O$ profiles on the timing of transitions (see also the 20 year resolved version of Fig. 3, provided as supplementary information). As pointed out by Mulvaney et al. (2000), the greater similarity of the [Ca^{2+}] records than the $\delta^{18}O$ records can be explained by the large distance to the dust sources, that are known to be located mainly in Asia (Biscaye et al., 1997). According to this argument, the amount of dust in Greenland ice cores is modulated primarily by the source efficiency and transport paths, leading to roughly similar dust input to the entire Central Greenland area, while the $\delta^{18}O$ profiles are less similar due to differences in source areas between the cores and the influence of local temperature and circulation effects.

6 Conclusion

We have presented a synchronization of the NGRIP, GRIP, and GISP2 ice cores from the onset of GI-1 to GI-5 (14.9 – 32.45 ka b2k). Together with the match points of Rasmussen et al. (2006), the synchronization has made it possible to extend the GICC05 time scale to the GRIP and GISP2 cores from the onset of the Holocene to GI-5. The matching reveals that the accumulation rate at the GISP2 drill site was elevated by 7 – 9% on average relative to GRIP and NGRIP over the 16.5 – 18.3 ka b2k period, possibly due to migration of the ice divide. Around this time, anomalous events in the NGRIP, GRIP, and GISP2 δ^{18}O and [Ca^{2+}] profiles are observed. Some of the same features are seen for the period 21 – 24 ka b2k, including the scarcity of good match points, but with smaller magnitude and without the strong anomaly in annual layer thickness. Over the remaining period, the synchronized profiles of δ^{18}O and [Ca^{2+}] show very good agreement, especially across the stadial-interstadial transitions and during the two characteristic dust events of GS-3.

The fact that the anomalies are all located within the same 3 ky long period (compare the timing of the anomalies in Fig. 3) indicates that their causes may very well be connected. However, from the δ^{18}O difference curves of Fig. 3 it is clear that the duration of the GRIP-GISP2 offset is not contemporaneous with the interval of high NGRIP δ^{18}O values. This offset in timing, and the stable δ^{18}O values of the GISP2 core, make it unlikely that the anomalies are caused by a movement of the polar front or other large-scale changes in atmospheric circulation (as suggested by Masson-Delmotte et al., 2005a, during stadial-interstadial transitions), as such changes would be observed all over Greenland, although possibly with different amplitudes at the different drill sites. Instead, we suggest that the anomalous values are related to changes in the source areas of the precipitation received at the three sites, probably due to circulation changes or changes in sea ice extent. More investigations using combined high-resolution δD and δ^{18}O data are needed to identify possible changes in source and drill site temperatures during this time interval. Indeed, such changes have been derived from δ^{18}O and δD profiles from the Holocene (Masson-Delmotte et al., 2005b), which is in line with the observed decoupling of δ^{18}O and accumulation rates in this period (Andersen et al., submitted; Svensson et al., submitted).

The synchronization provides improved basis for interpreting the climatic information from the three cores in the late glacial period, and the common time scale makes it possible to assess differences in the climatic information contained in these key records of the glacial climate. We hope that the advent of common chronological frameworks in ice core studies will improve the understanding of the climate system and add to our knowledge on the underlying dynamics.

7 Supplementary information

A figure similar to Fig. 3, but with 20 year resolution, is available as supplementary information.

8 Data access

An electronic version of Table 2 and the corresponding match points in the 8.2 – 14.8 ka b2k period from Rasmussen et al. (2006) are available from http://www.icecores.dk together with 20 and 50 year mean values of $\delta^{18}O$ and $[Ca^{2+}]$ from both the NGRIP, GRIP, and GISP2 ice cores on the GICC05 time scale. The customized Matlab application for ice core synchronization (”Matchmaker”) can be obtained from SOR upon request.

Acknowledgements

This work is a contribution of the Copenhagen Ice Core Dating Initiative which is supported by a grant from the Carlsberg Foundation. IKS is funded by the Danish Research Agency through the ESF RESOLuTION programme.

Tables

Core	Data series	Method	Data Coverage	Depth res. (cm)	Reference
GRIP	ECM		Continuous	0.1	Taylor et al. (1993); Moore et al. (1994); Wolff et al. (1997)
	DEP		Continuous pointwise	2	Taylor et al. (1993); Moore et al. (1994); Wolff et al. (1997)
	$[SO_4^{2-}]$	IC	Discontinuous, discrete	2.5 – 5	
	$[NH_4^+]$, $[Ca^{2+}]$	CFA	Continuous†	0.2	Fuhrer et al. (1993, 1996)
	$\delta^{18}O$		Continuous, discrete	6.9 – 13.8	Johnsen et al. (1997)
NGRIP	ECM		Continuous	0.1	Dahl-Jensen et al. (2002)
	DEP		Continuous pointwise	0.5	Dahl-Jensen et al. (2002)
	$[SO_4^{2-}]$, $[NH_4^+]$, $[Ca^{2+}]$	CFA	Continuous	0.1	Bigler (2004)
	$\delta^{18}O$		Continuous, discrete	5	NGRIP members (2004)
GISP2	ECM		Continuous	0.1	Taylor et al. (1993, 1997)
	$[SO_4^{2-}]$, $[NH_4^+]$, $[Ca^{2+}]$	IC	Continuous, discrete	20	Mayewski et al. (1997); Taylor et al. (1996)
	$\delta^{18}O$		Continuous, discrete	20	Stuiver and Grootes (2000); Grootes and Stuiver (1997)

† $[NH_4^+]$ data not available in the 2065 – 2281 m interval.

Table 1
Data series used for the matching (ECM, DEP, $[SO_4^{2-}]$, $[NH_4^+]$) and data presented in Fig. 2 ($\delta^{18}O$, $[Ca^{2+}]$).

No.	NGRIP depth (m)	GRIP depth (m)	GISP2 depth (m)	GICC05 age (years b2k)	GICC05 MCE (years)	No.	NGRIP depth (m)	GRIP depth (m)	GISP2 depth (m)	GICC05 age (years b2k)	GICC05 MCE (years)
1	1610.8	1760.19	1804.23	14915	195	34	-	2018.28^{s}	2049.96	27548	822
2	1612.00^{c,n}	1761.46^{c,n}	1805.41^{c,n}	14967	196	35	1862.58	2018.92^{s}	2050.57	27574	823
3	1614.72^{c,n}	1764.35^{c,n}	-	15083	199	36	1864.02^{n}	2020.43^{s,n}	2051.97	27622	825
4	1619.57^{c}	1769.52^{c}	1812.91^{c}	15297	209	37	1866.21^{w}	2022.53^{w}	2054.07^{w}	27693	827
5	1621.54^{N}	1771.62^{N}	-	15384	214	38	1866.87	2023.14^{s}	2054.62	27715	828
6	1625.58^{n}	1775.82^{n}	1818.89	15559	221	39	1868.55^{n}	2024.82^{n}	-	27763	831
7	1627.96^{n}	1778.34^{n}	1821.27	15671	226	40	-	2025.98^{s}	2057.25	27810	834
8	1642.66	1793.37	1835.43	16333	261	41	1870.39^{N}	2026.64^{N}	2057.85^{N}	27852	838
9	1645.83^{n}	1796.72^{n}	1838.60^{n}	16469	268	42	1871.39^{N}	2027.53^{N}	-	27912	842
10	1687.77	1840.78	1883.03	18296	361	43	1872.25^{n}	2028.27^{s,n}	2059.49	27967	847
11	1688.68	-	1883.92	18335	362	44	1880.01^{n}	2035.25^{n}	2066.16	28454	881
12	1692.63^{N,e}	1845.56^{N,e}	-	18518	370	45	1888.70^{n}	2043.41^{n}	2074.09	28807	895
13	1693.68^{N,e}	1846.60^{N,e}	-	18567	375	46	1889.86^{n}	2044.51^{n}	2075.17	28842	896
14	-	1847.87^{N,e}	1890.11^{N,e}	18623	378	47	1892.66	-	2077.4	28961	901
15	1699.82^{n}	1852.61^{w,n}	1894.73	18833	388	48	1894.01^{N}	2048.24^{N}	-	29045	905
16	1705.79	-	1900.61	19101	402	49	1902.84	2055.99	2086.38	29678	946
17	-	1863.67^{N}	1905.31^{N}	19325	413	50	-	2057.36^{N}	2087.71^{N}	29795	957
18	1714.18	1867.33	1908.76^{w}	19480	421	51	1916.8	2068.05	-	30641	1011
19	1716.15	1869.39	1910.69	19564	425	52	1918.95^{n}	2069.76	2099.52^{n}	30753	1020
20	1719.13^{N}	1872.49^{N}	-	19700	431	53	1929.87	2079.37^{w}	2108.9	31428	1067
21	1721.32^{w,n}	1874.76^{n}	1915.73^{w}	19806	435	54	1931.05	2080.41	2109.92^{w}	31506	1072
22	1728.59^{n}	1882.23^{n}	1922.77	20136	448	55	1939.51	2087.83	2117.07	32029	1105
23	-	1892.18	1932.03	20565	465	56	1939.94^{w}	2088.21	2117.40^{w}	32054	1107
24	1770.81^{u,w}	1926.34^{u}	1963.66^{u}	22244	544	57	1944.45	2092.24	2121.23	32248	1122
25	1782.66^{N,u}	1939.26^{N,u}	-	22851	571	58	1946.54	2094.09	2123.05	32324	1123
26	1783.70^{N,u}	1940.37^{N,u}	-	22905	574	59	1947.34	2094.83	2123.75	32354	1125
27	1798.35^{n,u}	1955.95^{s,n,u}	1990.98^{n,u}	23617	612	60	1947.94^{n}	2095.39	2124.27^{n}	32377	1128
28	1802.27	1960.03^{s}	-	23864	629	61	1948.72^{n}	2096.11	2124.95^{n}	32404	1129
29	1814.92	-	2006.77	24668	674	62	1949.23	2096.59	2125.4	32421	1130
30	1820.39^{w,n}	1978.58^{w,n}	2012.06	25018	691	63	1949.57	2096.92	2125.72	32431	1130
31	1831.58	-	2022.79	25759	735	64	1950.07	-	2126.15	32449	1130
32	1840.22	1997.83	2030.74	26282	760	65	1950.45	2097.75	2126.51	32461	1130
33	1843.68^{n}	2001.13^{n}	2033.89^{w}	26477	767	66	1951.09	2098.33	2127.05	32482	1131

^{n} Volcanic match supported by peak in [NH_4^+].
^{c} [Ca^{2+}] peak in addition to ECM, DEP and [SO_4^{2-}].
^{N} Match based on [NH_4^+] data.
^{s} GRIP [SO_4^{2-}] peak in addition to ECM and DEP data.
^{w} Wide peak and/or less well-defined match-point (depth uncertainty up to 20 cm).
^{u} Increased uncertainty. The estimated possible mismatch across this section is 1 m.
^{e} [NH_4^+] match 1692-1695 m NGRIP-depth is supported by minor ECM and [SO_4^{2-}] peaks in NGRIP and GISP2 at approx. 1689.9 m, 1690.6 m, and 1695.3 m NGRIP-depths.

Table 2
Match-points representing synchronous events in the NGRIP, GRIP, and GISP2 ice cores. The GICC05 ages and maximum counting errors (MCE) are taken from Andersen et al. (submitted)

References

Alley, R. B., Shuman, C. A., Meese, D. A., Gow, A. J., Taylor, K. C., Cuffey, K. M., Fitzpatrick, J. J., Grootes, P. M., Zielinski, G. A., Ram, M., Spinelli, G., Elder, B., 1997. Visual-stratigraphic dating of the GISP2 ice core: Basic, reproducibility, and application. Journal of Geophysical Research 102 (C12), 26367–26381.

Andersen, K. K., Svensson, A., Johnsen, S., Rasmussen, S. O., Bigler, M., Röthlisberger, R., Ruth, U., Siggaard-Andersen, M.-L., Steffensen, J. P., Dahl-Jensen, D., Vinther, B. M., Clausen, H. B., submitted. The Greenland Ice Core Chronology 2005, 15-42 kyr. Part 1: Constructing the time scale, Quaternary Science Reviews.

Bay, R. C., Bramall, N. E., Price, P. B., Clow, G. D., Hawley, R. L., Udisti, R., Castellano, E., 2006. Globally synchronous ice core volcanic tracers and abrupt cooling during the last glacial period. Journal of Geophysical Research 111, D11108.

Bay, R. C., Price, P. B., Clow, G. D., Gow, A. J., 2001. Climate logging with a new rapid optical technique at Siple Dome. Geophysical Research Letters 28 (24), 4635–4638.

Bender, M., Sowers, T., Dickson, M.-L., Orchardo, J., Grootes, P., Mayewski, P., Meese, D., 1994. Climate correlations between Greenland and Antarctica during the last 100,000 years. Nature 372 (6507), 663–666.

Bigler, M., 2004. Hochauflösende Spurenstoffmessungen an polaren Eisbohrkernen: Glaziochemische und klimatische Prozessstudien, Ph.D. dissertation, University of Bern, Switzerland.

Bigler, M., Wagenbach, D., Fischer, H., Kipfstuhl, J., Miller, H., Sommer, S., Stauffer, B., 2002. Sulphate record from a northeast Greenland ice core over the last 1200 years based on continuous flow analysis. Annals of Glaciology 35, 250–256.

Biscaye, P. E., Grousset, F. E., Revel, M., Van der Gaast, S., Zielinski, G. A., Vaars, A., Kukla, G., 1997. Asian provenance of glacial dust (stage 2) in the Greenland Ice Sheet Project 2 ice core, Summit, Greenland. Journal of Geophysical Research 102 (C12), 26765–26781.

Björck, S., Walker, M. J. C., Cwynar, L. C., Johnsen, S., Knudsen, K.-L., Lowe, J. J., Wohlfarth, B., INTIMATE Members, 1998. An event stratigraphy for the Last Termination in the North Atlantic region based on the Greenland ice-core record: a proposal by the INTIMATE group. Journal of Quaternary Science 13 (4), 283–292.

Blunier, T., Brook, E. J., 2001. Timing of millennial-scale climate change in Antarctica and Greenland during the last glacial period. Science 291, 109–112.

Blunier, T., Schwander, J., 2000. Gas enclosure in ice: Age difference and fractionation. In: Hondoh, T. (Ed.), Physics of Ice Core Records. Hokkaido University Press, Sapporo, pp. 307–326.

Clausen, H., Hammer, C., Hvidberg, C., Dahl-Jensen, D., Steffensen, J., Kipfstuhl, J., Legrand, M., 1997. A comparison of the volcanic records over the past 4000 years from the Greenland Ice Core Project and DYE-3 Greenland ice cores. Journal of Geophysical Research 102 (C12), 26707–26723.

Clausen, H. B., Gundestrup, N., Johnsen, S. J., Bindschadler, R., Zwally, J., 1988. Glaciological investigations in the Crête-area, Central Greenland. A search for a new deep-drilling site. Annals of Glaciology 10, 10–15.

Dahl-Jensen, D., Gundestrup, N. S., Miller, H., Watanabe, O., Johnsen, S. J., Steffensen, J. P., Clausen, H. B., Svensson, A., Larsen, L. B., 2002. The NorthGRIP deep drilling programme. Annals of Glaciology 35, 1–4.

Dansgaard, W., Johnsen, S., Clausen, H., Dahl-Jensen, D., Gundestrup, N., Hammer, C., Hvidberg, C., Steffensen, J., Sveinbjörnsdottir, A., Jouzel, J., Bond, G., 1993. Evidence for general instability of past climate from a 250-kyr ice-core record. Nature 364 (6434), 218–220.

Fisher, D., Koerner, R., Paterson, W., Dansgaard, W., Gundestrup, N., Reeh, N., 1983. Effect of wind scouring on climate records from ice-core oxygen-isotope profiles. Nature 301, 205–209.

Fisher, D. A., Reeh, N., Clausen, H. B., 1985. Stratigraphic noise in time series derived from ice cores. Annals of Glaciology 7, 76–83.

Fuhrer, K., Neftel, A., Anklin, M., Maggi, V., 1993. Continuous measurements of hydrogen peroxide, formaldehyde, calcium and ammonium concentrations along the new GRIP ice core from Summit, Central Greenland. Atmospheric Environment 27A (12), 1873–1880.

Fuhrer, K., Neftel, A., Anklin, M., Staffelbach, T., Legrand, M., 1996. High-resolution ammonium ice core record covering a complete glacial-interglacial cycle. Journal of Geophysical Research 101 (D2), 4147–4164.

Fuhrer, K., Wolff, E. W., Johnsen, S. J., 1999. Timescales for dust variability in the Greenland Ice Core Project (GRIP) ice core in the last 100,000 years. Journal of Geophysical Research 104 (D24), 31043–31052.

Grönvold, K., Óskarsson, N., Johnsen, S. J., Clausen, H. B., Hammer, C. U., Bond, G., Bard, E., 1995. Ash layers from Iceland in the Greenland GRIP ice core correlated with oceanic and land sediments. Earth and Planetary Science Letters 135, 149–155.

Grootes, P. M., Stuiver, M., 1997. Oxygen 18/16 variability in Greenland snow and ice with 10^{-3} to 10^{5}-year time resolution. Journal of Geophysical Research 102, 26455–26470.

Hammer, C., Clausen, H., Dansgaard, W., 1980. Greenland ice sheet evidence of post-glacial volcanism and its climatic impact. Nature 288, 230–235.

Hammer, C., Clausen, H., Dansgaard, W., Neftel, A., Kristinsdottir, P., Johnson, E., 1985. Continuous impurity analysis along the Dye-3 deep core. In: Langway, C.C., J., Oeschger, H., Dansgaard, W. (Eds.), Greenland Ice Core: Geophysics, Geochemistry, and the Environment. Geophys. Monogr. Ser., vol. 33. American Geophysical Union (AGU), Washington, D.C., pp. 90–94.

Hammer, C., Clausen, H., Langway, C.C., J., 1997. 50,000 years of recorded global volcanism. Climatic Change 35 (1), 1–15.

Hammer, C. U., 1980. Acidity of polar ice cores in relation to absolute dating, past volcanism, and radio-echoes. Journal of Glaciology 25 (93), 359–372.

Johnsen, S., Dahl-Jensen, D., Dansgaard, W., Gundestrup, N., 1995. Greenland palaeotemperatures derived from GRIP bore hole temperature and ice core isotope profiles. Tellus 47B, 624–629.

Johnsen, S. J., Clausen, H. B., Dansgaard, W., Fuhrer, K., Gundestrup, N., Hammer, C. U., Iversen, P., Jouzel, J., Stauffer, B., Steffensen, J. P., September 1992. Irregular glacial interstadials recorded in a new Greenland ice core. Nature 359, 311–313.

Johnsen, S. J., Clausen, H. B., Dansgaard, W., Gundestrup, N. S., Hammer, C. U., Andersen, U., Andersen, K. K., Hvidberg, C. S., Dahl-Jensen, D., Steffensen, J. P., Shoji, H., Sveinbjörnsdóttir, Á. E., White, J., Jouzel, J., Fisher, D., 1997. The δ^{18}O record along the Greenland Ice Core Project deep ice core and the problem of possible Eemian climatic instability. Journal of Geophysical Research 102 (C12), 26397–26410.

Johnsen, S. J., Dahl-Jensen, D., Gundestrup, N., Steffensen, J. P., Clausen, H. B., Miller, H., Masson-Delmotte, V., Sveinbjörnsdottir, A. E., White, J., 2001. Oxygen isotope and palaeotemperature records from six Greenland ice-core stations: Camp Century, Dye-3, GRIP, GISP2, Renland and NorthGRIP. Journal of Quaternary Science 16, 299–307.

Masson-Delmotte, V., Jouzel, J., Landais, A., Stievenard, M., Johnsen, S. J., White, J. W. C., Werner, M., Sveinbjornsdottir, A., Fuhrer, K., 2005a. GRIP deuterium excess reveals rapid and orbital-scale changes in Greenland moisture origin. Science 209, 118–121.

Masson-Delmotte, V., Landais, A., Stievenard, M., Cattani, O., Falourd, S., Jouzel, J., Johnsen, S. J., Dahl-Jensen, D., Sveinsbjornsdottir, A., White, J. W. C., Popp, T., Fischer, H., 2005b. Holocene climatic changes in Greenland: Different deuterium excess signals at Greenland Ice Core Project (GRIP) and NorthGRIP. Journal of Geophysical Research 110, D14102.

Mayewski, P., Meeker, L., Twickler, M., Whitlow, S., Yang, Q., Lyons, W., Prentice, M., 1997. Major features and forcing of high-latitude northern hemisphere atmospheric circulation using a 110,000-year-long glaciochemical series. Journal of Geophysical Research 102, 26345–26366.

Meese, D. A., Gow, A. J., Alley, R. B., Zielinski, G. A., Grootes, P. M., Ram, M., Taylor, K. C., Mayewski, P. A., Bolzan, J. F., 1997. The Greenland Ice Sheet Project 2 depth-age scale: Methods and results. Journal of Geophysical Research 102 (C12), 26411–26423.

Moore, J. C., Mulvaney, R., Paren, J., 1989. Dielectric stratigraphy of ice: A new technique for determining total ionic concentrations in polar ice cores. Geophysical Research Letters 16, 1177–1180.

Moore, J. C., Wolff, E. W., Clausen, H. B., Hammer, C. U., Legrand, M. R., Fuhrer, K., 1994. Electrical response of the Summit-Greenland ice core to ammonium, sulphuric acid, and hydrochloric acid. Geophysical Research Letters 21 (7), 565–568.

Mortensen, A., Bigler, M., Grönvold, K., Steffensen, J., Johnsen, S., 2005. Volcanic ash layers from the Last Glacial Termination in the NGRIP ice core. Journal of Quaternary Science 20 (3), 209–219.

Mulvaney, R., Röthlisberger, R., Wolff, E. W., Sommer, S., Schwander, J., Hutterli, M. A., Jouzel, J., 2000. The transition from the last glacial period in inland and near-coastal Antarctica. Geophysical Research Letters 27 (17), 2673–2676.

NGRIP members, 2004. High-resolution record of Northern Hemisphere climate extending into the last interglacial period. Nature 431, 147–151.

Palmer, A. S., van Ommen, T. D., Curran, M. A. J., Morgan, V., Souney, J. M., Mayewski, P. A., 2001. High-precision dating of volcanic events (A.D. 1301 – 1995) using ice cores from Law Dome, Antarctica. Journal of Geophysical Research 106 (D22), 28,089–28,095.

Rasmussen, S. O., Andersen, K. K., Svensson, A. M., Steffensen, J. P., Vinther, B., Clausen, H. B., Siggaard-Andersen, M.-L., Johnsen, S. J., Larsen, L. B., Dahl-Jensen, D., Bigler, M., Röthlisberger, R., Fischer, H., Goto-Azuma, K., Hansson, M., Ruth, U., 2006. A new Greenland ice core chronology for the last glacial termination. Journal of Geophysical Research 111, D06102.

Rasmussen, S. O., Vinther, B. M., Clausen, H. B., Andersen, K. K., accepted. Early Holocene climate oscillations recorded in three Greenland ice cores, Quaternary Science Reviews.

Röthlisberger, R., Bigler, M., Hutterli, M., Sommer, S., Stauffer, B., Junghans, H., Wagenbach, D., 2000. Technique for continuous high-resolution analysis of trace substances in firn and ice cores. Environmental Science and Technology 34 (2), 338–342.

Ruth, U., Wagenbach, D., Steffensen, J., Bigler, M., 2003. Continuous record of microparticle concentration and size distribution in the central Greenland NGRIP ice core during the last glacial period. Journal of Geophysical Research. 108, 4098.

Southon, J., 2004. A radiocarbon perspective on Greenland ice-core chronologies: Can we use ice cores for ^{14}C calibration? Radiocarbon 46 (3), 1239–1260.

Stuiver, M., Grootes, P. M., 2000. GISP2 Oxygen isotope ratios. Quaternary Research 53, 277–284.

Svensson, A., Andersen, K. K., Bigler, M., Clausen, H. B., Dahl-Jensen, D., Davies, S. M., Johnsen, S. J., Muscheler, R., Rasmussen, S. O., Röthlisberger, R., Steffensen, J. P., Vinther, B. M., submitted. The Greenland Ice Core Chronology 2005, 15-42 kyr. Part 2: Comparison to other records, Quaternary Science Reviews.

Taylor, K., Alley, R., Lamorey, G., Mayewski, P., 1997. Electrical measurements on the Greenland Ice Sheet Project 2 core. Journal of Geophysical Research 102, 26511–26517.

Taylor, K., Hammer, C., Alley, R., Clausen, H., Dahl-Jensen, D., Gow, A., Gundestrup, N., Kipfstuhl, J., Moore, J., Waddington, E., 1993. Electrical conductivity measurements from the GISP2 and GRIP Greenland ice cores. Nature 366, 549–552.

Taylor, K., Mayewski, P., Twickler, M., Whitlow, S., 1996. Biomass burning recorded in the GISP2 ice core: A record from eastern Canada? The Holocene 6 (1), 1–6.

Udisti, R., Becagli, S., Castellano, E., Delmonte, B., Jouzel, J., Petit, J. R., Schwander, J., Stenni, B., Wolff, E. W., 2004. Stratigraphic correlations between the European Project for Ice Coring in Antarctica (EPICA) Dome C and Vostok ice cores showing the relative variations of snow accumulation over the past 45 kyr.

Journal of Geophysical Research 109, D08101.
Vinther, B. M., Clausen, H. B., Johnsen, S. J., Rasmussen, S. O., Andersen, K. K., Buchardt, S. L., Dahl-Jensen, D., Seierstad, I. K., Siggaard-Andersen, M.-L., Steffensen, J. P., Svensson, A. M., Olsen, J., Heinemeier, J., 2006. A synchronized dating of three Greenland ice cores throughout the Holocene. Journal of Geophysical Research 111, D13102.
Walker, M. J. C., Björck, S., Lowe, J. J., Cwynar, L. C., Johnsen, S., Knudsen, K.-L., Wohlfarth, B., 1999. Isotopic 'events' in the GRIP ice core: a stratotype for the Late Pleistocene. Quaternary Science Reviews 18 (10–11), 1143–1150.
Wolff, E., Moore, J., Clausen, H., Hammer, C., 1997. Climatic implications of background acidity and other chemistry derived from electrical studies of the Greenland Ice Core Project ice core. Journal of Geophysical Research 102, 26325–26332.
Wolff, E. W., Basile, I., Petit, J.-R., Schwander, J., 1999. Comparison of Holocene electrical records from Dome C and Vostok. Annals of Glaciology 29, 89–93.
Zielinski, G., 2000. Use of paleo-records in determining variability within the volcanism-climate system. In: Alverson, K., Oldfield, F., Bradley, R. (Eds.), Past Global Changes and their Significance for the Future. Vol. Quaternary Science Reviews, 19(1-5). Pergamon, pp. 417–438.
Zielinski, G., Mayewski, P., Meeker, L., Whitlow, S., Twickler, M., Morrison, M., Meese, D., Gow, A., Alley, R., 1994. Record of volcanism since 7000 B.C. from the GISP2 Greenland ice core and implications for the volcano-climate system. Science 264, 948–952.